In situ Chemical Oxidation of Creosote/Coal Tar Residuals: Experimental and Numerical Investigation

by

Steven Philip Forsey

A thesis
presented to the University of Waterloo
in fulfillment of the
thesis requirement of the degree of
Doctor of Philosophy
in
Earth Sciences

Waterloo, Ontario, Canada, 2004

I herby declare that I am the sole author of this thesis. This is a true copy of the thesis, including any required final version, as accepted by my examiners.

I understand that my thesis may be made electronically available to the public

Steven Forsey

Abstract

Coal tar, coal tar creosote and oily wastes are often present as subsurface contaminants that may migrate below the water table, leaving a widely distributed residual source of contaminants leaching to the ground water. *In situ* chemical oxidation is a potentially viable technology for the remediation of aquifers contaminated with creosote and coal tars. The oxidant of choice would be flushed through the contaminated area to oxidize aqueous contaminants and enhance the mass transfer of contaminants from the oil phase. A series of batch and column experiments were performed to assess the ability of a chemical oxidizing reagent to oxidize creosote compounds and to increase mass transfer rates. Results from the column experiments were then simulated using a reactive transport model that considered 12 different creosote compounds undergoing dissolution, oxidation and advective-dispersive transport.

Three strong chemical oxidizing reagents, Fenton's Reagent, potassium persulfate with ferrous ions, and potassium permanganate were tested with batch experiments to determine their reactivity towards creosote compounds. All three reagents successfully decomposed aqueous creosote compounds and were able to reduce the mass of the monitored creosote compounds within the oil phase. However, both the Fenton's and persulfate reagents required large molar ratios of iron and peroxide because the precipitation of iron continually removed the iron catalyst from the aqueous phase. Fenton's and persulfate reagents could be used in systems that are allowed to become acidic to solubilize the iron, but the cost of adjusting the pH, potential impact on aquifer geochemistry and the short lived free radical reaction make these reagents less practical than $KMnO_4$. $KMnO_4$ oxidizes a wide variety of creosote compound, can be used at very high concentrations, and its concentration will not be reduced significantly as it moves through the zone of contamination.

The feasibility of using potassium permanganate as an oxidizing reagent for *in situ* treatment of creosote residuals was investigated using batch column experiments. Column experiments were conducted at a neutral pH in a carbonate rich sand matrix with creosote at 8 % saturation. The columns were treated intermittently with simulated ground water or $KMnO_4$ dissolved in simulated ground water (8 g/L) for 172 days. Under these experimental conditions the $KMnO_4$ decreased the initial mass of the monitored creosote compounds by 36.5%, whereas in the control column (no oxidizer) only 3.9% was removed. To remove all of the monitored creosote compounds from the columns it was calculated that the volume needed would be 40 times less for the $KMnO_4$ solution, compared to flushing alone with simulated ground water.

To evaluate the potential effectiveness of *in situ* chemical oxidation at field sites, numerical model simulations need to incorporate relevant chemical oxidation rates to assess system performance and to provide design guidance. In-depth kinetic studies were performed to determine rate constants and to gain insight into the oxidation of creosote compounds with $KMnO_4$. The study examined the kinetics of the oxidative treatment of a selected group of creosote/coal tar compounds in water using excess potassium permanganate and investigated the correlation between reactivity and physical/chemical properties of the organic pollutants.

The oxidation of naphthalene, phenanthrene, chrysene, pyrene, 1-methylnapthalene, 2-methylnaphthalene, acenaphthene, fluorene, carbazole, isopropylbenzene, ethylbenzene and methylbenzene closely followed first-order reaction kinetics, enabling calculation of second-order rate constants. Fluoranthene was only partially oxidized by permanganate and the oxidation of anthracene was too fast to be measured. Biphenyl, dibenzofuran, benzene and tert-butylbenzene failed to react in this study.

Comprehensive column experiments complemented by numerical modeling revealed an unequal enhancement of the removal of creosote compounds from the oil phase. For the more readily oxidizable compounds such as pyrene and naphthalene, a significant increase in the mass transfer rates was observed in the oxidation columns, compared to the oxidant free column.

For non-oxidizable compounds such as biphenyl and dibenzofuran, an increase in the rate of mass removal was also observed in the oxidation columns, even though their aqueous concentrations were not reduced in the column. This was due to the rapid removal of the more readily oxidizable compounds from the oil, which increases the mole fraction of the non-oxidizable compounds. Thus according to Raoult's Law, the concentration in the aqueous phase becomes closer to its pure phase liquid solubility and its aqueous concentration increases.

The most significant result of the experiments is the observed increase in the rate of removal of those compounds that have low aqueous solubilities and are readily oxidized, such as pyrene and fluorene. Compounds that have low aqueous solubilities and are not readily oxidizable, such as chrysene, may still take a long period of time to be removed, but the removal time is greatly reduced with oxidation compared to flushing the area with water alone.

Acknowledgments

I would like to thank my supervisor Dr. James Barker for helping me through the journey and for his professional and personal support.

I would also like to thank the members of my thesis committee Dr. Neil Thomson, Dr. Bob Gillham and Dr. Mike Chong for their help and encouragement and Dr. Lynn Roberts of Johns Hopkins University for generously offering her time as the external reader.

I would also like to acknowledge the help I received from Dr. Monica Barra and Dr. John Molson. I could not have successfully completed this thesis without their assistance. I thank Dr. M. Barra for the impromptu discussions concerning the kinetic studies. Her advice and comments were extremely valuable. Dr. J. Molson, I would like to thank, for allowing me to adapt his numerical modelling program to my oxidation experiments and for guiding me through its development.

The laboratory experiments could not have been accomplished without the help from the girls in the Organic Geochemistry lab, past and present: Kim Hamilton, Shirley Chatten and Marianne Vandergriendt. Thank you for doing the hundreds of GC samples, letting me perform my experiments in your fume hoods and generally letting me be in your way.

I would also like to thank the Chemistry Department for allowing me to have a full time position while juggling a part time Ph.D. and the Earth Science Department for their support and allowing me to take a little longer in completing my Ph.D.

I am very lucky to have very close friends that take the stress out of life. I would like to thank Jake Fisher, Ted and Laurie Spieker, Peter and Kim Hannam and Lorri Duke, for all their love and support.

I would especially like to thank my family; my parents and my wife's parents for always being there with encouragement and inspiration; my teenaged children Dan and Chrissy for introducing me to new experiences as a father, allowing me to be part of their lives and letting me embarrass them at every opportunity. Finally, I would like to thank my wife Barb, for her love, patience and understanding. We have been together since high school and I cannot imagine life without her.

Table of contents

Chapter 4

Degradation and Oxidative Kinetics of Polycyclic Aromatic Hydrocarbons and Alkylbenzenes Found in Creosote/Coal Tar by Potassium Permanganate

Chapter 5
Column Experiments with Numerical Simulation

Chapter 6
Summary, Conclusions and Recommendations

List of Figures

List of Tables

Chapter 1

Introduction: Creosote/Coal Tars and Chemical Oxidation

1.1 Creosote/Coal Tars

Creosote and coal tars (CCTs) are a complex mixture of mutually miscible organic compounds that can contain as many as 200 different chemicals with only a few present at greater than 1% by weight (Mueller et al., 1989). The composition of creosote depends on the coal tar from which it was produced; it generally contains 85% polynuclear aromatic hydrocarbons (PAHs), 10% phenolics and 5% heterocyclic compounds (nitrogen, sulfur and oxygen containing aromatics) (Mueller et al., 1989). CCTs are associated with manufactured gas plants, tar distillation works and wood preservative plants. Creosote contamination is a global problem. For example in Denmark and Germany there are approximately 457 and 1000 creosote contaminated sites respectively (Dyreborg and Avin, 1994). In the United States there are over 600 wood-preserving plants that use 454,000 metric tonnes of creosote annually (Mattraw and Franks, 1986).

The contamination of ground water with polycyclic aromatic hydrocarbons (PAHs) is of great concern because many of the PAHs are carcinogenic (Dipple et al., 1984) or mutagenic (Durant et al., 1996). CCTs are dense non aqueous phase liquids (DNAPLs) and contain compounds that have low aqueous solubilities, but can be present at aqueous concentrations far in excess of drinking water standards. Because of their low aqueous solubilities the rate of mass transfer from the non aqueous phase to the water phase is very slow. Sources of CCTs thus represent long-term contamination problems with organic compounds leaching into the ground water for decades or centuries until the source is depleted.

CCTs, being denser than water, will migrate upon release to the subsurface through the soil horizons and below the water table. Depending upon such factors as the initial mass of DNAPL released (pressure driving the migration); the physical properties of the DNAPL such as density and viscosity; the intrinsic permeability of the geological medium; and the degree of oil saturation of the pore space in the medium, the DNAPL will migrate downward until it meets an impermeable boundary. Impermeable boundaries are finer grained strata such as silts, clays or rocks having small-aperture fractures which exclude entry of the DNAPL. At these boundaries pools of DNAPL are formed, which may consist of 20 to 60% of the pore spaces (Kueper et al., 1992). Residual DNAPL is formed at the trailing edge of a migrating body due to hysteresis (Bear, 1972) and typically occupies from 1 to 20% of the pore space. Residuals are trapped as discontinuous blobs and are found as single discrete blobs below the range of the pore water dimensions, as doublets connected by two pore bodies linked by a bridge, or as branched segments with three or more connected pore bodies (Morrow et al., 1988, Sahoul et al., 2001).

Potential methods to remove residuals or pools of DNAPLs include the use of enhanced oil recovery methods (EOR) and pump and treat technologies. It is important to note that no *in situ* remediation method has totally restored a DNAPL contaminated aquifer and of the thousands of contaminated aquifers in North America only a few have fully been restored to drinking water use because of the difficulties associated with source-zone restoration (Cherry et al., 1992).

EOR methods flood the contaminated zone with one of the following: 1) hot water or steam, 2) carbon dioxide, 3) surfactant, 4) alcohol 5) alkaline, or 6) polymers (Mercer and Cohen, 1990). EOR methods mobilize the DNAPL by reducing the interfacial tension and/or viscosity and physically remove the DNAPL by pumping. Mobilization of a DNAPL can create a number of problems such as: contaminating previously clean portions of the subsurface, density driven migration of the DNAPL vertically downward, and the movement of DNAPL into lower permeable and less-accessible regions. Generally 10 to 40% of the

DNAPL can remain in the subsurface after EOR methods have been used. (Mercer and Cohen, 1990).

In situ pump and treat technologies can recover the DNAPL as either the oil phase itself or by pumping the contaminated ground water. Generally to remove the oil phase by pumping, the well has to be located directly in a pool of DNAPL. The removal of oil can be enhanced by injecting water under high pressures (water flooding) and displacing the DNAPL, but these methods only remove 30 to 40% of the initial DNAPL (Mercer and Cohen, 1990). To remediate the source by pumping and treating dissolved contaminants leached from the source, a long term program would be needed because of the low aqueous solubilities, small mass transfer rates and the large mass of DNAPLs commonly found at contaminated sites.

To improve mass removal and shorten the length of time required to pump and treat, the rate of mass transfer could be increased by increasing the ground water flow through the residual DNAPL. Laboratory studies with pools of trichloroethylene (TCE) and trichloroethane (TCA) have suggested that the rate of chemical mass transfer to the ground water should increase almost in proportion to the increased ground water velocity (Schwille, 1988). Also, laboratory column and tank experiments (Anderson et al., 1992, Imhoff et al., 1989) with chlorinated DNAPLs suggested that saturated ground water concentrations should be observed for water exiting a residual area for flow rates up to 1 m/day before the rate of mass transfer becomes limiting. Conversely, mass transfer limitations are observed in column experiments with creosote at residual saturation in which the effluent concentrations did not reach effective solubility values. This discrepancy was attributed to either mass transfer limitations (insufficient time to reach equilibrium) or dispersion and dilution by water which had not come into contact with the creosote oil (Priddle and MacQuarrie, 1994, Dryeborg and Avrin, 1994). Similarly mass transfer limitations were observed in the biodegradation of naphthalene from coal tar globules in which the observed rates of mass transfer were slower than the rate of biodegradation (Ghoshal et al., 1996). Their results

inferred that the overall rate of biodegradation was limited by the mass transfer rates.

Most recent research on non-equilibrium mass transfer processes has been based on some form of the stagnant layer model as shown in Figure 1.1 (Find, 1999).

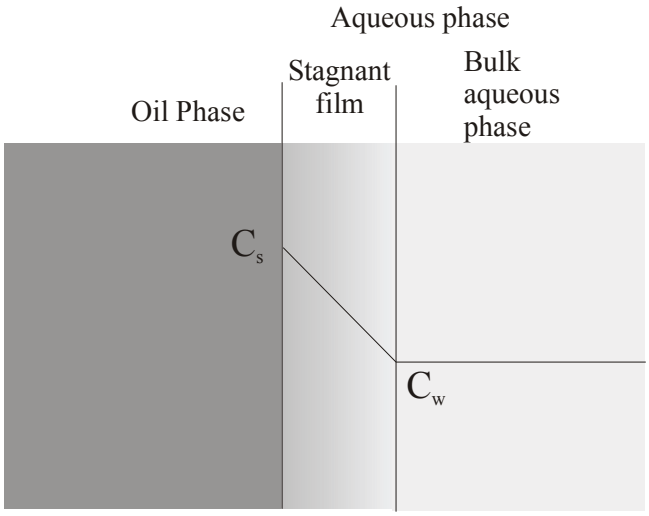

Figure 1.1 Conceptual drawing of a stagnant film layer in which diffusion-limited mass transport occurs across the film. .

The rate of mass transfer or dissolution for a single component can be expressed as,

$$J = \lambda(C_s - C_w) \qquad 1.1$$

where J is the solute mass flux, λ is the interfacial mass transfer coefficient, C_s is the effective solubility limit of the organic compound, and C_w is the aqueous concentration of the organic compound in the bulk flowing ground water. The stagnant film model assumes that resistance to mass transfer resides in the thickness of the thin film adjacent to the water/oil interface. This approach neglects possible mass transfer limitations within the oil phase and may be valid only as long as the oil phase resistance to mass transfer does not dominate the overall mass transfer (Ortiz et al., 1999). Thus for the above creosote column experiments a

contributing factor to the observed mass transfer limitations may be caused by the resistance of the different creosote compounds to diffuse from the oil phase into the water phase.

A possible explanation for the resistance of mass transfer from the oil phase into the water phase is the formation of a semi-rigid, skin like film on the surface of creosote/coal tar oils when exposed to water. Experiments have demonstrated that the coal-tar water interface undergoes a visible change as coal tar is aged in water (Luthy et al., 1993). The film that forms on the interface consisted mainly of the same creosote compounds found in the bulk oil phase. The primary difference was that the film contained water bound by weak intermolecular interactions between the coal tar components and water. It was hypothesized by the researchers that the coal tar-water interface is stabilized by the formation of an organized, semi-gelatinous film or thin emulsion-like layer (Nelson et al., 1996). The effect aged coal tar has on mass transfer rates was demonstrated with experiments using flow-through stirred tank reactors containing coal tar imbedded in microporous silica beads. The differences in mass transferred rates was measured by observing the rate of naphthalene dissolution, and their results showed that the aqueous concentrations of naphthalene was noticeable less for coal tar aged for one week compared to non aged coal tar. Calculations determined that the boundary layer mass transfer rates were significantly slower than pore diffusion rates and it was inferred that the observed decrease in aqueous concentrations was caused by a reduction in the mass transfer rate as a result of changes in the coal tar-water interfacial properties (Luthy et al., 1993).

Other studies have shown a significant relationship between the oil phase mass transfer coefficients and viscosity. Experiments with hydrophobic organic compounds dissolving from coal-derived oils showed that the mass-transfer coefficient or the rate of dissolution from the oil phase is greatest for low-viscosity oils and decreases with increasing viscosity (Southworth et al., 1983). A fifty fold decrease in the mass-transfer coefficient was observed between toluene and a highly aromatic synthetic mineral oil. Similar results were observed in flow-through dissolution experiments that measured the overall mass transfer

coefficient for the dissolution of naphthalene, phenanthrene and pyrene from low viscosity oils and semi solid hydrophobic materials into water (Ortiz et al., 1999). Observations and calculations demonstrated that for the low viscosity oil (pump oil 86 cP at 40 ^{o}C) mass transfer was dominated by aqueous phase transport, but for highly viscous materials (transmission oil, 800-1400 cP at 40 ^{o}C, Vaseline, hard paraffin.) nonaqueous phase mass transfer was dominated. For all nonaqueous phase materials a film or skin was not observed at the boundary between the nonaqueous phase and water.

Mass transfer rates can be increased significantly by increasing flow rate through a DNAPL contaminated area as demonstrated with the laboratory experiments with chlorinated solvents. However, other factors such as viscosity and the formation of semi-ridged films at the surface of the nonaqueous phase may limit the mass transfer process. Thus for oils such as creosote and coal tar the mass transfer rate may become limiting and increasing the water flow rate may have a diminishing benefit.

At a field site the DNAPL source can last for decades at normal ground water velocities, thus to have a significant impact on the rate of remediation, the ground water flow would have to be increased at least 5 to 10 times. In highly permeable aquifers, hydraulic gradients 10 times higher than the ground water would only exist near the pumping or injection wells. For less permeable aquifers, higher hydraulic gradients may be achieved but the radius of influence around such wells would be small. Thus, it is very difficult to increase ground water flow through residual DNAPL. It must also be noted that mass transfer only occurs at the up-gradient edge of the contaminated zone (Figure 1.2). As clean water flows over the surface of the residual DNAPL the concentration in the aqueous phase increases until its aqueous solubility has been reached. At this point mass transfer from the oil phase to the aqueous phase no longer occurs. This area over which mass transfer occurs is called the mass transfer zone and varies on the order of a few millimetres or centimetres depending on the linear velocity of the water and mass transfer coefficient (Geller and Hunt, 1993).

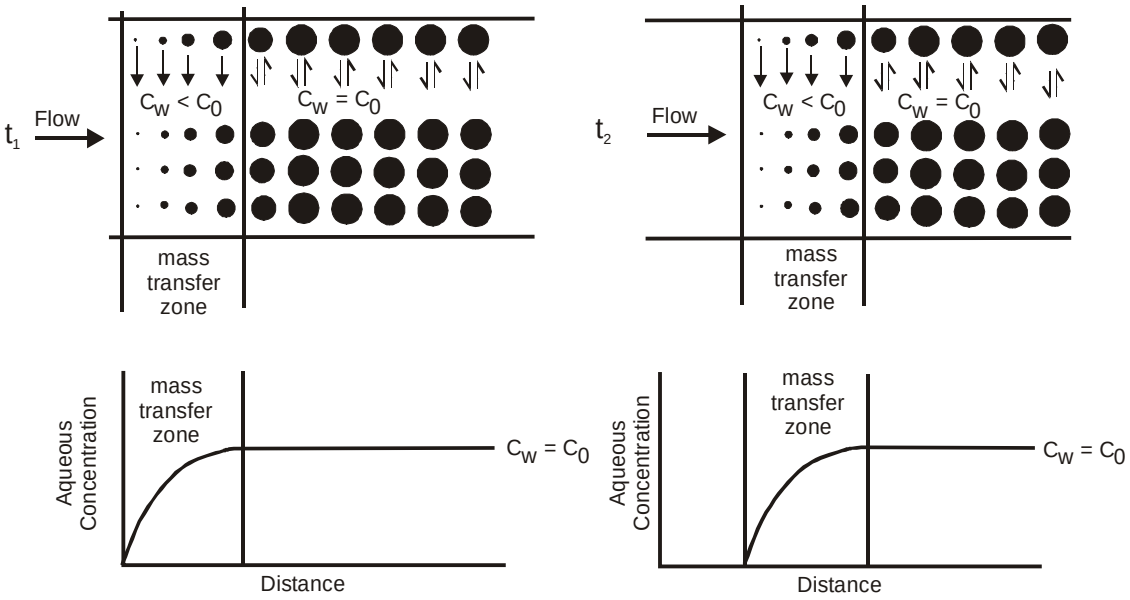

Figure 1.2 Conceptual model showing dissolution of an organic compound into flowing water and the propagation of the mass transfer zone through the residual oil at time t_1 and at a later time t_2. The black circles represent residual oil globules. (C_w = aqueous concentration, C_0 = pure phase solubility limit)

As mentioned above, laboratory studies have proven that the dissolution process can be increased by increasing the concentration differential, but to do this an increased ground water velocity must be imposed. Another method of increasing the concentration differential is to chemically remove or destroy the aqueous organics.

1.2 The Chemical Oxidation Process

The *in situ* chemical oxidation technology would be used after oil production is no longer observed and the creosote oil is trapped at residual saturations. In the *in situ* chemical oxidation process, the oxidizer would be flushed through a creosote contaminated zone to achieve mineralization of the contaminants to carbon dioxide or to oxidize organic contaminants to biodegradable acids and alcohols.

The removal of creosote oils from the subsurface is dependent on two processes: 1) the rate of dissolution of the compounds from the oil phase into the water phase, and 2) the rate of oxidation. The rate of chemical oxidation is dependant on the concentration of permanganate and the solute (assuming a second-order rate) and the driving force for the dissolution process, is the solute concentration gradient between the DNAPL and water phase. As shown in Figure 1.2 the rate of dissolution is greatest when fresh water first comes in contact with the oil, that is when $C_w = 0$ (equation 1.1). In the chemical oxidation process it is anticipated that the solutes will be oxidized to low aqueous concentrations throughout the contaminated area, not just at the up-gradient edge of the contamination. This would have the effect of increasing the mass transfer zone to possibly as large as the oxidant flushed area. The mass transfer zone can only be increased if the concentration of the chosen chemical oxidizing reagent does not decrease significantly as it travels through the residual DNAPL, otherwise the rate of oxidation will decrease and the desired effect will be diminished.

Flushing a contaminated area with an oxidizing reagent is a potentially effective technology for the remediation of creosote/coal tar contaminated aquifers. To the author's knowledge this is the first study to determine the kinetic data for the chemical oxidation of polycyclic aromatic hydrocarbons with permanganate and to incorporate this data into a model which includes dissolution of the residual, multicomponent, non-aqueous phase source as well as advective-dispersive transport and oxidation of the aqueous phase creosote compounds.

1.3 Research Goals and Objectives

The objective of this research was to investigate different oxidizing reagents, to determine which reagent is suitable for the *in situ* chemical oxidation process, and to gain insight into the complex oxidation/dissolution and mass transport of creosote compounds within a creosote contaminated soils. To meet these goals the following specific objectives were defined:

- using different powerful oxidizing reagents determine their reactivity towards creosote and individual creosote compounds;

- conduct batch column experiments to examine the oxidation potential of the chosen oxidizing reagent to enhance the removal of creosote compounds from the oil phase;

- complete an in-depth investigation into the oxidation/dissolution process that enhances the removal of creosote compounds from the oil by;

    a) carrying out extensive kinetic studies to determine the second-order rate constants for the oxidation of selected creosote compounds;
    b) performing column experiments to determine the effect that flow rate and permanganate concentration has on the rate of removal of creosote compounds from residual creosote oil;
    c) modifying and validating a numerical model for simulating residual creosote oil dissolution and chemical oxidation;
    d) performing simulations using the model to develop insight into the dynamic oxidation/dissolution process which can be used to provide a conceptual framework for implementation at a creosote contaminated field site.

1.4 Thesis Organization

Following the introduction, this thesis is divided into three main sections: two chapters examining the chemical oxidation of creosote and creosote compounds specifically designed to simulate conditions at CFB Borden, a chapter on the degradation and oxidative kinetics of polycyclic aromatic hydrocarbons found in creosote and a chapter on column experiments and numerical simulations which examine the oxidation/dissolution process.

Chapter 2 presents a review of three different chemical oxidizing reagents and examines their reactivity towards organic compounds.

Chapter 3 investigates the chemical oxidation of creosote and creosote compounds through batch reactions. Batch column experiments were also preformed to examine the ability of an oxidizing reagent to enhance the removal of creosote compounds from a sand media containing creosote at residual oil saturations.

Chapter 4 presents an oxidative kinetic study of polycyclic aromatic hydrocarbons and alkyl benzenes found in creosote with permanganate. This study determined second-order rate constants and related trends in reactivity to bond dissociation energies, ionization potentials and calculated heats of formation. The chapter also presents the Clar's aromatic sextet theory which relates topology with physical properties and shows how it can be used to predict the relative stability of arenes towards ring oxidation and the possible partially oxidized products that may form.

Chapter 5 investigates the rate of removal of different creosote compounds from the oil phase by examining the experimental data from 5 different column experiments. The experimental data was simulated by adapting a 3D finite element numerical model developed by Frind, Moslon, and Schirmer (1999). The model was then used to investigate the following questions: 1) what is the relationship between oxidant concentration and flow rate, 2) does

oxidation occur throughout the column and increase the length of the mass transfer zone, 3) what influence does the oxidation process have on the rate of removal of the non oxidizable compounds, and 4) how long will it take to remove the selected creosote compounds from the oil phase with and without oxidation? The chapter also looks at field site strategies for the use of $KMnO_4$ for the *in situ* treatment of creosote/coal tar residuals.

Chapter 6 provides a summary and conclusions.

A general abstract and summary is provided for the entire thesis but because chapters four and five were developed as separate stand-alone sections they have their own abstract, introductions and conclusions.

Chapter 2

Chemical Oxidizing Reagents

2.1 Introduction

Initial experiments were designed to investigate the feasibility of using a chemical oxidizing reagent as an *in situ* remediation technology in pH neutral, carbonate buffered aquifers. The pH constraints placed on the system were designed to simulate the conditions found at Canadian Forces Base (CFB) Borden.

The oxidizing reagents selected for laboratory studies were Fenton's Reagent (FR) (H_2O_2, Fe^{2+}), potassium persulfate (PS) with ferrous ion and potassium permanganate. All three reagents are strong oxidizing reagents that are capable of reacting with a wide range of organic compounds. This chapter presents an overview of the reaction conditions and mechanisms that are involved in the oxidation of organic compounds with these reagents.

2.2 Fenton's Reagent

Fenton's Reagent has been successful in the oxidation of alcohols, ketones (Merz and Waters, 1949; Kolthoff and Medalia, 1949), chlorobenzenes (Sedlak and Andren, 1991), nitrophenols, nitrobenzenes (Lipczynska-Kochany, 1991), benzene, phenols and other aromatic compounds (Walling and Johnson, 1975). Thus Fenton's Reagent has been investigated for the treatment of waste waters (Keating et al., 1978; Barbeni et al., 1987, Eisenhauer, 1964; Lou and Lee, 1995: Bergendahl et al. 2003) and soils (Watts et al., 1990; Flontron et al., 2003).

Fenton's Reagent is a strong oxidizing reagent which generates hydroxyl free radicals through the addition of ferrous iron with H_2O_2. The hydroxyl free radical is a powerful oxidant,

more powerful than ozone or H_2O_2 and is only surpassed by fluorine (Watts et al. 1990). The reaction mechanism for the oxidation of organic compounds involves a complex mixture of competing free radical reactions. The oxidation process is initiated with the addition of ferrous ions to H_2O_2.

$$H_2O_2 + Fe^{2+} \rightarrow HO\bullet + HO^- + Fe^{3+} \quad (2.1)$$

$k_{2.1} = 76\ M^{-1}\ s^{-1}$ (Walling, 1975)

The HO• initiated from the addition of ferrous ions can also terminate the reaction:

$$Fe^{2+} + HO\bullet \rightarrow HO^- + Fe^{3+} \quad (2.2)$$

$k_{2.2} = 3 \times 10^8\ M^{-1}\ s^{-1}$ (Walling, 1975)

Numerous other competing reactions are widely accepted and given below:

$$H_2O_2 + Fe^{3+} \rightarrow Fe\text{-}OOH^{2+} + H^+ \quad (2.3)$$

$k_{2.3} = 0.001 - 0.01\ M^{-1}s^{-1}$ (Walling and Goosen, 1973)

$$Fe\text{-}OOH^{2+} \rightarrow HO_2\bullet + Fe^{2+} \quad (2.4)$$

$$Fe^{2+} + HO_2\bullet \rightarrow Fe^{3+} + HO_2^- \quad (2.5)$$

$k_{2.5} = 1.3 \times 10^6\ M^{-1}s^{-1}$ (at pH = 3, Bielski et al., 1985)

$$Fe^{3+} + HO_2\bullet \rightarrow O_2 + H^+ + Fe^{2+} \quad (2.6)$$

$k_{2.6} = 1.2 \times 10^6\ M^{-1}s^{-1}$ (at pH = 3, Bielski et al., 1985)

$$HO\bullet + H_2O_2 \rightarrow HO_2\bullet + H_2O \quad (2.7)$$

$k_{2.7} = 2.7 \times 10^7\ M^{-1}s^{-1}$ (Buxtton et al., 1988)

Hydroxyl radicals can react with hydrocarbons (RH) by abstraction of hydrogen atoms (equation 2.8) or can add to aromatic rings (equation 2.9),

$$RH + HO\bullet \rightarrow R\bullet + H_2O \quad (2.8)$$

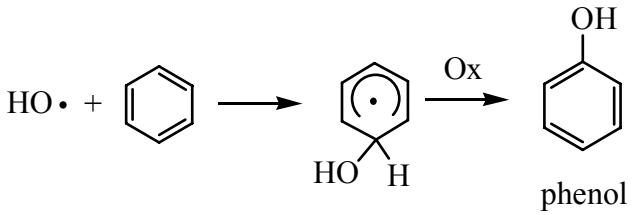

(2.9)

The organic radicals produced in equation 2.8 can initiate a radical chain oxidation as shown in equations 2.10 and 2.11 or can terminate the reaction through redox reactions (equations 2.12, 2.13) or by a coupling reaction if organic radical concentrations are significant (equation 2.14) (Walling 1975).

$$R\bullet + H_2O_2 \rightarrow ROH + HO\bullet \quad (2.10)$$

$$R\bullet + O_2 \rightarrow ROO\bullet \quad (2.11)$$

$$Fe^{2+} + R\bullet + H^+ \rightarrow \ Fe^{3+} + RH \quad (2.12)$$

$$Fe^{3+} + R\bullet \rightarrow \ Fe^{2+} + \text{products} \quad (2.13)$$

$$2R\bullet \rightarrow \ \text{dimer} \quad (2.14)$$

The ferrous ions produced from the above reactions can react with hydroxide ions to form ferric hydroxo complexes that can coagulate and form large amounts of small flocs. The ferric hydroxo complexes created during the oxidation process form according to the following reactions (Walling and Kato (1971), Lin and Lo (1997):

$$[Fe(H_2O)_6]^{3+} + H_2O \rightleftharpoons [Fe(H_2O)_5OH]^{2+} + H_3O^+ \quad (2.15)$$

$$[Fe(H_2O)_5OH]^{2+} + H_2O \rightleftharpoons [Fe(H_2O)_4(OH)_2]^{2+} + H_3O^+ \quad (2.16)$$

Within pH 3 and 7, the above complexes become

$$2[Fe(H_2O)_5OH]^{2+} \rightleftharpoons [Fe(H_2O)_8(OH)_2]^{4+} + 2H_2O \quad (2.17)$$

$$[Fe(H_2O)_8(OH)_2]^{4+} + H_2O \rightleftharpoons [Fe_2(H_2O)_7(OH)_3]^{3+} + H_3O^+ \quad (2.18)$$

$$[Fe_2(H_2O)_7(OH)_3]^{3+} + [Fe(H_2O)_5OH]^{2+} \rightleftharpoons [Fe_2(H_2O)_7(OH)_4]^{5+} + 2H_2O \quad (2.19)$$

From the above sequence of reactions it is seen that the stoichiometric ratio between H_2O_2, Fe^{2+}, organic compound and Fe^{3+} will have a significant impact on the success of the oxidation process. The effect of H_2O_2 and Fe^{2+} and pH is discussed in the subsequent sections.

2.2.1 Influence of Hydrogen Peroxide

Hydrogen peroxide, the reagent used to create the reactive hydroxyl radical, if used at too high of a concentration may inhibit the oxidation process. Studies performed at a pH of 7 with varying concentrations of H_2O_2 (10^{-5} M to 10^{-1}M) demonstrated that as the H_2O_2 concentration increased to between 10^{-4} to 10^{-3} M the oxidation rate increased, but at higher concentration levels poorer oxidation rates were observed (Beltran et al., 1998). Thus H_2O_2 acts as an initiator and inhibitor of hydroxyl radicals. When the H_2O_2 concentrations are high, its inhibiting character predominates likely through equations 2.8 and with the conjugate base of the H_2O_2, equation 2.20. The pK_a of hydrogen peroxide is 11.6 (CRC, 2003).

$$HO_2^- + \bullet OH \rightarrow O_2^- \bullet + H_2O \quad (2.20)$$

$k_{2.20} = 7.5 \times 10^9\ M^{-1}s^{-1}$ (Buxtton et al., 1988)

2.2.2 Influence of Ferrous Ion (Fe^{2+})

The influence of ferrous ion concentration is similar to that of H_2O_2 in that it promotes free radical reactions; however at higher concentrations it seems to have an inhibitory effect. Experiments with fluorene and Fenton's Reagent showed that in order to have 100% removal of fluorene a Fe^{2+} concentration of at least 7×10^{-5} M was needed (Beltran et al., 1998). At higher concentrations (2×10^{-4} M) a plateau in the rate of reaction was encountered and at concentrations above 2×10^{-4} M an inhibitory effect on fluorene oxidation resulted. The plateau value reached in the rate of oxidation was attributed to the disappearance of free Fe^{2+}, although this could not be confirmed and the inhibitory effect at higher concentrations was most likely due to the scavenging of free radicals by Fe^{2+} as given it in equation 2.4 (Beltran et al., 1998).

2.2.3 Influence of pH

The pH of the solution can dramatically influence the rate of reaction. At a pH between 2 and 4 the rate constant for oxidation of Fe^{2+} with H_2O_2 remains unchanged but increases dramatically by three orders of magnitude at a pH of 8 (Moffet and Zika, 1987). Similarly, the oxidation of fluorene with Fenton's Reagent in an unbuffered reaction mixture, showed that as the initial pH was increased from 2 to 7 the oxidation rate increased. However, a further increase in pH decreased the oxidation rate and became negligible at a pH of 12 (Beltran et al., 1998).

The optimal pH of 7 is most likely attributed to the formation of the $Fe(OH)^+$ species. $Fe(OH)^+$ reacts more readily with H_2O_2 to yield hydroxyl radicals than does Fe^{2+}. The rate

constant for the oxidation of Fe^{2+} is 76 $M^{-1}s^{-1}$ with H_2O_2, whereas with $Fe(OH)^+$ the rate constant is 1.9 x 10^6 $M^{-1}s^{-1}$ (Beltran et al., 1998),

$$Fe^{2+} + OH^- \rightarrow Fe(OH)^+ \quad (2.21)$$

$$H_2O_2 + Fe(OH)^+ \rightarrow Fe(OH)_2^+ + OH\bullet \quad (2.22)$$

Ferrous and ferric ions also compete for the hydroperoxide radicals through equations 2.11 and 2.15 so that as the pH increases the termination reaction (equation 2.6) becomes more important and the ferrous ion can be regenerated,

$$Fe^{3+} + HO_2\bullet \rightarrow O_2 + H^+ + Fe^{2+} \quad (2.6)$$

$$Fe^{2+} + HO_2\bullet \rightarrow HO_2^- + Fe^{3+} \quad (2.23)$$

At pH values greater than 8, Fe^{3+} exists mostly as hydroxide complexes like $FeOH^{2+}$ or $Fe(OH)_2^+$ or insoluble oxide-hydroxides such as Fe_2O_3 and $Fe(OH)_3$. These species, once formed, are not reactive and will not allow for the regeneration of ferrous ions.

2.2.4 The Reaction of Hydroxyl Radicals with PAHs

The reaction of hydroxyl radicals with aromatic compounds has been well documented (Walling, 1975; Lipczynska-Kochany, 1992). The mechanism is analogous to an electrophilic substitution reaction (Anbar et al., 1966) in which the attack on the aromatic ring results in the formation of the cyclohexadienyl radical (equation 2.24). The radical may either dimerize, be oxidized to phenol with Fe^{3+} or be converted back to the initial aromatic compound.

Most reaction rates of hydroxyl radicals with aromatic compounds approach the diffusion controlled limit (Buxton, 1988) but because the mechanism is analogous to an electrophilic substitution some effect of the substituents can be observed. For example, electron withdrawing substituents like nitro groups will impede the reaction and electron-donating substituents (OH, NH_2) will accelerate the reaction (Anbar et al., 1966).

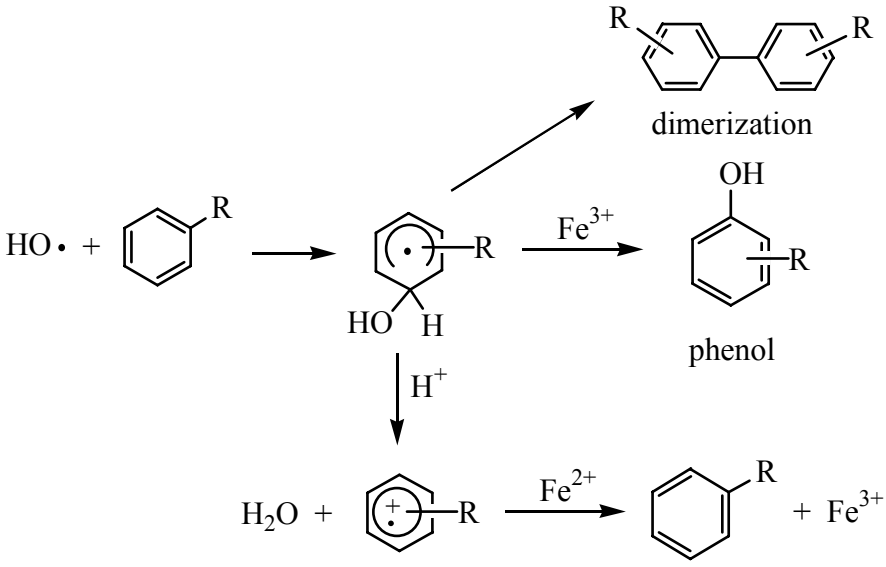

(2.24)

2.3 Persulfate with Ferrous Ion

The reaction of persulfate with Fe^{2+} is analogous to Fenton's Reagent in that it involves the homolytic cleavage of a peroxide bond to form a radical and an anion as shown in equation 2.25,

$$S_2O_8^{2-} + Fe^{2+} \rightarrow SO_4^{\bullet -} + SO_4^{2-} + Fe^{3+} \qquad (2.25)$$

Sulfate radicals, like the HO• radical are highly reactive to organic compounds, but the mechanism of the reaction can be quite different. For instance, the $SO_4^{\bullet -}$ radical frequently removes an electron from an organic molecule whereas the HO• radical adds to C=C or abstracts a hydrogen from the C-H bond (Norman, 1979).

An example is illustrated with carboxylate ions from saturated acids which react with $SO_4^{\bullet -}$ to give carboxy radicals, followed by decarboxylation to generate alkyl radicals (equation 2.26). In contrast, HO• reacts mainly by hydrogen abstraction at the C-H bond (equation 2.27),

$$CH_3CO_2^- + SO_4^{\bullet -} \rightarrow CH_3CO_2\bullet + SO_4^{2-} \rightarrow \bullet CH_3 + CO_2 \qquad (2.26)$$

$$CH_3CO_2^- + HO\bullet \rightarrow \bullet CH_2CO_2^- + H_2O \qquad (2.27)$$

There is also a marked difference between how the two radicals react with aromatic compounds. The reaction of $SO_4^{\bullet -}$ radicals with aromatic compounds occurs by an electron-transfer mechanism to produce the radical cation as shown in equation 2.28,

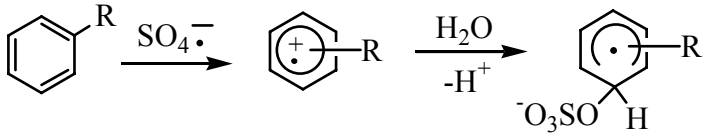

(2.28)

The rate of reaction toward aromatic compounds is governed by the electrophilicity of the $SO_4^{\bullet -}$ radical. Electron donating groups such as amino, hydroxyl or alkoxy increase the rate of reaction whereas electron-withdrawing groups such as nitro or carbonyl substituents significantly decrease the rate of reaction. Measured second-ordered rate

constants for the reaction of $SO_4^{\bullet -}$ with some aromatic compounds are given in Table 2.1 (Neta et al., 1977).

Aromatic compound	Rate constant, M^{-1} s^{-1}
Anisole	4.9×10^9
Benzene	3.0×10^9
Benzoic acid	1.2×10^9
Benzonitrile	1.2×10^8
Nitrobenzene	$\leq 10^6$

Table 2.1 Second-order rate constants for the reaction of $SO_4^{\bullet -}$ with various aromatic compounds.

2.4 Potassium Permanganate ($KMnO_4$)

Potassium permanganate can oxidize a wide variety of organic and inorganic compounds. It is used as an oxidizing reagent in chemical synthesis, hydrometallurgical separations, radioactive decontamination and as a microbiocide in waste water treatment. In drinking water it destroys organic compounds that cause color, taste and odour problems and oxidizes iron, manganese and hydrogen sulfide (Ficek, 1978).

The reaction mechanism and the reactivity of permanganate are dependent on the organic reactant as well as the reaction conditions, in particular the pH of the medium. The reduced form of permanganate produced is also dependent on the acidity of the solution. For example, the oxidation of an alkene under alkaline conditions produces *cis* diols and MnO_2, while the same reaction under acidic conditions causes cleavage of the double bond to produce carbonyl compounds and Mn^{3+} or Mn^{2+} (Lee and Chen, 1989).

In a neutral pH medium the dominant manganese product is manganese dioxide. The formation of MnO_2 may be beneficial for *in situ* applications, because MnO_2 can itself oxidize

phenols in groundwater (Stone, 1987, Ulrich and Stone, 1989). This may enhance the oxidation process by aiding in the destruction of partially oxidized products.

Rudakov, Loachev and Zaichuk have extensively studied the oxidation of benzene and alkylbenzenes with different permanganate species. Manganese(VII) in an aqueous solution can be present in the form of the permanganate anion MnO_4^-, permanganic acid $HMnO_4$, or permanganyl cation MnO_3^+ depending on the pH of the medium. It was determined through kinetic studies that the reaction with MnO_4^- dominates at a pH greater than 2.5, whereas at a pH less than 0.3 the reaction of $HMnO_4$ dominates. To study the reactivity of MnO_3^+ the reactions were carried out in very acidic perchloric acid solution ($HClO_4$ = 3.5 M) (Lobachev et. al., 1997). The following scheme represents the different reactive species that can form depending on the pH,

$$MnO_4^- \underset{-H^+}{\overset{H^+}{\rightleftharpoons}} HMnO_4 \underset{-H^+}{\overset{H^+}{\rightleftharpoons}} H_2MnO_4^+ \underset{+H_2O}{\overset{-H_2O}{\rightleftharpoons}} MnO_3^+ \qquad (2.29)$$

The pK_a of $HMnO_4$ is -2.2. $H_2MnO_4^+$ is a hydrated species, which upon loss of water can form a perchloric complex (ClO_3OMnO_3) (Lobachev et al., 1997).

2.4.1 MnO_4^-

The oxidation of alkylbenzenes can occur through two parallel routes: 1) the attack of the C-H bond of an alkyl substituent and 2) the attack of the aromatic ring.

The reaction mechanism of MnO_4^- with alkylbenzenes was studied by Rudakov and Lobachev (1994) with batch experiments performed at a pH of 5-7 at 70°C. At this pH the predominant permanganate species is the MnO_4^- ion. It was determined that the most important reaction of MnO_4^- ion with alkylbenzenes such as methylbenzene, ethylbenzene and

isopropylbenzene occurs through the abstraction of a benzylic hydrogen atom as shown in the reaction of toluene with MnO_4^-,

$$C_6H_5\text{-}CH_3 + OMnO_3^- \longrightarrow \{C_6H_5\text{-}H_2C\text{- -}H\text{- - -}OMnO_3^-\}$$
$$\longrightarrow C_6H_5\text{-}H_2COMn(VII)O_2(OH^-) \longrightarrow C_6H_5\text{-}H_2COH + Mn(V)O_3^- \qquad (2.30)$$

The benzyl alcohol that is formed is further oxidized to benzoic acid and manganese(V) is reduced to manganese dioxide ($Mn(IV)O_2$).

The order of reactivity for the alkylbenzenes follows the bond strength of the benzylic C-H bond or the C-H bond dissociation energy. Thus the stronger the C-H bond the more resistant to oxidation the compound will be. The bond strength decreases from primary, secondary to tertiary hydrogens and the order of reactivity increased in the same order: $C_6H_5CH_3 < C_6H_5CH_2CH_3 \leq C_6H_5CH(CH_3)_2$. The substrate selectivity by the MnO_4^- anion is similar to what is observed in H abstraction by radicals (Rudakov and Lobachev, 1994).

The oxidation of benzene is 2000 times slower than toluene and does not occur by hydrogen abstraction but involves an attack of MnO_4^- on the aromatic ring through an electrophilic addition reaction (Rudakov and Lobachev, 1994).

The general mechanism for the reaction of an electrophile with an arene initially involves a loose association of the reactants in which the complexing agent is not localized at a particular carbon atom, but is held near the π-electron cloud. This is called a π-complex or a charge transfer complex and the structure is usually drawn with an arrow indicating that the aromatic ring is electron donating. After the initial association there is a donation of two electrons from the π system to form an electron deficient σ-complex. It is the formation of the σ-complex, not the π-complex, that is the rate-determining step in electrophilic aromatic substitution (Taylor, 1990). This fact has allowed researchers to use ionization potentials, or

how tightly the electrons are held to the molecule, to improve the description of aromatic reactivity in electrophilic substitution reactions (Kachurin and Vysotskii, 1999),

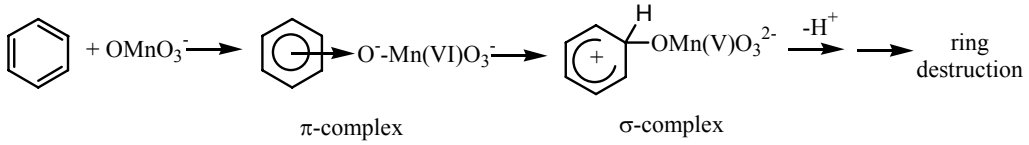

(2.31)

2.4.2 $HMnO_4$

The selectivity and reactivity of permanganic acid ($HMnO_4$) towards the oxidation of alkyl benzenes is slightly different from the MnO_4^- ion. Kinetic studies with toluene and $HMnO_4$ in aqueous perchloric acid solutions indicated that ring attack was the dominate route to oxidation unlike the MnO_4^- ion in which side chain oxidation takes place. However, like the MnO_4^- ion the oxidation of ethylbenzene and isopropylbenzene with $HMnO_4$ mainly occurs on the side chain (Lobachev et al., 1997).

Experiments performed by Lobachev et al., 1997 showed that ring oxidation of alkyl benzenes with $HMnO_4$ was simultaneously controlled by the basicity and by the ionization potentials of the substrate. Their research indicated a consecutive formation of a charge transfer complex (A) followed by σ-complex (B) (equation 2.32). The slow stage (2) and the preequilibrated stage (1) are governed by the basicity and by the ionization potentials respectively.

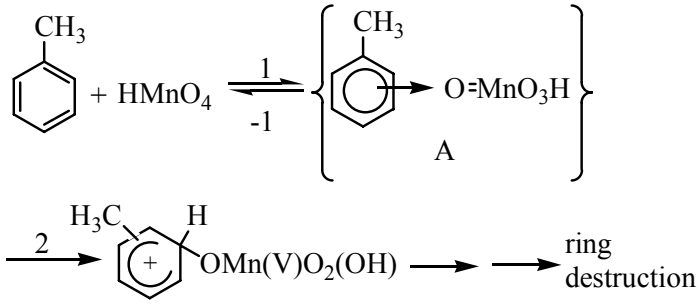

(2.32)

The main route of oxidation for other methylbenzenes such as 2,3,5-trimethylbenzene, 1,2,4,5-tetramethylbenzene and *ortho*, *meta* and *para*-dimethylbenzene (xylene), also occurs at the ring. However, the oxidation of ethyl- and isopropylbenzene occurs mainly on the side chain. It was assumed that the oxidation of the alkyl C-H bond by $HMnO_4$ occurs by a mechanism similar to the MnO_4^- ion,

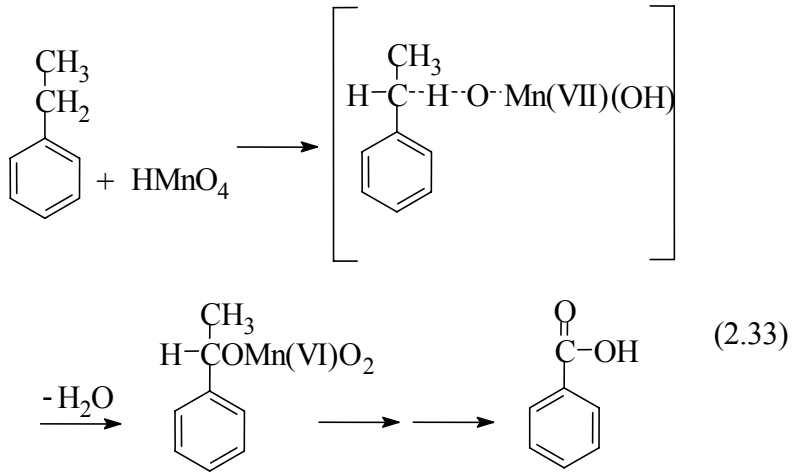

(2.33)

2.4.3 MnO_3^+

In very acidic conditions ($HClO_4$ = 3.5 M) the dominant species in solution is MnO_3^+ and the attack on benzene and alkylbenzenes is predominantly on the aromatic ring via an electrophilic substitution reaction (Lobachev et al., 1997). A comparison of the reactivity and substrate selectivity indicated that like $HMnO_4$ the reactions are controlled simultaneously by the basicity and the ionization potentials of the alkyl benzenes. MnO_3^+ was determined to be a stronger electrophilic reagent than $HMnO_4$ in the reactions with the aromatic ring.

2.5.4 Permanganate Conclusions

The rates of benzene and alkylbenzene oxidation by Mn(VII) species increases in the series MnO_4^- < $HMnO_4$ < MnO_3^+. Because MnO_3^+ attacks alkylbenzenes at the ring it can be concluded that the rate of electrophilic ring attack increases with an increase in the positive charge of the reagent faster than the oxidation rate of the alkyl C-H bonds. Thus for a system that is slightly acidic (pH < 2.5), neutral or basic in which the major Mn(VII) species is MnO_4^-, side chain oxidation will occur faster than ring oxidation for alkylbenzenes. As the system increases in acidity, ring oxidation becomes more dominant.

Chapter 3

Batch Experiments and Batch Column Experiments

Creosote was placed below the water table at residual concentrations at Canadian Forces Base (CFB) Borden to provide a site to study the dissolution of creosote compounds (King and Barker, 1999). The aquifer at CFB Borden is a pH-neutral carbonate-buffered system and initial batch and column experiments were designed to investigate the feasibility of using chemical oxidizing reagents as an *in situ* remediation technology for the removal of creosote/coal tar oils at this site. The pH constraints and reaction conditions placed on the experiments were designed to simulate the conditions found at CFB Borden.

3.1 Batch Experiments with Individual Creosote Compounds and Creosote Oil

3.1.1 Introduction

The chemical oxidizing reagents, Fenton's reagent, potassium persulfate with ferrous ions and potassium permanganate were investigated in batch experiments to determine the ability of these reagents to oxidize creosote and creosote compounds. The creosote compounds chosen were *para*-cresol (a hydroxybenzene), indole (an N-heterocyclic aromatic compound), pyrene (a PAH) and 1-methylnaphthalene (an alkyl substituted PAH).

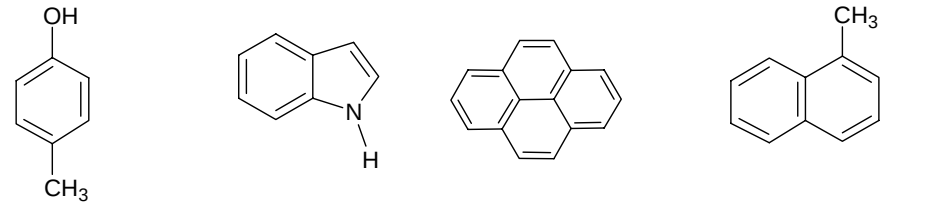

para-Cresol Indole Pyrene 1-Methylnaphthalene

Figure 3.1 Chemical structures of creosote compounds investigated.

3.1.2 Procedure

Experiments were conducted in a 1 litre, two-neck flask at room temperature (21 ± 1 ^{o}C). Oxidizing reagents were added to a 1 litre solution of 0.01 M phosphate buffered, organic free water (Organic Pure water purification system, Sybran/Barnstead). For the batch reactions in which creosote oil was added, the reaction vessel was stirred for 2 days before the addition of the oxidizing reagents. Reactions were performed under a positive pressure of nitrogen. The reaction vessels were not sealed because of the potential increase in pressure caused by the evolution of oxygen or carbon dioxide.

A phosphate buffer was used instead of a carbonate buffer because carbonates are known to act as free radical scavengers and can inhibit the oxidation of organic compounds. Thus, a phosphate buffer was used instead of a carbonate buffer to reduce side reactions that may occur. The dominant species at pH 7 for phosphate and carbonate buffers are $H_2PO_4^-$, HPO_4^{2-} and HCO_3^- respectively. The rate constant for the reaction of hydroxyl radicals with HCO_3^- (8.5×10^6 $M^{-1}s^{-1}$) is much larger than for the phosphate species $H_2PO_4^-$ (~2×10^4 M^{-1} s^{-1}) and HPO_4^{2-} (1.5×10^5 M^{-1} s^{-1}) (Buxton et al., 1988). Free radical reactions with a phosphate buffer would be less likely than with a carbonate buffer.

Analytical reagent grade $KMnO_4$, $K_2S_2O_8$, $FeSO_4 \cdot 7H_2O$, H_2O_2 (30% solution) and dichloromethane (glass distilled, 99.9% purity) were obtained from BDH and used without further purification. The solids were ground with a mortar and pestle and added to the reaction mixture as solids. Hydrogen peroxide solution was added *via* a syringe. Pyrene, indole, and 1-methylnaphthalene were obtained from Aldrich at 99, 99, and 98% purity, respectively. p-Cresol was obtained from Sigma at 99% purity. Creosote was obtained from Carbochem Mississauga, Ontario.

3.1.3 Chemical Analysis

Water samples obtained from the reaction vessels were collected as either 13 or 45 mL samples. A 13 mL sample was added to 3 g of NaCl and 0.3 mL of 1N HCl in a 18 mL crimp top vial. After shaking the vial to dissolve the NaCl, 1 mL of CH_2Cl_2 (spiked with an internal standard) was added and the vial was shaken for 15 minutes on an orbital shaker set at 400 rpm. The CH_2Cl_2 was then withdrawn and analysed. The same procedure for a 45 mL sample was followed except 9 g of NaCl, 1 mL of 1 N HCl and 3 mL of CH_2Cl_2 was used in a 60 mL crimp top vial.

The majority of the samples were analysed on a temperature programmed Hewlett Packard HP5890A gas chromatograph using a 30 m DB5 (Chrom. Spec.) capillary column with a 0.25 mm i.d. and 0.25 μm film thickness. A split/splitless auto injector was used in the splitless mode and maintained at 275^o C. Chromatographic conditions were: initial oven temperature 40^o C for 0.5 min; ramp to 300^o C at 15^o C/min, and hold for 10 min. A flame ionizing detector (FID) was maintained at 325^o C with a helium carrier gas flow rate of 25 mL/min. Other samples were analysed on a gas chromatograph mass selective detector system (GC/MSD). The same column and operating conditions were used. Samples were injected manually and the injector was held at 250^o C. The transfer lines and the MSD were both held at 280^o C.

Quantification was by external and internal standard methods. The internal standard used was 2-fluorobiphenyl (Sigma). The external standard used is a mixture of 16 PAHs (benzene, toluene, ethylbenzene, p-xylene, o-xylene, naphthalene, acenaphthylene, acenaphthene, fluorene, phenanthrene, anthracene, fluoranthene, pyrene, B(A)anthracene, chrysene and B(b+k)fluoranthene, Ultra Scientific #Us-106) augmented with m-xylene, dibenzofuran, 2-methylnaphthalene (Rose Scientific #s 000202, 000261, 000562) biphenyl, indole, carbazole and 1-methylnaphthalene (Sigma).

3.1.4 Oxidation of *p*-Cresol with Fenton's Reagent

When performing the Fenton's reaction at a pH of 7, the loss of the iron catalyst is a major concern. Ferrous ions once converted to ferric ions (Fe^{3+}) can form hydroxy complexes that form small flocs during the oxidation process (Walling and Kato (1971), Lin and Lo (1997). The importance of the decrease of catalyst concentration over time has been reported by Watts (1990), Sedlak (1991) and Walling (1975). Watts observed in a silica sand system that the decomposition of pentachlorophenol (PCP) and hydrogen peroxide was initially rapid but slowed after 3 hours. The concentration of Fe^{2+} decreased with time and reached a quasiequilibrium soluble iron concentration of 9 mg/L. Sedlak (1991) also observed a decrease in Fe^{2+} during the oxidation of chlorobenzene. The decomposition of chlorobenzene ceased after approximately 4 hours and the concentration of Fe^{2+} dropped from approximately 5 mM to 0.5 mM during this time interval. In the batch oxidation of fluorene, acenaphthene and phenanthrene the oxidation process stopped within 10 minutes and analysis of Fe^{2+} showed that none remained (Beltan et al., 1998).

The oxidation of p-cresol with Fenton's Reagent at a molar ratio of 1:30:4 (p-cresol : H_2O_2 : Fe^{2+}) is shown in Figure 3.2. After the initial decomposition, the reaction stopped. The oxidation process could be continued if additional ferrous ions or Fenton's Reagent (Fe^{2+} and H_2O_2) was added, but could not be continued if H_2O_2 alone was added. This is presumably caused by a decrease in the Fe^{2+} concentration during the reaction since the addition Fe^{2+} resumed the oxidation of p-cresol.

As stated in Chapter 2 the concentration of ferrous ions and H_2O_2 influences the overall rate of oxidation of organic compounds with Fenton's Reagent. Sufficient concentrations of the reagents are needed to create the hydroxyl radicals to complete the oxidation but if either Fe^{2+} or H_2O_2 concentrations are too large the concentration of hydroxyl radicals may diminish as shown in equations 2.2, 2.7 and 2.20,

$$Fe^{2+} + HO\bullet \rightarrow HO^{-} + Fe^{3+} \quad (2.2)$$

$$HO\bullet + H_2O_2 \rightarrow HO_2\bullet + H_2O \quad (2.7)$$

$$HO_2^{-} + \bullet OH \rightarrow O_2^{-}\bullet + H_2O \quad (2.20)$$

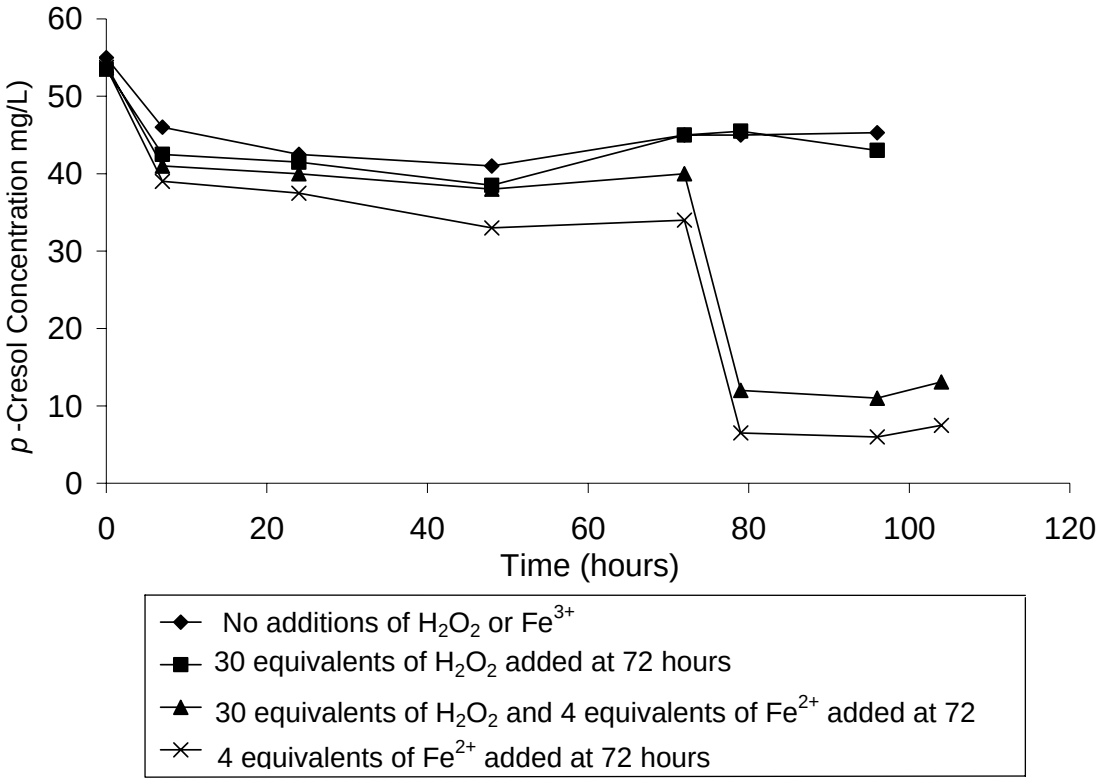

Figure 3.2 Oxidation of p-cresol with Fenton's Reagent. Initial concentration of p-cresol = 5 x 10^{-4} M; molar ratio of reagents, p-cresol : H_2O_2 : Fe^{2+}; 1: 30 : 4.

The oxidation of p-cresol with different molar ratios of H_2O_2 and iron is shown in Figure 3.3. The results showed that the most favourable conditions for the oxidation reaction was at a molar ratio of 1:30:8 (p-cresol:H_2O_2:Fe^{2+}). The concentrations of p-cresol, H_2O_2, and Fe^{2+} were 4.6 x 10^{-4}, 1.4 x 10^{-2} and 3.7 x 10^{-3} M, respectively. At lower concentrations of H_2O_2 less than

70% of the p-cresol was oxidized and no significant increase in oxidation was observed for ferrous iron concentrations above 3.7 x 10^{-3} M.

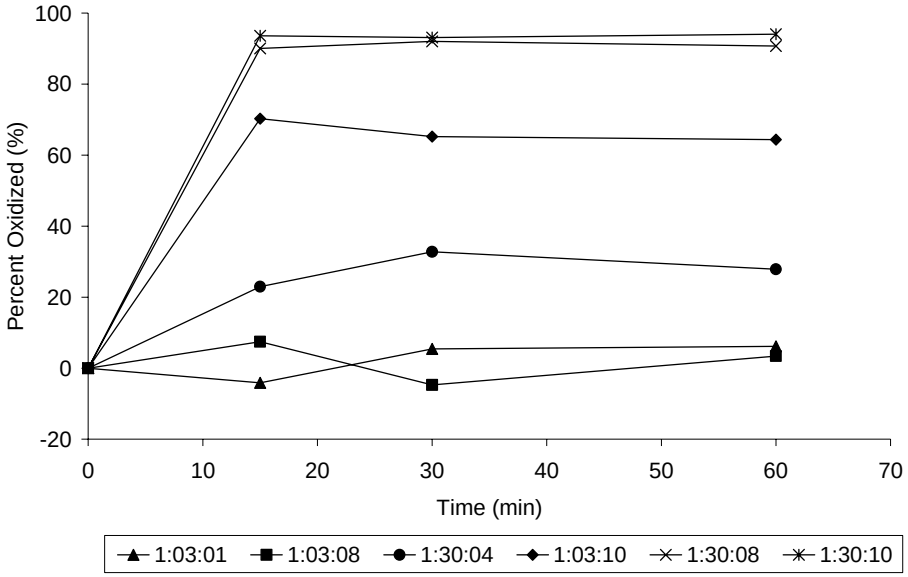

Figure 3.3 Oxidation of *p*-cresol using different ratios of *p*-cresol:H_2O_2:Fe^{2+}.

3.1.5 Oxidation of p-Cresol with Potassium Persulfate and Fe^{2+}

The reaction of persulfate is analogous to the Fenton's Reagent reaction. Ferrous ions will decrease in concentration and will become limiting. The main difference with this reagent is that oxygen will not be produced during the reaction.

The reaction dynamics were investigated by varying the molar ratio of the reactants. If the iron concentration was increased while maintaining a constant molar ratio between p-cresol and $S_2O_8^{2-}$ (1:8) the amount of p-cresol oxidized decreased. This may be caused by the reduction of the sulfate radicals by Fe^{2+}(equation 3.1).

$$Fe^{2+} + SO_4 \bullet^{-} \rightarrow SO_4^{2-} + Fe^{3+} \qquad (3.1)$$

When the molar ratio of persulfate was increased to 1:10 the amount of p-cresol removed increased, although increasing the ratio to as much as 1:33 did not significantly change the amount of p-cresol oxidized. When the molar ratio of p-cresol: $S_2O_8^{2-}$: Fe^{2+} was adjusted to 1:10:8, 95% of the p-cresol could be oxidized. The concentration of S_2O_8 and Fe^{2+} were 4.2 x 10^{-3} and 3.4 x 10^{-3} M respectively. The concentration of the iron corresponds closely to the optimal concentration encountered in the Fenton's reaction, 3.7 x 10^{-3} M.

Thus it can be concluded that an iron concentration of approximately 3.5 x 10^{-3} M or in a molar ratio of p-cresol:iron of 1:8 will generate sufficient quantities of free radicals to oxidize p-cresol. Larger concentrations of iron may inhibit the reaction by reacting with the sulfate radical as shown in equation 3.1.

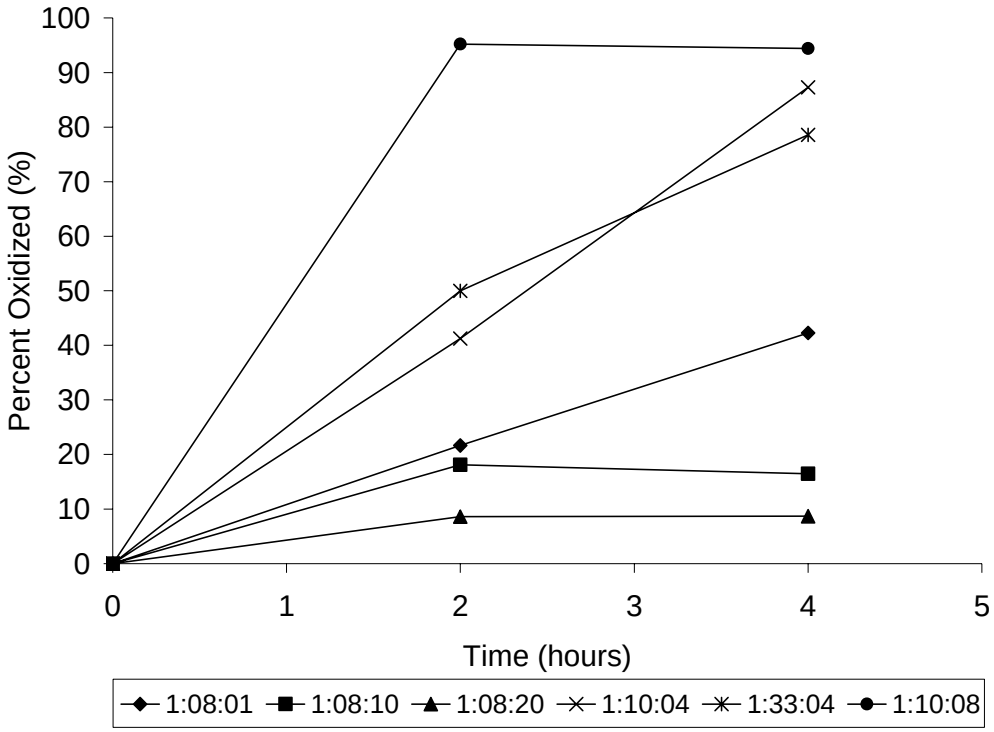

Figure 3.4. Oxidation of *p*-cresol using different ratios of *p*-cresol:$S_2O_8^{2-}$:Fe^{2+}.

3.1.6 Oxidation of p-Cresol by Potassium Permanganate

The oxidation of p-cresol by permanganate at a pH of 7 was very rapid (data not shown). Decomposition was complete within five minutes at a 1 to 1 molar ratio ($KMnO_4$: p-cresol).

3.1.7 Oxidation of Representative Creosote Compounds, 1-Methylnaphthalene, Indole and Pyrene by Various Oxidants

The oxidation of indole by $KMnO_4$ in a 1:1 molar ration removed 82% of the organic compound. With the addition of a second equivalence of $KMnO_4$, indole was decomposed to below detection limits (Figure 3.5). Fenton's reagent also reacted rapidly with indole and decreased the indole concentration by 92%, using a molar ratio of 1:10:8 (indole:H_2O_2:Fe^{2+}). Further additions of Fenton's reagent using the same initial molar ratios did not completely oxidize indole to below detection limits. Incomplete oxidation of indole was also observed using persulfate in the molar ratio 1:10:8 (indole:$S_2O_8^{2-}$:Fe^{2+}).

1-Methylnaphthalene was oxidized by all three reagents. Persulfate, $KMnO_4$ and Fenton's Reagent reduced the concentration of 1-methylnaphthalene by 33, 28 and 17 % respectively in batch reaction after 25 minutes. Using the same initial molar ratios additional reagents were then added to the reactors to determine if the concentration of 1-methylnapthalene could be reduced to below detection limits. After 8 additions of the reagents to the batch reactors the concentration of 1-methylnaphthalene was decreased to 96, 75, and 48 percent by persulfate, $KMnO_4$ and Fenton's Reagent, respectively (Figure 3.6). The control experiment in which no reagent was added shows a slight decrease in concentration, presumably from volatilization.

The pH was also monitored during the reaction. The pH decreased upon addition of the persulfate or Fenton's reagent. The pH increased slightly on addition of the $KMnO_4$ from 7.0 to 7.2 (Figure 3.7).

Fenton's Reagent and persulfate failed to oxidize pyrene using the reaction conditions in this study. The oxidation of pyrene with $KMnO_4$ was rapid, and is discussed in depth in Chapter 4.

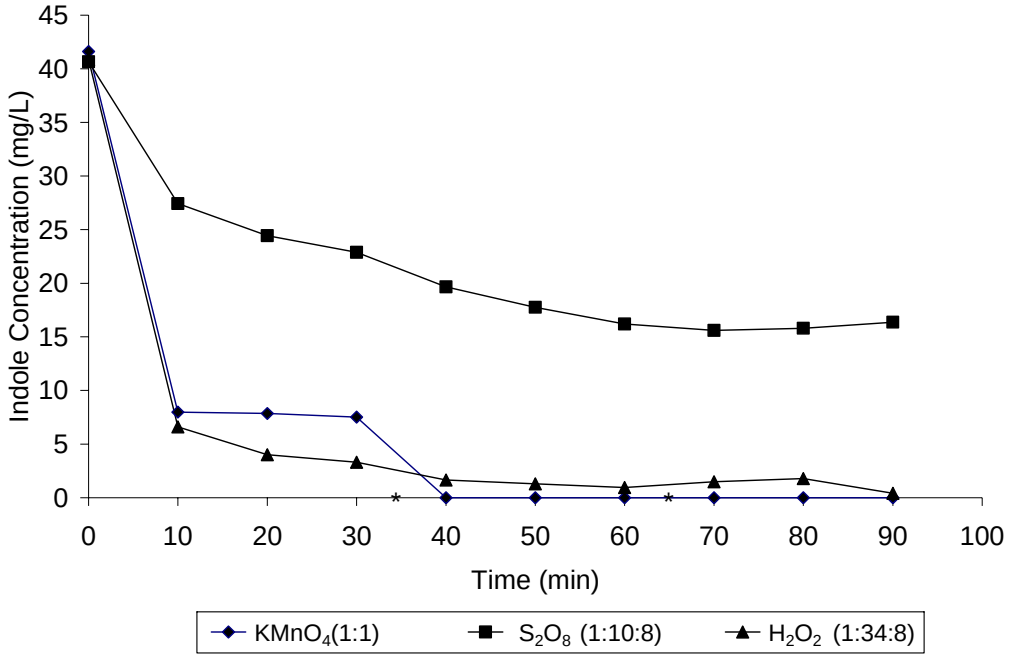

Figure 3.5 Oxidation of indole with $KMnO_4$ in a 1:1 molar ratio, S_2O_8 in a 1:10:8 (indole:$S_2O_8^{2-}$:Fe^{2+}) molar ratio and H_2O_2 in a 1:10:8 (indole:H_2O_2:Fe^{2+}) molar ratio. At 35 and 65 minutes additional reagents were added at the given initial molar ratios.

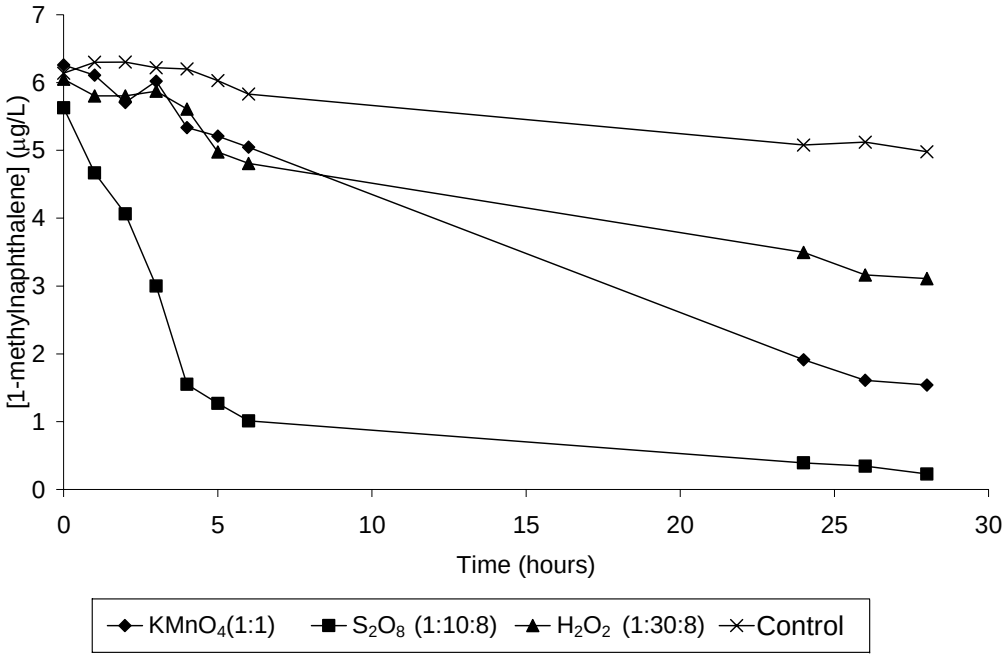

Figure 3.6 Oxidation of 1-methylnaphthalene. Additional reagents were added at 1, 2, 3, 4, 5, 6 and 24 hours.

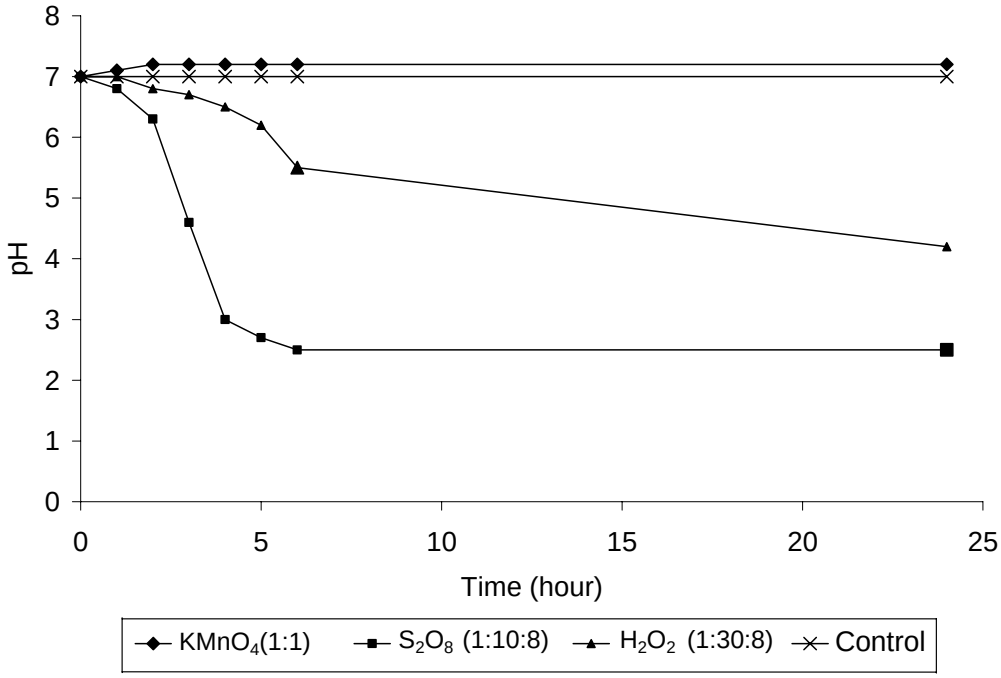

Figure 3.7 pH in batch reactions after each addition of reagents at 1, 2, 3, 4, 5, 6 and 24 hours.

3.1.8 Batch Oxidation of Creosote Oil

Creosote (0.1 mL) was added to one litre of 0.01 M phosphate buffered (pH=7) organic free water and was stirred for 2 days. This allowed the complex mixture of compounds to equilibrate between the oil phase and water. Oxidizing reagents were added according to the molar ratios used in studying the reaction of p-cresol with various oxidants. To estimate the number of moles of creosote added an average molecular weight of 200 g/mol was assumed. This molecular weight was estimated by examining the mass spectrum of a creosote sample. The mass spectra showed that the unknown fraction was predominately made up of heavy molecular weight PAHs with a smaller percentage of unknown phenols and heterocyclic compounds. The density of the creosote was measured to be 1.10 g/mL. The oxidizing reagents were added daily for the first 5 days and then every other day for the next 22 days for a total of 27 days with 15 additions of reagents.

The mass of the monitored creosote compounds added to each reaction flask was determined by finding the average concentration of 5 (0.01 mL) creosote oil samples then multiplying by the volume of oil added to the flask. The initial masses, aqueous concentrations during the reactions, and final mass of creosote compounds extracted at the end of the experiment are given in Tables 3.1 to 3.3.

The more soluble compounds such as phenol, p-cresol, m-xylene and indole were quickly removed from the aqueous phase. The less soluble compounds such as fluorene, dibenzofuran, pyrene, naphthalene and phenanthrene were gradually oxidized to very small aqueous concentrations over the 27 day experiment (15 additions of oxidizing agents).

The oxidation and mineralization of creosote compounds from the aqueous phase is shown in Figures 3.8, to 3.11. Figure 3.8 is a gas chromatogram of pure phase creosote oil. Figures 3.9 to 3.11 show the initial spectra of creosote compounds in the water phase and the

concentration of creosote compounds after three days. Table 3.5 identifies the peaks in the chromatograms.

At the end of the experiment unreacted creosote globules could still be seen in all of the reaction mixtures. Analysis of the oil phase revealed that even though the concentrations of many compounds were below detection limits in the aqueous phase they were still present in the oil phase.

Permanganate is ionic and is not soluble in hydrophobic liquids like creosote, thus it is expected that oxidation mainly occurs in the water phase or on the surface of the creosote oil. However, oxidation may occur in the creosote oil. The upper limit of the solubility of water in coal tar expressed as a mole fraction is estimated to be 0.01, $x_{water}^{coal\ tar}$. This is comparable to water solubilities in other organic liquids, such as 0.003 for water in benzene and 0.0034 in 1-methylnaphalene (Peters and Luthy, 1993). This implies that limited oxidation may occur in the oil phase but mainly occurs in the aqueous phase or on the surface of the oil. Thus the rate of removal of creosote compounds from a contaminated site will not only depend on the rate of oxidation but also on the rate of dissolution from the oil phase. In any event, more than 90 percent of the less soluble polyaromatic compounds that were analyzed were removed from the creosote phase.

The pH values of the reaction mixtures for the persulfate and hydrogen peroxide solutions were 1.6 and 1.1, respectively, at the end of the experiment. After two reagent additions, the pH of the solution dropped to 4 for both persulfate and hydrogen peroxide systems.

Using a mass selective spectrometer detector, the major oxidized products were tentatively identified using the National Institute of Standards and Technology Mass Spectrometer Library and are given in Table 3.4

	Masses in oil phase (mg)	Masses in the aqueous phase (μg)			Masses in oil phase (mg)
Compound	Before Oxidation	Before the addition of H_2O_2	After 2 days and 2 additions of H_2O_2	After 15 days and 9 additions of H_2O_2	At the end of the experiment
m-xylene	1.91	1.75	0.19	<.006	<.006
phenol	1.26	0.99	0.04	<0.03	<0.03
p-cresol	0.34	0.97	0.12	<.009	ND
naphthalene	4.59	6.17	0.50	0.03	0.03
phenanthrene	5.63	1.10	0.91	0.08	0.39
anthracene	0.75	0.25	0.03	ND	0.01
dibenzofuran	2.66	1.24	0.66	ND	0.10
carbazole	0.67	0.56	0.26	ND	0.02
pyrene	2.38	0.55	0.20	ND	0.43
indole	0.31	0.65	ND	ND	ND
2-methylnaphthalene	1.57	0.11	0.41	ND	ND
1-methylnaphthalene	0.57	0.61	0.25	ND	0.11
biphenyl	0.91	0.33	0.25	ND	0.03
acenaphthene	4.50	1.62	0.77	0.04	0.03
fluorene	3.45	0.83	0.69	ND	0.07
1-methylphenanthrene	1.32	0.05	0.04	ND	0.10
fluoranthene	4.61	0.28	0.24	ND	1.32

ND - concentrations below the detection limit of FID.
Detection Limits are given in Appendix 3.

Table 3.1 Masses of creosote compounds before during and after oxidation with Fenton's Reagent.

	Masses in oil phase (mg)	Masses in the aqueous phase (μg)			Masses in oil phase (mg)
Compound	Before Oxidation	Before the addition of S_2O_8 and Fe^{2+}	After 2 days and 2 additions of S_2O_8 and Fe^{2+}	After 15 days and 9 additions of S_2O_8 and Fe^{2+}	At the end of the experiment
m-xylene	1.91	0.58	0.20	<.006	<.006
phenol	1.26	0.98	<0.03	<0.03	<0.03
p-cresol	0.34	0.96	0.52	0.04	0.04
naphthalene	4.59	4.43	2.55	ND	0.11
phenanthrene	5.63	2.31	1.07	ND	0.58
anthracene	0.75	0.28	0.12	ND	0.02
dibenzofuran	2.66	1.72	1.17	ND	0.15
carbazole	0.67	0.88	0.09	ND	0.03
pyrene	2.38	0.73	0.03	0.08	0.71
indole	0.31	0.68	ND	ND	ND
2-methylnaphthalene	1.57	1.12	0.68	ND	ND
1-methylnaphthalene	0.57	0.62	0.41	ND	0.16
biphenyl	0.91	0.41	0.30	0.06	0.04
acenaphthene	4.50	2.20	0.34	0.02	0.05
fluorene	3.45	1.28	0.79	0.05	0.11
1-methylphenanthrene	1.32	0.26	0.07	0.01	0.15
fluoranthene	4.61	0.36	0.23	ND	1.99

ND - concentrations below the detection limit of FID.
Detection Limits are given in Appendix 3.

Table 3.2 Masses of creosote compounds before during and after oxidation with S_2O_8 and Fe^{2+}.

	Masses in oil phase (mg)	Masses in the aqueous phase (μg)			Masses in oil phase (mg)
Compound	Before Oxidation	Before the addition of $KMnO_4$	After 2 days and 2 additions of $KMnO_4$	After 15 days and 9 additions of $KMnO_4$	At the end of the experiment
m-xylene	1.91	0.66	0.45	0.19	<.006
phenol	1.26	0.96	<0.03	<0.03	<0.03
p-cresol	0.34	0.95	ND	ND	ND
naphthalene	4.59	6.25	4.37	1.14	0.02
phenanthrene	5.63	9.32	3.21	4.33	0.62
anthracene	0.75	0.62	0.12	0.02	ND
dibenzofuran	2.66	4.27	2.21	3.29	0.68
carbazole	0.67	1.16	0.190	0.20	ND
pyrene	2.38	3.69	0.55	0.73	0.23
indole	0.31	0.76	ND	ND	ND
2-methylnaphthalene	1.57	2.27	1.18	0.14	ND
1-methylnaphthalene	0.57	1.20	0.58	0.04	ND
biphenyl	0.91	1.00	0.56	0.40	0.04
acenapthalene	4.50	5.44	0.04	0.05	ND
fluorene	3.45	3.99	1.05	ND	ND
1-methylphenanthrene	1.32	1.03	0.07	0.07	ND
fluoranthene	4.61	3.89	1.13	2.16	1.15

ND - Concentrations below the detection limit of FID.
Detection Limits are given in Appendix 3.

Table 3.3 Masses of creosote compounds before during and after oxidation with $KMnO_4$

$KMnO_4$	Fenton's Reagent	Persulfate and Iron
fluorene-9-one	fluorene-9-one	fluorene-9-one
phthalic anhydride	phthalic anhydride	phthalic anhydride
2-hydroxy-9-fluoreneone	9, 10-anthracenedione	2-hydroxy-9-fluoreneone
isoindoledione	isoindoledione	isoindoledione
benzofuran	benzofuran	benzofuran
	1,4-dihydroethanonaphthalene	9, 10-anthracenedione
		9,10-phenanthrenedione

Table 3.4 Tentative identification of oxidation products formed during the reactions with the oxidizing reagents.

3.1.9 Conclusions

Oxidation of p-cresol at pH 7 using a molar ratio of 1:3:1 (p-cresol : H_2O_2 : Fe^{2+}), was ineffective, but by increasing the ferrous ion and peroxide molar ratios to 1:30:8 (p-cresol : H_2O_2 : Fe^{2+}), 92% of the p-cresol was decomposed. Similarly, the oxidation of p-cresol with persulfate required a large molar ratio of persulfate and iron. At a molar ratio of 1:10:8 (p-cresol : S_2O_8 : Fe^{2+}), 95% of the p-cresol was oxidized. Permanganate decomposed p-cresol (100%) in a 1:1 molar ratio within 5 minutes.

Laboratory batch experiments indicated that for the iron catalyzed reagents the Fe^{2+} concentration decreased during the experiments, which reduces the rate at which free radicals are produced and thus reduces the rate of organic contaminant oxidation. The decrease in catalyst is most likely caused by the precipitation of iron oxyhydroxides and by the inability of the organic radicals to reduce Fe^{3+} back to Fe^{2+}. Permanganate decomposed 1-methylnaphthalene, pyrene, indole and p-cresol at pH 7. Fenton's Reagent and persulfate with Fe^{2+} were able to decompose 1-methylnaphthalene, indole and p-cresol but not pyrene at pH 7.

It was demonstrated that in the creosote oil oxidation experiments, all three oxidizing reagents decomposed aqueous creosote compounds and were able to reduce the mass of the monitored creosote compounds in the oil phase. Fenton's and persulfate reagents can oxidize creosote compounds at pH 7, but the mass of creosote that would decompose at pH 7 is not known because the pH of the reactions decreased during the experiment.

To yield optimal reaction conditions at a pH of 7 with Fenton's and persulfate reagents, large molar ratios of iron and peroxide must be used. It has been noted in the decomposition of pentachlorophenol, that the natural iron from soils (e.g., hematite, magnetite, goethite) are able to promote the free radical reaction (Watts et al., 1990). Therefore the amount of iron catalyst needed for *in situ* remediation may be less than what is needed for the batch experiments. Conversely, other minerals such as calcite and dolomite can be detrimental to the free radical

oxidation process. As stated in section 3.1.2, free radicals are scavenged by carbonates; as a result, typical water treatment processes are more effective at pH<6.3, where the less reactive carbonic acid species is dominant (Montgomery, 1985). Thus delivery of the reagent in an aquifer containing a significant carbonate mineral fraction may only impact a small area because the free radicals are being consumed by the geological media. This may be overcome by adding a large excess of the reagents but the reactions are exothermic and would produce high temperatures. In the case of H_2O_2, oxygen would also be produced and reduce the efficiency of the injection well. The reagents could be used at lower concentrations if the pH of the aquifer were adjusted, but in an aquifer containing carbonate minerals the cost of adding acid as well as the detrimental impact on the aquifer makes the use of Fenton's and persulfate reagents impractical.

$KMnO_4$ would be the preferred oxidizing reagent for pH neutral, carbonate buffered aquifers because it oxidizes a wide variety of organic compounds, it can be used at high concentrations and once the oxidant demand of the aquifer material has been met $KMnO_4$ should remain at high concentration throughout the contaminated area.

Number	Compound	Number	Compound
1	phenol	10	fluorene
2	p-cresol	11	anthracene
3	naphthalene	12	phenanthrene
4	indole	13	carbazole
5	2-methylnaphthalene	14	methylphenanthrene
6	1-methylnaphthalene	15	fluoranthene
7	biphenyl	16	pyrene
8	acenaphthene	17	Benzo[a]anthracene
9	dibenzofuran	18	chrysene

Table 3.5 Identification of creosote compounds for Figures 3.8 to 3.11.

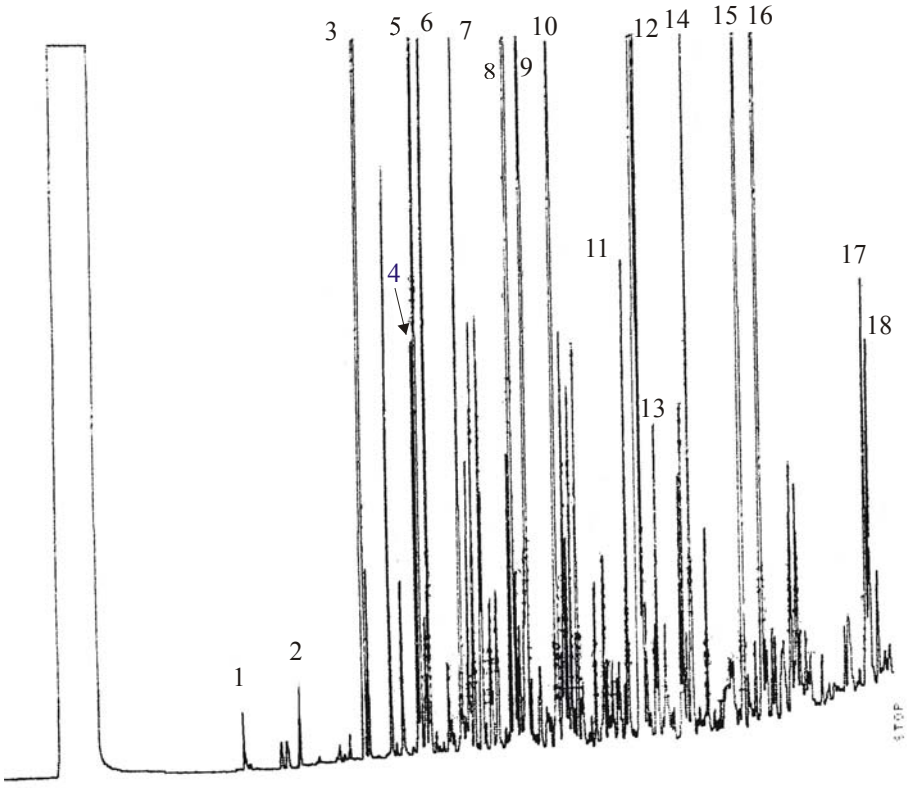

Figure 3.8 Gas chromatogram of a 0.01 mL creosote sample in 100 mL of CH_2Cl_2.

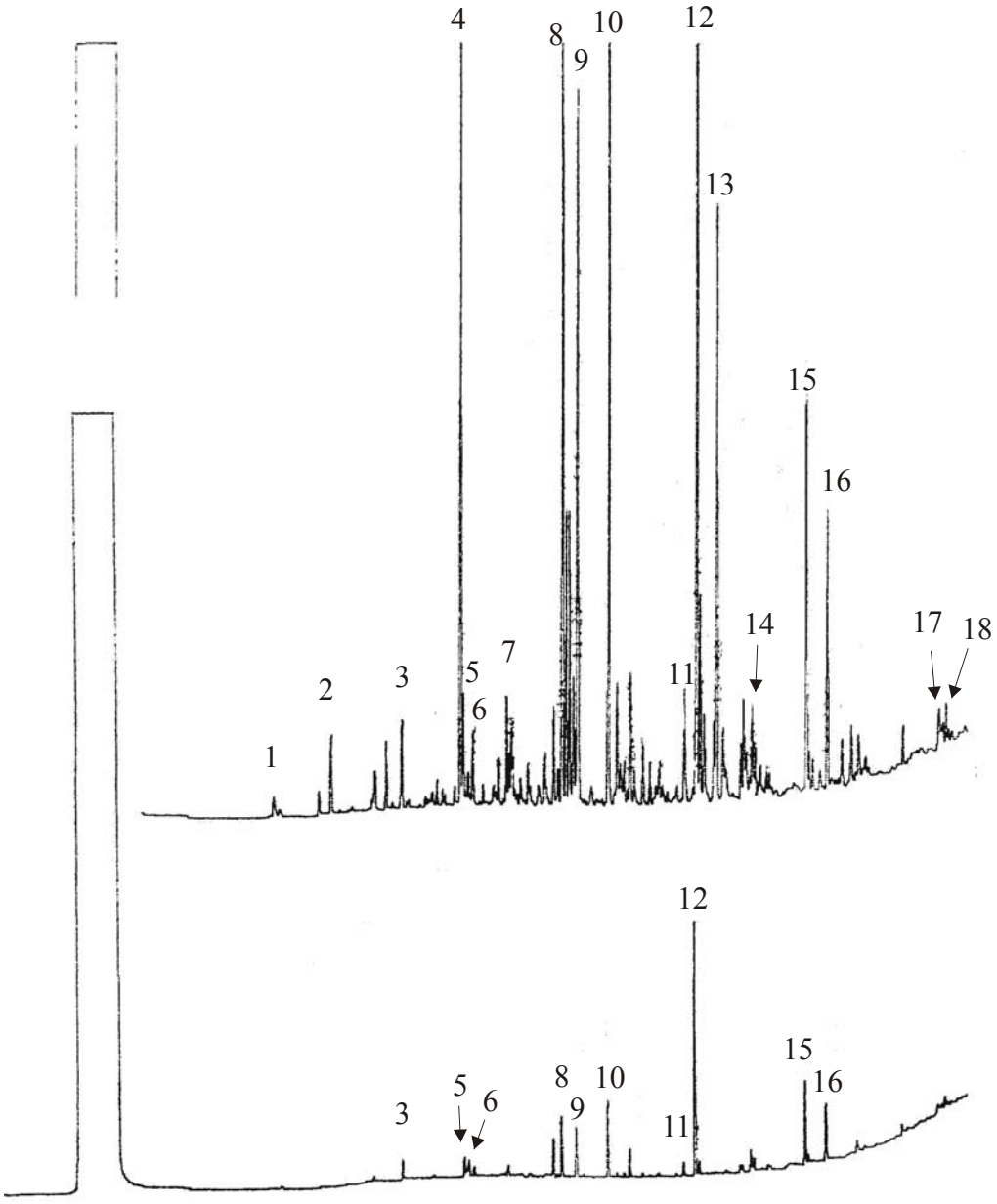

Figure 3.9 Fenton's Reaction. Gas chromatogram of the water phase before (top) and after (bottom) three days and three additions of Fenton's reagent. The concentration of H_2O_2 and Fe^{2+} after their addition to the reaction vessel was 1.8×10^{-2} and 4.1×10^{-3} M, respectively.

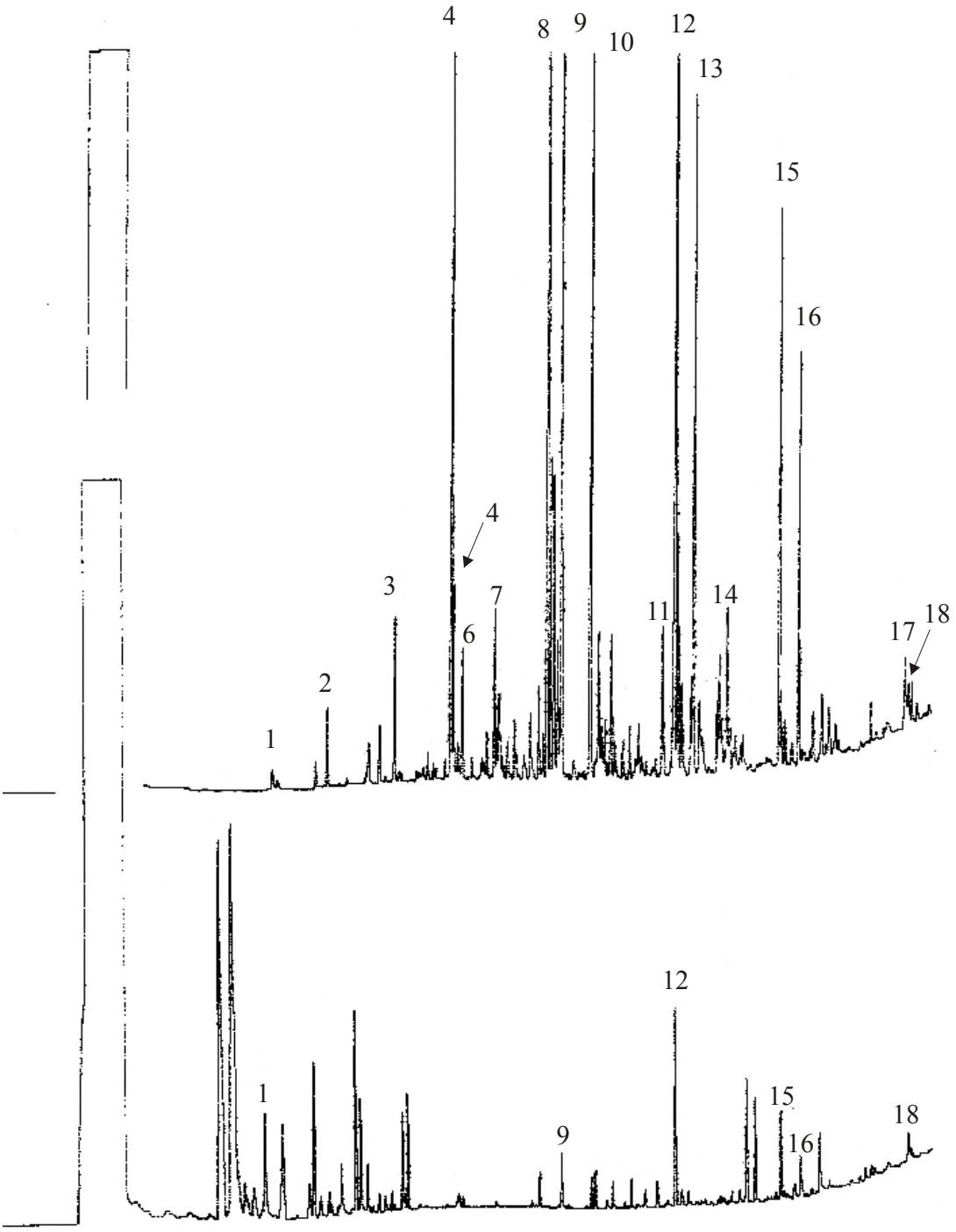

Figure 3.10 Persulfate and Fe^{2+} reagent. Gas chromatogram of the water phase before (top) after (bottom) three days and three additions of persulfate and iron. The concentration of S_2O_8 and Fe^{2+} after their addition to the reaction vessel was 1.8 x 10^{-2} and 4.1 x 10^{-3} M, respectively.

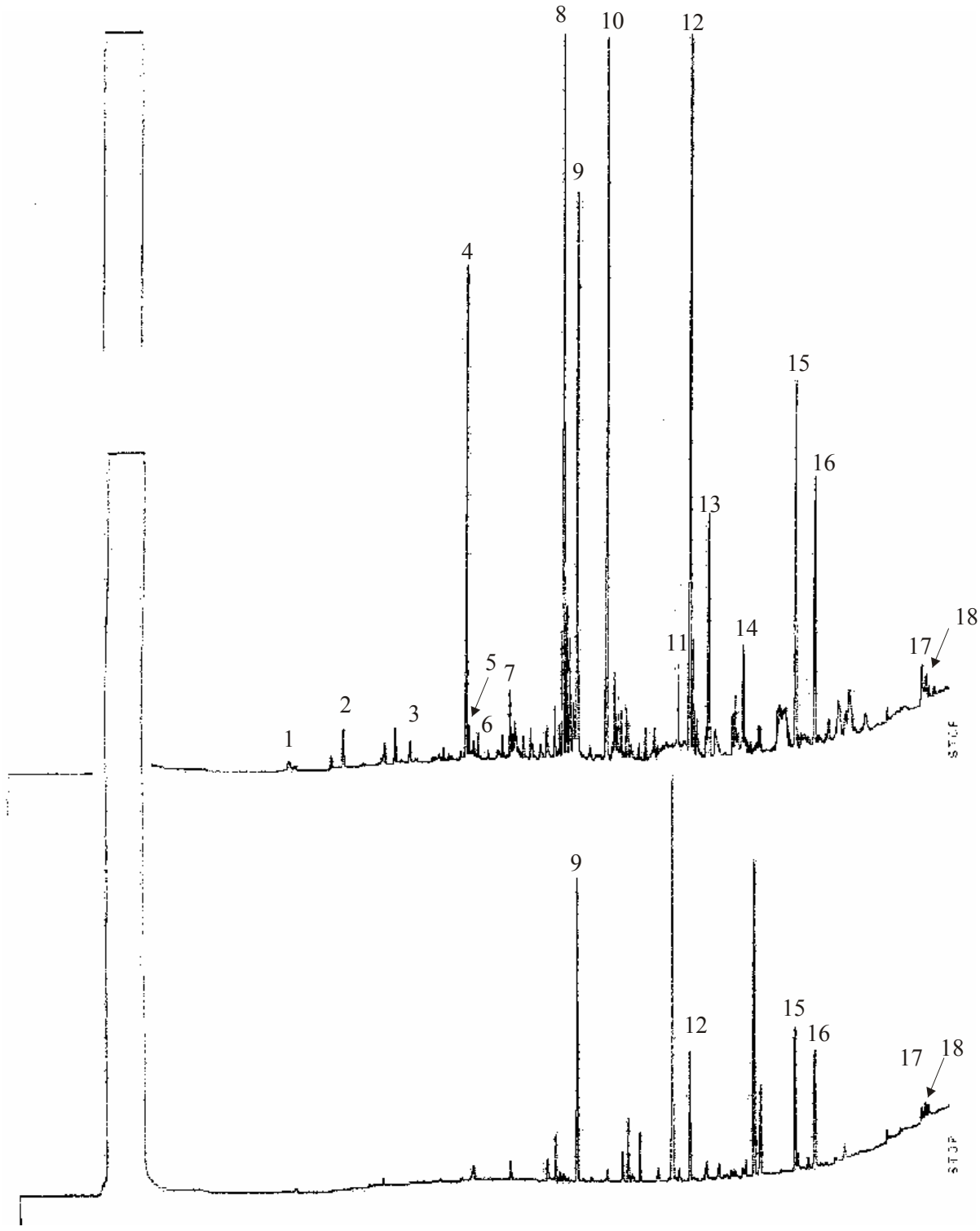

Figure 3.11 Permanganate Reagent. Gas chromatogram of the water phase before (top) and after (bottom) three days and the additions of permanganate.

3.2 Investigative Batch Column Experiment with $KMnO_4$

3.2.1 Introduction

Laboratory studies have confirmed the ability of a number of chemical oxidizing reagents (Fe-catalyzed peroxide or persulfate and permanganate) to oxidize phenolics, polycyclic aromatic hydrocarbons and heterocyclic compounds in solution. Permanganate appears to be the preferred oxidizing reagent in carbonate buffered soils/ground waters, while Fenton's Reagent and Fe^{2+} catalyzed persulfate are better suited to unbuffered (pH) or acidic environments.

Column experiments were conducted to assess the ability of $KMnO_4$ to enhance the removal of creosote residual oils from a carbonate sand matrix. To simulate the conditions found at CFB Borden, column experiments were performed, with the same filter sand used to backfill the emplaced source at CFB Borden. The columns with creosote at 8% saturation were treated intermittently with simulated groundwater or $KMnO_4$ dissolved in simulated groundwater (8 g/L) for 172 days.

3.2.2 Dissolution of Creosote, a Multi-Component DNAPL

Coal tars and creosotes (which are derived from distillation of coal tars) are chemically complex. The exact composition will vary from site to site because the composition is a function of the bituminous coal feedstock and the nature of the carbonization, distillation, condensing and purifying operations. The chemical composition of the creosote obtained from Carbochem Ltd. is shown in Table 3.6. The selected compounds represent 56.5% of the total mass in the creosote assuming the molecular weight of the unknown fraction was 200 g/mol. The molecular weight of the unknown fraction was estimated by examining the mass spectrum of a creosote sample. The mass spectra showed that the unknown fraction was predominately made up of heavy molecular weight PAHs with a smaller percentage of

unknown phenols and heterocycles. The density of the creosote was measured to be 1.10 g/mL at 21 ^{o}C.

To determine the aqueous concentration of specific compounds found in creosotes it is assumed that the complex mixture behaves ideally and follows a simplified version of Raoult's Law, which states the concentration of a component above an ideal solution is proportional to the mole fraction of the components in the organic phase,

$$C_s = X_n C_l \tag{3.2}$$

where C_s is the dissolved phase concentration or effective solubility limit of the organic in equilibrium with the oil phase, X_n is the mole fraction of n, and C_l is the liquid phase solubility of component n. This assumes that the properties of a complex organic mixture are determined by the properties of its pure components and their concentrations in the mixture. This is generally a valid assumption for DNAPLs composed of chemically similar species, such as creosote that is composed predominantly of PAHs (Mackay et al., 1991). Raoult's Law also assumes that there are no influences from co-solvents, surfactants or electrolytes that can alter the solubility of the individual compounds in the aqueous phase.

The majority of individual PAHs found in creosotes and coal tars are solids at normal temperatures but are liquids in the creosote oil. The liquid solubility is always higher than the solid solubility at temperatures below the melting point and must be calculated. The correct liquid solubility to be used in equation 3.2 is that of the subcooled chemical (Miller et al., 1985) which can be estimated from,

$$C_l = C_s \exp[\Delta S(T_m/T^{-1})/R] \tag{3.3}$$

where T is the system temperature, C_s is the solid phase solubility, T_m is the melting point of the pure compound, ΔS is the entropy of fusion and R is the gas constant. ΔS can be

calculated from experimentally measured enthalpies of fusion or $\Delta S/R$ can be estimated using Walden's rule as 6.8 ±1.0 (Miller et al., 1985).

Several studies have shown that equation 3.2 is a good assumption and dissolution from oily mixtures follows Raoult's Law within a factor of 2. These studies include batch experiments with eight different PAHs from four diesel fuels (Lee et al., 1992a) and 13 different PAHs from eight different coal tar samples (Lee et al., 1992b). Priddle and MacQuarrie (1994) examined the dissolution of creosote compounds with a dynamic column experiment and showed that five of the seven PAHs conformed to ideal behaviour within a factor of two. The calculated effective solubility using equations 3.2 and 3.3 of the selected creosote compounds is shown in Table 3.6.

3.2.3 Experimental

The columns were constructed of thick walled glass tubing fitted with stainless steel end plates (Figure 3.12). A seal was maintained between the end plates and the glass with a Teflon O-ring. The end plates were secured to the glass column with a universal beaded coupling joint. Creosote was obtained from Carbochem Ltd in Missisauga Ontario. Simulated groundwater was prepared by adding sufficient quantities of reagent grade $NaHCO_3$ and $CaCl_2$ to organic free water (Milli-Q water purification system) to precipitate a thin film of $CaCO_3$ after bubbling with purified CO_2. This method was used to minimise precipitation or dissolution of $CaCO_3$ during the experiment. $KMnO_4$ solutions were made by dissolving solid $KMnO_4$ into the simulated groundwater. All reagents were obtained from BDH and used without further purification. The filter sand used in the columns was obtained from the field site at CFB Borden (carbonates 45%, quartz 28%, feldspar 2%) (Devlin, 1994).

To provide a homogeneous mixture of creosote and filter sand the mixing was completed outside the column. Filter sand (300 mL) was placed into a 1 L beaker and weighed. Water (30 mL) was then added to the sand and stirred to wet the sand. Creosote (10 mL) was

Compound	fraction by Weight wt %	Molecular Weight (g/mol)	Melting Point ^{o}C	Solubility of Pure Solid-Phase Compound S_s (µg/L)	Solubility of Pure Compound in Liquid-Phase S_l (µg/L)	Effective Aqueous Solubility c^e_w (µg/L)	Estimated % Mass removed per gram sand (ug/g)
m-xylene	0.0001	106.20	-48.00		160.[1]	0.0383	9.4
phenol	0.0007	94.10	43.00	82000.[2]	123650.	175.0564	100.
o-cresol	0.0004	108.10	33.00	25920.[2]	31111.	19.4887	100.
p and m-cresol	0.0012	108.10					
2,6-dimethyl-phenol	0.0002	122.20	27.00	6049.[2]	6331.	2.1254	100.
2,4 and 2,5-dimethylphenol	0.0005						
2,3-dimethylphenol	0.0008	122.20	74.00	4570.[2]	13980.	18.0008	100.
3,5-dimethylphenol	0.0001	122.20	66.00	4888.[2]	12457.	1.1019	100.
naphthalene	0.0808	128.20	80.20	30.60	102.0[1]	12.2175	5.0
indole+2-methyl-naphthalene	0.0389						
1-methylnaphthalene	0.0182	142.20	-22.00		28.40[1]	0.6913	1.2
biphenyl	0.0151	154.20	71.00	7.50[2]	21.4252	0.3990	0.87
acenaphthylene	0.0020	152.20	82.00				
acenanpthene	0.0603	154.20	93.00	3.93	21.6000[1]	1.6048	0.87
dibenzofuran	0.0404	168.20	86.00	10.00[2]	40.2267	1.8360	1.5
fluorene	0.0470	166.20	116.50	1.18	11.6000[1]	0.6229	0.44
phenanthrene	0.1043	178.20	100.00	1.30[2]	7.1978	0.8000	0.25
anthracene	0.0107	178.20	216.30	0.731	7.0900[1]	0.0808	0.25
carbazole	0.0087	167.20	247.00	1.00[2]	158.5027	1.5611	5.91
fluoranthene	0.0516	202.30	107.00	0.263	1.8500[1]	0.0897	0.057
pyrene	0.0401	202.30	202.30	0.135	2.6700[1]	0.1006	0.082
B(a)anthracene	0.0115	228.20	156.00	0.014	0.3040[1]	0.0029	0.008
chrysene	0.0112	228.20	254.00	0.002	0.3790[1]	0.0035	0.010
B(b)fluoranthene	0.0064	252.30	168.00				
B(k)fluoranthene	0.0030	252.30	217.00				
B(a)pyrene	0.0044	252.32	179.00	0.00378	0.1160[1]	0.0004	0.003
indeno(1,2,3,c,b) pyrene + dibenzo(a,h)anthracene	0.0048						
benzo(g,h,i)perylene	0.0014	276.34	278.00	0.00026	0.0840[1]	0.0001	0.0002

[1] Mackay et al., 1991
[2] Mueller, 1989

Table 3.6 Creosote composition, calculated effective aqueous solubility using equations 3.2 and 3.3 and estimated mass loss for 3.61L of solutions passing through the control column.

then added to the water wet sand and stirred thoroughly with a spatula. The column (5 cm ID, 12 cm long) was packed with material from the middle of the mixture (i.e. not from along the edge of the beaker) in approximately 1 cm steps. After each 1 cm step the sand was gently packed with a bent spatula.

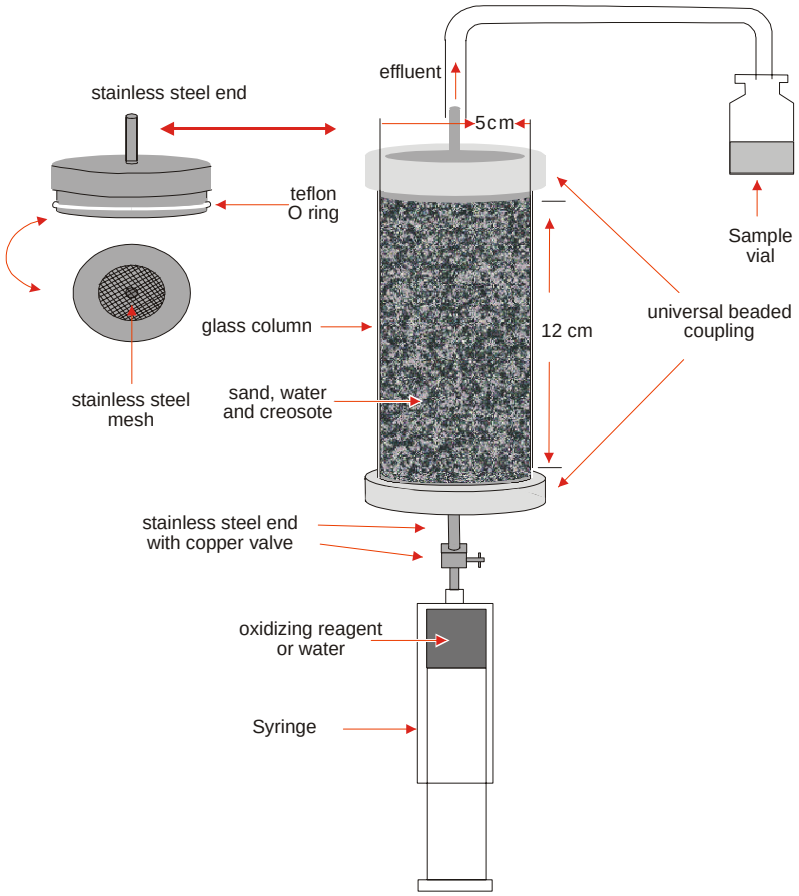

Figure 3.12 Column Design

Before adding solutions to the columns the columns were flushed with CO_2 for one hour. The columns were then slowly wetted from the bottom upward. This was necessary to remove trapped air in the sand. $KMnO_4$ or simulated groundwater were then added intermittently at room temperature ($21 \pm 2\ ^{o}C$) at rate of approximately 13 mL per min. from the bottom of the columns and samples from the effluent were analysed to provide a snapshot of the pore water chemistry. The columns were then left overnight to equilibrate before another flushing.

The effective porosity for both columns was not determined and it was not known to what extent the effective porosity would decrease due to the precipitation of manganese oxides. The overall porosity of the columns was determined gravimetrically (Table 3.7). Because the effective pore volume for the columns was not known, it was decided to add the permanganate solution to the oxidation column first and stop the flow when the concentration of $KMnO_4$ in the effluent was approximately the same as the influent concentration. In all cases the volume added was smaller than the measured porosity. An equivalent volume of simulated groundwater was passed through the control column to observe the removal of creosote compounds due to flushing alone. After 6, 40, 61 and 91 days the screen in the $KMnO_4$ column became plugged. A needle was used to make holes in the screen so that more $KMnO_4$ could be added. At 95 days the $KMnO_4$ could no longer be added to the column even after poking with a needle. Ten millilitres of a saturated sodium bisulfite solution was then added to remove magnesium oxides on the surface of the screen. An equal amount of the water was also flushed through the control column. After 4 hours $KMnO_4$ was then added to the column until approximately the same concentration of $KMnO_4$ was observed from the effluent. The screen did not become plugged again.

	$KMnO_4$	Control
initial mass of sand in 1L beaker (g)	520.92	520.90
volume of creosote added to 1L beaker (L)	0.010	0.010
volume of column (cm^3)	237.3	237.6
mass of sand added to column (g)	377.3	392.1
bulk density of sand (g/cm^3)	1.59	1.65
volume of creosote added (L)	0.00724	0.00753
porosity	0.39	0.41
oil saturation	0.078	0.077
pH of effluent	6.9 - 8.5	5.8 - 6.7
volume of solutions added (L)	3.61	3.61
total number of days	172.0	172.0
overall flow rate (cm^3/d)	21.0	21.0

Table 3.7. Operational characteristics of sand columns

3.2.4 Chemical Analysis

Water samples from the effluent were collected as either 13 or 45 mL samples and analyzed as given in section 3.1.3. Sand samples containing residual creosote were Soxhlet extracted with a 200 mL mixture of CH_2Cl_2 and acetone (1:1) for 24 hours. The solvent volume was reduced to 25 mL with a Kuderna-Danish concentrator and analysed for the monitored creosote compounds. After extraction the sand was dried in an oven at 90 ^oC overnight, cooled in a desiccator and then weighed to determine the mass of sand. At the end of the experiment the sand from the control column could be weighed directly after the extraction but the sand from the permanganate column was covered with manganese oxides. The manganese oxides were removed with an acidified solution of hydroxylamine hydrochloride (Choa, 1972).

To a sand sample, 70 mL of hydroxylamine hydrochloride (0.025M in 0.01M HNO_3) and 10 mL of 6M HNO_3 was added and stirred for 5 min. The final pHs of the solutions were between 1 and 2. The concentration of manganese removed by the extraction was determined by atomic adsorption at the Water Quality Laboratory, University of Waterloo, Department of Earth Sciences. The instrument used was a Varian Model 1475 Atomic Absorption Spectrophotometer. The concentrations were then converted to mass of MnO_2.

Because the sand and creosote were mixed outside the column before packing, it was difficult to assess directly the mass of creosote added to each column. To calculate initial mass of individual creosote compounds added to each column, samples of sand from the beaker were Soxhlet extracted and the concentrations were determined (μg of creosote compounds per g of sand). At the conclusion of the experiment the mass of the targeted creosote compounds per gram of sand was determined and compared to the initial values to estimate the mass lost for each column. This assumes that a homogeneous mixture was in fact added to the column.

3.2.5 Results and Discussion

When $KMnO_4$ was first added to the column the oxidizing reagent rapidly faded from the characteristic dark pink colour as it was reduced to manganese oxides by easily oxidizable creosote compounds and minerals on the sand. As more $KMnO_4$ was added the pink persisted and preferred pathways through the column were clearly marked by the pink $KMnO_4$ solution. After each addition the pink colour visibly diffused into pore spaces that were initially bypassed. After 6 injections the sand was completely covered with manganese oxides which made it difficult to observe the movement of the permanganate solution through the porous media

It is expected, in the column in which simulated ground water was used that the effluent concentrations for the PAHs will reach their calculated aqueous solubility concentrations. Studies examining mass transfer rates have shown that equilibrium concentrations can be reached quickly (minutes or hours) with petroleum based hydrocarbons and chlorinated organics (Shui et al., 1990; Anderson et al., 1992) but in column experiments with creosote (Priddle, 1994) it took ~ 60 h for all the components in creosote to come to equilibrium with the aqueous phase. The contact time between flushing the creosote DNAPL with water for this experiment was 24 hours or more. This contact time is believed to be sufficient to allow the concentrations of the more abundant and soluble PAHs to reach equilibrium concentrations.

The effluent concentrations of the less soluble PAHs should also remain relatively constant because the mass of the PAHs removed by flushing is small compared to the initial mass added to the column. The mole fraction should therefore not change significantly nor change the solubility of the different PAHs. The expected mass lost for the PAHs due to flushing can be roughly estimated by multiplying the effective solubilities by the volume of water passed through the column (3.61 L) (Table 3.6). This calculation assumes that equilibrium between the two phases is attained after 24 hours, that Raoult's Law for effective

solubilities is obeyed, that the mole fraction does not change, and that water comes in contact with the oil phase throughout the column.

Effluent concentrations for both columns showed a rapid decrease in the aqueous concentrations for the more soluble compounds such as phenol, o-cresol and m-xylene (data not shown). The less soluble PAHs such as naphthalene, dibenzofuran, phenanthrene or fluorene were continually leached from the creosote phase as shown in Figures 3.13 and 3.14. The effluent concentrations were generally higher in the control column compared to the $KMnO_4$ column and were approximately equal to or lower than the calculated effective aqueous solubility values.

Initially, the effluent concentrations for both columns were greater than the calculated values. This may be caused by the facilitated transport of creosote organics sorbed onto fine sand grains or colloidal material, or by creosote oil droplets discharge from the column. As seen in Figures 3.13 and 3.14 spikes of high concentrations were observed.

The filter sand used was poorly sorted with a coefficient of uniformity of 3.5 (Devlin, 1994). The sand was sieved (#7, 2.8 mm) to remove the coarse material but fine sand grains were not removed. Fine grains of sand transported out of the columns containing sorbed organic compounds would also be extracted with the aqueous phase and contribute to the effluent concentrations. The samples were not filtered because of the potential for sorption of PAHs onto filter paper.

After 172 days the columns were sectioned into 12 divisions, the creosote/sand mixture was Soxhlet extracted, and the mass of sand was measured to determine the mass of creosote per gram of sand vertically through the column.

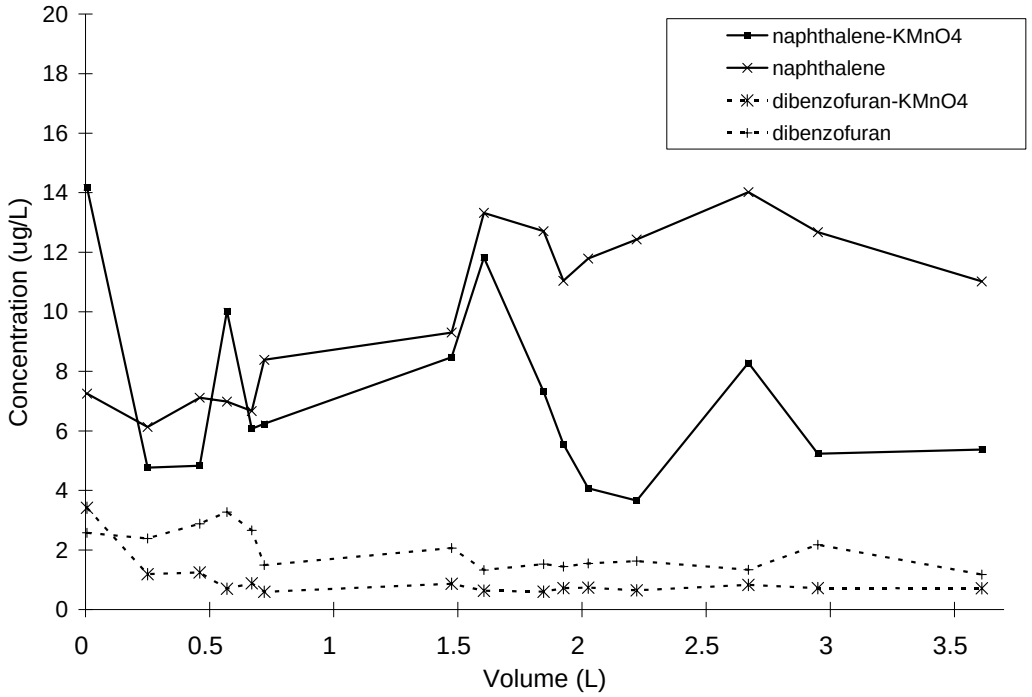

Figure 3.13 Naphthalene and dibenzofuran effluent concentrations for the $KMnO_4$ and water columns.

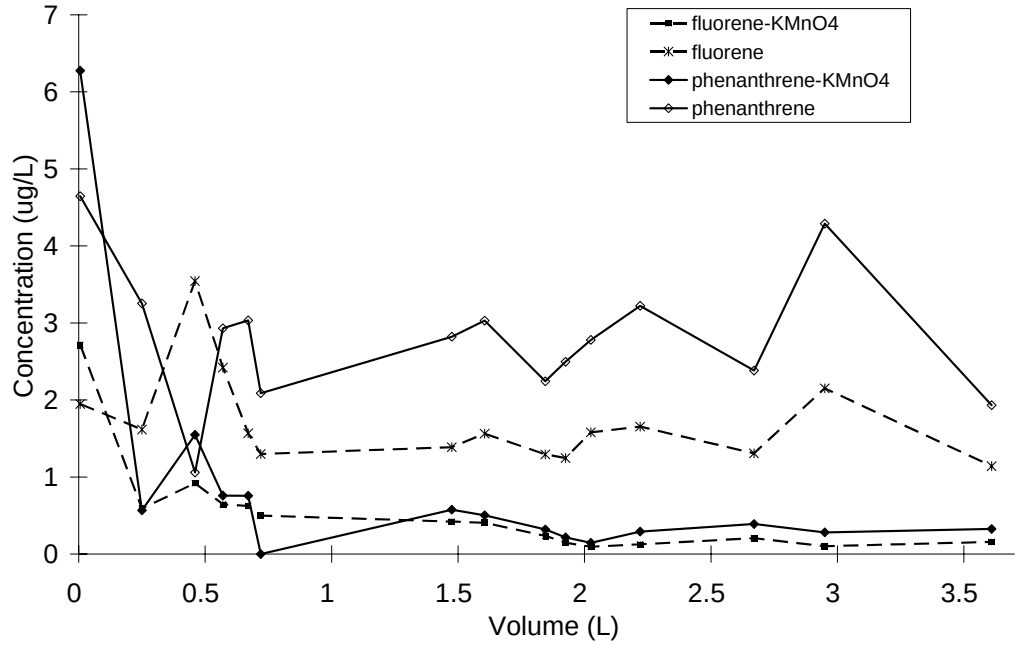

Figure 3.14 Fluorene and phenanthrene effluent concentrations for the $KMnO_4$ and water columns.

To determine the mass of sand that was covered with MnO_2 in the $KMnO_4$ column the manganese oxides were selectively removed with an acidified solution of hydroxylamine hydrochloride. It was very important that the hydroxylamine only removed the precipitated manganese oxides and not the manganese oxides on the sand grains themselves in order to establish the mass of sand added to the column. To determine the mass of MnO_2 removed during the procedure three samples of filter sand were analyzed. This procedure only removed 2 x 10^{-4} grams of MnO_2 per gram of sand (Table 3.8). The average concentration of MnO_2 precipitated on the sand grains after 172 days was 2.081 x 10^{-2} (g/g). As seen in Table 3.8 the concentration of manganese oxides was greater at the bottom of the column. This was also visually observed. The top of the column contained an orange/brown precipitate of manganese oxides that became blacker downward through the column. At the bottom of the column a hard precipitate of manganese oxides had formed within the sand matrix.

	sand samples from $KMnO_4$ column	Mass of sand before extraction of MnO_2 (g)	Mass of MnO_2 on the filter sand (g)	Mass of sand after extraction of MnO_2 (g)	Weight Percent of MnO_2 (MnO_2/Sand) (g/g)	
top of column	$MnO_4$1	36.0059	0.5228	35.6723	1.452 x 10^{-2}	
	$MnO_4$2	33.2541	0.3999	32.9989	1.203 x 10^{-2}	
	$MnO_4$3	28.8152	0.4626	28.5200	1.605 x 10^{-2}	
	$MnO_4$4	32.7829	0.5654	32.4221	1.725 x 10^{-2}	
	$MnO_4$5	34.1771	0.6669	33.7515	1.951 x 10^{-2}	
	$MnO_4$6	40.0211	0.7346	39.5523	1.836 x 10^{-2}	
	$MnO_4$7	28.7455	0.7259	28.2823	2.525 x 10^{-2}	
	$MnO_4$8	28.4085	0.7259	27.9453	2.555 x 10^{-2}	
	$MnO_4$9	35.2654	0.8299	34.7358	2.353 x 10^{-2}	
	$MnO_4$10	25.1784	0.6832	24.7424	2.714 x 10^{-2}	
bottom of column	$MnO_4$11	32.6255	0.7998	32.1151	2.452 x 10^{-2}	
	$MnO_4$12	27.0809	0.7058	26.6305	2.606 x 10^{-2}	
	total	382.3605		377.3685	2.081 x 10^{-2}	average
	Extraction of clean Filter Sand					
	standard 1	42.0584	0.0073	42.0537	1.744 x 10^{-4}	
	standard 2	34.1747	0.0056	34.1711	1.651 x 10^{-4}	
	standard 3	17.3427	0.0049	17.3396	2.797 x 10^{-4}	
					2.064 x 10^{-4}	average

Table 3.8 Hydroxylamine hydrochloride extraction of manganese covered sand and clean filter sand.

Extraction of the control column revealed an increase in creosote concentration downward through the column with the bottom third of the control column containing the highest concentration of creosote (Table 3.9). This was also observed visually through the glass column. After 5 additions of water to the control column, small black creosote globules could be seen within the pore spaces and as the experiment continued a band of creosote approximately 3 cm thick formed 1 cm from the bottom of the column. Extraction of the column showed fluctuating PAH concentrations throughout the column.

These observations may have major implications at the Borden field site in that the creosote and sand was mixed using a similar method. The initial homogeneous mixture that was added to the aquifer will, as time passes, become heterogeneous as the density driven migration of the oil occurs. It should be expected that pockets of oil will form as it migrates downward through the filter sand and is trapped by finer grained strata.

Creosote globules were not observed in the $KMnO_4$ column and extraction of this column showed a more uniform distribution of the creosote compounds (Table 3.10). Comparison of concentrations of creosote compounds left in the sand matrix before and after flushing with $KMnO_4$ or water are shown in Table 3.11. In the $KMnO_4$ column there is an actual increase in concentrations for 1-methylnaphthalene and benzo(b)fluoranthene. This increase in mass could be the result of oxidized compounds in the gas chromatogram co-eluting with the monitored creosote compounds. If oxidized products have similar retention times as the above compounds, the area count for those peaks would be inflated and give concentrations larger than the true values. For the remaining compounds the extraction showed that the percent mass removed was greater in the oxidation column than in the control column.

To assess the degree of variability inherent in the extraction procedure, creosote, sand and water were mixed in a beaker as outlined in the procedure and four samples were soxhlet

extracted. The standard deviation for the four samples is given in Table 3.11. The creosote used for this analysis was taken from a different can of creosote and unfortunately did not contain lighter, more volatile phenolic compounds.

The percent mass removed (per gram of sand) for each compound given in Table 3.11 is potentially inflated due to the facilitated transport of creosote compounds on fine sand grains or through the discharge of creosote oil. The degree to which they are inflated can be assessed by comparing the expected mass loss calculated from aqueous solubilities and the experimental values obtained for the control column (Table 3.6). In all cases except naphthalene, the percent mass loss per gram of sand in the control column was only slightly greater than the calculated values. The increased mass loss due to facilitated transport in the $KMnO_4$ column cannot be assessed directly, although the smaller effluent concentrations indicate that the mass removed due to facilitated transport would be smaller than that found in the control column.

To calculate the overall percent mass removed per gram of sand, the masses of all the compounds were summed and divided by the total mass of sand added to the column. The $KMnO_4$ column reduced the overall targeted creosote compounds by 36.5 % compared to only 3.85% for the control column. The total mass loss for PAH compounds only (naphthalene to benzo(g,h,i)perylene) was 36.2 % and 2.44 % for the $KMnO_4$ and control columns respectively.

In the $KMnO_4$ and control column the chemicals that had the lowest percent mass loss were chrysene and benzo(g,h,i)perylene. To estimate the volumes needed to remove 100 percent of these compounds a simple ratio can be used,

$$\frac{\text{Volume needed to totally remove compound (L)}}{100\%} : \frac{3.61\text{L}}{\%\text{ removed after 3.61L}} \qquad (3.4)$$

This assumes that the physical/chemical properties of the oil phase do not change as compounds are leached from the oil and that oxidation and mass transfer rates remain constant. Using the above ratio, 62 L for the $KMnO_4$ column and 2,481 L for the control column would be required to remove the chemicals from the creosote phase. Thus at flow rates of 21 cm^3/d, 40 times the volume of water would be used to totally remove all the monitored creosote compounds compared to a solution of $KMnO_4$ at a concentration of 8 g/L. At this flow rate it would take 8 and 325 years for the $KMnO_4$ and control columns, respectively, to remove the monitored compounds.

The rate of mass transfer could also be increased by increasing the concentration of the $KMnO_4$ solution. Experiments with chlorinated solvents and $KMnO_4$ have shown that the rate of dissolution is increased with increasing $KMnO_4$ concentration due to the increased rate of oxidation (Schnarr, 1992). A concentration of 8 g/L was used in this experiment, but concentrations up to its solubility limit of 36.2 g/L (5 ^oC) (Perry at al., 1994) could be used. However, as the $KMnO_4$ concentration increases there may be a point at which the rate of contaminant dissolution becomes limiting. To optimize the reaction, a series of columns could be performed with increasing concentrations of $KMnO_4$ to determine when the rate of mass loss is maximized.

The procedure of intermittently flushing the column with an oxidizer did not maintain $KMnO_4$ concentrations. For example, the effluent was colourless after 24 hours indicating little residual $KMnO_4$. The rate of reaction would decrease as the concentration in the liquid decreased. To sustain the rate of reaction and improve the mass removed, the concentration of $KMnO_4$ should remain high. This could have been accomplished by having the reagent flush through the column constantly.

3.2.6 Conclusions

At a neutral pH in a carbonate rich sand matrix containing creosote at 8 % residual saturation, $KMnO_4$ (8 g/L) decreased the initial mass of creosote compounds by 36.5%. In the column in which no oxidizer was used, only 3.85 % was removed. The $KMnO_4$ and control columns removed 36.2 % and 2.44 % of the PAHs respectively.

The observed increase in mass loss from the $KMnO_4$ column verifies that the chemical oxidation process increased the dissolution process above that of flushing alone. Extraction of the column at the end of the experiment did not show a general trend in decreasing or increasing concentration of compounds through the column. This observation suggests that the oxidation process may have occurred throughout the column.

	Top of column										Bottom of column		Total
mass of sand Extracted (g)	2514	37.55	37.18	26.72	30.90	36.11	36.53	28.77	28.47	40.93	29.65	34.18	392.09
Compound	Concentration (µg of compound/g of sand)												Overall Concentration (µg /g)
naphthalene	566	688	634	906	706	681	883	910	2429	8717	6385	3537	2369
indole+2-methyl-naphthalene	116	149	107	189	151	147	156	185	347	1465	1125	710	423
1-methylnaphthalene	389	432	255	512	412	425	196	272	483	1686	1224	805	609
biphenyl	68	87	78	109	88	83	98	106	231	781	625	417	241
acenaphthylene	15	28	23	33	26	25	ND	ND	ND	132	103	72	40
acenaphthene	355	415	449	533	421	404	548	513	1335	4441	3549	2577	1354
dibenzofuran	214	234	215	317	248	239	261	289	645	2343	1894	1330	716
fluorene	334	380	353	460	429	377	425	445	1067	3614	2978	2251	1142
phenanthrene	801	1060	926	1408	1105	1084	1175	1300	2838	8946	7414	5659	2922
anthracene	ND	101	55	135	65	103	112	125	201	645	558	398	217
carbazole	ND	36	25	42	25	30	41	39	ND	276	268	156	83
fluoranthene	ND	696	634	912	752	716	813	951	2098	6962	5872	4474	2182
pyrene	ND	224	209	297	245	233	338	348	840	2687	2264	1721	834
B(a)anthracene	ND	90	76	117	82	81	91	95	237	794	682	501	253
chrysene	ND	81	80	108	90	88	93	99	203	729	620	464	237
B(b)fluoranthene	ND	ND	ND	ND	ND	ND	ND	ND	171	539	475	357	136
B(k)fluoranthene	27	55	51	82	61	58	63	77	ND	ND	ND	ND	39
B(a)pyrene	ND	ND	ND	ND	ND	22	22	ND	56	210	183	133	56
indeno(1,2,3,c,b) pyrene + dibenzo(a,h) anthracene	ND	ND	ND	ND	ND	ND	ND	ND	ND	90	91	50	21
benzo(g,h,i)perylene	ND	ND	ND	ND	ND	ND	ND	ND	ND	45	67	24	12
Total concentration (µg/g)	3375	4757	4171	6189	4908	4796	5315	5754	13182	45103	36378	25635	13885

Table 3.9 Results obtained after flushing with 3.61 L of ground water over 172 days.

	Top of column										Bottom of column		Total
mass of sand Extracted (g)	35.67	33.0	28.52	34.42	33.75	39.55	28.28	27.95	34.74	24.74	32.12	26.63	377.37
Compound	Concentration (µg of compound/g of sand)												Overall Concentration (µg /g)
naphthalene	384	628	1074	1757	1734	1046	1127	698	1257	1280	629	499	1012
indole+2-methyl-naphthalene	119	192	234	323	324	254	289	214	357	358	220	252	259
1-methylnaphthalene	335	491	564	785	785	264	660	459	761	780	510	542	600
biphenyl	105	153	ND	262	ND	ND	ND	ND	ND	ND	ND	276	65
acenaphthylene	22	36	54	46	48	38	ND	ND	49	69	33	66	38
acenaphthene	114	224	413	621	605	350	387	236	377	413	264	487	371
dibenzofuran	261	364	566	763	788	637	748	511	903	900	596	790	645
fluorene	102	199	330	423	430	266	287	185	291	315	234	398	285
phenanthrene	974	1593	2334	3119	3131	2289	2664	1897	3069	3164	2205	2934	2420
anthracene	ND	ND	ND	ND	ND	ND	ND	ND	ND	ND	ND	30	2
carbazole	3	ND	3	54	56	43	5	3	61	32	38	6	27
fluoranthene	1003	1386	1888	2460	2495	1972	2336	1786	2803	2873	129	2663	1952
pyrene	220	336	505	801	804	582	569	414	775	735	422	636	564
B(a)anthracene	75	115	179	237	237	168	187	137	223	227	131	212	176
chrysene	114	153	205	251	252	198	233	198	275	292	201	266	217
B(b)fluoranthene	ND	ND	207	221	237	182	172	140	242	231	184	214	166
B(k)fluoranthene	86	117	ND	ND	ND	ND	ND	ND	ND	ND	ND	ND	18
B(a)pyrene	19	27	ND	ND	ND	ND	ND	ND	ND	ND	ND	ND	4
indeno(1,2,3,c,b) pyrene + dibenzo(a,h) anthracene	ND	4	53	ND	ND	ND	ND	ND	ND	ND	ND	ND	4
benzo(g,h,i)perylene	ND	ND	ND	ND	ND	ND	ND	ND	ND	ND	ND	ND	0
Total concentration (µg/g)	3936	6018	8609	12123	11927	8589	9664	6876	11445	11669	5796	10270	8827

Table 3.10 Results obtained after flushing with 3.61 L of a $KMnO_4$ solution (8 g/L) over 172 days.

	$KMnO_4$ Column			Control Column			Standard Deviation of four Soxhlet extracted samples (ug/g)
	mass of compound per mass of sand (µg/g)		Percent mass lost per gram of sand (%)	mass of compound per mass of sand (µg/g)		Percent mass lost per gram of sand (%)	
Compound	Initial	Final		Initial	Final		
m-xylene	2.82	ND	100.00	2.01	ND	100.00	
phenol	14.80	ND	100.00	12.02	ND	100.00	
o-cresol	7.52	ND	100.00	6.89	ND	100.00	
p and m-cresol	24.39	ND	100.00	19.05	ND	100.00	
2,6-dimethyl-phenol	4.56	ND	100.00	3.66	ND	100.00	
2,4 and 2,5-dimethylphenol	9.94	ND	100.00	5.82	ND	100.00	
2,3-dimethylphenol	17.48	ND	100.00	3.18	ND	100.00	
3,5-dimethylphenol	1.20	ND	100.00	7.01	ND	100.00	
naphthalene	2367.72	1012.38	57.24	2461.48	2368.89	3.76	±18.23
indole+2-methyl-naphthalene	465.36	259.39	44.26	503.18	423.39	15.86	±13.49
1-methylnaphthalene	595.00	600.25	-.88	630.12	609.02	3.35	±6.16
biphenyl	319.01	65.23	79.55	249.74	240.97	3.51	±7.46
acenaphthylene	41.25	35.02	15.10	42.25	40.12	5.04	±0.81
acenanpthene	1331.84	370.84	72.16	1377.11	1354.00	1.68	±93.74
dibenzofuran	708.02	644.64	8.95	733.80	715.69	2.47	±20.23
fluorene	1128.70	285.21	74.73	1157.44	1141.66	1.36	±18.66
phenanthrene	2869.21	2420.27	15.65	2949.68	2922.11	0.93	±108.03
anthracene	219.06	2.09	99.04	224.51	217.21	3.25	±3.62
carbazole	96.91	26.54	72.61	91.11	82.75	9.18	±3.78
fluoranthene	2158.60	1952.42	9.55	2195.06	2181.94	0.60	±22.40
pyrene	781.84	563.75	27.89	845.99	834.35	1.38	±16.84
B(a)anthracene	249.64	175.58	29.67	259.60	253.22	2.46	±4.61
chrysene	230.53	216.94	5.90	239.99	237.01	1.24	±4.12
B(b)fluoranthene	138.05	166.40	-20.54	141.18	135.69	3.89	±1.71
B(k)fluoranthene	35.06	18.39	47.57	39.69	39.14	1.39	±1.39
B(a)pyrene	52.22	4.14	92.07	56.50	55.53	1.71	±1.42
indeno(1,2,3,c,b) pyrene+dibenzo(a,h)anthracene	22.01	4.34	80.31	22.03	20.63	6.35	±1.05
benzo(g,h,i) perylene	10.50	0.00	100.00	11.89	11.87	0.15	±0.28
total	**13903.25**	**8823.82**	**36.53**	**14440.69**	**13885.20**	**3.85**	

ND = Not detected after extraction of sand

Table 3.11 Initial and final mass of selected creosote compounds per mass of filter sand.

Chapter 4

Degradation and Oxidative Kinetics of Polycyclic Aromatic Hydrocarbons and Alkylbenzenes Found in Creosote/Coal Tar by Potassium Permanganate

4.1 Abstract

The ability of permanganate to oxidize polycyclic aromatic hydrocarbons is well known but little kinetic information is available. This study examined the kinetics of the oxidative treatment of a selected group of creosote/coal tar compounds in water using excess potassium permanganate and investigated the correlation between reactivity and physical/chemical properties. The oxidation of naphthalene, phenanthrene, chrysene, 1-methylnapthalene, 2-methylnaphthalene, acenaphthene, fluorene, carbazole isopropylbenzene, ethylbenzene and methylbenzene closely followed first-order reaction kinetics and second-order rate constants were calculated. The oxidation of pyrene was initially very rapid and did not follow the pseudo-first-order rate decay at early times, although a correlation was observed at later times. Fluoranthene was only partially oxidized by permanganate and the oxidation of anthracene was too fast to be measured. Biphenyl, dibenzofuran, benzene and tert-butylbenzene failed to react under the conditions of this study. The rate at which an electrophilic aromatic substitution reaction occurs is controlled by the ability of the arene to donate electrons. This relationship was investigated by comparing the second-order rate constants with ionization potentials and with semi-empirical molecular orbital calculations of the relative heats of formation of the σ-complex intermediate. The rate of oxidation was shown to increase with increasing number of rings because less energy is typically required to overcome the aromatic character of a polycyclic ring than is required for benzene. Thus the rate of oxidation increased in the series naphthalene < phenanthrene < pyrene. The interaction of MnO_4^- ion with alkyl substituted

benzenes and substituted polyaromatic hydrocarbons (PAHs) may occur via two different routes: through the attack at the on the benzylic C-H bond and through the attack at the ring. The reactivity of these compounds is controlled by both the benzylic C-H bond strength and the ability of the aromatic ring to donate electrons. Alkyl substituted benzenes and substituted PAHs showed a good correlation between second-order rate constants and bond dissociation energies, but not between second-order rate constants and calculated heats of complexation. Also presented is the Clar's aromatic sextet theory which relates topology with physical properties and how this theory can be used to predict the relative stability of arenes towards ring oxidation.

4.2 Introduction

Creosote and coal tar may contain as many as 200 different chemicals with only a few present at a concentration greater than 1%. The composition of creosote depends on the coal tar from which it was produced but it generally contains 85% polycyclic aromatic hydrocarbons (PAHs), 10% phenolics and 5% heterocyclic compounds (nitrogen, sulfur and oxygen containing aromatics) (Mueller et al., 1989).

The contamination of ground water with polycyclic aromatic hydrocarbons is of great concern because many are carcinogenic (Dipple et al., 1984) or mutagenic (Durant et al., 1996). One potential method for the removal of PAHs from soils, sediments and ground water is the *in situ* application of permanganate (Gates-Anderson et al., 2001, Lamarche, 2002). To evaluate the potential effectiveness of *in situ* chemical oxidation at field sites, it is likely that numerical model simulations will need to incorporate relevant chemical oxidation rates to provide design guidance and to assess system performance.The purpose of this study was to examine the rates of reaction between representative groups of creosote/coal tar compounds (Table 4.1) and aqueous permanganate, and to investigate the relationships between rates of reaction and physical/chemical properties of the organic compounds.

The oxidation of benzene and alkylbenzenes by different permanganate species has been extensively studied by Rudakov, Loachev and Zaichuk. The oxidation of alkylbenzenes can occur through the attack of the MnO_4^- ion either on the C-H bond of an alkyl substituent, or on the aromatic ring (Rudakov and Loachev, 1994). It was determined that the dominant reaction of MnO_4^- with alkylbenzenes such as methylbenzene, ethylbenzene and isopropylbenzene at a pH 5-7 (70°C) occurs through the abstraction of a benzylic hydrogen atom as shown in the reaction of toluene with MnO_4^-,

$$\begin{aligned} &C_6H_5\text{-}CH_3 + OMnO_3^- \longrightarrow \{C_6H_5\text{-}H_2C\text{- -}H\text{- - -}OMnO_3^-\} \\ &\longrightarrow C_6H_5\text{-}H_2COMn(VII)O_2(OH^-) \longrightarrow C_6H_5\text{-}H_2COH + Mn(V)O_3^- \end{aligned} \qquad (4.1)$$

The benzylalcohol that is formed is further oxidized to benzoic acid and manganese (V) is reduced to manganese dioxide ($Mn(IV)O_2$).

The order of reactivity for alkylbenzenes follows the bond strength of the benzylic C-H bond or the basicity of the arene. Thus, the stronger the C-H bond, the more resistant to oxidation the compound will be. The bond strength decreases from primary, secondary to tertiary hydrogens and the order of reactivity increases in the same order: $C_6H_5CH_3 < C_6H_5CH_2CH_3 \leq C_6H_5CH(CH_3)_2$. The substrate selectivity by the MnO_4^- anion is similar to that observed in H abstraction by radicals (Rudakov and Loachev, 1994).

It was also determined that the rate at which ring oxidation occurred increased with increasing positive charge of the reagent or in the series $MnO_4^- < HMnO_4 < MnO_3^+$ (Lobachev et al., 1997). Because $HMnO_4$ and MnO_3^+ only form in very acidic systems, side chain oxidation in slightly acidic, neutral or basic conditions in which the major Mn(VII) species is MnO_4^-, will occur faster than ring oxidation for alkylbenzenes. For example, under neutral conditions the oxidation of benzene, which involves an attack of MnO_4^- anion on the aromatic ring is 2000 times slower than the oxidation of toluene which proceeds through a hydrogen atom abstraction mechanism (Rudakov and Loachev, 1994).

The general mechanism for the reaction of an electrophile with an arene initially involves a loose association of the reactants in which the complexing agent is not localized at a particular carbon atom, but is held near the π-electron cloud. This is called a π-complex or a charge transfer complex and the structure is usually drawn with an arrow indicating that the aromatic ring is electron donating. After the initial association there is a donation of two electrons from the π system to form an electron deficient σ–complex. It is the formation of the σ–complex, and not the π–complex, that is the rate-determining step in electrophilic aromatic substitution (Taylor, 1990). This fact has allowed researchers to use ionization potentials, or how tightly the electrons are held to the molecule, to improve the description of aromatic reactivity in electrophilic substitution reactions (Kachurin and Vysotskii, 1999),

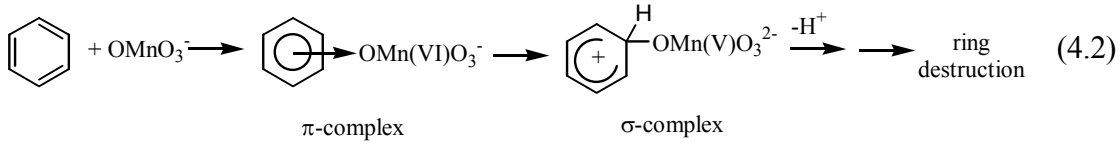

(4.2)

Creosote and coal tars contain a vast variety of PAHs which will react similarly to the examples given above. The attack of the MnO_4^- ion on a creosote/coal tar compound may occur on the aromatic ring, or if the arene has a side chain, the MnO_4^- ion may also attack a benzylic hydrogen; it is also possible that both reactions could occur on the same molecule. It can be expected that the mechanisms and the rates of reactions will be quite diverse for the different creosote/coal tar compounds, and the reactivity of the arenes to oxidation will be dependant on its chemical structure.

4.3 Experimental Methods

4.3.1 Overview

The rate at which the aromatic compounds were degraded was measured using two methods. In the first method the concentration of the $KMnO_4$ was varied while the concentration of the aromatic compound was held constant. In the second method the $KMnO_4$ concentration was held constant and the concentration of the aromatic compound

was varied. For all reactions $KMnO_4$ was in at least a 10 fold molar excess above that of the organic compound. The concentration range of $KMnO_4$ used for the reactions varied between 0.09 and 15 g/L. See Appendix 1 for the balance oxidation/reduction reactions.

4.3.2 Materials

The aromatic compounds benzene (>99%), methylbenzene (>99%), ethylbenzene (>99%), isopropylbenzene (99%), tert-butylbenzene (99%), naphthalene (99%), 1-methylnaphthalene (98%), 2-methylnaphthalene (97%), biphenyl (99%), anthracene (99.9%), phenanthrene (98%), fluoranthene (98%), chrysene (98%), pyrene (99%), acenaphthene (99%), fluorene (98%), carbazole (99%) and dibenzofuran (99%) were obtained from Aldrich Chemical (Milwaukee, WI) and used as received. Analytical reagent grade $KMnO_4$ and sodium bisulfite used to quench the reactions were obtained from BDH and used without further purification. All reactions were performed in unbuffered Milli-Q water.

4.3.3 Kinetic Experiments with Naphthalene, 1-Methylnaphthalene, 2-Methylnaphthalene, Biphenyl, Anthracene, Phenanthrene, Fluoranthene, Chrysene, Pyrene, Acenaphthene, Fluorene, Carbazole and Dibenzofuran

Kinetic experiments with the creosote compounds were performed in a two neck round bottom flask (500 mL) under a positive pressure of nitrogen at room temperature (21 ± 1 ^{o}C). Individual or groups of organic compounds were dissolved in acetone. 1 ml of the acetone stock solution was added to 500 mL of Milli-Q pure water and stirred for one hour. A sample was then taken, extracted with methylene chloride (CH_2Cl_2) and analyzed on a gas chromatograph (GC) to determine the concentration of the organic compound initially added. $KMnO_4$ was then added as a freshly prepared concentrated solution via a syringe through a septum. For the chemical reactions with carbazole, phenanthrene, fluorene, pyrene and chrysene, permanganate was ground with a mortar and pestle to a very fine powder and quickly added as a solid to a stirring solution through the septum. $KMnO_4$ is very soluble in

water with an aqueous solubility limit of 32.6 g/L at 5 ^{o}C (Perry et al., 1984). To test the method, finely ground solid $KMnO_4$ was added to 0.5 L of water to give concentrations of 5, 1 and 0.5 g/L. For each trial the concentration had reached its maximum concentration within 5 to 10 seconds. The error associated with the time needed to dissolve solid $KMnO_4$ was considered to be small with respect to the time frame of the experiments. The experimental data were also very reproducible (see Appendix 2) which supports the statement that the dissolution of the solid $KMnO_4$ was rapid compared to the oxidation of these compounds. Water samples from the reaction mixtures were collected during the experiments as either 13 or 50 mL samples *via* a glass syringe. The water samples were added to 15 mL or 60 mL crimp topped hypervials containing 1 mL or 3 mL of a saturated solution of sodium bisulfite ($NaHSO_3$) in order to quench the reaction by reducing $KMnO_4$ to Mn^{2+}. CH_2Cl_2 (2 mL) containing an internal standard (2-fluorobiphenyl) was then added to the mixture. The vials were sealed with a tegrabond Teflon septum and aluminum seal (20 mm) and were shaken on an orbital shaker set at 3500 rpm for 20 minutes before analysing. The CH_2Cl_2 extracts were analyzed on a temperature programmed Hewlett Packard HP5890A gas chromatograph using a 30 m DB5 (Chromatographic Specialties) capillary column with a 0.25 mm i.d. and 0.25 μm film thickness. A split/splitless auto injector was used in the splitless mode and maintained at 275° C. Chromatographic conditions were: initial oven temperature 40° C for 0.5 min; ramp to 300° C at 15° C/min., and hold for 10 min. The flame ionization detector (FID) was maintained at 325° C with a helium carrier gas flow rate of 25 mL/min. Quantification was accomplished by an internal standard method using augmented standards prepared from commercially available PAH mixtures (Supelco, Bellefonte, PA).

Chrysene and anthracene have aqueous solubilities of 2 and 40 μg/L with minimum detection limits of 6.30 and 3.63 μg/L respectively. To obtain concentrations of chrysene and anthracene that could be measured during the experiments the compounds were dissolved in acetone and added very slowly to obtain concentrations above their aqueous solubility limits. The volume of stock anthracene or chrysene added to 500 mL of water was between 0.2 to 0.5 mL. The solutions were stirred for one hour and solids were not observed in the saturated

solution. This method was tested by adding 0.2 mL of a stock chrysene solution to 1L of water. Six trials gave an average concentration of 50 μg/L with an uncertainty of 9.4 μg/L, as given by the 95% confidence interval.

The above compounds are semivolatile and the method used did not minimize head space during the reaction. To monitor any potential loss of organic compound due to volatilisation, controls were performed using the same procedure with Milli-Q water instead of the $KMnO_4$ solution. The controls showed no significant loss of the PAHs and were not used to adjust experimental data.

4.3.4 Kinetic Experiments with Benzene and the Alkylbenzenes, Methylbenzene, Ethylbenzene, Isopropylbenzene and tert-Butylbenzene

Benzene, methylbenzene, ethylbenzene, isopropylbenzene and tert-butylbenzene are volatile organic compounds and the method used minimized head space. The reactions were performed in 22 mL crimp topped hypovials. The vials were filled with a freshly prepared $KMnO_4$ solution. To the $KMnO_4$ solution a stock solution (12.5 μL) containing a mixture of benzene, methylbenzene, ethylbenzene, isopropylbenzene and tert-butylbenzene in methanol was added and the vial was quickly sealed with a tegrabond Teflon septa and aluminium seal (20 mm). The vials were shaken on an orbital shaker set at 3500 rpm. After a specific amount of time 14 mL of the solution was removed and added to a 22 mL crimp top vial containing sodium bisulfite (1 g) sealed, and then shaken to quench the reaction. Head space analysis was then performed on the vial as described below. Controls and blanks were also performed during the experiments. Calibration standards were prepared by filling a 22 mL vial with organic-free water and removing 8 mL from the total volume. Vials were quickly spiked with a methanolic stock solution, sealed and then analyzed.

4.4 Chemical Analysis

4.4.1 Analysis of Naphthalene, 1-Methylnaphthalene, 2-Methylnaphthalene, Biphenyl, Anthracene, Phenanthrene, Fluoranthene, Chrysene, Pyrene, Acenaphthene, Fluorene, Carbazole and Dibenzofuran

The CH_2Cl_2 extracts were analyzed on a temperature programmed Hewlet Packard HP5890A gas chromatograph using a 30 m DB5 (Chrom. Spec.) capillary column with a 0.25 mm i.d. and 0.25 μm film thickness. A split/splitless auto injector was used in the splitless mode and maintained at 275° C. Chromatographic conditions were: initial oven temperature 40° C for 0.5 min; ramp to 300° C at 15° C/min., and hold for 10 min. The flame ionizing detector (FID) was maintained at 325° C with a helium carrier gas flow rate of 25 mL/min. Quantification was accomplished by an internal standard method using augmented standards prepared from commercially available PAH mixtures (Supelco, Bellefonte, PA). The internal standard used was 2-fluorobiphenyl.

4.4.2 Analysis of Benzene, Methylbenzene, Ethylbenzene, Isopropylbenzene and tert-Butylbenzene

The reaction samples and calibration spikes were run on a Hewlett Packard 5890 gas chromatograph equipped with a split injection port, capillary column, PID and a Varian Genesis headspace autosampler. Peak areas were measured by a HP 3392A integrator and an ESTD method of calibration was used. Detection limits for these compounds were found to be 2-15 ppb (μg/L) using the EPA procedure for Method Detection Limit (MDL). The column used was a Stabilwax 30 m x 0.32 mm column with an internal diameter of 0.5 μm film thickness. The carrier gas used was helium at 3.5 mL/min. The injector was split 10:1 and was set at 150^{o}C. Column conditions were: oven 65^{o} C, isothermal, and detector PID (10.2 eV), 150^{o}C with helium makeup gas at 30 mL/min.

4.4.3 Identification of Oxidation Intermediates

The CH_2Cl_2 extracts were analyzed on a Varian CP-3800 GC using the same column and chromatographic conditions as given in section 4.4.1. The Varian Saturn 2000 mass spectrometer was run in the E.I. mode. Identification of 9,10-anthraquinone and 9-fluorenone was accomplished by matching mass spectra to those of authentic samples of 9,10-anthraquinone (99%) or 9-fluorenone (98%) obtained from Aldrich. Tentative identification of acenaphthenone was conducted through the mass spectrum library search because no authentic standard was available.

4.4.4 Analysis of $KMnO_4$

Permanganate concentrations were measured using an Ultraspec Plus(4054) UV/Vis spectrophotometer at 525 nm. Experimental samples were diluted with Milli-Q water to a concentration between 0.01 and 0.1 g/L so that the measured concentration would fall within the calibration range. The permanganate concentration was determined after the solid or concentrated solution of $KMnO_4$ was added to the reaction mixture and also at the end of each experiment.

4.5 Results and Discussion

4.5.1 Kinetics

The overall general equation for the irreversible bimolecular reaction for the destruction of an aromatic compound with $KMnO_4$ is given by,

$$\text{Aromatic compound} \xrightarrow{MnO_4^-} \text{oxidized products} \qquad (4.3)$$

The kinetic rate law for equation 4.3 can be described by,

$$r_C = \frac{dC}{dt} = -k_C [C]^{\alpha} \left[\mathrm{MnO_4^-}\right]^{\beta} \tag{4.4}$$

where C is the aromatic compound, r_C is the decay rate, k_C represents the oxidation rate constant, and α and β are the reaction orders with respect to [C] and [$KMnO_4$].

In all the experiments the concentration of $KMnO_4$ was at least in a 10 fold molar excess and should not change significantly during the course of the experiment. Hence, the reaction becomes pseudo-first-order and equation 4.4 can be simplified as equations 4.5 and 4.6,

$$r_C = -k_{\mathrm{obs}} [C]^{\alpha} \tag{4.5}$$

$$k_{\mathrm{obs}} = k_C \left[\mathrm{KMnO_4}\right]^{\beta} \tag{4.6}$$

where k_{obs} is a pseudo-first-order rate constant and the order of the reaction is α. By varying the values of [C] and measuring the reaction rate, the order α with respect to [C] can be determined by a log-log form of equation 4.5,

$$\log r = \log k_{obs} + \alpha \log[C] \tag{4.7}$$

To avoid complications from subsequent reactions or catalysts an initial rate method was used (Casado et al., 1986) and equation 4.5 can be expressed as,

$$\log r_0 = \log k_{obs} + \alpha \log[C]_0 \tag{4.8}$$

Similarly by varying the concentration of [$KMnO_4$] for each experiment and determining k_{obs}, the order β with respect to [$KMnO_4$] can be obtained by a log-log form of equation 4.6,

$$\log k_{obs} = \log k_C + \beta \log[MnO_4^-] \quad (4.9)$$

k_{obs} is obtained by using the integrated form of equation 4.5,

$$\ln [C]_t = - k_{obs}\, t + \ln [C]_0 \quad (4.10)$$

Based on the equation 4.8, α can be estimated using initial rates of reaction. Experiments were conducted in which the $KMnO_4$ concentration for each trial was held constant while the initial arene concentration was varied. $KMnO_4$ concentrations were chosen to allow the reactions to proceed within a reasonable time frame. Reaction conditions are given in Table 4.2. The order of the reaction was calculated through a linear regression of the logarithm of initial rate versus the logarithm of initial organic concentration as shown in Figure 4.1 for naphthalene. The oxidation of naphthalene is representative of the data obtained for the oxidation of arenes that reacted with $KMnO_4$, except for fluoranthene and pyrene which is discussed in later sections. As seen in Table 4.3, the order of the reaction (α) for the PAHs is approximately one. Thus the reaction order with respect to the organic compounds is approximately unity and k_{obs} represents a pseudo-first-order rate constant.

To establish the value of β, experiments were conducted in which the concentration of $KMnO_4$ was varied for each trial while holding the initial concentration of the arene constant. The pseudo-first-order rate constant, k_{obs} for each reaction at the specified $KMnO_4$ concentration, was obtained based on equation 4.10. The value of β was then determined by the plot of the logarithm of k_{obs} versus the logarithm of $KMnO_4$, as shown for naphthalene in Figure 4.1. The values obtained for β are given in Table 4.3. Biphenyl and dibenzofuran did not react under these conditions and the reaction rate for anthracene was too fast to be measured.

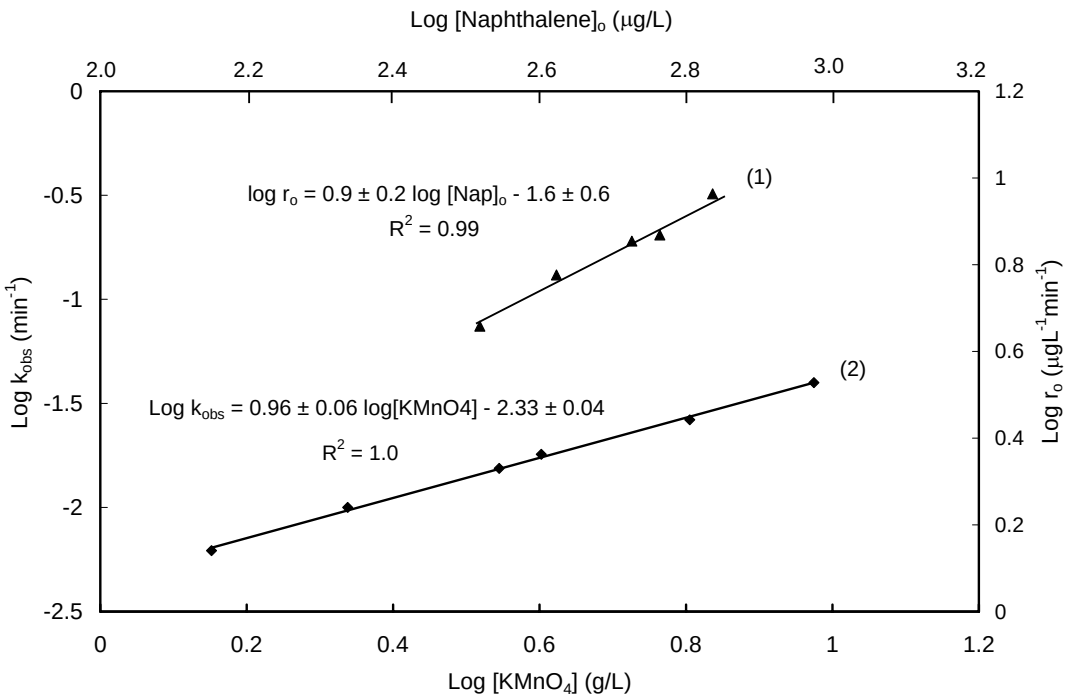

Figure 4.1 (1) Plot of initial rates versus initial concentration for five naphthalene experiments. The slope of 0.91 ± 0.06 confirms a first-order reaction with respect to naphthalene. (2) Plot of pseudo-first-order rate constant k_{obs} versus $KMnO_4$ concentration for Naphthalene. A slope $\beta = 0.96 \pm 0.02$ confirms a first-order reaction with respect to $KMnO_4$. The stated uncertainties reflect the 95% confidence limits.

Hence, the results from both experiments demonstrate that the initial reaction between the majority of the compounds and $KMnO_4$ can be approximated as second-order reactions with $\alpha = 1$ and $\beta = 1$. The values for α and β for chrysene, pyrene and fluoranthene vary more significantly from one. The oxidation of pyrene and fluoranthene is discussed in later sections and the larger deviation for chrysene could be the result of the method used. Chrysene was at concentrations above its aqueous solubility limit and errors would have been introduced if chrysene precipitated out of solution before or during the reactions. However, because of the reproducibility of the data (see Appendix 2) chrysene was included in the results.

Both sets of data can be used independently to calculate the second-order rate constants. The second-order rate constant can be determined by using equation 4.9 with $\beta = 1$ and plotting k_{obs} versus initial $KMnO_4$ concentration. The slope of the line provides the second-order rate constant (Figure 4.2). The second-order rate constant can also be determined by using the data set in which the initial concentration of the organic compound was varied; a plot of ln[C] versus time gives the pseudo-first-order rate constant k_{obs} and by dividing this value by the $KMnO_4$ concentration the second-order rate constant can be obtained (Figure 4.3). The second-order rate constants using both sets of data are given in Table 4.4. The uncertainties in k_C for the experiments in which the $KMnO_4$ concentration was varied are the 95% confidence intervals of the slope given by the linear regression calculation. For the experiments in which the initial arene concentration was varied, the uncertainty in k_C is given by the 95% confidence interval of experimental data.

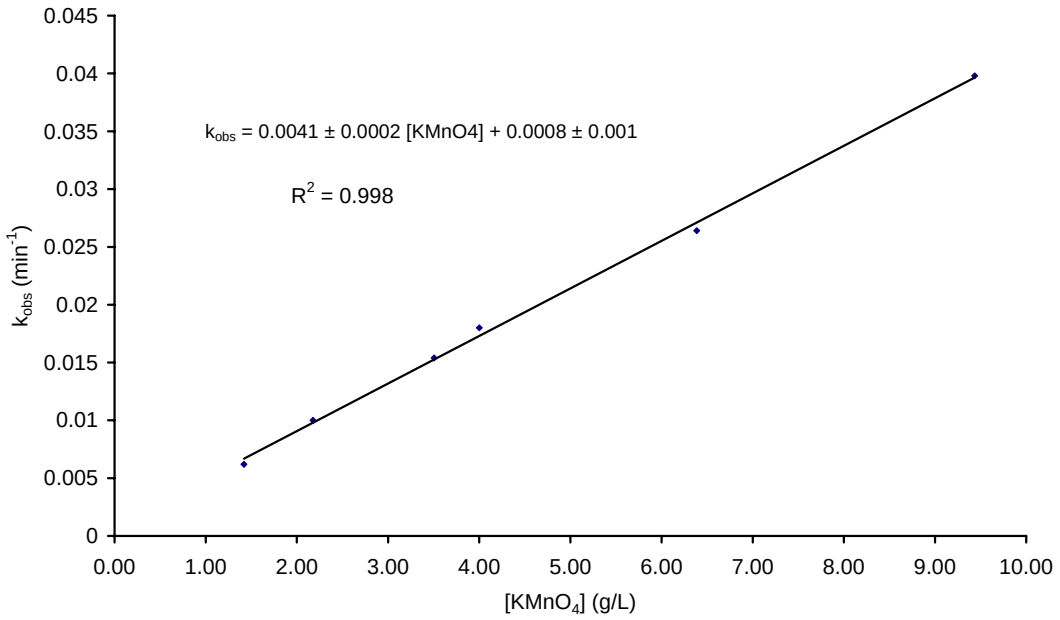

Figure 4.2. Determination of the second-order rate constant for naphthalene with $KMnO_4$. Naphthalene at 753 ± 26 μg/L was oxidized by $KMnO_4$ at concentrations varying from 1.42 to 9.44 g/L. The slope provides the second-order rate constant for naphthalene: $4.11 \times 10^{-3} \pm 8 \times 10^{-5}$ $(g/L)^{-1}min^{-1}$.

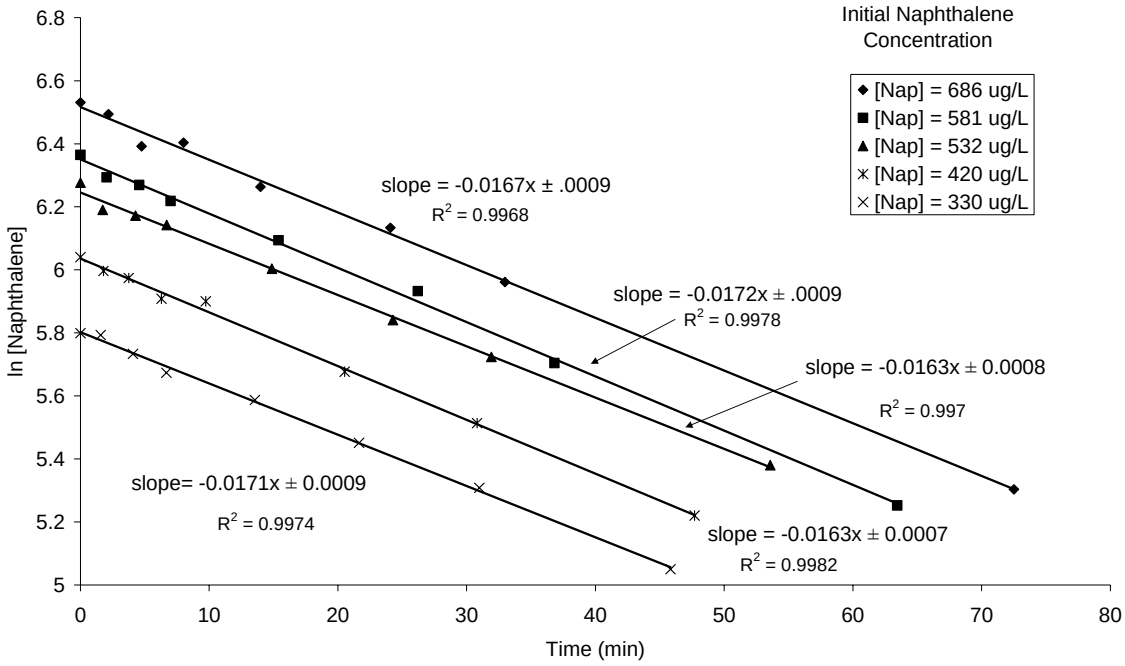

Figure 4.3. Pseudo-first-order plots of naphthalene ranging in initial concentrations from 686 to 330 μg/L with a constant concentration of $KMnO_4$ (3.83 g/L). Dividing the slope of the plots (k_{obs}) by the $KMnO_4$ concentration provides the second-order rate constant for naphthalene: $4.36 \times 10^{-3} \pm 6 \times 10^{-4}$ $(g/L)^{-1}min^{-1}$.

4.5.2 Oxidation of Fluorene

The oxidation of fluorene produced the intermediate 9-fluorenone (equation 4.11) as confirmed by GC/MS analysis. 9-Fluorenone was then oxidized to below detection limits over a 4 day time period. No other partially oxidized products were observed in the CH_2Cl_2 extracts, although oxidized products may have been present in the water phase. The percent conversion of fluorene to 9-fluorenone was not determined in these experiments but should be determined in future studies. This reaction has been reported as early as 1894 in which fluorene was readily oxidized with sodium dichromate in acetic acid to produce 9-fluorenone (Clar, 1964a).

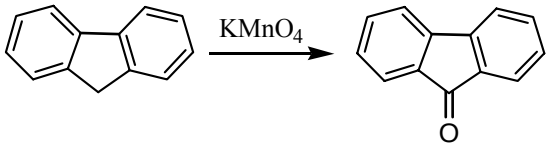

(4.11)

4.5.3 Oxidation of Acenaphthene

The oxidation of acenaphthene followed pseudo-first-order decay but also formed an unstable by-product, tentatively identified as acenaphthenone. The concentration versus time graph of acenaphthenone showed a rapid increase in concentration followed by a rapid decrease in concentration, indicating further oxidation of the ketone (Figure 4.4). The molar conversion of acenaphthene to acenaphthenone was not determined. No other partially oxidized products were observed in the CH_2Cl_2 extracts, although oxidized products may well have been present in the water phase.

The observed oxidation rate for acenaphthene could be a combination of two mechanisms, either through the oxidation of the side chain of acenaphthene to acenaphthenone followed by ring destruction or through the direct oxidation of the naphthalic ring system (equation 4.12). Both reactions are equally likely to occur since both pathways would have similar rate constants, as seen in the oxidation of naphthalene and ethylbenzene with rate constants of 4.23×10^{-3} and 2.27×10^{-3} g $L^{-1}min^{-1}$ respectively. Reactivity and chemical structure are further discussed in section 4.6.

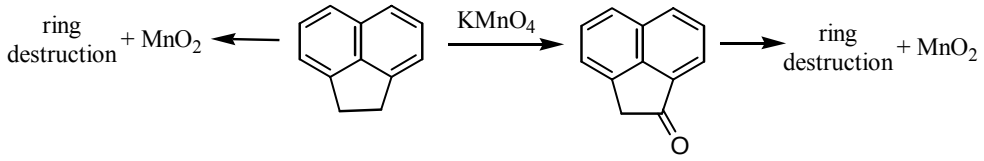

(4.12)

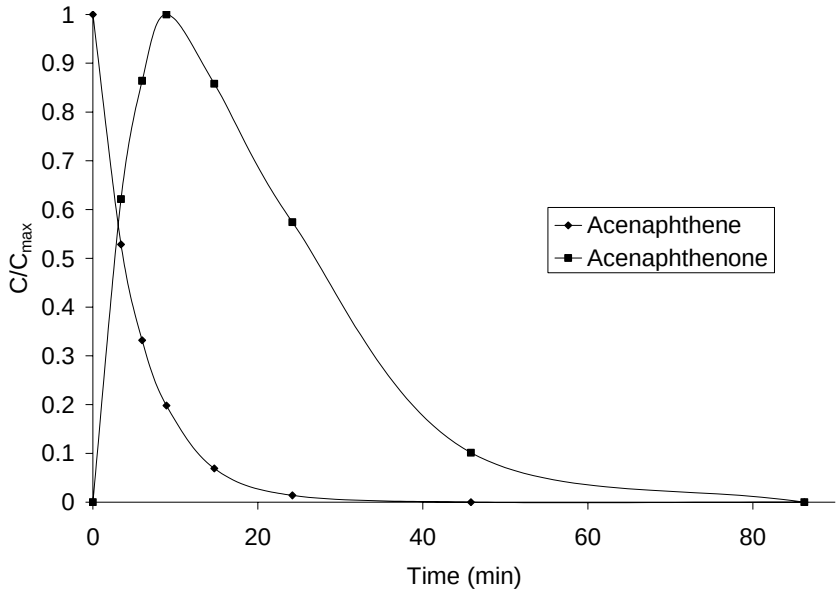

Figure 4.4 Oxidation of acenaphthene and its unstable byproduct acenaphthenone. Concentrations are relative to the maximum concentration observed for each compound based on GC/FID peak areas.

4.5.4 Oxidation of Fluoranthene

Fluoranthene did not follow a normal degradation curve, as seen in Figure 4.5 in which data from both methods is given. The initial reaction occurred within approximately the first minute and then the concentration remained relatively constant for at least 7 hours (not shown). Control experiments, in which no oxidant was added, showed no significant loss of fluoranthene. To determine α, β and the second-order rate constant, only the initial two or three data points were used. Thus the values are approximate and only apply to the initial reaction rates before the reaction stops. Interestingly, the second-order rate constants determined using the two different experimental methods were extremely close, 0.37 ± 0.09 and 0.34 ± 0.06 $(g/L)^{-1}min^{-1}$.

Analysis of the CH_2Cl_2 extracts by GC did not show any partially oxidized products although oxidized products could have present in the aqueous phase. It was interesting to

note that as the concentration of $KMnO_4$ increased, the percentage of fluoranthene removed increased (Figure 4.6). A possible explanation is the formation of an equilibrium between the σ-complex intermediate and the starting material. When the concentration of $KMnO_4$ is increased the equilibrium is shifted to the formation of oxidized products.

As stated in the Introduction, the mechanism for an electrophilic aromatic substitution reaction involves the addition of an electrophile to form an intermediate σ-complex which is followed by the loss of a proton from the adduct.

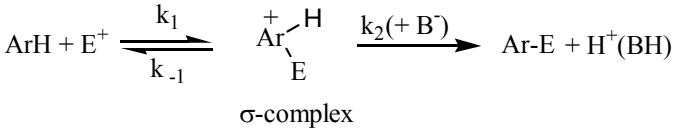

(4.13)

As seen in equation 4.13, if $k_2 >> k_{-1}$, the overall rate of the reaction is determined by the rate of the first step, but if k_2 is equal to or less than k_{-1}, the intermediate is partitioned between product formation and reversion to the starting material. Examples of electrophilic aromatic substitution reactions that follow a similar pathway include sulfonation, diazonium coupling of phenols, iodination of phenol and aniline. Kinetic understanding of these reactions involves observing deuterium and tritium isotopic effects in the formation of the product. These experiments show a positive isotope effect which supports the two-step mechanism. The equilibrium between k_1 and k_{-1} can be altered through steric effects, changing the concentration of base, or by using a more reactive electrophile (Taylor, 1990).

Fluoranthene could undergo a similar mechanism, but in this case the substituted product was not isolated and the reaction involved many more steps in the oxidation process. It was beyond the scope of this study to determine the more complex kinetics and the mechanism is only present here as a possible explanation of the results observed.

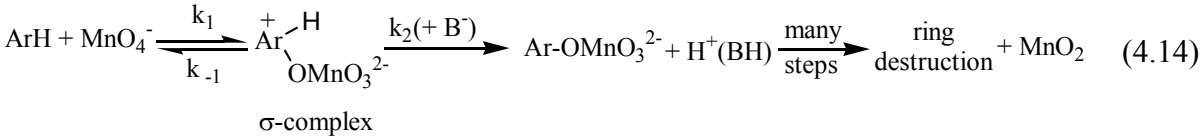

(4.14)

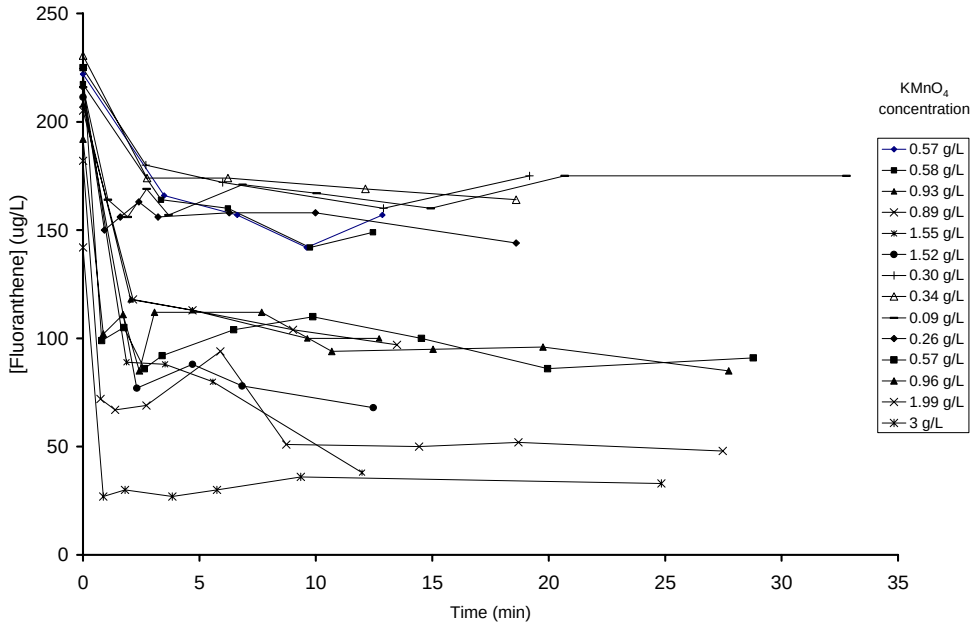

Figure 4.5. Oxidation of fluoranthene with $KMnO_4$ using all data. Fluoranthene and $KMnO_4$ concentration were varied between 144 and 499 μg/L, 0.09 and 3 g/L respectively. Only early times are shown. The fluoranthene concentration remains relatively constant for at least 7 hours.

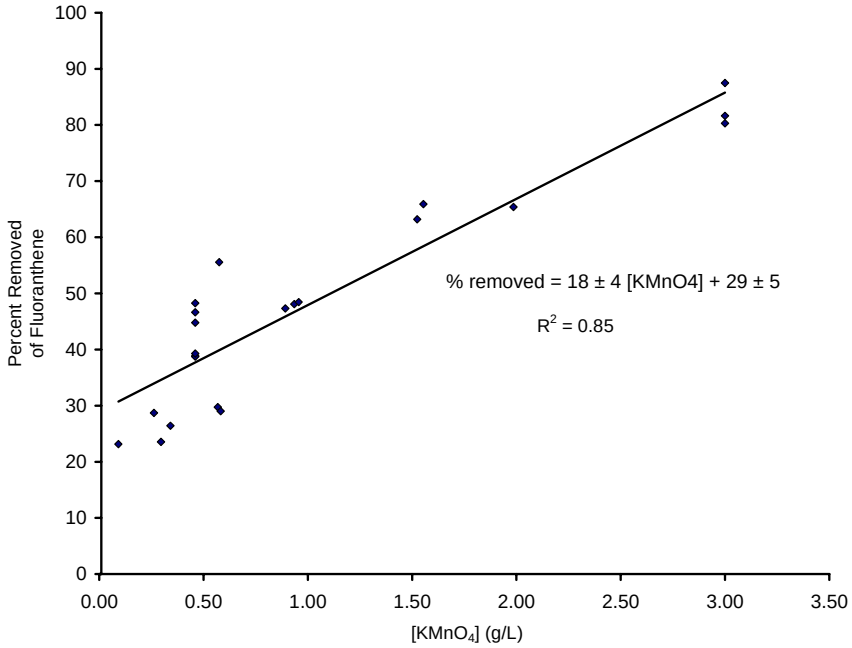

Figure 4.6. Oxidation of fluoranthene with $KMnO_4$ at various concentrations of fluoranthene and $KMnO_4$. As the concentration of $KMnO_4$ is increased, the percentage of fluoranthene removed also increased.

4.5.5 Oxidation of Anthracene

Anthracene reacted similarly to fluoranthene, in that an initial rapid decrease was observed, however a correlation between the concentration of $KMnO_4$ added and percentage of anthracene removed was not observed. The percentage of anthracene oxidized varied between 30 and 100%. The procedure was slightly modified to try to monitor early times of the reaction. In a 22 mL crimp top hypovial containing a $KMnO_4$ solution (20 mL) and sealed with a tegrabond Teflon septum, a stock solution of anthracene (0.5 mL) was added with a glass syringe through the septum. The entire reaction was then quickly quenched by adding 1 mL of a saturated bisulfite solution via a syringe. The water was then extracted as outlined in the Materials and Methods section. Using this method the reaction could be stopped in 5 seconds. In a series of reactions starting with the same initial concentration of anthracene (167 μg/L) and $KMnO_4$ (5.2 g/L), five experiments were run with increasing reaction times from 5 to 19 seconds. All five experiments produced the same decrease in concentration indicating that, like fluoranthene, a rapid initial reaction occurs and then no further oxidation is observed. Reactions were only monitored for a maximum of one hour.

The oxidation of anthracene produced a stable oxidized product, 9,10-anthraquinone which was identified using GC/MS. The partial oxidation product formed in this reaction was not an unexpected result because it is well known that the oxidation of anthracene with chromic acid, electrolytic oxidation and catalytic oxidation with air readily forms the very stable 9,10-anthraquinone (Clar, 1964b). The percent conversion of anthracene to 9, 10-anthraquinone was not determined.

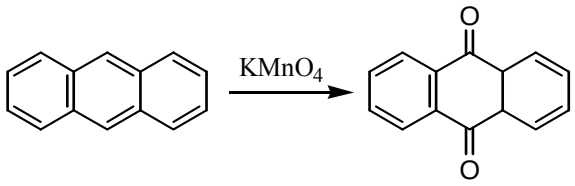

9,10-anthraquinone

(4.15)

4.5.6 Oxidation of Pyrene

The oxidation of pyrene was very rapid. The plot of concentration versus time showed an initial rapid decrease in concentration followed by a slowing in the oxidation rate. As seen in Figure 4.7, the experimental data for the decomposition did not follow the pseudo-first-order rate decay at earlier times, although a correlation was observed at later times (greater than 1 minute). The data also did not fit a second-order rate expression. Deviation from a pseudo-first-order reaction becomes more evident in the calculation of k_c in that the plots of k_{obs} versus $KMnO_4$ concentration produced the most scatter (r^2 =0.69). Also, k_c, (determined from the set of data in which the $KMnO_4$ concentration was held constant for each trial), differs by approximately a factor of two (Table 4.4). The reaction of pyrene could be similar to that of fluoranthene, except in equation 4.14, k_{-1} would be smaller than that for fluoranthene and complete oxidation of pyrene occurs. Further investigation is necessary to arrive at a better understanding of the mechanism that is occurring.

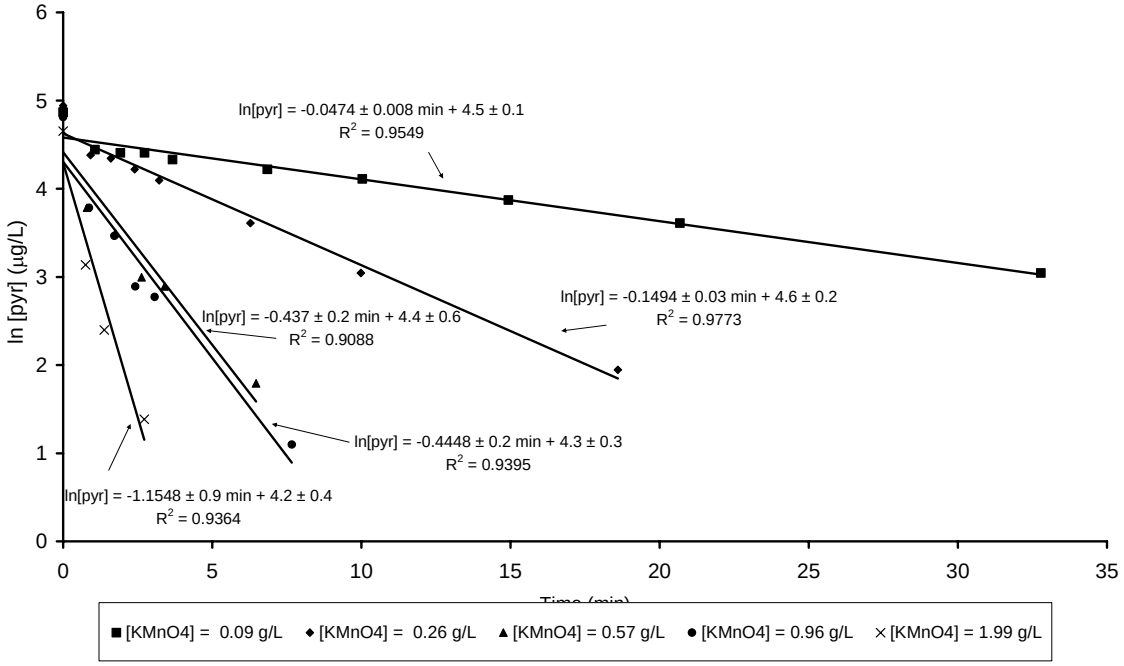

Figure 4.7 Oxidation of pyrene; rapid initial oxidation followed by a decrease in the rate of decomposition. Reaction appears to follow pseudo-first-order kinetics at later times [Pyrene] = 127 ± 15 µg/L

4.5.7 Oxidation of Benzene and Substituted Benzenes

To complement the study of the oxidation of polyaromatic hydrocarbons by $KMnO_4$, benzene and a series of substituted benzenes were also studied. For these compounds a series of reactions was performed in which the $KMnO_4$ concentration was varied while holding the initial concentration of the organic constituents constant. The concentration of $KMnO_4$ was in excess.

The oxidation of methylbenzene, ethylbenzene and isopropylbenzene showed a typical pseudo-first-order decay and the value of β and the second order rate constants were determined as described in section 4.5.1. The reaction conditions, β and the second-order rate constants are shown in Tables 4.2 to 4.4. For the calculations it was assumed that the value of α is one. No partially oxidized products were observed in the head space analysis although, water soluble oxidized products may be present in the aqueous phase.

Both benzene and t-butylbenzene failed to react at room temperature. Neither compound posses benzylic hydrogens, thus the most probable pathway to oxidation is through an electrophilic attack by the MnO_4^- ion on the aromatic ring. Under these conditions at room temperature, $KMnO_4$ is not a sufficiently strong electrophile, and no measurable rate of reaction was observed.

The oxidation of methylbenzene, ethylbenzene and isopropylbenzene followed the order of reactivity that was determined by Loachev and Rudakov, i.e. the order of reactivity for the alkylbenzenes follows the bond strength of the benzylic C-H bond or their bond dissociation energies. The bond strength decreases from primary, secondary to tertiary hydrogens and the order of reactivity increased in the same order: $C_6H_5CH_3 < C_6H_5CH_2CH_3 \leq C_6H_5CH(CH_3)_2$. Data for each compound are shown in Appendix 2.

4.6 Chemical Structure and Reactivity

In addition to calculating rates of reaction, it is desirable to relate reactivity to a readily available chemical or physical property in order to predict the rate of oxidation of different polycyclic aromatic compounds. As stated in the Introduction, it has been shown that the reaction of arenes with MnO_4^-, either occurs through the abstraction of a benzylic hydrogen atom in which case the rate is controlled by the C-H bond dissociation energy (bond strength), or through an electrophilic aromatic substitution reaction in which case it maybe possible to relate reactivity to the compounds ionization potential (the ability to donate electrons). Both bond dissociation energy and ionization potentials are gas phase properties and therefore can only approximate the energies involved in an aqueous solution since the values neglect solvent effects, the ionic nature of permanganate and the steric interactions between the reacting species.

4.6.1 Electrophilic Aromatic Substitution and Reactivity

For compounds that do not possess benzylic hydrogens, the major pathway to ring destruction is through an electrophilic attack of the MnO_4^- ion on the aromatic ring. A key intermediate for all electrophilic aromatic substitution reactions (nitration, sulfonation, halogenation, etc.) involves the formation of the arene-reagent σ-complex through the donation of two π electrons to the electrophile. A measure of the ability of a molecule to donate electrons is its gas phase ionization potential. As shown in Figure 4.8 a trend is observed between second-order rate constants for pyrene, fluoranthene, phenanthrene and naphthalene and their ionization potentials. As the ionization potential decreases, or the ability to donate an electron increases, the rate of the reaction also increases. Chrysene reacts much slower than predicted from its ionization potential. This could be due to experimental errors or due to the over simplification of relating a gas phase physical measurement to a reaction that occurs in a solution with a slightly soluble compound and does not take into account solvent effects or steric interactions between the arene and the electrophile.

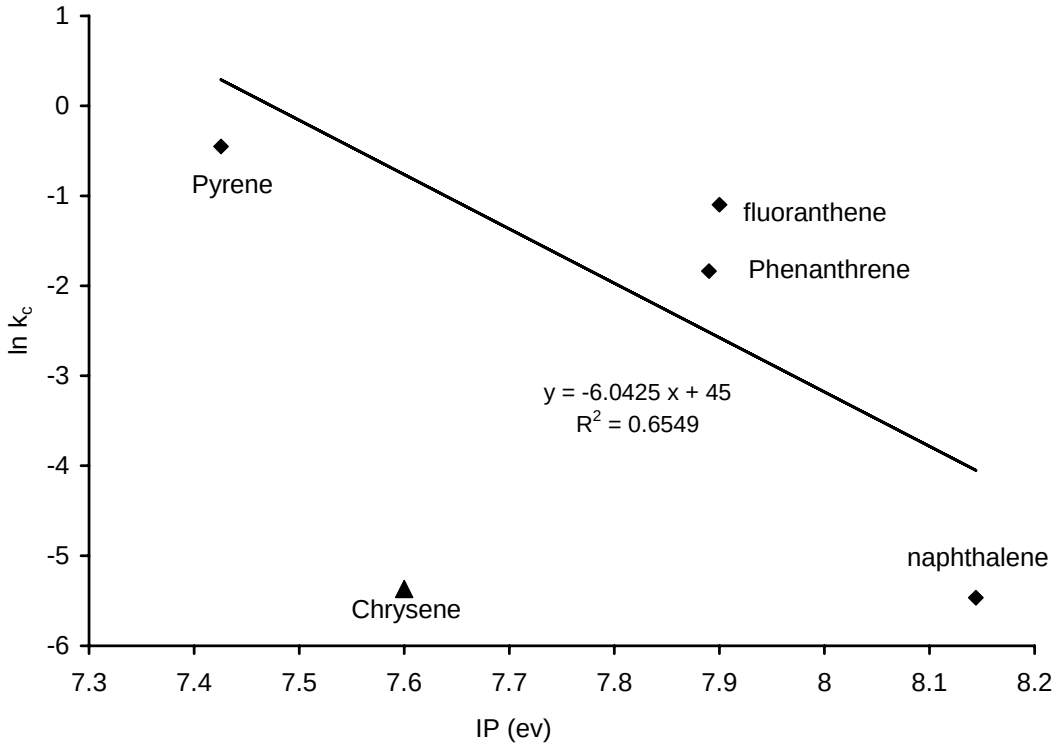

Figure 4.8. Correlation between second-order rate constants (k_C) and ionization potential (IP) for the polycyclic aromatic hydrocarbons pyrene, chrysene, phenanthrene, fluoranthene and naphthalene.

In most electrophilic aromatic substitution reactions the formation of the σ-complex is an endothermic process, and the free energy of the transition state is closely related to the intermediate that is formed. Thus there is parallelism between the formation of the intermediate and the transition state energy and it can be assumed that the more stable the intermediate, the faster it will form. This associates a thermodynamic property to a kinetic rate but relative reactivities of groups of polycyclics have shown good correlation with localization energies (Taylor, 1990).

To investigate this phenomenon, semi-empirical molecular orbital calculations were used to determine the relative change in the heat of reaction in the formation of the sigma complex. Calculations were performed using AM1 calculations as implemented in the

HyperChem™ program which gives the standard enthalpies of formation at 298 K, ΔH_f expressed as kilocalories per mole. The geometry of each structure was fully optimized followed by a single point calculation.

The heat of reaction in forming the sigma complex can be expressed as,

$$\Delta H_r = \Delta H_f(\sigma - complex_{(MnO_4^-)}) - \Delta H_f(MnO_4^-) - \Delta H_f(arene) \qquad (4.16)$$

The formation of the sigma complex is common to each molecule, thus for comparative purposes, it is only necessary to derive the energy required to reorganize the electrons in the formation of the sigma bond and the heat of formation of $KMnO_4$ can be left out of the equation. AM1 calculations do not calculate energies involving transition metals accurately, therefore, the sigma complex was simplified to a hydroxyl intermediate. The relative differences in complexation energy were thus calculated after the relationship,

$$\Delta H_{compl} = \Delta H_f(\sigma - complex_{(OH)}) - \Delta H_f(arene) \qquad (4.17)$$

For polyaromatic hydrocarbons there is more than one possible location in which the sigma complex could form. For example, in the oxidation of naphthalene the electrophilic aromatic ring attack could occur at positions 1 or 2, as shown in equation 4.18. The calculated heat of formation of the hydroxyl σ-complexes at position 1 and 2 shows that the σ complex resulting from electrophilic addition at position 2 is less stable than that resulting from addition at position 1. The more stable form was used in the calculation of ΔH_{compl}. This assumes that the most stable σ-complex corresponds to the most reactive position i.e., the relative stability of the intermediates determines the position under kinetically controlled conditions.

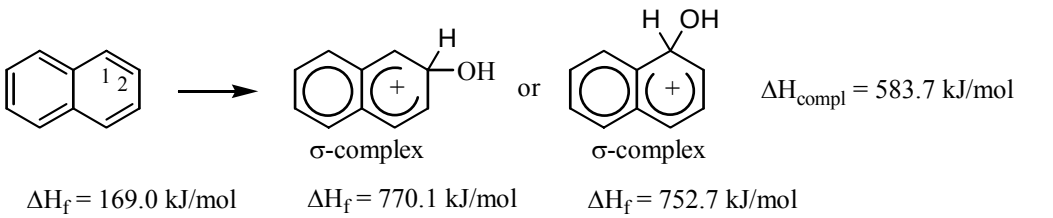

(4.18)

The trend between calculated stability of the σ-complex intermediate and reactivity is similar to the trend obtained for ionization potentials and reactivity as shown in Figure 4.9.

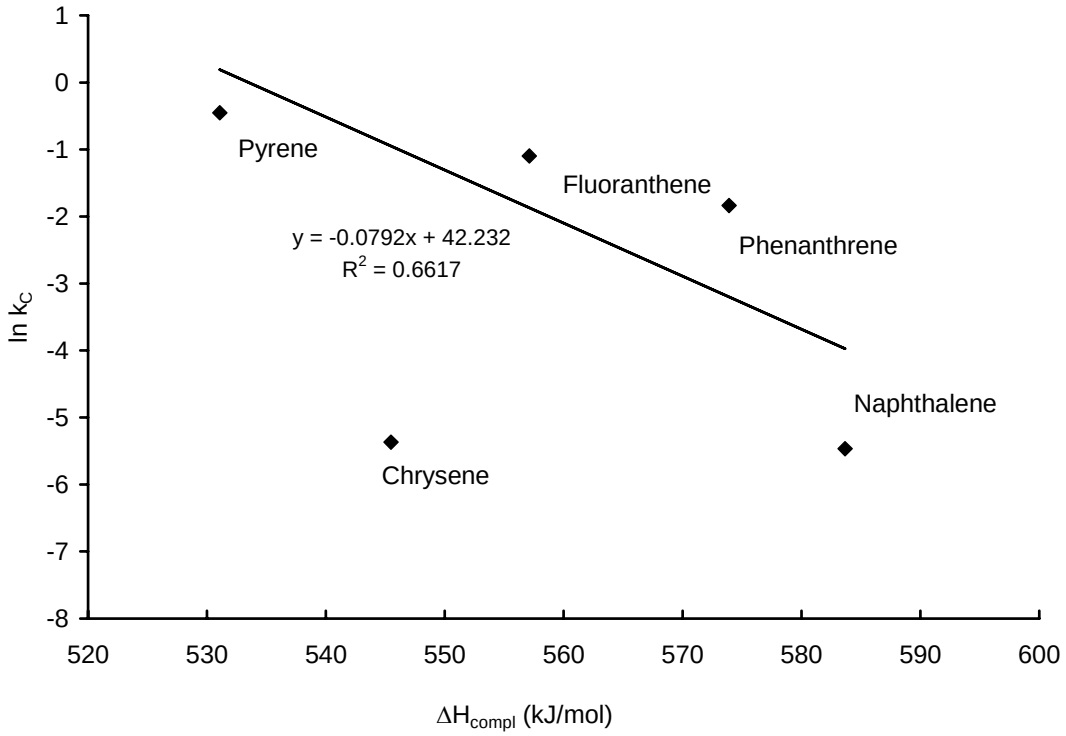

Figure 4.9. The dependency of the second-order-rate constants (k_C) of arene oxidation by $KMnO_4$ and calculated heat of complexation (ΔH_{compl}).

The ionization potential for anthracene is similar to that of pyrene, 7.439 and 7.426 eV respectively, but the rate of oxidation for anthracene is much faster than that of pyrene. The ionization potential of anthracene does not correctly predict its reactivity. In contrast, the calculated heat of complexation or the energy needed to form the σ-complex is much smaller

for anthracene than it is for pyrene, ΔH_{compl} = 519.2 and 531.1 kJ/mol respectively. This suggests that anthracene should react much faster than pyrene. Using the value of 519.2 kJ/mol in the equation given in Figure 4.9, a second-order rate constant of 3.3 $(g/L)^{-1}min^{-1}$ is obtained. The second-order rate constant calculated this way is only an approximation since the heats of formation of the true σ-complex intermediate was not calculated and was estimated using a hydroxyl group. Also more data points are needed to obtain a better correlation.

4.6.2 Side Chain Reactivity

Compounds that possess an alkyl side chain can either be attacked by the MnO_4^- ion through extraction of a benzylic hydrogen atom or through an electrophilic aromatic substitution reaction. Thus two possible reactions may occur on the same compound. If the reaction proceeds mainly through an alkyl side chain attack, the rate of reaction should correlate with the benzylic C-H homolytic bond dissociation energy, because the rate determining step involves the rupture of the C-H bond (Rudakov et al., 1994).

The relationship between the second-order rate constant for alkyl substituted benzenes and PAH's and their bond dissociation energies is shown in Figure 4.10. The second order rate constants were divided by the number of equivalent hydrogens to statically correlate for the number of active benzylic hydrogens. Carbazole, which has a N-H bond dissociation energy similar to that of isopropylbenzene, reacted far more readily than the bond dissociation energy implied. Carbazole did not follow the trend and was not included in the correlation given in Figure 4.10.

A trend was not found between reaction rates and σ-complex formation for carbazole, acenaphthene, 1-methylnaphthalene, and 2-methylnaphthalene. The poor correlation between rate constants and heats of formation of the sigma complex and good correlation between bond dissociation energies implies that side chain attack contributes significantly to

the observed rate of reaction. However, both reaction mechanisms could be occurring at the same time and the measured second-order rate constants are thus a combination of both mechanisms.

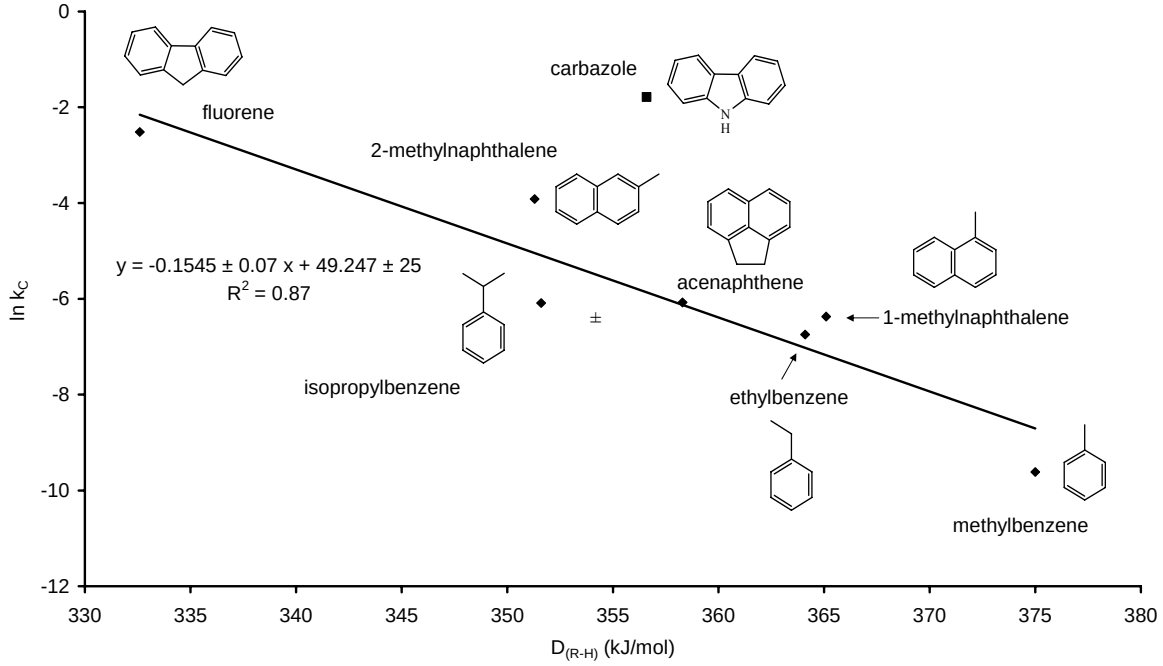

Figure 4.10. Correlation between second-order oxidation rates (k_c) divided by the number of equivalent benzylic hydrogens and bond dissociation energies (D_{R-H}).

4.6.3 Reactivity of the Heterocycles, Carbazole and Dibenzofuran

Carbazole and dibenzofuran have very similar structures; they both have a biphenyl aromatic ring system joined together by either nitrogen or oxygen. However, their reactivity towards MnO_4^- is considerably different. Carbazole reacts very rapidly whereas dibenzofuran does not react at all. The attack of MnO_4^- on carbazole may occur by the abstraction of the hydrogen atom bonded to the nitrogen or on attack on the aromatic ring. As seen in Figure 4.10 the rate of reaction is much faster than implied by the bond dissociation energy. This suggests ring oxidation is contributing significantly to the observed oxidation rate.

Both carbazoles and dibenzofurans are known to undergo electrophilic aromatic substitution reactions such as bromination and nitration (Gilman et al., 1935, Hand et. al, 1997, Hall 1992, Zhang et. al., 1995). A possible reason for the difference in reactivity is the ability of the heteroatom to activate the aromatic ring towards electrophilic aromatic substitution reactions. It is well known that both nitrogen and oxygen activate aromatic rings, through the donation of electrons into the σ-complex, but nitrogen, being less electronegative than oxygen, is a more powerful activating group. The biphenyl arene ring system is very stable (see section 4.7). Under these reaction conditions, it is possible that only nitrogen is a strong enough activator to assist the attack of MnO_4^- on the stable biphenyl ring system. However, it is not known which pathway, ring attack or hydrogen atom abstraction is the reason for carbazoles enhanced susceptibility to oxidation compared to dibenzofuran. The oxidation of carbazole by MnO_4^- is very complex and further experiments are needed to elucidate the mechanism.

4.7 Visual Inspection of Arene Topography and Reactivity towards $KMnO_4$

There are many factors that affect the rate at which a reaction proceeds and it is not until kinetic studies are performed that it can be said with certainty that one compound will react faster than another. But hydrogeologists and engineers are often faced with a suite of chemicals at a contaminated site and it would be advantageous to be able to predict whether a particular compound would be oxidized by MnO_4^-, what possible partially oxidized products could be formed and what compounds should be monitored for. Presented below is a simple method to determine if an aromatic compound will be oxidized by MnO_4^- and what possible oxidation products may be formed based on its chemical structure.

4.7.1 Polycyclic Aromatic Hydrocarbons

Clar (1972) presented an empirically based theory that elegantly described aromaticity in a very simple way that correlated topology with physical properties without the use of more complex molecular orbital calculations. The Clar structural formula for arenes was based on the Armit and Robinson's aromatic sextet. For example, in Figure 4.11 the structures for pyrene, phenanthrene and triphenylene are given. The dots represent isolated 2p electrons, whose interaction leads to formation of π molecular orbitals. Clar's proposal was to group the electrons to give the maximum number of rings consisting of six π electrons, i.e. benzenoid π-electron sextets. Thus Clar's formulas for pyrene and phenanthrene show that not all the rings can contain six π electrons. Phenanthrene is composed of two benzene-like regions and a double bond. Likewise pyrene consists of two benzenoid rings and two rings each with one double bond. Triphenylene, on the other hand, does not possess double bonds and is called an all-benzenoid compound. Just by looking at the Clar structure one would predict that phenanthrene and pyrene would be reactive because they possess regions with double bond characteristics. In contrast, triphenylene has three isolated benzene rings and so should be very stable. In fact this is what is observed: both phenanthrene and pyrene readily undergo electrophilic aromatic substitution reactions (Streitwieser and Heathcock, 1981), whereas triphenylene and other all-benzenoid hydrocarbons exhibit a pronounced chemical inertness (Gutman and Cyvin, 1989).

The structures of naphthalene and anthracene are also given in Figure 4.11. For naphthalene and anthracene the sextet could be in any of the rings. By convention, Clar proposed to describe naphthalene as structure (A) and assumed a migration from one ring to another. Again both of these compounds have double bond characteristics in their structures and both are readily oxidized in chromic acid (Fessenden and Fessenden, 1998).

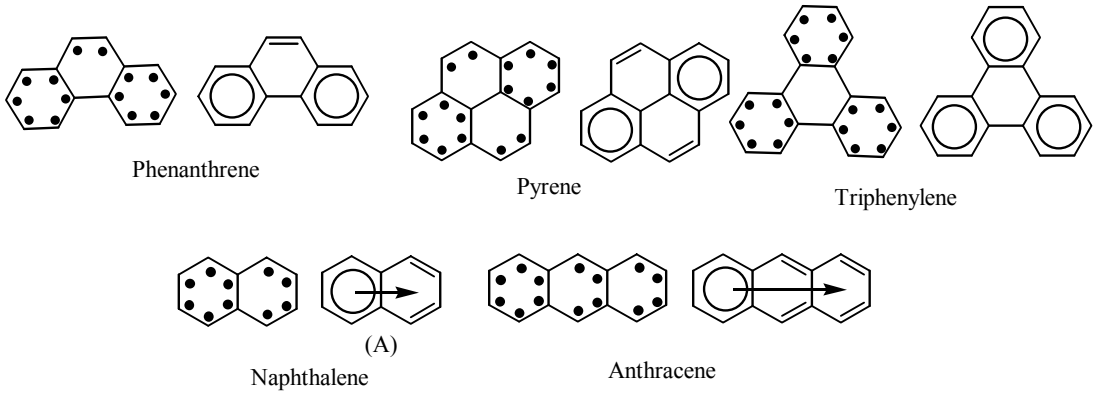

Figure 4.11. Clar's π sextet model of phenanthrene, pyrene, triphenylene, naphthalene and anthracene.

Generally, the rate of reactivity towards oxidation, reduction and electrophilic substitution reactions increases as the number of aromatic rings increases. This occurs because a polycyclic compound can undergo a reaction at one ring and still have one or more intact benzenoid rings in the intermediate and in the product. Thus, less energy is required to overcome the aromatic character of a single ring of the polycyclic compounds than is required for benzene. However, this is a generalization because the rate of a reaction can be affected by many factors such as steric interactions, reaction conditions and the connectivity of the aromatic rings.

The Clar model provides a quick and easy method to look at possible oxidation products that may form during the oxidation process. For example, in this study, the oxidation of anthracene by MnO_4^- readily produced 9,10-anthraquinone. Two potential reactions could have occurred: one in which the oxidation took place on an end ring, or in the central ring. Using the Clar structures it is observed that the most stable intermediate is formed when the attack is on the central ring because two benzenoid rings are formed instead of one. The product, once formed, is also very stable because the two benzene rings are isolated (Figure 4.12).

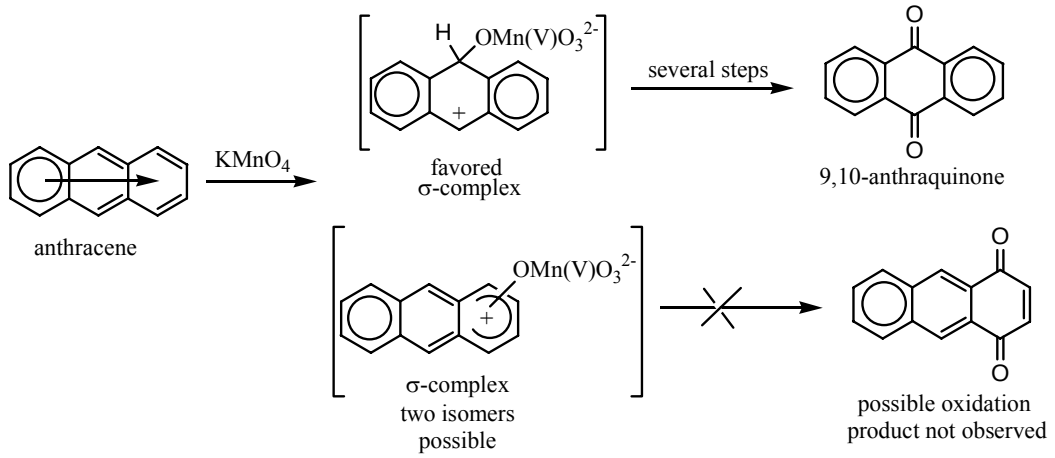

Figure 4.12. Oxidation of anthracene using the Clar sextet model to predict the oxidation product. Oxidized product will have the maximum number of sextets or benzenoid rings.

The oxidation of phenanthrene, chrysene and pyrene is shown in Figure 4.13 (Clar, 1964a and 1964b). Using Clar structures clearly helps to predict the major products in each reaction. The products that are formed all have the maximum number of benzenoid rings.

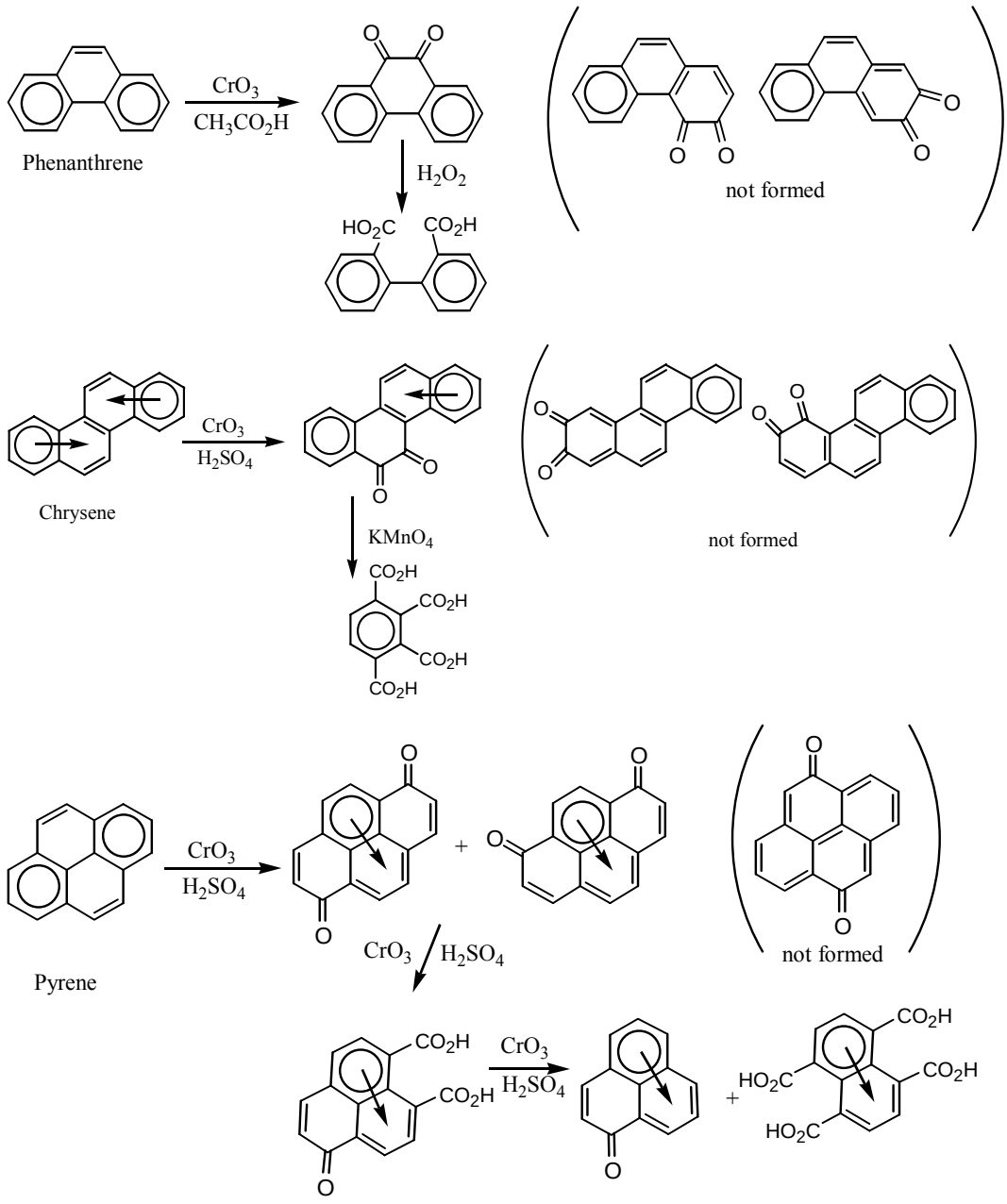

Figure 4.13 Oxidized products of phenanthrene, chrysene and pyrene that are formed contain the maximum number of benzenoid rings.

4.7.2 Substituted Arenes and Heterocycles

Benzene was not oxidized by MnO_4^- under the condition employed in this study. Benzene, being the simplest form of the Clar sextet, is very stable and is resistant to oxidation; although it is well known that alkylbenzenes with benzylic primary, secondary and tertiary hydrogens are oxidized by MnO_4^- to form benzoic acid. Thus, benzoic acids are potential oxidation products whose presence should be monitored for at a remediation site. If the alkyl benzene does not posses benzylic hydrogens as in the case with t-butylbenzene, oxidation at room temperature may not occur with MnO_4^-.

As previously discussed, oxidation of alkyl substituted polycyclic aromatic hydrocarbons could occur through a side chain attack or by an attack on the aromatic ring system. Thus the partial oxidation of compounds such as methylnaphthalenes would produce both naphthalic acids as well as ring oxidation products.

The partial oxidation of arenes containing secondary benzylic carbons that are part of a ring system will produce ketones as seen in the oxidation of fluorene and acenaphthene to fluorenone and acenaphthenone. In fact, peri-condensed hydrocarbons consisting of six-membered rings in which one carbon atom is bonded to two hydrogen atoms are more reactive than the methylene group in fluorene and its benzologues (Clar, 1964b). Thus ketones as well as carboxylic acids are potential oxidation products that may form in the oxidation of creosote/coal tars by MnO_4^-.

The Clar structures for biphenyl, dibenzofuran, and carbazole show two separate benzenoid rings linked by a C-C bond. The heterocycles dibenzofuran and carbazole are also biphenyl systems with an additional bond connecting the benzenoid rings through either an oxygen or nitrogen atom. Clar structures indicate a very stable aromatic system. This is indeed what is observed: biphenyl and dibenzofuran are both resistant to oxidation.

Carbazole, because of nitrogen's ability to donate electrons into the ring system and acidic hydrogen is more reactive than might be predicted by the Clar structures. Therefore, heterocycles that contain oxygen and nitrogen may or may not increase the reactivity of the arene toward oxidation and other considerations must be taken when contemplating their reactivity.

4.8 Conclusions

Room temperature oxidation of a selected group of creosote/coal tar compounds with excess MnO_4^- was successful in oxidizing naphthalene, phenanthrene, chrysene, pyrene, anthracene, carbazole, 1-methylnaphthalene, 2-methylnaphthalene, acenaphthene, methylbenzene, ethylbenzene and isopropylbenzene. The room temperature oxidation of benzene, tert-butylbenzene, biphenyl and dibenzofuran was unsuccessful. For the compounds that reacted with MnO_4^-, pseudo-first-order kinetic calculations were performed and the second-order rate constants were determined.

The mechanism of oxidation for the polycyclic aromatic hydrocarbons is most likely *via* an electrophilic aromatic ring attack. The rate of oxidation was shown to increase with an increasing number of rings because less energy is required to overcome the aromatic character of a polycyclic ring than is required for benzene. Thus the reactivity increased in the series: naphthalene < phenanthrene < pyrene. To assess the trend in reactivity and the ability of an arene to donate its aromatic π electrons to an electrophile, the second-order rate constants were compared to the arenes ionization potential and calculated heat of formation of the σ-complex intermediate. Both methods provided good correlations for naphthalene, phenanthrene, pyrene and fluoranthene but not for chrysene. Chrysene reacted much slower than predicted by either its ionization potential or calculated heat of complexation. This may be due to the oversimplification of relating gas phase physical constants and calculations to a highly ionic aqueous system with a compound that has a very low aqueous solubility and

does not take into account solvent effects or steric interactions between the arene and the electrophile.

The second-order rate constants derived in this study for pyrene and fluoranthene assume that the reaction follows first-order kinetics. In the case of pyrene the initial reaction is very rapid, slows down after approximately 1 minute, then closely follows a first-order rate decay. Fluoranthene also reacts rapidly but the reaction stops after one minute. Thus the second-order rate constants for these compounds are approximations and care must be taken when using these values for ground water numerical simulations.

In the oxidation of fluoranthene it was found that as the concentration of MnO_4^- was increased, the amount of fluoranthene oxidized also increased. A possible explanation for this phenomenon is the creation of a stable intermediate that is partitioned between product formation and reversion to the starting material. By increasing the concentration of MnO_4^- the equilibrium was shifted to the oxidation of fluoranthene. Similarly, in the oxidation of pyrene, the deviation from first-order kinetics could be caused by the formation of a stable intermediate, but in this case the intermediate is transient and complete oxidation of pyrene occurs.

Methylbenzene, ethylbenzene, isopropylbenzene, acenaphthene, fluorene, 1-methylnaphthalene, and 2-methylnaphthalene were all decomposed by MnO_4^-. Oxidation of the above compounds may occur via two different routes: by attacking the benzylic C-H bond or by attacking at the aromatic ring. The reactivity of these compounds is controlled by both the benzylic C-H bond strength (bond dissociation energy) and the ability of the aromatic ring to donate electrons in an electrophilic aromatic substitution reaction. Both alkyl substituted benzenes and substituted PAHs showed a good correlation between second-order rate constants and bond dissociation energies, but not between the rate constants and the calculated heats of complexation. This implies that side chain oxidation contributes significantly to the observed rate of reaction.

Compounds that have stable aromatic ring systems that do not possess benzylic hydrogens will be resistant to oxidation. In this study benzene, tert-butylbenzene, biphenyl and dibenzofuran did not react at measurable rates with MnO_4^- at room temperature.

Compounds	Structure	C_w (g/m^3)
PAH's		
Biphenyl	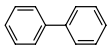	7.2 ± 0.5[a]
Naphthalene		31.5 ± 2[a]
Anthracene	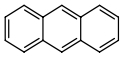	0.04 ± 0.005[a]
Phenanthrene	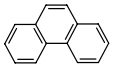	1.10 ± 0.02[a]
Fluoranthene	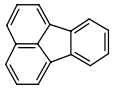	0.26 ± 0.06[a]
Chrysene	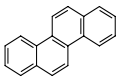	0.002 ± .001[a]
Pyrene	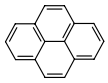	0.132 ± 0.02[a]
Heterocyclic PAH's		
Carbazole	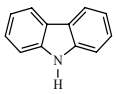	1.2 ± 0.4[b]
Dibenzofuran	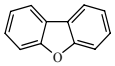	7.0 ± 0.8[b]

Compound	Structure	C_w (g/m^3)
Substituted PAH's		
1-methylnaphthalene		28 ± 2[a]
2-methylnaphthalene	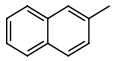	25.0 ± .7[b]
Fluorene	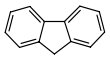	1.9 ± 0.1[a]
Acenaphthene		3.8 ± 2[a]
Benzene and substituted benzenes		
Benzene		1780 ± 20[a]
Methylbenzene		530 ± 20[a]
Ethylbenzene	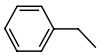	160 ± 20[a]
Isopropylbenzene	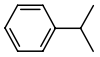	50 ± 5[a]
t-Butylbenzene	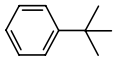	32[c]

[a] Shui et al., 2000.
[b] Pearlman et al., 1984.
[c] CRC Handbook of Chemistry and Physics, 2003.

Table 4.1 Selected creosote compounds; structures and aqueous solubilities (C_w).

Compound	$[C]_0$ Constant for each Trial			$[KMnO_4]$ Constant for each Trial		
	$[KMnO_4]$ (g/L)	$[C]_0$ (μg/L)	# of Trials	$[KMnO_4]$ (g/L)	$[C]_0$ μg/L	# of Trials
Polyaromatic						
Biphenyl	5.1 – 15	655 ± 5	6			
Naphthalene	1.42 – 9.44	753 ± 26	6	3.8 ± 0.1	330 – 686	5
Anthracene	0.04 – 5.3	50 ± 5	4			
Phenanthrene	0.57 – 1.55	491 ± 14	8	0.46 ± 0.02	144 – 369	6
Fluoranthene	0.09 – 1.99	217 ± 9	6	0.46 ± 02	66 – 163	6
Chrysene	2.07 – 4.83	129 ± 51	4	3.8 ± 0.1	9 – 26	5
Pyrene	0.57 – 1.57	90 ± 3	8	0.46 ± 0.02	27 – 73	6
Pyrene	0.09 – 1.99	127 ± 15	5			
Heterocyclic PAH						
Carbazole	0.57 – 1.55	471± 14	8	0.46 ± 0.02	128 – 344	6
Dibenzofuran	5.1 – 15	664 ± 42	6			
Substituted PAH's						
1-methylnaphthalene	1.42 – 9.44	650 ± 20	6	3.8 ± 0.1	292 – 597	5
2-methylnaphthalene	1.42 – 9.44	719 ± 23	6	3.8 ± 0.1	320 – 662	5
Fluorene	0.57 – 1.55	505 ± 13	8	0.46 ± 0.02	148 – 371	6
Acenaphthene	1.42 – 9.44	630 ± 42	6	3.8 ± 0.1	282 – 590	5
Benzene and substituted benzenes						
Benzene	7.0 – 14.5	4076 ± 56	4			
Methylbenzene	7.0 – 14.5	4397 ± 307	4			
Ethylbenzene	7.0 – 14.5	4995 ± 406	4			
Isopropylbenzene	7.0 – 14.5	5418 ± 268	4			
t-Butylbenzene	7.0 – 14.5	5494 ± 123	4			

Table 4.2 Experimental reaction conditions for the oxidation of selected creosote compounds by $KMnO_4$. The uncertainties specified are the standard deviation of the concentration for the given number of trials.

Compound	Alpha	r^2	Beta	r^2
Polyaromatic				
Biphenyl			NR[b]	
Naphthalene	0.9 ± 0.2	0.99	0.96 ± 0.06	1.00
Anthracene[a]				
Phenanthrene	0.9 ± 0.3	0.96	1.01 ± 0.07	0.99
Fluoranthene	0.7 ± 0.5	0.81	1.3 ± 0.1	1.0
Chrysene	1.3 ± 0.4	0.97	1.6 ± 0.7	0.98
Pyrene	0.86 ± 0.09	0.99	0.9 ± 0.3	0.80
Heterocyclic PAH				
Carbazole	0.9 ± 0.2	0.97	1.1 ± 0.1	0.93
Dibenzofuran			NR	
Substituted PAH's				
1-metlnaphthalene	1.0 ± 0.2	0.99	0.93 ± 0.1	1.00
2-metlnapphthalene	1.1 ± 0.1	1.0	0.93 ± 0.05	1.00
Fluorene	1.0 ± 0.5	0.90	1.1 ± 0.1	0.99
Acenaphthene	1.1 ± 0.2	0.99	0.96 ± 0.04	1.00
Benzene and substituted benzenes				
Benzene			NR	
Methylbenzene			1 ± 1	0.85
Ethylbenzene			0.86 ± 0.1	1.00
Isopropylbenzene			0.86 ± 0.5	0.95
t-Butylbenzene			NR	

[a] Reaction too fast to be measured
[b] No Reaction

Table 4.3. Reaction orders α and β with respect to the organic compound, [C] and [$KMnO_4$]. The uncertainties specified reflect the 95% confidence level.

Compound	k_C $[C]_0$ Constant $((g/L)^{-1}\ min^{-1})$	r^2	k_C $KMnO_4$ Constant $((g/L)^{-1}\ min^{-1})$	k_C Average $((g/L)^{-1}\ min^{-1})$	k_C Average $(M^{-1}\ s^{-1})$
PAHs					
Chrysene[1]	$4.1 \times 10^{-3} \pm 2.0 \times 10^{-3}$	0.98	$5.0 \times 10^{-3} \pm 5 \times 10^{-3}$	$4.7 \times 10^{-3} \pm 5 \times 10^{-3}$	$1.2 \times 10^{-2} \pm 1 \times 10^{-2}$
Naphthalene	$4.11 \times 10^{-3} \pm 2 \times 10^{-4}$	1.0	$4.3 \times 10^{-3} \pm 7 \times 10^{-4}$	$4.2 \times 10^{-3} \pm 7 \times 10^{-4}$	$1.1 \times 10^{-2} \pm 2 \times 10^{-3}$
Phenanthrene	$0.156 \pm 9 \times 10^{-3}$	1.0	$0.163 \pm 9 \times 10^{-3}$	$0.16 \pm 1 \times 10^{-2}$	$0.42 \pm 3 \times 10^{-2}$
Fluoranthene[2]	$0.37 \pm 9 \times 10^{-2}$	0.97	$0.34 \pm 6 \times 10^{-2}$	0.3 ± 0.1	0.9 ± 0.3
Pyrene[3]	0.4 ± 0.2	0.69	$0.836 \pm 7 \times 10^{-2}$	0.6 ± 0.2	1.7 ± 0.6
Anthracene					
Substituted PAHs and benzenes					
Methylbenzene	$2.01 \times 10^{-4} \pm 2 \times 10^{-4}$	0.85		$2.0 \times 10^{-4} \pm 6 \times 10^{-5}$	$5.3 \times 10^{-4} \pm 5 \times 10^{-4}$
Ethylbenzene	$2.34 \times 10^{-3} \pm 3 \times 10^{-4}$	0.96		$2.3 \times 10^{-3} \pm 8 \times 10^{-5}$	$6.0 \times 10^{-3} \pm 8 \times 10^{-4}$
Isopropylbenzene	$2.27 \times 10^{-3} \pm 1 \times 10^{-3}$	1.0		$2.4 \times 10^{-3} \pm 3 \times 10^{-4}$	$6.2 \times 10^{-3} \pm 2 \times 10^{-3}$
1-metnaphthalene	$5.9 \times 10^{-3} \pm 2 \times 10^{-4}$	1.0	$4.38 \times 10^{-3} \pm 7 \times 10^{-4}$	$5.1 \times 10^{-3} \pm 7 \times 10^{-4}$	$1.4 \times 10^{-2} \pm 2 \times 10^{-3}$
2-metnapphthalene	$6.5 \times 10^{-3} \pm 4 \times 10^{-4}$	1.0	$7.3 \times 10^{-3} \pm 1 \times 10^{-3}$	$7.3 \times 10^{-3} \pm 1 \times 10^{-3}$	$1.8 \times 10^{-2} \pm 3 \times 10^{-3}$
Acenaphthene	$0.077 \pm 4 \times 10^{-3}$	1.0	$0.082 \pm 1 \times 10^{-2}$	$8.0 \times 10^{-2} \pm 1 \times 10^{-2}$	$0.21 \pm 3 \times 10^{-2}$
Fluorene	$0.16 \pm 1 \times 10^{-2}$	0.99	$0.157 \pm 8 \times 10^{-3}$	$0.16 \pm 1 \times 10^{-2}$	$0.43 \pm 3 \times 10^{-2}$
Carbazole	$0.18 \pm 3 \times 10^{-2}$	0.97	$0.157 \pm 1 \times 10^{-2}$	$0.17 \pm 3 \times 10^{-2}$	$0.44 \pm 8 \times 10^{-2}$
Benzene	NR		NR		
t-Butylbenzene	NR		NR		
Biphenyl	NR		NR		
Dibenzofuran	NR		NR		

[1] Second-order rate constant has been tentatively assigned due to possible solubility experimental errors.

[2] Second-order rate constant has been assigned tentatively because only initial data used to determine rate constant. Also the reaction does not go to completion.

[3] Second-order constant has been tentatively assigned because there is an initial rapid decrease in concentration followed by a pseudo-first-order decay.

NR - No reaction

Table 4.4 Second-order rate constants (k_C) for the selected creosote compounds. The uncertainties specified reflect the 95% confidence level.

Compound	IP (eV)[a]	D_{R-H} (kJ/mol)	ΔH_f (kJ/mol)	$\Delta H_{f(\sigma\text{-compl.})}$ (kJ/mol)	$\Delta H_{compl.}$ (kJ/mol)
PAHs					
Biphenyl	8.23				
Naphthalene	8.144		169.0	752.7	583.7
Phenanthrene	7.89		239.4	813.3	573.9
Anthracene	7.439		262.3	781.6	519.2
Fluoranthene	7.9		367.0	924.1	557.1
Chrysene	7.60		317.7	863.1	545.5
Pyrene	7.426		280.7	811.8	531.1
Heterocyclic PAHs					
Carbazole	7.57	356.6[b]	283.3	808.8	525.5
Substituted PAHs					
1-methylnaphthalene	7.97	365.1[c]	141.1	704.2	563.1
2-methylnaphthalene	7.91	358.3[c]	137.4	703.0	565.5
Fluorene	7.91	332.6[c]	226.5	798.6	572.1
Acenaphthene	7.75	351.3[c]	177.2	730.5	553.3
Benzene and substituted benzenes					
Benzene	9.24				
Methylbenzene	8.828	375[c]			
Ethylbenzene	8.77	364.1[c]			
Isopropylbenzene	8.73	351.6[c]			
t-Butylbenzene	8.68				

[a] CRC Handbook of Chemistry and Physics 2003
[b] Barckholtz et al., 1999
[c] Kromkin et al., 2002

Table 4.5. Selected Creosote compounds; ionization potential (IP), and benzylic C-H bond dissociation energies (D_{R-H}), calculated heat of formation of the organic compound (ΔH_f), calculated heat of formation of the most stable hydroxyl σ-complex ($\Delta H_{f\,(\sigma\text{-compl})}$) and the heat of complexation (ΔH_{compl}).

Chapter 5

Column Experiments with Numerical Simulations

5.1 Abstract

Five column experiments were performed to investigate the effect that the strong oxidizing reagent, potassium permanganate ($KMnO_4$), has on increasing mass removal rates of creosote compounds from sand contaminated with residual creosote at 3% saturation. Several different flow rates and $KMnO_4$ concentrations were tested. The results were simulated using a reactive transport model that considered 12 different creosote compounds undergoing dissolution, oxidation and advective-dispersive transport.

In situ chemical oxidation with $KMnO_4$ greatly enhanced the rate of removal of creosote compounds from the oil phase compared to flushing with water. For example, at a $KMnO_4$ concentration of 15 g/L, 56% of the monitored creosote compounds were removed from the column after 5 days. With water as the flushing agent, only 8% of the compounds were removed after 6 days.

The oxidation process enhanced the removal of creosote compounds from the oil phase by a) increasing the length of the mass transfer zone by decreasing the concentration of creosote compounds in the aqueous phase; b) increasing the aqueous solubility of less readily oxidizable compounds by increasing their mole fraction in the oil phase and c) increasing the mass transfer process possibly through the diffusion of permanganate into areas of low permeability.

Experimental results and model simulations showed that the degree of enhanced dissolution was different for each compound. For the more readily oxidizable compounds such as pyrene and naphthalene a significantly higher rate of mass removal was observed in the oxidation columns compared to the column without oxidation. The aqueous concentrations of these compounds were reduced to below their aqueous solubility limits and the length of the mass transfer zone from the oil phase to the aqueous phase became equivalent to the column length

For non-oxidizable compounds such as biphenyl and dibenzofuran an increase in the rate of mass removal was also observed in the oxidation columns, even though their aqueous concentrations were not reduced in the column by oxidation. This was due to the rapid removal of the more readily oxidizable compounds from the oil, which increased the mole fraction of the non-oxidizable compounds. Thus, according to Raoult's Law, the concentration in the aqueous phase becomes closer to its pure phase aqueous solubility. For these compounds, the length of the mass transfer zone was not increased and mass transfer only occurred at the influent end of the column. The removal of these compounds from the oil phase may still take a long time, but the interval is greatly reduced with oxidation compared to flushing with water alone.

The most significant result of the experiments is the observed increase in rate of removal of those compounds that have low aqueous solubilities and are readily oxidized such as pyrene and fluorene.

5.2 Introduction

The rate of mass transfer of chemical compounds from a DNAPL to flowing ground water can be expressed as the product of a mass transfer coefficient, a concentration differential and the contact area between the dense non aqueous phase liquid (DNAPL) and ground water,

Mass Transfer Rate [M/T]	=	Mass Transfer Coefficient [L/T]	x	Concentration Differential [M/L^3]	x	Contact Area [L^2]	(5.1)

Mass Transfer Flux
[M/L^{2}T]

The mass transfer coefficient is related to the DNAPL component properties and the ground water flow conditions. The concentration differential is defined as the difference between the effective solubility of the component and the dissolved concentration in the ground water in contact with the DNAPL (Cussler, 1997).

The most rapid mass transfer from the oil phase to the aqueous phase will occur when the concentration in the aqueous phase of a compound is significantly below its effective aqueous solubility. For water that is flowing through a contaminated aquifer, this only occurs when the water initially comes in contact with the DNAPL. As water travels over the residual oil, the concentration of the components in the aqueous phase increases until the aqueous solubility limit has been reached. At this point mass transfer between the DNAPL and aqueous phase has reached equilibrium. The area over which this mass transfer occurs is called the mass transfer zone (Geller and Hunt, 1993), and is defined as the flow distance necessary to reach equilibrium (Figure 5.1). Under normal ground water velocities in a porous media such as sand, the mass transfer zone is on the order of a few millimeters or centimeters.

In the column experiments performed by Geller and Hunt (1993), three stages were observed as water travelled through the column: 1) increasing aqueous concentration during water flooding as the mass transfer zone was established, 2) a quasi-steady effluent concentration as the mass transfer zone propagated downstream and 3) a decline in effluent concentration as the DNAPL-containing region decreased to less than the length of the mass transfer zone.

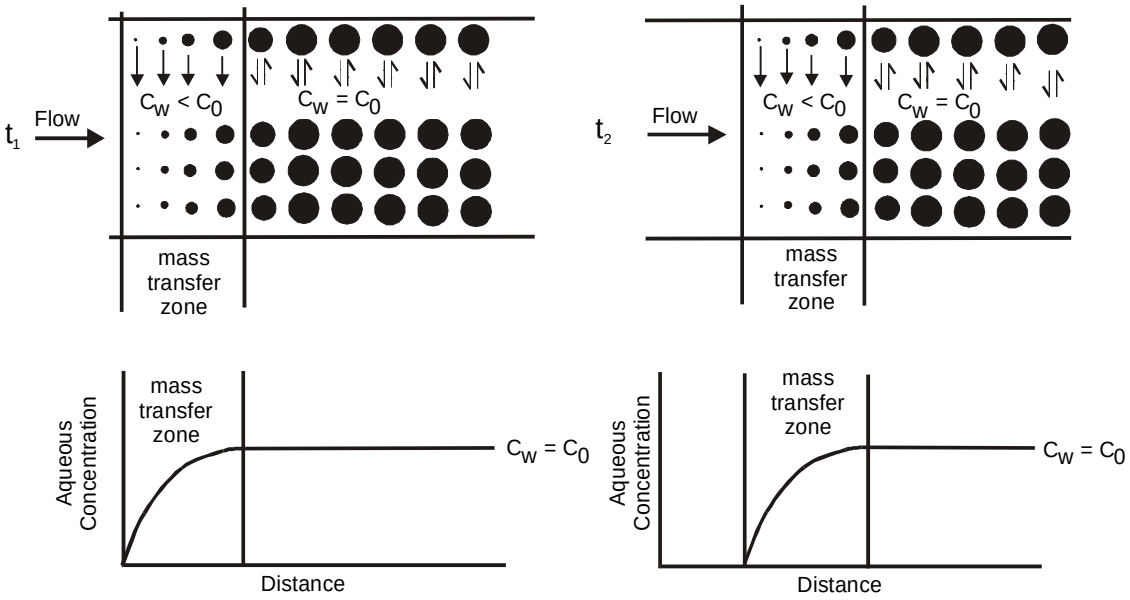

Figure 5.1 Conceptual model showing dissolution of an organic compound into flowing water and the propagation of the mass transfer zone through the residual oil at time t_1 and at a later time t_2. The black circles represent residual oil globules. (C_w = aqueous concentration, C_0 = pure phase solubility limit)

For a multi-component system, the dissolved phase concentration of each component in equilibrium with the oil can be expressed as a variation of Raoult's Law,

$$C_s^m = X_n^m C_0^m \tag{5.2}$$

where C_s^m is the effective solubility limit of component *m*, X_n^m is the mole fraction of *m* in the DNAPL, and C_0^m is the aqueous solubility of component *m*. Equation (5.2) indicates that when an organic liquid mixture contains more than one compound, each with different solubilities, C_s^m, the mole fraction of each compound will change as the oil dissolves. As a more soluble compound dissolves, its mole fraction and effective solubility decreases. In the same mixture, however, the mole fraction of a less soluble compound increases and its

aqueous concentration increases. Thus, for a multi-component system one would expect many mass transfer zones propagating downstream.

A chromatographic effect will also take place due to the varying mole fractions throughout the contaminated area. At the upgradient front of the DNAPL zone, for example, a less soluble compound whose mole fraction has increased will dissolve to a greater extent. But further downstream where the globules are larger and the mole fraction in the oil is small, the compound would partition back into the oil. The mass transfer zone for a multi-component system will therefore be a function of the local solubilities of each component.

The objective of the *in situ* chemical oxidation process is to not only oxidize and mineralize compounds in the aqueous phase, but also to increase the length of the mass transfer zone. The oxidation process increases the mass transfer zone by decreasing the aqueous phase concentrations throughout the contaminated area, not just at the upgradient front (Figure 5.2).

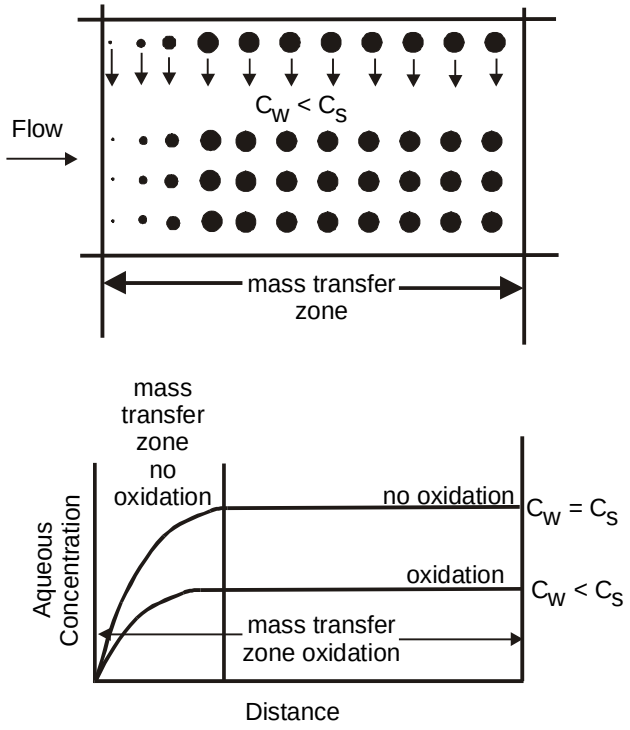

Figure 5.2. Conceptual model showing chemical oxidation will decrease the aqueous concentrations throughout the contaminated area and increase the length of the mass transfer zone.

The length of the mass transfer zone can only be increased if the concentration of the chemical oxidizing reagent does not decrease significantly as it travels through the treatment area. $KMnO_4$ was chosen as the reagent because it is a powerful oxidizer that can be used at very high concentrations and its concentration will not be reduced significantly as it moves through the zone of contamination.

5.3 Column Experiments

Five column experiments were performed with residual creosote. Four columns were flushed with potassium permanganate at high and low concentrations and at high and low flow rates. The fifth column was flushed with water containing no oxidizing reagent in order to calibrate the model and to determine experimentally the amount of creosote mass removed due to dissolution and advective-dispersive transport alone.

5.3.1 Column Design

The columns were constructed of thick-walled glass tubing fitted with stainless steel end plates (Figure 5.3). A seal was maintained between the end plates and the glass with a Teflon O-ring. The end plates were secured to the glass column with a universal beaded coupling joint. The experimental columns were cylindrical with an internal radius of 2.5 cm, an internal length of 11.7 cm, with a total volume 229.8 cm^3. All tubing was either glass or Teflon and the reagents were added with a peristaltic pump.

The sand used for the columns experiments was obtained from an unconfined aquifer at CFB Borden. The sand consists primarily of quartz (58%), feldspars (19%) and calcite (14%) with smaller quantities of amphiboles (7%) and chlorite (2%). The organic content of the sand was 0.02% (Mackay et al., 1986). The creosote source was obtained from Carbochem Ltd. in Mississauga.

To pack the columns, sand was first added to a beaker and weighed. Next, 40 mL of water was added to the sand and mixed with a spatula. 4 mL of creosote was added to the water-wet sand, which was then thoroughly mixed with a spatula. The creosote/sand/water mixture was then added in approximately 0.5 cm lifts to the column and packed after each lift. During packing, two or three creosote/sand/water samples were taken to determine the initial mass of creosote per mass of sand added to the column. After packing, the column was slowly flushed with carbon dioxide for approximately 1 hour to displace air that was trapped in the sand. Water was then added slowly from the bottom of the column until 50 mL of water was collected from the top of the column. The bottom of the column was then closed and the flask containing the water was raised above the column. The reservoir provided water to fill the pore spaces as CO_2 dissolved into the water. The column was left for approximately 15 hours and a visual examination showed no sign of entrapped air. A falling head test was then conducted to determine the hydraulic conductivity of the column. The reagents, water or potassium permanganate were then added *via* a peristaltic pump. Sodium chloride (0.1M) was added initially to the solutions to provide a tracer. Chloride concentrations were determined by adding 0.1g of dextrin and 5 drops of the indicator (0.1% 2',7'-dichlorofluorescien) to 2 mL samples then titrating with a standardized silver nitrate solution to a permanent pink colour. At the conclusion of the experiment, another falling head test was completed to determine the permeability of the columns.

5.3.2 Analytical Procedures

Permanganate solutions were prepared by dissolving solid $KMnO_4$ with Milli-Q pure water in a 500 mL or 1 L volumetric flask. $KMnO_4$ solutions were made fresh approximately every two to three days. Analytical reagent-grade $KMnO_4$ was obtained from BDH and used without further purification.

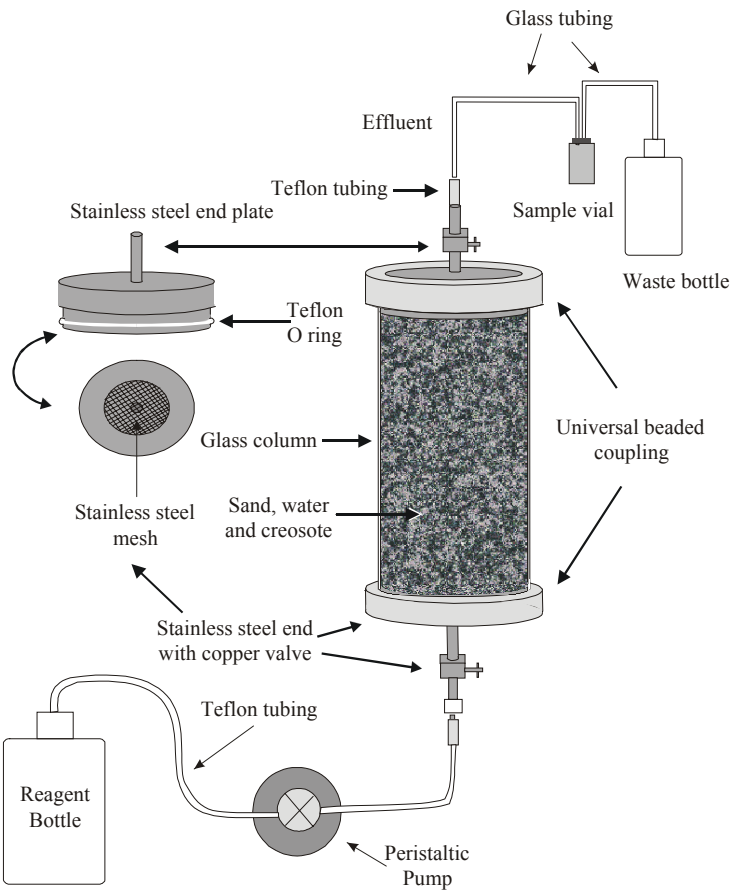

Figure 5.3 Column Design.

To determine initial and final concentrations of creosote compounds on the column material, sand samples coated with creosote were Soxhlet extracted with a 400 mL mixture of methylene chloride and acetone (1:1). Depending on the concentration of the creosote compounds, the samples were either diluted after extraction or concentrated to 25 mL with a Kuderna-Danish concentrator and then analyzed for the monitored creosote compounds.

Effluent water samples were collected with a syringe at the in-line sampling vial (Figure 5.3). To a 13 mL sample, 3 g of NaCl, 0.3 mL of 1N HCl and 1 mL of methylene chloride was added and shaken for 15 minutes on an orbital shaker set at 400 rpm. The methylene chloride was then extracted and analyzed.

The samples were analyzed on a temperature programmed Hewlett Packard HP5890A gas chromatograph using a 30 m DB5 (Chrom. Spec.) capillary column with a 0.25 mm i.d. and 0.25 μm film thickness. A split/splitless auto injector was used in the splitless mode and maintained at 275° C. Chromatographic conditions were: initial oven temperature 40° C for 0.5 min; ramp to 300° C at 15° C/min and hold for 10 min. The flame ionizing detector (FID) was maintained at 325° C with a helium carrier gas flow rate of 25 mL/min. Quantification was accomplished by an internal standard method using augmented standards prepared from commercially available PAH mixtures (Supelco, Bellefonte, PA). The internal standard was 2-fluorobiphenyl.

5.3.3 Estimation of the Initial Mass of Creosote Compounds Added to the Columns.

To determine the mass of creosote compounds added to the column, samples of the sand/creosote/water were taken during packing and Soxhlet extracted. After the extraction the sand was dried in an oven at 90°C overnight, cooled in a desiccator and then weighed. This provided the mass of each compound per gram of sand: the mass fraction. The mass of creosote compounds added to the column was calculated by multiplying the mass fraction by the mass of sand added to the column.

The creosote was obtained from Carbochem Ltd. in Mississauga, Ontario, and was a mixture of liquids and suspended solids. The mixture was not homogeneous and taking samples from the 1-gallon container gave different concentrations of the creosote compounds. Obtaining creosote in this way would not give the consistency needed for the five different experiments. To minimize this problem, the container of creosote was left undisturbed for one week. Then 20 mL of creosote was syringed from the top layer of the oil and was stored in a 25 mL crimp topped vial which was sealed with a Teflon septum. The creosote for all experiments was obtained from this vial which was thoroughly shaken before use. No visible solids were observed in the liquid. The density of the oil was measured gravimetrically as 1.1 g/mL ± 0.02. The uncertainty represents the 95% confidence interval.

To determine the homogeneity of the 20 mL creosote sample, four 0.5 mL samples were added to 100 mL volumetric flasks and diluted with methylene chloride. This solution was further diluted by adding 10 μL to 1 mL of methylene chloride in a volumetric flask. Each 1 mL sample was analyzed twice (Table 5.1). To determine the effectiveness of the Soxhlet extraction, four 0.5 mL samples of creosote were added to a Soxhlet thimble containing 165 grams of sand which was mixed with 30 mL of water. The creosote-sand source material was mixed with a spatula and then Soxhlet extracted with a mixture of methylene chloride and acetone (1:1) overnight. After soxhlet extraction the sample was diluted to 500 mL and then 100 μL of this was added to 1 mL of methylene chloride before injecting two samples into the gas chromatograph (Table 5.1).

Table 5.1 shows the mass of each of the monitored creosote compounds in the four 0.5 mL creosote samples and the 95 % confidence interval between the 8 GC analyses as well as the uncertainty obtained from the Soxhlet extraction. In general the uncertainty between samples was only slightly larger for the Soxhlet extraction of the oil from the sand than the analysis of the oil itself.

Compound	Average mass in a 0.5 ml Sample from a 20 mL sample of Creosote (mg)	95 % confidence interval	Average mass in a 0.5 ml Sample After Soxhlet Extraction (mg)	95 % confidence interval
Naphthalene (Nap)	46.90	± 1.76	44.33	± 3.01
1-methylnaphthalene (1-Metnap)	9.04	± 0.27	8.97	± 0.44
Biphenyl (Biph)	6.48	± 0.30	6.45	± 0.33
Acenaphthene (Acen)	33.02	± 0.87	33.34	± 1.42
Dibenzofuran (Dibenz)	22.44	± 0.70	22.65	± 0.93
Fluorene (Flu)	25.30	± 0.66	25.96	± 1.04
Carbazole (Carb)	4.24	± 0.14	4.09	± 0.83
Phenanthrene (Phen)	58.93	± 1.61	61.16	± 2.14
Anthracene (Anth)	6.14	± 0.16	6.38	± 0.23
Fluoranthene (Fluouran)	27.27	± 0.79	28.49	± 0.98
Pyrene (Pyr)	21.34	± 0.60	22.34	± 0.78
Chrysene (Chr)	6.05	± 0.77	5.27	± 1.56

Table 5.1 Analysis of a creosote sample and determination of the errors associated with the Soxhlet extraction.

5.4 Numerical Model

The model used to simulate the oxidation/dissolution process was BIONAPL/3D: a 3D finite element numerical model developed by J. Molson and E. Frind at the University of Waterloo (Frind et al., 1999). The model includes dissolution of a residual, multicomponent, non-aqueous phase source as well as advective-dispersive transport and biodegradation of the aqueous phase compounds.

The dissolution process is based on a stagnant boundary layer in which mass is transferred from a residual non-aqueous phase to the flowing ground water (Figure 5.4). The solute mass flux across the stagnant boundary is a function interfacial area between the two phases and the concentration gradient (equation 5.1). This is one of the simplest ways to represent interfacial mass transfer and the boundary layer or unstirred layer is almost always hypothetical, for fluid motions commonly occur at the surface of the interface (Miller et al., 1990).

The model also assumes that the solute, present at high dilution is slowly diffusing across the interface. In many cases diffusion itself can cause convection. The assumption that the solute is at high dilution allows one to neglect the diffusion-induced convection perpendicular to the interface (Cussler, 1997). The steady-state flux across the stagnant film in terms of a mass coefficient can be written as,

$$J_1 = \lambda \left(C_{1i} - C_{1l} \right) \tag{5.3}$$

where J_1 is the mass solute flux per unit area relative to the interface ($ML^{-2}T^{-1}$), λ is the mass transfer coefficient (LT^{-1}), C_{1l} (ML^{-3}) is the concentration of in the bulk solution and C_{1i} is the concentration at the interface that is in the same fluid as the bulk concentration.

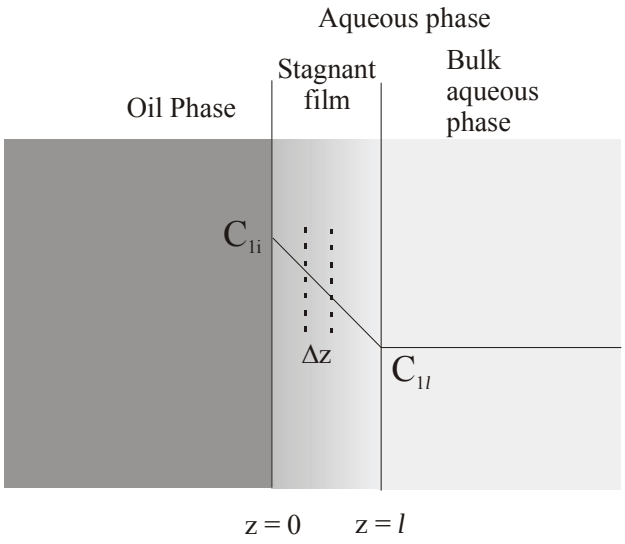

Figure 5.4 Conceptual drawing of a stagnant film layer in which diffusion-limited mass transport occurs across the film. Note that C_{li} is constant and implies no resistance to mass transfer in the oil phase.

The flux across the stagnant film can also be described in terms of the diffusion coefficient as described by the following equation,

$$J_1 = -D\frac{dC_1}{dz} = \frac{D}{l}\left(C_{1i} - C_{1l}\right) \tag{5.4}$$

where D is the aqueous diffusion coefficient (MT^{-1}) and l is the thickness of the thin film or stagnant layer (L). Note that at z = 0 C_{li} is constant and implies that there is no resistance to mass transfer in the oil phase. The diffusion across the stagnant film follows the basic relationship for the diffusion across a thin film as described by Fick's Law. Because the system is at steady-state C_{li} and C_l are independent of time. Physically, this means the volumes of the adjacent solutions must be much greater than the volume of the film. Combining equation 5.3 and 5.4 gives,

$$\lambda = \frac{D}{l} \tag{5.5}$$

The mass transfer coefficient is frequently described as a nondimensional expression; the Sherwood number (Sh),

$$\mathrm{Sh} = \frac{\lambda l}{D} = 1 \tag{5.6}$$

Equation 5.5 implies that the mass transfer coefficient is directly proportional to the diffusion coefficient and by doubling the diffusion one would double the mass transfer. However, the mass transfer coefficient still varies in some unknown fashion with variables like fluid viscosity and stirring, because these variations are lumped into the unknown film thickness (Cussler, 1997). The film thickness is almost never known and must be found experimentally. In the modeling of ground water flow through a porous media the length scale is usually equal to the media grain diameter (Geller and Hunt, 1993).

The stagnant film model provides a simple physical insight into the resistance of solute mass transfer from a nonaqueous phase liquid into flowing water. Many mass transfer models have been based on some form of the stagnant layer model (Miller et al., 1991; Powers et al., 1992, Imhoff et al., 1994) and the correlations are written in terms of the Sherwood number,

$$\mathrm{Sh} = \frac{\begin{pmatrix}\text{mass transfer}\\ \text{coefficient}\end{pmatrix}\begin{pmatrix}\text{a characteristic}\\ \text{length}\end{pmatrix}}{\begin{pmatrix}\text{diffusion}\\ \text{coefficient}\end{pmatrix}} = F\begin{pmatrix}\text{other system}\\ \text{variables}\end{pmatrix} \tag{5.7}$$

By using a characteristic length, it is implied from equation 5.6,

$$\begin{pmatrix}\text{mass transfer}\\ \text{coefficient}\end{pmatrix} = \frac{(\text{diffusion coefficient})}{(\text{some characteristic length})}\begin{pmatrix}\text{a correction}\\ \text{factor } F\end{pmatrix} \tag{5.8}$$

For a multi-component DNAPL like coal tar and creosote the steady-state flux across the stagnant film for component *m* at a point *i* can be written as,

$$J_i^m = \lambda_i^m \left(C_s^m - C_w^m \right) \tag{5.9}$$

where J_i^m is the mass flux of component m relative to the interface at point *i* (ML^3T^{-1}), λ_i^m is the mass transfer coefficient (LT^{-1}), C_s^m is the effective solubility of component *m* (see equation 5.2), and C_w^m is the concentration of component *m* in the bulk flowing water.

In the porous medium, the diffusion length across which mass transfer occurs will vary due to heterogeneities caused by areas which have reduced permeabilities (Figure 5.5). The blob shape and the exposed surface area in contact with water will also vary throughout the source. Thus the stagnant layer as discussed above is a physically-based empirical concept rather than a measurable quantity. In the stagnant film model there is no attempt to define the rate coefficient, λ_i^m, in terms of primary variables of the porous medium; the rate will instead be calibrated by the model.

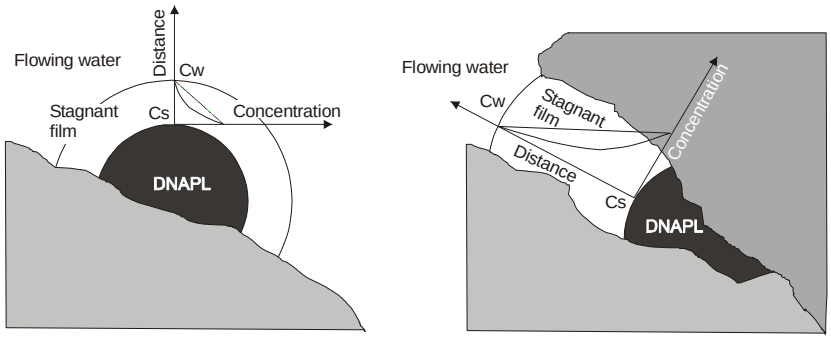

Figure 5.5 Conceptual drawing of a stagnant film layer in a porous media in which diffusion-limited mass transport occurs.

The mass transfer rate coefficient that was adopted by Frind et al. (1999) is given by the following equation,

$$\lambda_i^m = \mathrm{Sh}\frac{D^m}{(d_{50})^2}\left(\frac{f_i^m S_{n_i}}{S_{n_0}}\right)^{\beta^m} \qquad (5.10)$$

where D^m is the aqueous diffusion constant for multi-component m, d_{50} is the median grain size diameter (a characteristic length of the system), S_{ni} is the NAPL saturation at i, S_{no} is the initial DNAPL saturation, Sh is the Sherwood number, f_i^m is the local volume fraction of NAPL component m and β^m is a nonlinear coefficient.

The physical meaning of the Sherwood number as defined by equation 5.7 and rearrangement of equation 5.10 is the ratio of the total interfacial mass transferred relative to the mass transferred by diffusion. The Sherwood number is an empirical property of the NAPL-contaminated porous medium that controls the aqueous diffusion processes. It represents the effects of the thickness of the diffusion layer and the surface area of the oil blobs. Since these factors are geometric, they should be the same for each component in the NAPL (Frind et al., 1999).

In viscous oils like creosote and coal tar, resistance to mass transfer in the oil phase may occur, thus the component volume fraction $f_i^m S_{n_i} / S_{n_0}$ is used to represent the possible time dependence of the mass transfer process. The NAPL-specific fraction f_i^m and the exponent β^m serve as an empirical representation of the different rates at which different compounds may diffuse through the oil phase to the surface of the oil (Frind et al., 1999). The different rates of diffusion could be caused by differing adhesive intermolecular forces within the oil that could possible impede the movement of the compound within the oil. Since the rate of diffusion within the oil may be different for each compound the β value is allowed to be different for each compound. A more physical approach would be to use a dual film model

(Reitsma, 1996) but this was beyond the scope of the study for which the model was developed (Frind et al., 1999). It was felt that for this study, a dual film model was not necessary to model the one-dimensional column experiments. To allow for component-based variations in the creosote, the exponent β^m is allowed to be distinct for each component.

The calibration parameters Sh_i^m and β^m are defined as averages over a representative elementary volume (REV) encompassing a sufficiently large number of pores. With the column experiment the REV is measured in millimeters along the 12 cm column. This provides a small enough spacing to capture the transient processes of dissolution, mass transfer and oxidation. The REV should also be smaller than the mass transfer zone in which dissolution takes place. For the 1D column experiment, this was a straightforward calculation (Table 5.2).

The oil phase in the column experiments is assumed to be immobile because of the low residual saturation (0.03) used in column experiments which is below the level where movement due to hydraulic conditions will occur (Chatzis et al., 1983). Also because the aqueous concentrations of the creosote compounds are very dilute, density-dependent flow will not be considered. Thus the ground water continuity equation can be written as,

$$-\frac{\partial}{\partial x_i}\left(K_{ij} k_{rw} \frac{\partial h}{\partial x_i}\right) + S_w S_s \frac{\partial h}{\partial t} + \theta \frac{\partial S}{\partial t} = 0 \qquad (5.11)$$

where *h* is the hydraulic head, K_{ij} is the hydraulic conductivity tensor, S_w is the aqueous phase saturation, S_s is the specific storage, k_{rw} is the relative permeability of water, θ is the porosity and t is the time. The relative hydraulic conductivity can be expressed as a function of the aqueous phase saturation (Corey, 1986),

$$k_{rw} = \left(\frac{S_w - S_{rw}}{1 - S_{rw}} \right)^4 \tag{5.12}$$

where S_{rw} is the irreducible degree of water saturation. The degree of saturation with respect to water, S_w, and NAPL, S_n are related by,

$$S_w + S_n = 1 \tag{5.13}$$

Equation (5.11) is subject to the usual Dirichlet and Neumann boundary conditions.

The solute transport equation for m components can be expressed as,

$$R\theta S_w \frac{\partial C_w^m}{\partial t} + q_i \frac{\partial C_w^m}{\partial x_i} - \frac{\partial}{\partial x_i}\left(S_w \theta D_{ij}^m \frac{\partial C_w^m}{\partial x_j} \right) - \theta S_w \lambda^m (C_s^m - C_w^m) + \theta \lambda_{Ox}^m C_w^m = 0 \tag{5.14}$$

where R is the retardation factor, λ^m is the NAPL mass trasfer coefficient and λ_{Ox}^m is the pseudo first-order oxidation rate constant for component *m*. D_{ij}^m is the hydrodynamic dispersion tensor (L^2/T), which has principle components $D_L = \alpha_L v$ and $D_T = \alpha_T v$ in the longitudinal and transverse flow directions respectively, with α_L and α_T being respective dispersivities (L) and q_i is the Darcy Flux in the x_i-direction (L/T) given by,

$$q_i = -K_{ij} k_{rw} \frac{\partial h}{\partial x_j} \tag{5.15}$$

Equation (5.14) is subject to Dirichlet and Cauchy boundary conditions for mass transport.

The linear retardation coefficient is described by (Freeze and Cherry, 1979),

$$R = 1 + \frac{\rho_b K_d}{\theta} \tag{5.16}$$

where ρ_b is the bulk density and K_d is the linear sorption distribution coefficient which can be estimated using an empirical correlation with the octanol-water partition coefficient given by Schwarzenbach et al. (1993) as,

$$\log K_{oc} = 0.82 \log K_{ow} + 0.14 \tag{5.17}$$

and

$$K_d = K_{oc} f_{oc} \tag{5.18}$$

where K_{oc} is the organic carbon-water partitioning coefficient, K_{ow} is the octanol-water partitioning coefficient and f_{oc} is the fraction of organic carbon.

The mass-conservation equation for component m within the DNAPL mixture is,

$$(\partial / \partial t)(M^m) + \theta S_w \lambda^m (C_s^m - C_w^m) = 0 \tag{5.19}$$

where M^m is the mass component *m* per volume of porous medium. The individual masses satisfy,

$$\theta S_n \rho_n = \sum_m M^m \tag{5.20}$$

where the NAPL density ρ_n is defined as,

$$\rho_n = \sum_m M^m \rho^m / \sum_m M^m \tag{5.21}$$

with ρ^m being the density of component m. The total mass depleted from the NAPL phase through dissolution is the sum of the individual component masses M^m lost in the same time interval. The mass balance is expressed as,

$$\theta(\partial/\partial t)(S_n \rho_n) + \sum_m \left[\theta S_w \lambda^m_{Dis}(C^m_s - C^m_w)\right] = 0 \tag{5.22}$$

Creosote is an oil but many of the compounds are solids in their pure phase. Thus, the correct C_s^m value to be used in equation (5.2) is that of the subcooled liquid chemical (Mackay et al., 1991). This solubility is larger than that of the solid at temperatures below the melting point by the multiple (1/*F*) where *F* is the fugacity ratio, which at temperature *T* is given approximately by,

$$F = \exp\left[\frac{\Delta S(1 - T_m/T)}{R}\right] = \frac{C_s^m}{C_0^m} \tag{5.23}$$

where ΔS is the entropy of fusion, R is the ideal gas constant and C^m_s is the pure solid solubility. ΔS can be calculated for some but not all of the creosote compounds (J. of Phy. Ref. Data., 1993) thus $\Delta S/R$ is approximated to be 6.8 ± 1 (Miller et al., 1985).

The model developed by Frind et al. (1999) included Monod kinetic terms for biodegradation but did not include the direct input of pseudo-first-order oxidation rate constants. Thus the Monod biodegradation terms were modified to represent the first order rate of oxidation.

The biodegradation rate coefficient λ_{Bio}^{m} for organic component *m* was expressed in terms of N_A parallel degradation reactions as,

$$\lambda_{Bio}^{m} = \sum_{n=1}^{N_A} \left[k^{m,n} M_{mic}^{n} \left(\frac{1}{K_C^{m,n} + C_w^M} \right) \left(\frac{A^n}{K_A^{m,n} + A^n} \right) \cdot I^n \right] \tag{5.24}$$

where $k^{m,n}$ is the maximum utilization rate (day^{-1}) of component *m* with electron acceptor *n*, M_{mic}^{n} is the microbe concentration (kg/m^3), $K_C^{m,n}$ and $K_A^{m,n}$ are the half-utilization rate concentrations (kg/m^3) for the organic and electron acceptor, respectively, I^n is the electron inhibition function and (A^n) is the electron acceptor concentration.

Equation 5.24 was adapted to account for the oxidation reaction by treating $KMnO_4$ as the "electron acceptor" (A), setting $M_{mic}^{n} = I^n = 1$ and setting $K_C^{m,n} >> C_w^m$. The oxidation rate coefficient is then given by,

$$\lambda_{Ox}^{m} = k_{Ox}^{m} \left(\frac{[KMnO_4]}{K_{KMnO_4}^{m,n} + [KMnO_4]} \right) \tag{5.25}$$

where k_{Ox}^{m} is the maximum oxidation rate (day^{-1}) for component m, and $K_{KMnO_4}^{m}$ is the half-utilization concentration (kg/m^3). $KMnO_4$ is dissolved in the aqueous phase and therefore its transport is also assumed to be governed by advective-dispersive transport. Thus the rate of oxidation for component *m* will increase as the concentration of $KMnO_4$ increases in the pore spaces according to equation 5.25. Figure 5.6 depicts the relationship between the oxidation rate coefficient and $KMnO_4$ concentration. The program treated the transport of $KMnO_4$ as a conservative tracer (no retardation) and did not consider the initial decrease in concentration due the oxidant demand of the sand.

A more accurate relationship between rate coefficient and $KMnO_4$ concentration would be to multiply the concentration by the second order rate constant. However, since dispersion in the sand columns was small, as seen in the tracer breakthrough curves (see below), the $KMnO_4$ concentration should reach its maximum concentration within a relatively short distance compared to the column length, as the $KMnO_4$ front moves up the column. Thus the errors associated with correlating the second order rate constant with $KMnO_4$ concentration using this method was considered small. At the time of development, the model was adapted to incorporate the oxidation process as apposed to rewriting the code. On a larger scale simulation or field site simulations dispersions will be much larger and the linear relationship should be incorporated into the model. Also the oxidant demand by the aquifer material should be incorporated into the model design since this will greatly delay the time it will take to deliver the oxidant to the contaminant.

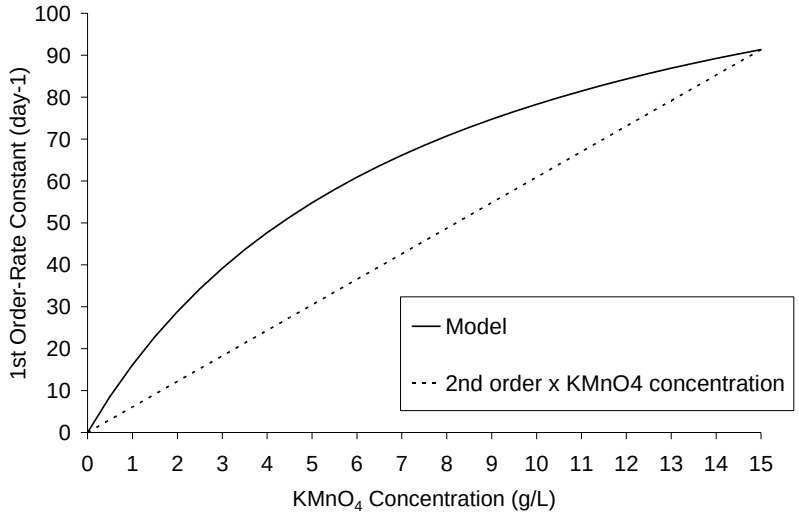

Figure 5.6. Model and actual correlations between $KMnO_4$ concentration and the pseudo-first-order rate constant for naphthalene. The pseudo-first-order rate constant for naphthalene at 15 g/L is 90.4 day^{-1}.

5.5 Results and Discussion

5.5.1 Columns Experiments

Column experiments were designed to examine the effect of flow rate and permanganate concentration has on the rate of removal of creosote compounds. Four oxidation column experiments with creosote at 3% oil saturation were performed. Experimental conditions were kept as uniform as possible with the volumetric flow rate and $KMnO_4$ concentration being the main two variables. Two columns were flushed with $KMnO_4$ at a concentration of 3 g/L with volumetric flow rates of 2.72×10^{-3} and 3.59×10^{-4} m^3d^{-1}. Two more columns were flushed with a higher concentration of $KMnO_4$ (15 g/L) with volumetric flow rates of 2.83×10^{-3} and 3.59×10^{-4} m^3d^{-1}. Since the same volumes of reagents were added at different flow rates the time the oil phase was exposed to the oxidizing reagent was different for the two different flow rates. Thus, these four column experiments were designed to show, for a defined volume of reagent flushed through the column, which concentration of $KMnO_4$ (3 or 15 g/L) and which flow rate (2.7×10^{-3} or 3.59×10^{-4} m^3d^{-1}) would remove the largest amount of creosote compounds from the oil phase.

The control column (no oxidizing reagent added) was used to observe the mass lost under non-oxidation dissolution conditions and to calibrate the oxidation/dissolution model. The physical characteristics of the 5 columns are shown in Table 5.2. The effective porosity was determined experimentally with a NaCl tracer and the hydraulic conductivity of the columns was determined using the falling head method. Tracer experiments were not performed at the conclusion of the oxidation experiments because $KMnO_4$ interferes with the titration used to determine NaCl concentrations.

In the control column the effective porosity and hydraulic conductivity decreased after the 6 day experiment. After approximately one day creosote globules began forming in the pore spaces in the lower half of the column. This is caused by the density driven migration of creosote oils downward along the sand grains until the oil migration is stopped by constricted

pore throats (Morrow et al., 1988, Chatzis et al., 1983). The oil becomes entrapped in larger pore spaces and reduces the number of pores available to conduct water. This physical change in the pore spaces reduces the permeability and increases the dispersivity of the column. Comparison of the initial and final NaCl breakthrough curves in the control column (Figure 5.7) shows an increase in the dispersion and a decrease in the effective pore volume, which are the expected results for the formation of creosote globules in the pore spaces of the sand. No creosote oil was observed exiting the influent tubes and indicates that once entrapment occurred the oil phase was immobile.

In all of the $KMnO_4$ experiments, a decrease in hydraulic conductivity was observed. This could be caused by the precipitation of manganese oxides on sand grains and screens, and from the formation of creosote globules. Creosote globules were not observed in the $KMnO_4$ columns and detailed extraction of the initial column experiment (Sec. 3.2.6) showed a relatively even distribution of creosote compounds throughout the column. This suggests that the main decrease in hydraulic conductivity was due to the precipitation of manganese oxides.

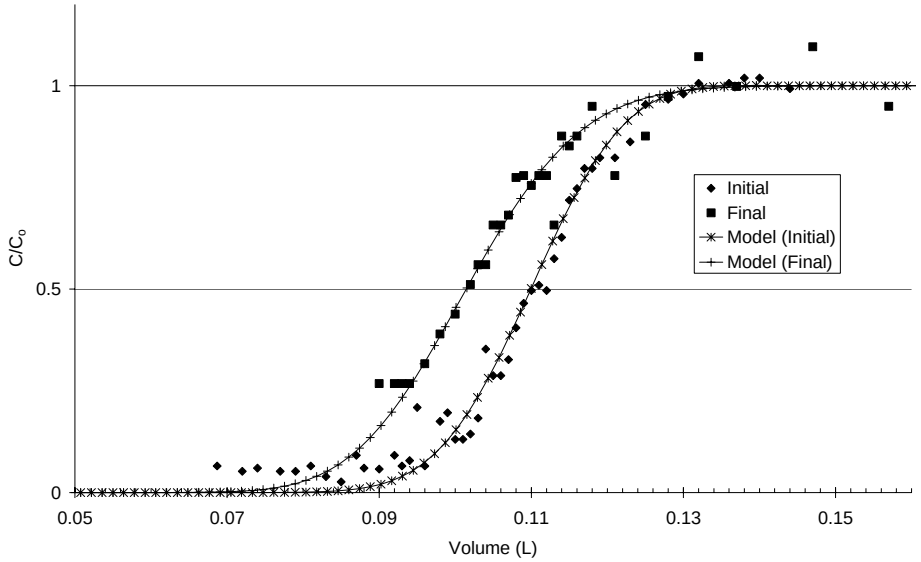

Figure 5.7 Sodium chloride breakthrough curves for the control column at the beginning and end of the experiment. The initial model parameters were:θ=0.47, v=1.72 x 10^{-5} m/s, α_L=0.0004m and the final parameters were: θ=0.45, v=1.85 x 10^{-5} m/s, α_L=0.0008 m.

The initial masses added to the columns and final masses of the selected creosote compounds remaining in the columns for the experiments are given in Tables 5.3 to 5.5. The initial mass of creosote compounds added to each column was relatively constant for compounds like 1-methylnaphthalene, biphenyl and chrysene but was quite variable for others such as naphthalene, phenanthrene, acenaphthene and anthracene. The largest error associated with the experiment is the mixing of the sand, water and oil in a beaker to form a homogeneous mixture and subsequently packing of the column. As stated in Section 5.2.3, while the column was being packed, two to three samples of the sand/water/oil mixture were taken and soxhlet extracted to give the mass of creosote compound per gram of sand. This value was then multiplied by the mass of sand added to the column to determine the mass of creosote compound added to the column. The error given for the initial mass added to the columns is the standard deviation between the samples. The error associated with the soxhlet extraction process is not included in this value. For some compounds like naphthalene, the deviation between columns was quite large. The large errors are most likely associated with mixing and packing of the column. At the end of the experiment, the column was sectioned into three or four samples and soxhlet extracted to determine the mass in the sample. The error associated with the mass of creosote compounds remaining on the sand was determined by using the errors in the soxhlet extraction given in Table 5.1. A percent deviation (standard deviation divided by mass of sand) was calculated and multiplied by the mass of sand for each extraction. These values most likely underestimate the errors involved in the final mass since they do not consider the errors that occurred while removing the creosote/sand mixture from the column. Also, it is assumed that the precipitation of manganese oxides does not effect the soxhlet extraction efficiency. The error for the percent removed was calculated using the propagation of errors computation as given in Skoog and West (1976).

Results of the control column show that compounds which have high aqueous solubilities and high mole fractions have the greatest mass lost. For example naphthalene which has a large mole fraction was reduced in the oil phase by approximately 54% and carbazole that

has a relatively high aqueous solubility, was reduced by approximately 33%. Very little mass was removed for compounds with low aqueous solubilities such as pyrene and chrysene, after the 6.29 day experiment.

All of the oxidation columns significantly enhanced the percentage of creosote compounds removed from the oil phase compared to the control column. Comparison between the oxidation columns reveals that for the same volume of oxidizing reagent passing through the columns, the percentage of creosote compounds removed was much greater for the columns with the slower flow rates. In the two columns with the lower flow rates, more mass of the more readily oxidized compounds such as 1-methylnaphthalene, carbazole and pyrene were removed compared the columns performed at the higher flow rates. For the non-reactive compounds like biphenyl and dibenzofuran, there was only a slight increase in the mass removed from the columns with the lower flow rates.

The results from the column experiments indicate that at a specified $KMnO_4$ concentration the lower flow rate was more successful in removing creosote compounds form the column using the same volume or mass of $KMnO_4$. For example, 56% of the monitored creosote compounds were removed from the column at a flow rate of 3.6×10^{-4} m^3d^{-1} ($[KMnO_4]$ =15 g/L, 21.7 g of $KMnO_4$), after 5.04 days, where as only 20 % of the monitored compounds were removed from the column at a flow rate of 2.72×10^{-3} m^3d^{-1} ($[KMnO_4]$ =15 g/L, 26.6 g of $KMnO_4$), after 0.63 days. Increasing the concentration of $KMnO_4$ also increased the mass of creosote compounds removed from the columns. For example, 56% of the monitored creosote compounds were removed from the column at a flow rate of 3.59×10^{-4} m^3d^{-1} ($[KMnO_4]$ =15 g/L, 21.7 g of $KMnO_4$), after 5.04 days, where as only 33 % of the monitored compounds were removed from the column at a flow rate of 3.59×10^{-4} m^3d^{-1} ($[KMnO_4]$ =3 g/L, 5.4 g of $KMnO_4$), after 4.97 days. These observations indicate that for these experiments the rate of mass transfer was significantly affected by the $KMnO_4$ concentration and that flow rate had less of an impact on the rate of removal of the readily oxidizable creosote compounds from the columns; however several questions still need to be

answered, including:

1. Was there an enlargement of the mass transfer zone?
2. Did oxidation occur throughout the column and for what compounds?
3. Is there an increase in the rate of removal of the more recalcitrant compounds?
4. How long would it take to remove the monitored compounds from the creosote oil?

These questions can be addressed through model simulations of the oxidation/dissolution process.

Column Experiment	1	2	3	4	5
$KMnO_4$ (g/L)	0	3	3	15	15
Mass of sand before packing column (g)	499.24	499.22	499.28	499.31	499.26
Volume of creosote added to sand (mL)	4	4	4	4	4
Mass of sand added to column (g)	355.6	372.25	377.33	372.19	379.61
Volume of creosote added to column using mass ratio (mL)	2.85	2.98	3.02	2.98	3.04
effective pore volume from tracer (mL)	111	93	88	88	100
effective pore volume from tracer at the end of the experiment (mL)	102				
effective porosity (mL)	0.47	0.40	0.38	0.38	0.44
effective porosity at the end of the experiment (mL)	0.43				
Total pore volume (mL) (Effective porosity plus volume of creosote added)	113.85	95.98	91.02	90.98	103.44
Creosote oil saturation (%)	2.50	3.11	3.32	3.28	2.95
Volumetric flow rate (m^3/d)	1.41×10^{-3}	2.72×10^{-3}	3.59×10^{-4}	3.59×10^{-4}	2.83×10^{-3}
Darcy's velocity (m/s)	8.30×10^{-6}	1.60×10^{-5}	2.12×10^{-6}	2.12×10^{-6}	1.67×10^{-5}
Average linear velocity (m/s)	1.77×10^{-5}	4.08×10^{-5}	5.68×10^{-6}	5.68×10^{-6}	3.94×10^{-5}
Duration of Experiment (days)	6.29	0.64	4.97	5.04	0.63
Total volume of solution added (L)	8.601	1.749	1.785	1.809	1.771
Number of pore volumes passed through the columns (mL)	79.85	18.81	20.28	20.56	17.71
Mass of $KMnO_4$ used (g)	0	5.25	5.36	27.14	26.56
Initial hydraulic conductivity (m/s)	7.5×10^{-5}	4.4×10^{-5}	4.6×10^{-5}	5.8×10^{-5}	1.2×10^{-5}
Final hydraulic conductivity (m/s)	1.9×10^{-6}	5.9×10^{-6}	9.2×10^{-8}	5.1×10^{-7}	3.9×10^{-7}
L_{mtz} (cm)[a]	2.5	3.9	1.0	1.0	4.0

[a] Estimation of the length of the mass transfer zone $L_{mtz} \approx \frac{0.27\theta}{S_n}\left(\frac{q}{D}\right)^{\frac{2}{3}} d_{n,0}^{5/3}$ where oil saturation $S_n = 0.03$, molecular diffusion $D = 5.0 \times 10^{-10}$ (m^2/s), porosity $\theta = 0.42$ and initial diameter of oil droplet = 0.001 (m). For detailed discussion see Geller and Hunt (1993)

Table 5.2 Column operating conditions

$[KMnO_4]$ = 0 g/L
Flow rate 1.41 x 10^{-3} (m^3/day)
Pore volumes 77.5
Duration 6.29 days

Liquid Phase Aqueous solubility (g/L)	PAH	Initial mass (mg)	Wt %	Final mass (mg)	% removed
0.121	Nap	279.2 ± 76	8.9	128.2 ± 3.7	54.1 ± 42
0.028	1-Metnap	57.3 ± 11	1.8	50.3 ± 0.5	12.2 ± 19.5
0.022	Biph	46.9 ± 7.7	1.5	40.8 ± 0.4	12.9 ± 16.7
0.020	Acen	217.7 ± 34	6.9	210.0 ± 1.7	3.5 ± 15.6
0.029	Dibenz	177.1 ± 27	5.6	171.7 ± 1.1	3.1 ± 15.3
0.016	Flu	170.9 ± 26	5.5	170.3 ± 1.3	0.28 ± 15.0
0.20	Carb	32.5 ± 5.0	1.0	22.8 ± 1.1	30.0 ± 17.0
0.0065	Phen	403.5 ± 60	12.9	418.0 ± 2.6	-3.7 ± 14.7
0.0034	Anth	47.5 ± 7.1	1.5	46.2 ± 0.3	2.7 ± 15.0
0.0019	Fluoran	189.18 ± 29	6.0	201.5 ± 1.2	-6.5 ±15.3
0.0024	Pyr	154.6 ± 24	4.9	155.0 ± 1.0	-0.24 ± 15.5
0.00039	Chr	39.3± 9.1	1.3	40.4 ± 1.9	-2.7 ± 23.8
	Total	1815 ± 117		1655.4 ± 70	8.8 ± 7.5
	Unknown	1319.4	42.2		

Table 5.3 Mass of monitored creosote compounds removed from the control column (no oxidation).

$[KMnO_4]$ (g/L)	3			3		
Flow rate (m^3/day)	2.72 x 10^{-3}			3.59 x 10^{-4}		
Pore volumes	17.9			18.9		
Duration (days)	0.64			4.97		
PAH	Initial mass (mg)	Final mass (mg)	% removed	Initial mass (mg)	Final mass (mg)	% removed
Nap	290.0 ± 50	246.2 ± 8.1	15.1 ± 18	298.0 ± 31	138.6 ± 8.2	53.5 ± 12.2
1-Metnap	62.3 ± 9.8	55.8 ± 1.2	10.4 ± 15.8	63.3 ± 6.7	42.7 ± 1.2	32.5 ± 11.2
Bip	51.6 ± 7.8	47.3 ± 0.9	8.4 ± 15.2	51.7 ± 6.1	49.7 ± 0.9	4.0 ± 11.9
Acen	230.3 ± 34	176.2 ± 3.8	23.5 ± 15.3	230.0 ± 37	125.0 ± 3.9	45.6 ± 17.9
Diben	203.5 ± 31	193.6 ± 2.5	4.9 ± 15.1	204.1 ± 34	180.6 ± 2.5	11.5 ± 16.9
Flu	176.4 ± 26	141.6 ± 2.8	19.8 ± 15.0	171.0 ± 26	88.3 ± 2.8	48.4 ± 16.2
Carb	33.9 ± 4.0	25.5 ± 2.2	24.9 ± 13.8	34.2 ± 4.3	11.7 ± 2.3	65.6 ± 16.6
Phen	421.7 ± 65	405.0 ± 5.8	4.0 ± 15.5	429.6 ± 97	302.7 ± 9.0	29.5 ± 23.7
Anth	18.3 ± 15	1.3 ± 0.45	93.2 ± 115	27.4 ± 29	0.8 ± 0.6	97.0 ± 132
Fluoran	165.8 ± 20	162.0 ± 2.6	2.3 ± 12.4	186.3 ± 30	164.7 ± 5.6	11.6 ± 16.4
Pyr	133.6 ± 17	126.2 ± 2.1	5.6 ± 13.0	150.2 ± 26	118.8 ± 2.1	20.9 ± 18.0
Chr	31.0 ± 4.7	30.7 ± 4.2	0.84 ± 20	35.3 ± 3.0	30.4 ± 4.3	13.8 ± 14.8
Total	1818.± 103	1611.3 ± 52	11.4 ± 6.4	1880.± 127	1254.0 ± 13	33.3 ± 7.2

Table 5.4 Mass of monitored creosote compounds removed from the oxidation columns with $KMnO_4$ at a concentration of 3 g/L.

[$KMnO_4$] (g/L)	15			15		
Flow rate (m^3/day)	3.59×10^{-4}			2.72×10^{-3}		
Pore volumes	19.01			15.4		
Duration (days)	5.04			0.63		
PAH	Initial mass (mg)	Final mass (mg)	% removed	Initial mass (mg)	Final mass (mg)	% removed
Nap	325.7 ± 29	55.4 ± 8.1	83.0 ± 12	304.2 ± 11.7	255.9 ± 8.3	15.9 ± 5.2
1-Metnap	71.7 ± 4.1	28.5 ± 1.2	60.3 ± 7.0	66.5 ± 6.9	57.2 ± 1.2	14.0 ± 4.0
Bip	60.0 ± 2.7	49.6 ± 0.9	17.3 ± 12.5	55.2 ± 1.8	45.3 ± 0.9	17.8 ± 3.7
Acen	277.1 ± 9.6	41.2 ± 3.8	85.1 ± 4.7	255.5 ± 8.1	185.8 ± 3.9	27.3 ± 3.6
Diben	246.1 ± 7.3	208.5 ± 2.5	15.3 ± 3.0	224.7 ± 7.4	185.9 ± 5.9	17.3 ± 3.5
Flu	214.6 ± 4.9	33.8 ± 1.4	84.2 ± 3.2	190.8 ± 5.6	136.0 ± 2.9	28.7 ± 7.0
Carb	46.3 ± 1.2	8.9 ± 2.2	80.8 ± 5.8	36.0 ± 0.93	12.6 ± 2.3	64.9 ± 6.7
Phen	548.3 ± 26	251.8 ± 5.8	54.1 ± 5.5	497.8 ± 16	392.8 ± 5.9	21.1 ± 3.5
Anth	39.5 ± 0.2	1.5 ± 0.61	96.3 ± 1.7	0	0	0
Fluoran	252.0 ± 12	201.4 ± 2.7	20.1 ± 5.0	211.0 ± 6.8	182.9 ± 2.7	13.3 ± 3.5
Pyr	201.7 ± 11	103.1 ± 2.1	48.9 ± 6.2	168.6 ± 6.4	140.9 ± 2.14	16.4 ± 4.1
Chr	38.4 ± 0.7	32.0 ± 4.2	16.7 ± 11.1	33.0 ± 0.41	36.46 ± 4.28	-10.5 ± 13
Total	2321 ± 57	1015.6 ± 12.8	56.2 ± 1.0	2043 ± 26	1631.9 ± 19	20.1 ± 1.5

Table 5.5 Mass of monitored creosote compounds removed from the oxidation columns with $KMnO_4$ at a concentration of 15 g/L.

5.5.2 Model Assumptions and Calibration

The BIONAPL/3D finite element numerical model (Frind et al., 1999; Molson, 2002) was used to simulate all column experiments. The column (11.7 x 4.43 cm) was discretized with 80 elements and a time step of 0.001 days was used for higher flow rates-shorter time experiments and a time step of 0.005 days was used for the control column and lower flow rate-longer time $KMnO_4$ experiments. Spatial resolution and time step size were constrained by the grid Peclet and Courant criteria (Daus et al., 1985).

The flow rates in the model were fixed to match the experimental conditions in which the solutions were flushed through the columns with a peristaltic pump. For the higher flow rate experiments, the linear velocity was set to 3.87×10^{-5} m/s, for the lower flow rate experiments the linear velocity was set to 5.38×10^{-6} m/s and for the control column, 1.72×10^{-5} m/s was used. The simulations assumed that the bulk porosity did not change during the

experiment. The linear velocity, bulk porosity and dispersivities were calibrated using the data obtained from the breakthrough curves of the conservative tracer. The porosity used for the $KMnO_4$ columns and control columns was 0.42 and 0.47 respectively. Dispersivities values of 0.0008, and 0.0004 were assigned for the $KMnO_4$ columns and control column respectively. Experimental tracer data and model simulations are shown in Figures 5.8 and 5.9.

The hydraulic conductivity was set equal to the average of the initial falling head determinations (4.5×10^{-5} m/s) and the diffusion coefficient of 5×10^{-10} m^2s^{-1} was used for all columns. The simulations were completed assuming a bulk density of 1500 kg/m^3, a mean grain diameter of 7.3×10^{-4} m, a residual water saturation of 0.07 as determined for Borden sand (Mackay et al., 1986).

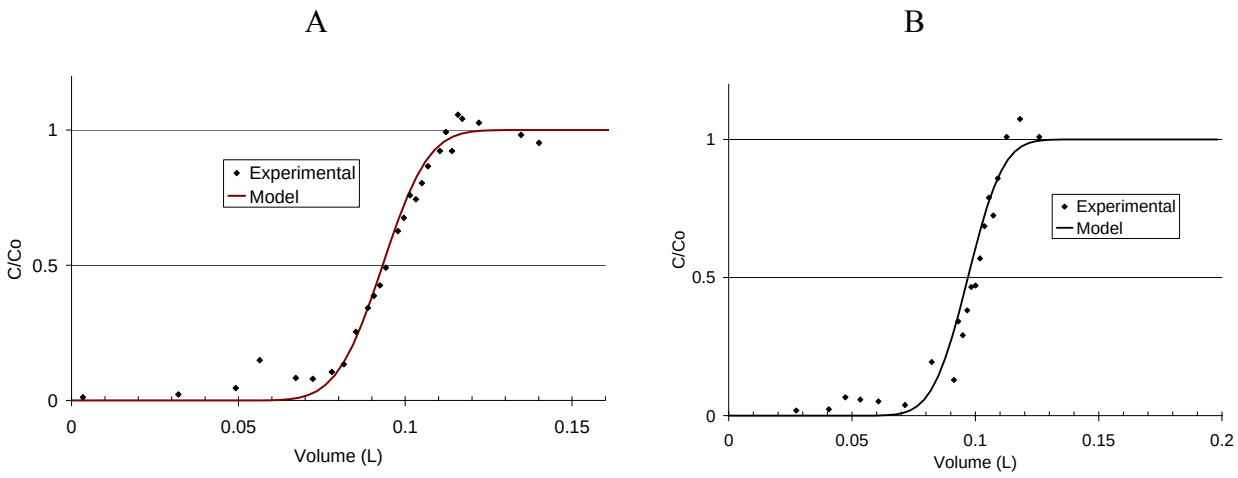

Figure 5.8 Sodium chloride initial breakthrough curves for the oxidation columns: Linear velocity v= 3.87 10^{-5} m/s, bulk porosity θ = 0.42, longitudinal dispersivity α_L= 0.008 m. Graph A: [$KMnO_4$] = 3g/L, Graph B: [$KMnO_4$] = 15 g/L

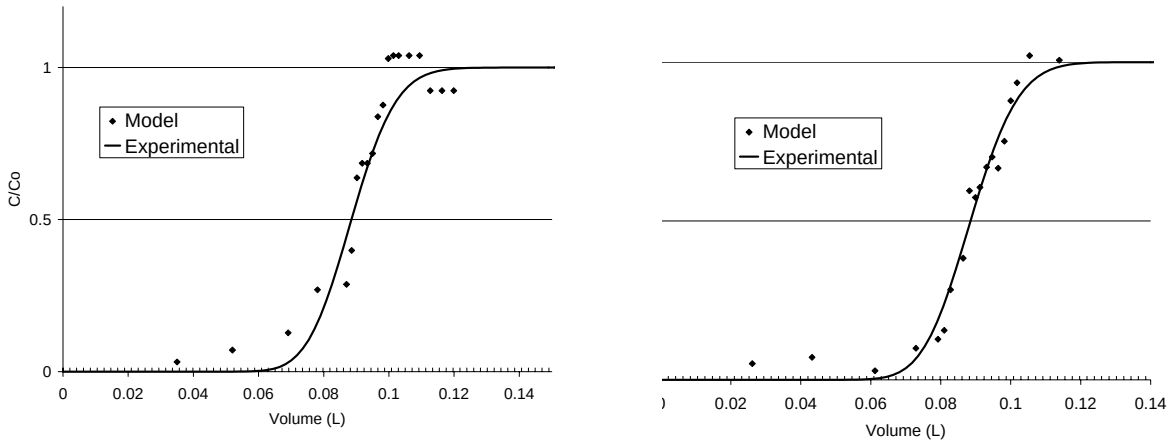

A B

Figure 5.9 Sodium chloride initialbreak through curves for oxidation columns. Linear velocity v= 5.38 10^{-6} m/s, bulk porosity Θ= 0.42, longitudinal dispersivity α_L = 0.008 m Graph A: [$KMnO_4$] = 3 g/L, Graph B:[$KMnO_4$] = 15 g/L

The Sherwood number and dissolution coefficient (β^m), which affects the DNAPL dissolution rate (Equation 5.10), were calibrated to the observed breakthrough data (control column only) and the observed mass of selected creosote compounds remaining in the column. The molecular weight, solubility and retardation values for the unknown fraction were also determined concurrently with the Sherwood number and β values by calibration of the model to the observed breakthrough data of the control column.

It is important to note that approximately 40% by weight of the creosote oil used for these experiments was unidentified and was modeled as a single compound. The unknown fraction in coal tars and creosote will, in reality, contain a mixture of lighter and heavier molecular weight compounds with varying solubilities. As dissolution proceeds, the unknown average molecular weight will change as the more soluble compounds are removed. Fortuitously, the creosote oil in this study did not contain light, highly soluble compounds like phenols, cresol or xylenes. Thus, the unknown fraction predominately consisted of heavier molecular weight and less soluble compounds and it was assumed that the molecular weight of the unknown fraction did not change during the dissolution process.

The molecular weights of coal tars and creosotes have been reported to range from 230 to 1600 g/mol (Peters and Luthy, 1993). Lee et al. (1992b) examined the partitioning of polyaromatic hydrocarbons from 8 different coal tars into water. The molecular weights for these coal tars ranged from 230 to 780 g/mol with densities ranging from 1.083 g/mL to 1.25 g/L. The molecular weight of the unknown fraction was determined through model calibration to be 260 g/mol, which is consistent for a creosote oil with a density of 1.1 g/mL (Lee et al., 1992b).

The liquid phase aqueous solubility, retardation and oxidation rate of the unknown fraction were chosen to be similar to known creosote compounds with heavier molecular weights, like chrysene, pyrene and fluoranthene. The liquid phase aqueous solubility of the unknown fraction was chosen to be 0.001 g/L and was given a retardation of 58. The first-order oxidation rate constant was chosen to be 10 times that of chrysene, 200 day^{-1} for 3 g/L and 1000 day^{-1} for 15 g/L.

Retardation values were calculated using equation 5.16 and a f_{oc} value of 0.0002 was used on the basis of measurements by Mackay et al. (1986) (Table 5.6).

The following assumptions were made in the numerical model:

- Residual creosote is immobile,
- Creosote dissolution occurs at equilibrium according to Raoult's Law (no oxidation),
- The molecular weight of the unknown creosote fraction does not change over time,
- The aqueous solubility of the unknown fraction does not change over time,
- The retardation value of the unknown fraction does not change over time,
- Mixing of the sand and creosote created a homogenous mixture.

Additional assumptions for the oxidation model include:

- Batch first-order rate constants are the same as the column oxidation rates,
- The oxidation rates are not affected by the formation of other manganese species (MnO_3^-, MnO_2),
- The model assumes that the $KMnO_4$ progresses through the column under normal advection and dispersion and does not initially decrease in concentration due to reaction with the sand,
- Oxidation occurs in the aqueous phase.

Compound	Log K_{ow} [a]	Log $_{oc}$ [b]	k_d [c] (cm^3/g)	R [d]
Naphthalene	3.35	2.89	0.15	2.0
1-methylnaphthalene	3.87	3.31	0.41	2.5
Biphenyl	3.95	3.38	0.48	2.8
Acenaphthene	3.92	3.35	0.45	2.7
Dibenzofuran	4.12	3.52	0.66	3.4
Fluorene	4.18	3.57	0.74	3.7
Carbazole	3.29	2.84	0.14	1.5
Phenanthrene	4.57	3.89	1.54	6.7
Anthracene	4.45	3.79	1.23	5.5
Fluoranthene	5.22	4.42	5.27	20.4
Pyrene	5.18	4.39	4.88	19.0
Chrysene	5.79	4.89	15.5	58.0

[a] Miller et al., 1985

[b] $\log K_{oc} = 0.82 \log K_{ow} + 0.14$

[c] $K_d = K_{oc} f_{oc}$ where $f_{oc} = 0.002$

[d] $R = 1 + \frac{\rho_b K_d}{\theta}$ where $\theta = 0.42$ and $\rho_b = 1.55$ (g/cm^3)

Table 5.6 Retardation values calculated for the 12 monitored creosote compounds

5.5.3 Control Column Results

The Sherwood number, dissolution coefficient (β^m) and the molecular weight of the unknown fraction were used to calibrate the model to the experimental breakthrough data and to the mass remaining in the control column. The best match to the experimental data was obtained with a molecular weight of the unknown fraction of 260 g/mol and a Sherwood number of 6.

Using these values, the percentage removed from the column was close to the experimental values with a slight over-estimation of the mass removed for acenaphthene, dibenzofuran and fluorene. However, the mass of carbazole removed was over-estimated by 45%. The simulation also over-estimated the effluent aqueous concentrations of carbazole, dibenzofuran, fluorene and phenanthrene.

After adjusting the values of β, the simulated breakthrough data and percentage of mass removed correlated well with the experimental data (Table 5.7, Figures 5.10 to 5.12). The model underestimated the aqueous concentrations of 1-methylnaphthalene and anthracene. The aqueous concentrations determined by the model for 1-methylnapthalene and anthracene differ by a factor of 1.4 and 3.7 respectively. The over estimation could be caused by incorrectly determining the subcooled liquid aqueous solubility limits or by co-solvency effects in which there is an enhancement in their aqueous solubilities.

The rate at which the compounds reached their aqueous solubility limits in the experiments was slower than the rate simulated by the model as seen in the break through curves. This implies that at early times the system was not at equilibrium and that there was a time lag before dissolution reached equilibrium.

Compound	Experimental % removed	Model Simulation Sh = 6, β = 0 % removed	Model Simulation % removed	
			β	Sh = 6
Naphthalene	54.1 ± 42	54.6	0.0	54.19
1-methylnaphthalene	12.2 ± 12	14.72	0.0	14.3
Biphenyl	12.9 ± 17	11.4	0.0	10.9
Acenaphthene	3.5 ± 16	10.5	0.0	10.0
Dibenzofuran	3.1 ± 15	13.4	1.0	7.5
Fluorene	0.28 ± 15	8.6	1.1	4.3
Carbazole	30.0 ± 17	66.4	0.8	31.4
Phenanthrene	-3.7 ± 15	9.5	1.8	6.7
Anthracene	2.7 ± 15	2.4	0.0	2.2
Fluoranthene	-6.5 ± 15	1.5	0.5	1.0
Pyrene	-0.24 ± 16	1.9	1.4	0.32
Chrysene	-2.7 ± 24	0.51	0.0	0.46

Table 5.7 Comparison between experimental and model simulations for the column without oxidation

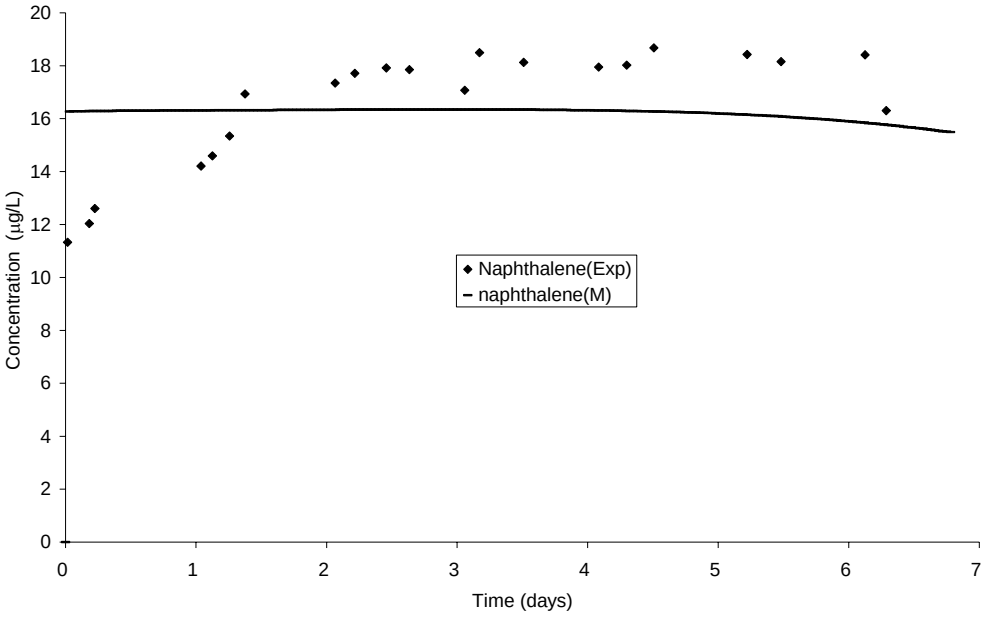

Figure 5.10 Naphthalene effluent concentrations for the Control column. Sh = 6, β = values given in table 5.7.

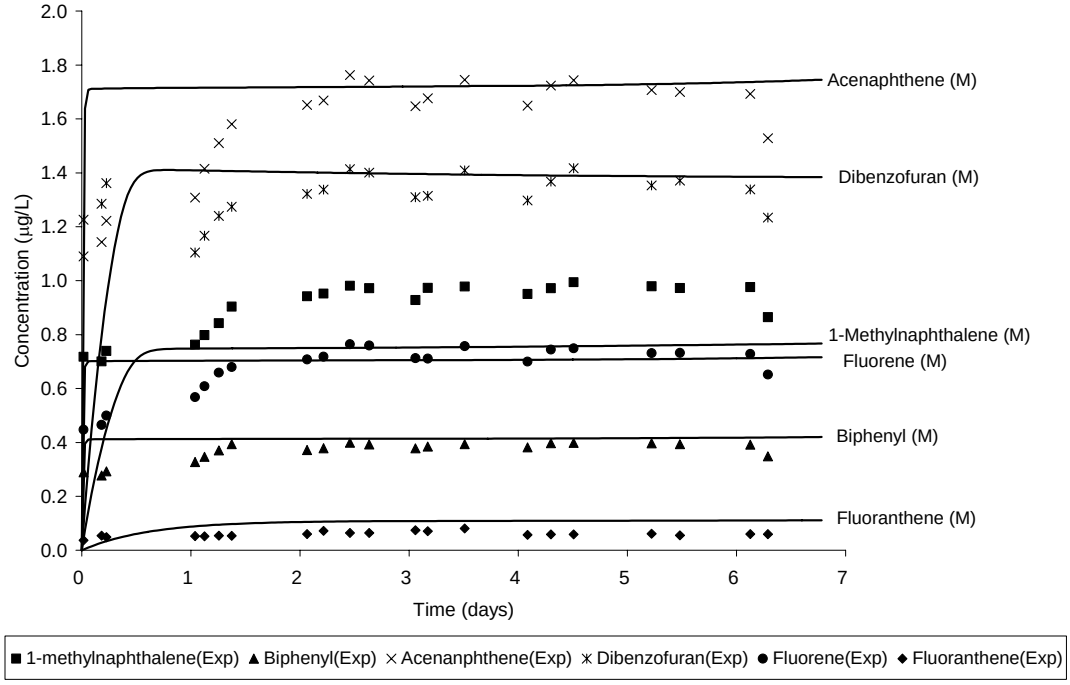

Figure 5.11 Experimental (Exp) and model (M) effluent concentrations for the Control column. Sh = 6, β values given in table 5.7. (Acenaphthene, Dibenzofuran, 1-Methylnaphthalene, Fluorene, Biphenyl and Fluoranthene).

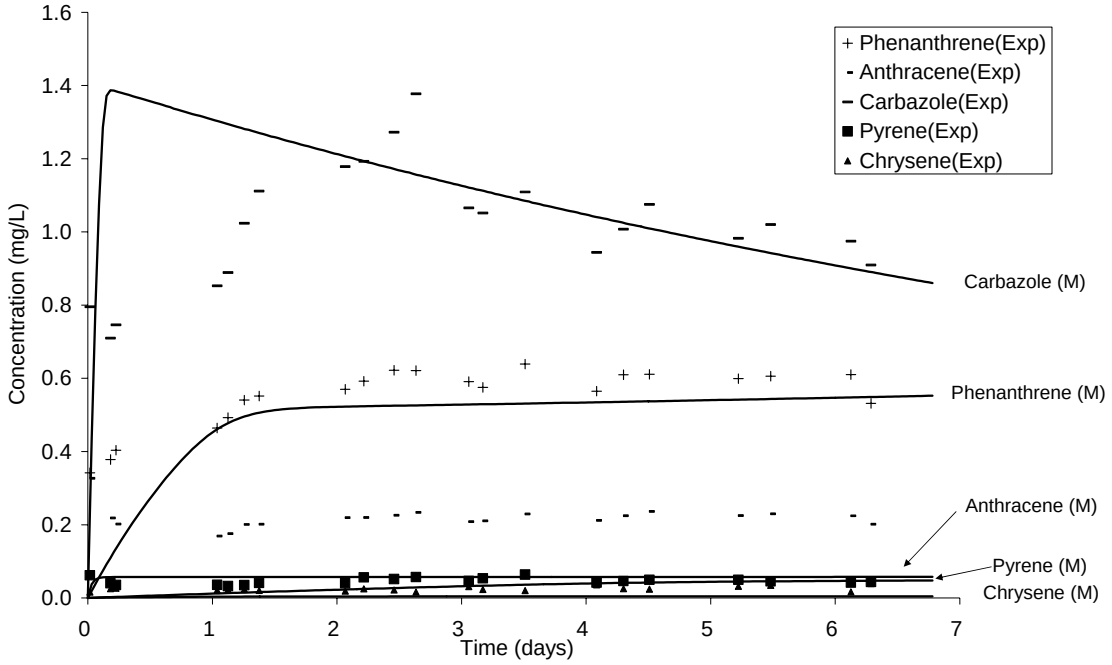

Figure 5.12 Experimental (Exp) and model (M) effluent concentrations for the Control column. Sh = 6, β values given in table 5.7. (Phenanthrene, Anthracene, Carbazole, Pyrene, Chrysene).

5.5.4 Oxidation Column Simulations

Comparison between the oxidation/dissolution model and experimental data was achieved by comparing the mass of the creosote compounds left in the columns and calculating the percentage removed. When the oxidation column was simulated using the Sherwood number and β values obtained from the control column far less mass of creosote compounds was removed in the simulation than determined experimentally. If the Sherwood number was increased, the results matched more closely to the experimental data. For the columns flushed with 3 g/L of $KMnO_4$, the Sherwood number was increased to 15 and for the columns flushed with 15 g/L of $KMnO_4$ the number was increased to 60. The β values also had to be changed to obtain a better agreement with the experimental data. The comparison of the experimental data and model simulation is shown in Table 5.8. The simulated data are generally in good agreement with the experimental data and are within the calculated experimental errors.

A change in the Sherwood number between the columns with, 0, 3 and 15 g/L of $KMnO_4$, suggests a change in the mass transfer coefficient and/or thickness of the thin film as described by the relationship given in equation 5.6,

$$\mathrm{Sh} = \frac{\lambda l}{D} \tag{5.6}$$

However, in the model used to simulate the mass of creosote compounds removed from the columns the characteristic length or film thickness was held constant and set as the median grain diameter. Since the aqueous diffusion coefficient is constant, the Sherwood number and the mass transfer coefficient are directly proportional to each other in the model. Thus, any change in the observed mass transfer rate must be adjusted in the model with the Sherwood number. A possible reason for the difference in the solute mass fluxes between the columns with different $KMnO_4$ concentrations could be the diffusion of $KMnO_4$ into areas of diffusive transport.

The stagnant layer model is based on the diffusion-limited mass transport of constituents across a thin film. Since the stagnant film will vary within the column it is defined as an average over a representative elementary volume which includes areas of low flow or hydraulically isolated areas as well as oil droplets exposed to the flowing water. The scenario shown in Figure 5.13 represents the varying path lengths a solute must travel before becoming part of the advective flow. At the front of the column when the concentration of the compound is below its effective solubility, mass transport will occur though the stagnant layer into the flowing water. Downstream, mass transfer will no longer take place once the compound has reached its aqueous solubility limit. The thickness of the stagnant layer or the characteristic length scale used in the model is the median grain size diameter.

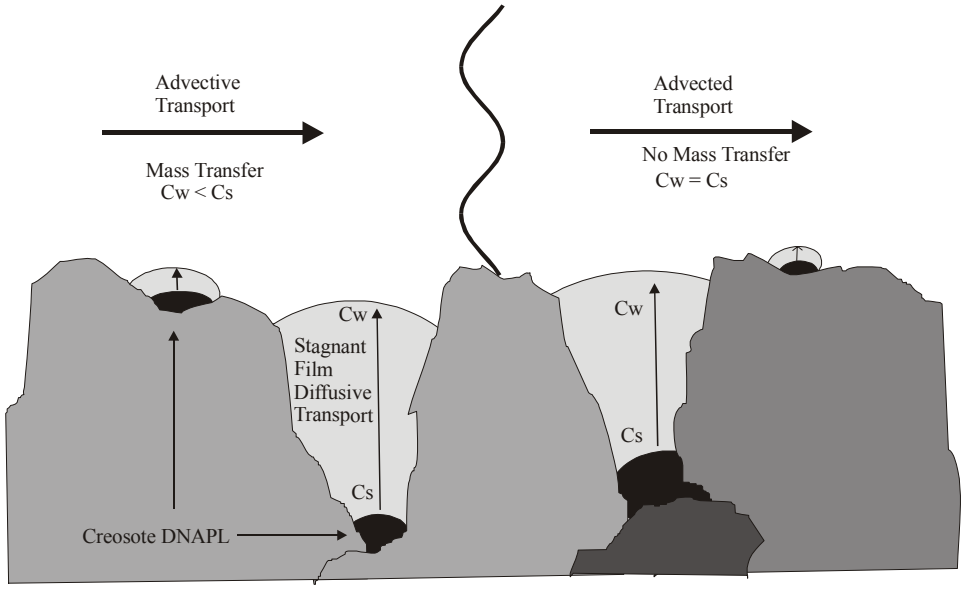

Figure 5.13 Conceptual diagram of diffusion-limited mass transport of creosote compounds from the oil into flowing water.

When $KMnO_4$ was added to the column the mass removed by the model underestimated the observed mass lost. To match the model to the experimental data the Sherwood number had to be increased to reflect the increase in the mass transfer. A possible explanation for the increased mass lost in the oxidation columns is a shrinking of the stagnant layer caused by the diffusion of $KMnO_4$ from mobile zones into areas of no or low flow. As $KMnO_4$ travels through the pore spaces, $KMnO_4$ will diffuse into the stagnant layer and decrease the thickness of the thin film (Figure 5.14). The rate at which diffusion into these areas occurs will decrease as the concentration of $KMnO_4$ increases, but because $KMnO_4$ reacts with oxidizable compounds, its concentration in the areas of diffusive transport will always be lower than the areas of advective transport (as long as there is oxidation occurring). Thus $KMnO_4$ will continuously be diffusing into the stagnant layer. When the concentration of $KMnO_4$ was increased from 3 g/L to 15 g/L the Sherwood number in the model had to be increased further from 15 to 60 to match the increased mass loss observed in the experimental data. This could possibly be caused by an increase in the rate of $KMnO_4$ diffusion into the stagnant layer caused

by the higher concentration gradients imposed by the higher concentration of $KMnO_4$, which subsequently decreases the thickness of the thin film.

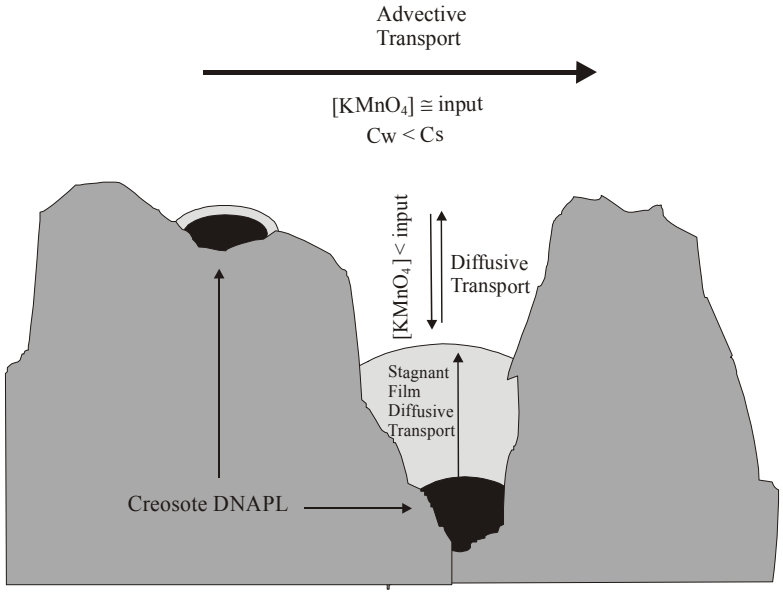

Figure 5.14 Conceptual diagram of diffusion-limited mass transport of creosote compounds from the oil into advective flow and $KMnO_4$ into areas hydraulically isolated which decreases the stagnant film.

The equation used in the model to describe the mass transfer coefficient was given by,

$$\lambda_i^m = Sh \frac{D^m}{(d_{50})^2} \left(\frac{f_i^m S_{n_i}}{S_{n_0}} \right)^{\beta^m} \tag{5.10}$$

In this equation the characteristic length at which diffusion occurs is estimated and fixed as the median grain size. However in the above discussion the characteristic length scale could be decreasing due to the diffusion of $KMnO_4$ into areas at which diffusive mass transport is occurring. The characteristic length is no longer the median grain diameter but an unknown value that can not be measured. The Sherwood number was changed because it is directly proportional to a change in the mass transfer rates experimentally observed. However

conceptually in the model it is the ratio of the Sherwood number to film thickness that is changing and not the Sherwood number directly.

Similar results have been observed in the oxidation of perchloroethylene and trichloroethylene with $KMnO_4$ in which the numerical model included both multi-phase flow and multi-component reactive transport equations and used kinetic mass transfer and oxidation reaction rates (Hood, 2002). Their results indicated enhancement of mass transfer occurred because of the diffusion of the oxidant into non-advective zones containing advectively-isolated DNAPL and in general, the magnitude of the enhancement was shown to be dependant upon the diffusion path length.

The β values for the oxidation models decreased for dibenzofuran, fluorene, phenanthrene and pyrene and remained the same for carbazole and fluoranthene in comparison with the non oxidation column. This could be caused by a change in the surface of the creosote oil and change the rate of diffusion out of the oil into the stagnant film. The change could also be caused by the high ionic strength of the $KMnO_4$ solution that is in contact with the oil or by the precipitation of manganese dioxides on the surface of the oil. It was beyond the scope of this research to investigate this phenomenon.

Thus the model provides a reasonable approximation of the complex oxidation/dissolution process and provides a good estimation of enhanced removal of creosote compounds at two different flow rates and $KMnO_4$ concentrations. The model also provides an opportunity to improve our understanding of the complex oxidation/dissolution process by examining the 1D linear profiles within the column; an observation that is very difficult to obtain through experimental procedures. Simulations can also be run for longer periods of time in order to estimate the length of time it would take to remove the monitored compounds from the oil phase.

		$[KMnO_4]$ = 3g/L Flow rate = 2.72 x 10^{-3} m^3/day Sherwood number = 15		$[KMnO_4]$ = 3g/L Flow rate = 3.59 x 10^{-4} m^3/day Sherwood number = 15	
Compound	β	Experimental % removed	Model % removed	Experimental % removed	Model % removed
Naphthalene	0.0	15.1 ± 18	18.1	53.5 ± 12.2	49.8
1-methylnaphthalene	0.0	10.4 ± 15.8	5.1	32.5 ± 11.2	16.7
Biphenyl	0.0	8.4 ± 15.2	2.7	4.0 ± 11.9	3.7
Acenaphthene	0.0	23.5 ± 15.3	13.6	45.6 ± 17.9	66.9
Dibenzofuran	0.0	4.9 ± 15.1	3.4	11.5 ± 16.9	4.5
Fluorene	0.5	19.8 ± 15.0	6.9	48.4 ± 16.2	40.9
Carbazole	0.8	24.9 ± 13.8	11.8	65.6 ± 16.6	54.3
Phenanthrene	0.8	4.0 ± 15.5	2.4	29.5 ± 23.7	17.1
Fluoranthene	0.5	2.3 ± 12.4	0.8	11.6 ± 16.4	6.5
Pyrene	0.5	5.6 ± 13.0	1.0	20.8 ± 18	8.1
Chrysene	0.0	0.8 ± 20.0	0.3	13.8 ± 14.8	0.5
		$[KMnO_4]$ = 15g/L Flow rate = 2.72 x 10^{-3} m^3/day Sherwood number = 60		$[KMnO_4]$ = 15g/L Flow rate = 3.59 x 10^{-4} m^3/day Sherwood number = 60	
	β	Experimental % removed	Model % removed	Experimental % removed	Model % removed	Model % removed no oxidation
Naphthalene	0.0	15.9 ± 5.2	36.4	83.0 ± 12	98.1	13.3
1-methylnaphthalene	0.0	14.0 ± 4.0	11.6	60.3 ± 7.0	64.4	4.2
Biphenyl	0.0	17.8 ± 3.7	3.5	17.3 ± 12.5	4.8	3.2
Acenaphthene	0.0	27.3 ± 3.6	46.4	85.1 ± 4.7	99.9	4.0
Dibenzofuran	0.0	17.3 ± 3.5	4.3	15.3 ± 3.0	6.1	2.8
Fluorene	0.5	28.7 ± 7.0	24.8	84.2 ± 3.2	90.1	1.5
Carbazole	0.8	65.0 ± 6.7	35.9	80.8 ± 5.8	92.1	13.6
Phenanthrene	0.8	21.1 ± 3.5	10.0	54.1 ± 5.5	63.4	0.7
Fluoranthene	0.5	13.3 ± 3.5	3.4	20.1 ± 5.0	34.3	0.6
Pyrene	0.5	16.4 ± 4.1	4.3	48.9 ± 6.2	40.3	0.3
Chrysene	0.0	-10.5 ± 13	0.52	16.7 ± 11.1	2.0	0.4

Table 5.8 Comparison between experimental data and model simulations for the oxidation columns. Also included; simulation without oxidation for $KMnO_4$ column at 15 g/L, flow rate = 3.59 x 10^{-4} m^3/day.

5.5.5 Enhanced Mass Transfer

The rate at which an organic compound is removed from the oil phase is dependant on the rate of dissolution and on the rate of oxidation. For compounds that are readily oxidized by

$KMnO_4$ it is expected that their aqueous concentration will decrease throughout the column and the mass transfer of these compounds from the oil phase will be significant because of the large imposed concentration gradient through the stagnant film. Conversely, for compounds that are not oxidized by $KMnO_4$ their aqueous concentration will be a function of their mole fraction and enhanced removal of these compounds may not be observed. Model simulations were used to investigate the dynamic oxidation/dissolution process by examining the 1D profiles of the aqueous concentrations of the modeled compounds as well as the oil saturation through the column. The model was also used to compare the length of time or the number of pore volumes it would take to remove the selected creosote compounds from the oil phase with and without oxidation.

The oxidation column ([$KMnO_4$] =15 g/L, 3.59 x 10^{-4} m^3/day) was modeled with and without oxidation and the results are shown in Table 5.8. The Sherwood number and β values used for the numerical model without oxidation were the same as those determined by the control column experiment. These results provide a direct comparison for the dissolution of creosote compounds with and without oxidation. Three types of compounds were examined; 1) pyrene, a readily oxidizable compound that has a low aqueous solubility, 2) dibenzofuran and biphenyl, which are stable non-oxidizable compounds, and 3) and naphthalene, a compound that has a high mole fraction, a relatively high solubility in water and is reactive towards $KMnO_4$.

The 1D profiles of naphthalene's aqueous concentration through the column at 0.5 and 5.0 days for the oxidation and no oxidation simulations are shown in Figure 5.15. The no oxidation curves clearly demonstrate the propagation of the mass transfer zone. As water enters the column, the aqueous phase concentration increases until it reaches its aqueous solubility limit and at this point mass equilibrium has been reached. As dissolution occurs, the mass transfer zone propagates down the column as naphthalene is removed from the oil phase at the influent end of the column. The concentration profile for the oxidation simulations shows a decrease in the aqueous concentration throughout the length of the column. Thus dissolution or mass transfer from the oil phase into the aqueous phase is now occurring throughout the entire

column. After 5 days approximately 98% of the naphthalene had been removed from the oil phase and its mole fraction within the oil had dropped dramatically; consequently, its aqueous phase concentration also decreased dramatically.

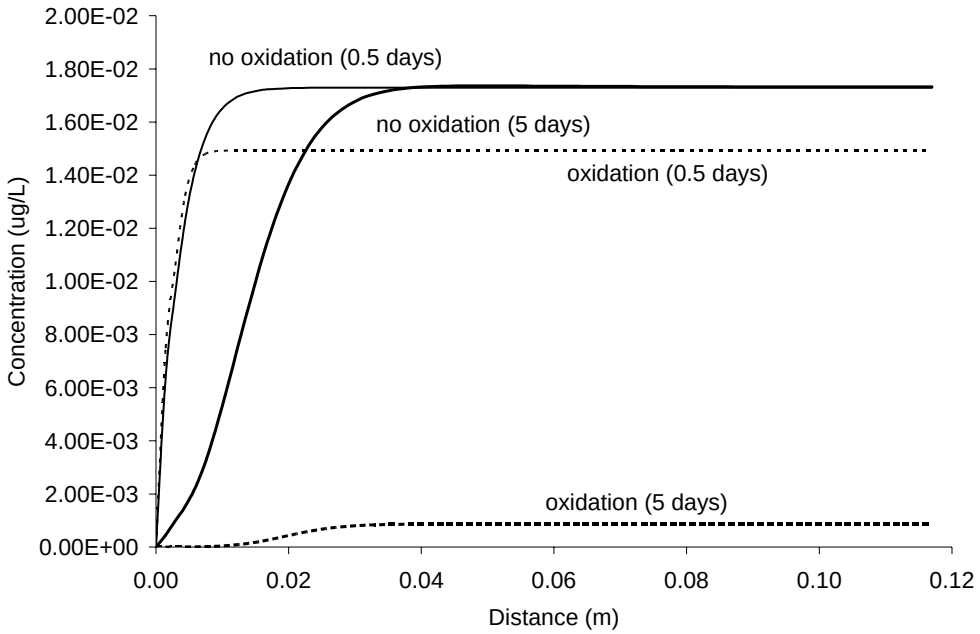

Figure 5.15 1D profiles of the simulated naphthalene concentrations with the column

Pyrene is a readily oxidizable PAH but has a very low aqueous solubility. The 1D profile showed that after 5 days in the no oxidation model, the aqueous concentration actually increased (Figure 5.16), because as the more soluble compounds are removed from the oil phase, the mole fraction and aqueous solubility of pyrene increases (equation 5.2). In the oxidation simulation, as expected with this rapidly oxidizable compound, the concentration in the aqueous phase decreased significantly. It is interesting to note that the pyrene concentration after 5 days is approximately the same as it was after 0.5 days. This is most likely due to the fact that the rate of dissolution is limiting. After 5 days, 40% of the pyrene was removed in the oxidation column and only 0.3 % in the no-oxidation simulation. This indicates that the mass transfer zone for pyrene is the entire column, but the rate of removal for this sparingly soluble compound may be limited by the rate of dissolution.

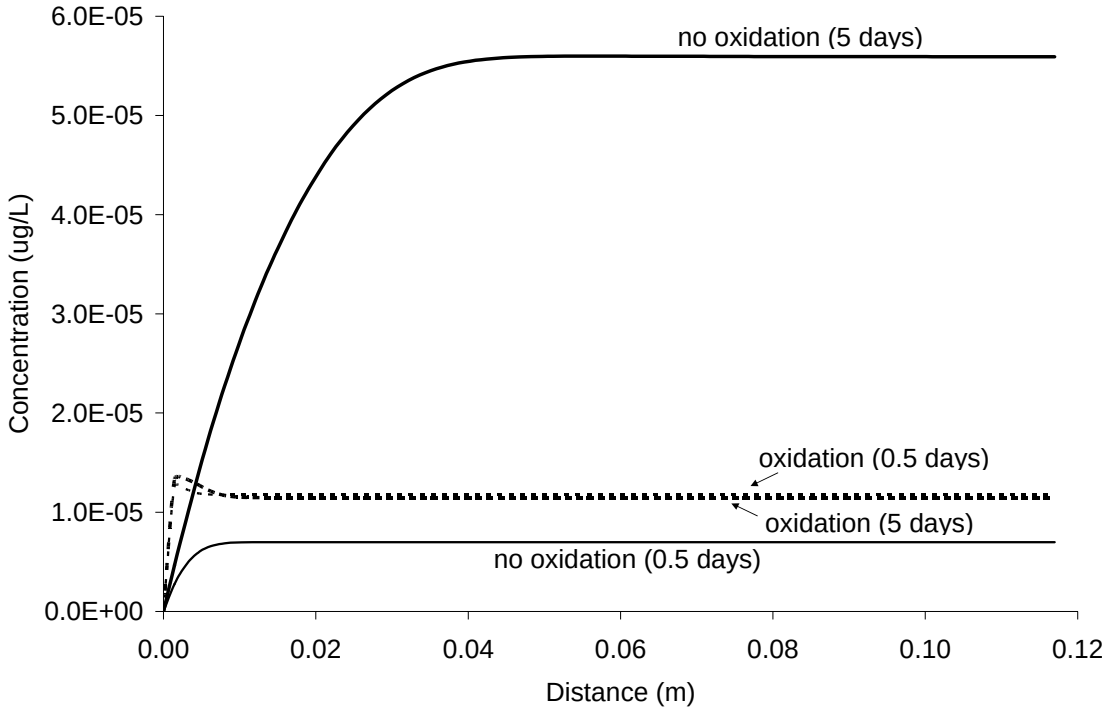

Figure 5.16 1D profile of the simulated pyrene concentrations within the column.

The most recalcitrant compounds, such as dibenzofuran and biphenyl have very low aqueous solubilities and are not oxidized by $KMnO_4$. For these compounds, mass transfer will only occur at the influent end of the column. The concentration profiles for dibenzofuran and biphenyl is shown in Figure 5.17. The no-oxidation simulations showed that after 5 days the aqueous concentrations of biphenyl and dibenzofuran had increased because of an increase in their mole fraction as the more soluble compounds were removed from the oil phase. In the oxidation simulations a large increase in the aqueous concentration was observed after 5 days. The increase in aqueous concentrations is again due to the increased mole fraction in the oil phase. The significance of this observation is that the oxidation process, which enhances the dissolution of more oxidizable compounds, also increased the mass transfer of the non oxidizable compounds at the influent end of the column by increasing their mole fractions in the creosote oil.

The model developed by Frind et al. (1999) also calculates oil saturation through the column (Figure 5.18). The no-oxidation 1D profile illustrates that mass transfer only occurred at the influent end of the column and that the oil saturation was only reduced at the front of the column. For the oxidation column the oil saturation was reduced from 0.03 to 0.016 throughout the column after 5 days denoting that there is an enhanced mass transfer for the more oxidizable compounds along the entire length of the column.

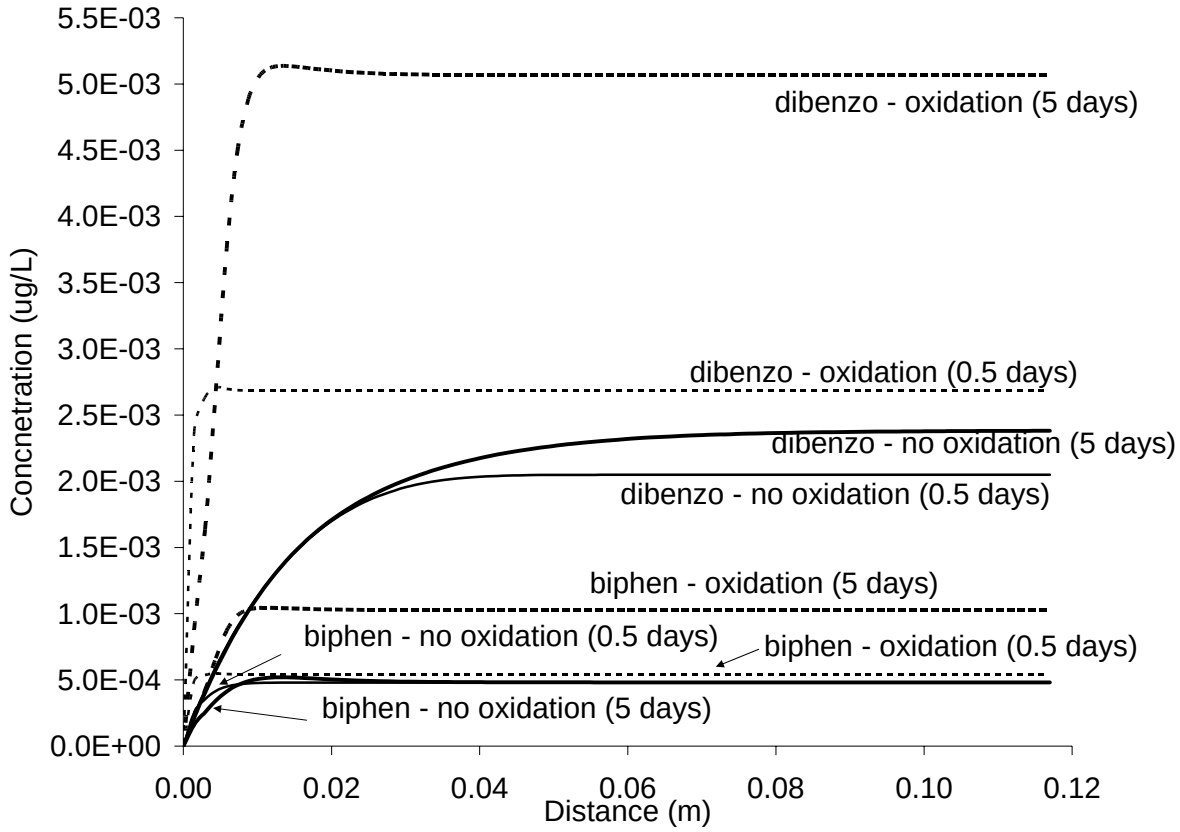

Figure 5.17 1D profiles of simulated dibenzofuran and biphenyl aqueous concentrations in the column.

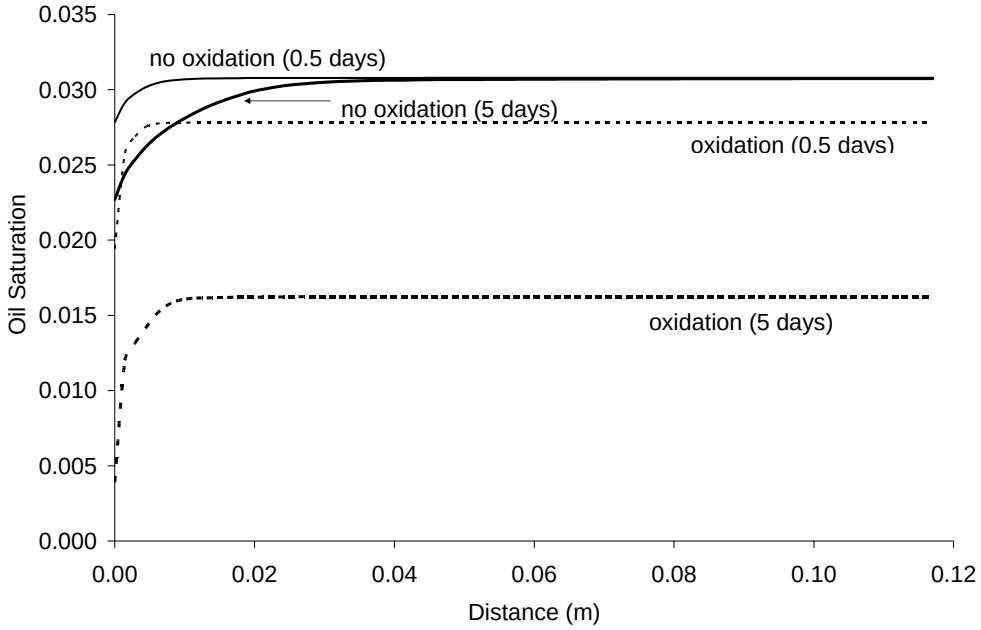

Figure 5.18 Simulated oil saturations along the column.

To determine the effect of oxidation on the length of time it takes to remove 99% of the selected compounds from the oil phase, model times were extended (Table 5.9). It was assumed that the physical/chemical parameters of the unknown fraction and of the sand column did not change during the simulation. The longer time simulation for the control column in which normal advection/dispersion and dissolution occurs depicts the recalcitrant nature of creosote and why it is of environmental concern. Compounds that are sparingly soluble and have a high mole fraction such as pyrene and phenanthrene would take over 12 years and more than 5000 pore volumes to completely dissolve from the 12 cm long column. For other compounds like chrysene, fluoranthene and fluorene, it would take over 3 years to reduce their masses to 1/100 of their initial value.

Using the same initial conditions but now with the addition of $KMnO_4$ at a concentration 15 g/L, the length of time it takes to reduce the mass of the monitored creosote compounds was greatly reduced. The greatest decrease in time was observed for compounds that are readily oxidized such as naphthalene and pyrene. For naphthalene and pyrene the time was reduced

from 22.4 to 4.5 days and from 12.6 years to 27.2 days respectively. For compounds that are not oxidized by $KMnO_4$, such as biphenyl and dibenzofuran, the time was reduced from 117.5 to 24.7 days and 835.8 to 23.7 days respectively. As stated above in the discussion with 1D profiles, the rapid removal of the more readily oxidizable compounds from the oil phase increases the mole fraction of the non oxidizable compounds and in accordance with Raoult's Law, the concentration in the aqueous phase moves closer to its pure phase liquid solubility and more mass is removed from the oil. For very sparingly soluble compounds that do not react quickly with $KMnO_4$ such as chrysene, there was also a remarkable decrease in time from 3.8 years to 40 days.

A major factor that must be considered with the application of $KMnO_4$ at a field site is the rate at which the reagent is injected. Because the flow rate affects the rate of dissolution, the volume of reagent used and ultimately the cost of remediation will be affected. Shown in Table 5.9 is a simulation of the same column but at a linear ground water velocity 10 times slower.

For compounds that are readily oxidized by $KMnO_4$, the length of time that was required to reduce their mass by 99% was not greatly increased in the low flow rate scenario. For example, naphthalene, which has a high aqueous solubility and is fairly reactive towards $KMnO_4$, took 5.1 days as opposed to 4.5 days at the higher flow rate. Pyrene, which is much more reactive than naphthalene but is far less soluble, took a little longer, at 37.7 as opposed to 27.2 days at the higher flow rate. Compounds that are not reactive towards $KMnO_4$ took significantly longer to remove at the slower flow rate. Chrysene, for example, takes 89 days to reduce its mass by 99% at the slower flow rate as opposed to 39 days. This is not unexpected, for the non-reactive sparingly soluble compounds, because the enhanced mass transfer process is not directly due to their oxidation but due to an increase in their mole fraction. Also, mass transfer only occurs at the influent end of the column for non oxidizable compounds.

The removal of creosote compounds from the oil phase will take longer at lower flow rates but the volume of $KMnO_4$ needed to remove the compounds is considerably less. With

naphthalene, for example, only 6.5 pore volumes are needed to reduce its mass by 99% at the slower flow rate as opposed to 56.5 pore volumes at the higher flow rate. This is because the enhanced rate of dissolution is mainly due to the reduction in aqueous phase concentrations, caused by the chemical oxidation process throughout the column. Similarly, the time needed to reduce the more recalcitrant compounds like chrysene was significantly longer but the pore volume needed was approximately 4.5 times less using the lower flow rate.

Thus increasing the flow rate will not significantly increase the rate of the mass removal for compounds that are readily oxidized. Increasing the flow rate for less reactive compounds increased the rate of removal, however, by increasing the flow rate larger volumes of reagent are then needed.

Linear Velocity (m/s)	1.72×10^{-5}		1.72×10^{-5}		1.72×10^{-6}	
[$KMnO_4$] (g/L)	0.0		15.0		15.0	
Compound	Days	Pore Volumes	Days	Pore Volumes	Days	Pore Volumes
Naphthalene	22.4	284.5	4.45	56.5	5.12	6.5
1-methylnaphthalene	88.5	1124.2	12.62	160.3	14.01	17.8
Biphenyl	117.5	1492.6	24.65	313.1	87.08	110.6
Acenaphthene	129.3	1642.5	3.07	39.0	3.11	3.9
Dibenzofuran	835.8	10616.9	23.74	301.6	85.85	109.1
Fluorene	1243.3	15793.3	11.9	151.2	12.37	15.7
Carbazole	265.4	3371.3	17.1	217.2	18.69	23.7
Phenanthrene	4536.6	57627.1	25.9	329.0	37.27	47.3
Fluoranthene	1081.4	13736.7	26.78	340.2	40.85	51.9
Pyrene	4618.2	58663.6	27.16	345.0	37.69	47.9
Chrysene	1408.5	17891.8	39.48	501.5	89.42	113.6

Table 5.9 Model simulations used to determine the time and pore volumes needed to reduce the mass of creosote compound to 1/100 of its original mass.

5.6 Conclusions

Permanganate is a powerful oxidant that readily oxidizes a wide range of polycyclic aromatic hydrocarbons. A column flushed with $KMnO_4$ greatly enhances the mass transfer of creosote compounds from the oil phase into the water phase. Experimentally it was determined

that for the same volume of reagent passed through the columns the slower flow rate and higher $KMnO_4$ concentration removed more of the monitored creosote compounds from the oil phase at a faster rate. For example, 56% of the monitored creosote compounds were removed from a column containing creosote at 3% oil saturation and a $KMnO_4$ concentration of 15 g/L (flow rate = 3.6×10^{-4} m^3/day) compared to only 11% for a column that was flushed with $KMnO_4$ at a concentration of 3 g/L (flow rate = 2.7×10^{-3} m^3/day).

Simulations of the $KMnO_4$ column experiments indicated that the mass removed from the columns was significantly greater than what could be attributed to the aqueous chemical oxidation of solutes alone. A possible explanation for the increased mass transfer is the diffusion of $KMnO_4$ into less permeable or hydraulically isolated areas. Diffusion of $KMnO_4$ occurs because of the concentration gradient between flowing water and hydraulically isolated areas. Conceptually, this would reduce the stagnant film and increase the rate of mass transfer across the interfacial boundary between the two phases.

The most significant result is in the removal of compounds that have low aqueous solubilities and are readily oxidized, such as pyrene and fluorene. Compounds that have low aqueous solubilities and are not readily oxidizable, such as biphenyl and chrysene may still take a long period of time to be removed but the interval is greatly reduced compared to flushing the contaminated area with water alone. Numerical model simulations indicate that for the more readily oxidizable compounds the percentage of mass removed from the column was not significantly increased by increasing the flow rate; whereas, for the non-oxidizable compounds, the rate at which their mass was removed increased with increasing flow rate.

Thus the chemical oxidation process enhances the removal of creosote oil by: a) increasing the mass transfer zone by decreasing concentration of creosote compounds in the aqueous phase, b) increasing the aqueous solubility of less readily oxidizable compounds by increasing their mole fraction and c) increasing the mass transfer process possibly through the diffusion of permanganate into areas of low permeability or hydraulically isolated areas.

5.7 Field Site Strategies for the use of $KMnO_4$ for the *in situ* Remediation of Creosote/Coal Tar Residuals

It is most likely impossible to remove all the coal tar/creosote oils from a contaminated subsurface area unless it is excavated. Thus, after treatment of the contaminated area, it is desirable to leave the site in a condition that no longer represents an environmental hazard. The chemical oxidation technology enhances the dissolution process and preferentially removes the more abundant, more soluble, and more reactive compounds at a faster rate than the less soluble, less reactive compounds, leaving behind the compounds that have large molecular weights and low aqueous solubility. This causes a net increase in viscosity of the oil and yields a more stable recalcitrant residual mass. As such, this chemical weathering or hardening of the oil decreases the flux of creosote compounds released into the flowing ground water and natural attenuation processes are more readily capable of managing the associated plumes.

The goal of the oxidation technology is not only to remove the oil by enhancing the oxidation/dissolution process, but also to stabilize the residual contaminants so that lower concentrations of creosote compounds are leaching into the ground water.

Chemical weathering of the oil and the potential precipitation of MnO_2 along the oil interface may decrease the flux of creosote compounds dissolving into the flowing ground water. The main product of the oxidation process is manganese dioxide, which is insoluble and can cause a reduction in aquifer permeability. Initially this was thought to be undesirable, but recent studies have shown that this undesirable effect can have a positive outcome.

Precipitation of MnO_2 is undesirable because it reduces the permeability of the soil by clogging pore spaces. This in turn reduces the ability to deliver the reagent to the contaminated area. Recent work by MacKinnon and Thomson (2002) has shown that

treatment of a pool of perchloroethylene (PCE) with $KMnO_4$ not only oxidized PCE and greatly enhanced the mass transfer rate, but also precipitated a layer of MnO_2 above the pool. It was observed that after the initial enhanced removal of PCE the observed rate of oxidation slowly decreased over time. This is probably due to the deposition of MnO_2. It was also observed that the MnO_2 deposits decreased the velocity of water above the pool, decreased the hydraulic conductivity of the aquifer system and decreased the mass transfer from the remaining pool.

One of the main problems with any *in situ* application is the delivery of the oxidant to oils trapped in immobile areas that have no flow or have greatly reduced permeability. The implication from the above experiment is that even if the oxidant cannot reach the entrapped oils, the precipitation of MnO_2 into pore spaces around the entrapped contamination will hydraulically isolate the oil from flowing water. This in turn would greatly diminish the mass flux of contaminants emanating from the contaminated area.

It is believed that this same process will occur with residual creosote. As permanganate is flushed through the contaminated area, the chemical oxidation process will enhance the removal of creosote compounds from the oil phase. Permanganate will also diffuse into areas of low permeability. Chemical weathering of the oil occurs and precipitation of MnO_2 will physically coat the surface of the oil. Both processes will reduce the mass flux of creosote compounds being released to the ground water. These hypotheses are currently being investigated with a field scale experiment at CFB Borden (Lemarche, 2002).

Advantages of $KMnO_4$ for Stabilization of Creosote Residuals

1. High concentrations of $KMnO_4$ ensures that the oxidizing reagent concentration does not become limiting and that the rate of chemical oxidation is optimal.

2. A high concentration of permanganate also means that its concentration can be maintained throughout the contaminated area unlike many oxidants such as Fenton's reagent that becomes non-reactive only a few meters away from the injection well.

3. Permanganate exhibits fast reaction times with organic material, but non-reacted $KMnO_4$ will persist in the subsurface for several months. Thus delivery of $KMnO_4$ can be accomplished by injecting the oxidant into up-gradient wells and allowing it to flow through the contaminated area under natural ground water flow.

4. Encapsulating of residual oils in the targeted zone with MnO_2 may decrease the concentrations of creosote compounds leaching from the DNAPL to very low or negligible concentrations, thereby stabilizing the source area.

5. $KMnO_4$ is an easily handled free flowing solid available as 99% active ingredient. Delivery of the material to the subsurface can be accomplished using standard equipment and routine health and safety operations.

Disadvantages of $KMnO_4$ for Stabilization of Creosote Residuals

1. Being a strong oxidizing reagent, permanganate will oxidize any minerals or natural organics in the subsurface. Thus humic substances and reduced mineral species provide a natural reductive capacity which results in oxidant consumption, implying that oxidant will be consumed during the initial phases of an oxidant flush until the reduction capacity is satisfied. The natural reduction capacity may vary throughout the aquifer due

to spatial variability and will be different for each site. The natural reduction capacity or oxidant demand is an important design component of any *in situ* chemical oxidation.

2. A source of trace metals such as manganese will be added.

3. Precipitation of manganese dioxides on injection well screens or surrounding filter packs may plug or reduce the efficiency of the injection wells.

Chapter 6

Summary, Conclusions and Recommendations

6.1 Summary and Conclusions

This research investigated the ability of a chemical oxidizing reagent to oxidize selected creosote compounds and evaluated the performance of an oxidizing reagent to enhance the removal of creosote oils from contaminated soils. This was accomplished through batch oxidation experiments, column experiments, kinetic studies and numeric model simulations.

Batch oxidation experiments with Fenton's reagent, persulfate and $KMnO_4$ demonstrated that all three reagents oxidized creosote compounds in water. Both Fenton's and persulfate reagents oxidize creosote compounds by the generation of reactive free radicals with the addition of ferrous ions. Free radicals, while very reactive towards organic compounds, are short lived and are scavenged by carbonate species. Thus, delivery of the reagents into an aquifer containing a significant carbonate mineral fraction may only impact a small area because the radicals could be consumed by the geological media. Also precipitation of the ferrous ion catalyst as iron hydroxides may limit the effectiveness of these reagents for *in situ* applications. $KMnO_4$ can be used at very high concentrations and will possibly remain at high concentrations throughout the contaminated area. Thus $KMnO_4$ was considered the most promising oxidant and further studies were conducted.

Initial column experiments with $KMnO_4$ demonstrated the ability of this oxidant to enhance the removal of creosote compounds from the oil phase during an oxidant flush.

$KMnO_4$ at a concentration of 8 g/L was intermittently flushed through a carbonate rich filter sand containing creosote at 8% residual saturation. An equal volume of water was flushed through a control column. The oxidation column removed 36.5% of the monitored creosote compounds from the oil phase, whereas in the control column only 3.85% of the compounds were removed. It was estimated that approximately 40 times the volume of water would be needed to remove sparingly soluble compounds like chrysene and benzo(g,h,i)perylene compared to using $KMnO_4$ at 8 g/L.

The oxidation of representative creosote compounds with $KMnO_4$ was then investigated to determine kinetic data needed for model simulation. Polycyclic aromatic hydrocarbons, alkyl substituted polycyclic aromatic hydrocarbons, heterocycles, benzene and alkyl substituted benzenes were studied in oxidative batch reactions. Oxidation of creosote compounds can either initially occur through an electrophilic aromatic ring addition or by the abstraction of a benzylic hydrogen. In the oxidation of polycyclic aromatic hydrocarbons the rate of oxidation increased as the number of rings increased (naphthalene < phenanthrene < pyrene) because as the number of rings increases less energy is required to overcome the aromatic character of the polycyclic ring. For heterocyclic and alkyl substituted polycyclic hydrocarbons the mechanism of oxidation can either occur through the attack of the MnO_4^- ion on the ring or benzylic hydrogens and thus the rate constant derived for these compounds is a combination of both mechanisms. Alkyl-substituted benzenes and substituted PAHs showed a good correlation between second-order rate constants and bond dissociation energies, but not between second-order rate constants and calculated heats of complexation. This implies that side chain oxidation contributes significantly to the observed rate of reaction. Not all creosote compounds are reactive towards oxidation by $KMnO_4$. Compounds such as benzene, t-butylbenzene, dibenzofuran, and biphenyl that do not contain benzylic hydrogens and have stable benzenoid rings were not be oxidized by $KMnO_4$ in this study.

Having determined the second-order rate constants for the reaction of $KMnO_4$ with a selected group of creosote compounds, in-depth column experiments and numerical model simulation were performed.

Column experiments with creosote at 3% oil saturation were designed to observe the effect of flow rate and $KMnO_4$ concentration has on enhancing the removal of creosote compounds from the residual oil. The experiments were kept as uniform as possible with the volumetric flow rate and the $KMnO_4$ concentration being the main two variables. Results from the experiments indicated that for the same volume of reagent passed through the columns the slower flow rate and higher $KMnO_4$ concentration removed more of the monitored creosote compounds from the oil phase at a faster rate. For example, 56% of the monitored creosote compounds were removed from a column flushed with $KMnO_4$ (1.7L) at a concentration of 15 g/L at a flow rate of 3.6×10^{-4} m^3/day compared to only 11% for a column that was flushed with $KMnO_4$ (1.7 L) at a concentration of 3 g/L and a flow rate of 2.7×10^{-3} m^3/day.

Results from oxidation/dissolution model simulations indicated that the enhanced dissolution of creosote was achieved by:

1. Increasing the mass transfer zone by decreasing the concentration of creosote compounds in the aqueous phase.
2. Increasing the aqueous solubility of less readily oxidizable compounds by increasing their mole fraction in the residual creosote oil.
3. Increasing the mass transfer process possibly through the diffusion of permanganate into areas of low permeability or hydraulically isolated areas.

In general, enhanced mass transfer will be greatest for compounds that are readily oxidizable because of the large concentration gradients imposed by the oxidation process.

The mass transfer zone for these compounds becomes the entire area in contact with $KMnO_4$ and causes the oil saturation to decrease throughout the contaminated area. The rate at which mass transfer occurs is dependant on the rate of oxidation and the rate of dissolution. For chemically reactive compounds with higher solubilities like naphthalene, the oxidation process will greatly enhance its removal. For sparingly soluble compounds that are highly reactive towards $KMnO_4$ like pyrene, the mass transfer rate is increased but may be limited by the rate of dissolution. Mass transfer rates will not increase as significantly for compounds that have low aqueous solubilities and are not very reactive towards $KMnO_4$, like chrysene, because both dissolution and oxidation rates are small. Enhanced mass transfer for these compounds is due to an increase in their mole fraction. As the more readily oxidizable and soluble compounds are removed from the oil phase their mole fraction increases and thus their aqueous solubility becomes closer to its aqueous solubility limit. For such compounds, mass transfer mainly takes place up-gradient where fresh reagent is in contact with the residual oils.

Model simulations demonstrated the potential reduction in time required to reduce the mass of creosote residuals by flushing the area with $KMnO_4$. To remove 99% of naphthalene, pyrene and chrysene from the 12 cm long column with water at a flow rate of 1.41×10^{-3} m^3/d it would take approximately 22, 4618, and 1408 days, respectively. However, flushing the same column at the same flow rate with $KMnO_4$ at 15 g/L it would take 4.5, 27.2 and 39.5 days, respectively.

Creosote and coal tars contain a vast variety of compounds that have varying degrees of aqueous solubilities and reactivities towards $KMnO_4$. The chemical complexity of the oil introduces additional design considerations for the field scale applications of an oxidant flush. Experimental and model results determined that for the more readily oxidizable compounds the percentage of mass removed from the column was not significantly increased by increasing the flow rate; whereas, for the non-oxidizable compounds, the rate at which

their mass was removed increased with increasing flow rate. Thus, to enhance the removal of all creosote compounds from the contaminated area the ideal remediation system would inject $KMnO_4$ at higher flow rates while maintaining high concentrations of $KMnO_4$. However, the volume of reagent needed to produce larger hydraulic gradients would be much greater than injection at lower flow rates. This could be overcome by using a recirculation system in which the oxidant is injected, extracted down-gradient, adjusted to the initial $KMnO_4$ concentration, and then re-injected. While this is a good method, limitations at the field site might make this method impractical.

If it is more practical to inject $KMnO_4$ as a pulse or at lower flow rates the oxidant flush would preferentially remove the more readily oxidizable compounds and the length of time needed to remediate the site may increase.

6.2 Recommendations

Research should now be focused on the *in situ* application of $KMnO_4$ to enhance the removal of creosote compounds from a creosote contaminated aquifer. A rigorous evaluation of the field data is necessary to evaluate the potential effectiveness of this remediation technology. From this research it is expected that the oxidation process will deplete the source of the more oxidizable creosote compounds and leave behind the higher molecular weight and less soluble creosote compounds. After treatment with $KMnO_4$ the mass flux of creosote compounds eluding from this weathered residual creosote oil should then be greatly reduced. Thus, field scale monitoring strategies should include measuring the chemical changes of the oil phase, within the creosote source and the reduction of contaminant mass flux into the ground water plume.

The effect of manganese oxide precipitation within and around the contaminated zone should also be examined to determine its effect on the mass transfer of the oxidant into the residual creosote and mass transfer of creosote compound out of the contaminated area.

Modeling at a field site should also take place to determine the limitations of the existing model to incorporate soil oxidation rates and field scale mass transfer rates. In the column experiments, the mixing of the oil and sand created a homogeneous mixture with the oil distributed primarily in the smaller pore spaces. At a creosote field site the source would be heterogeneous. As a consequence, the creosote source will have a wide distribution of oil in different sized pore spaces with varying relative permeability's and varying diffusion path lengths. Thus, the mass transfer process will be considerably more complex at a typical field site than compared to the mass transfer processes within a column. Accurate predictions of mass removal will require site specific calibration of the model, incorporation of oxidant demand by the aquifer material and may require a better understanding of the fundamental processes of the oxidation, dissolution, diffusion and mass transport of creosote compounds at the field scale.

This research has shown that, by flushing $KMnO_4$ through a creosote contaminated soil, the rate of mass transfer or the rate of removal of creosote compounds from the oil phase is greatly accelerated compared to flushing with water. This has great potential in the remediation of a creosote contaminated site, since the oxidation/dissolution process will not only reduce the oil saturation but should also weather and stabilize the residual oil so that the concentration of creosote compounds leaching into the ground water is greatly reduced.

References:

Anbar, M., D. Meyerstein, and P. Neta, The reactivity of aromatic compounds toward hydroxyl radicals, *J. Phys. Chem.,* 70(8):2660-2662, 1966.

Anderson, M.R., R.L. Johnon, and J.F. Pankow, Dissolution of dense chlorinated solvents in groundwater: 1. Dissolution from a well-defined residual source, *Ground Water*., 30(2):250-256, 1992.

Barbeni, M., C. Minero, E. Pelizzetti, E. Borgarello, and N. Serpone, Chemical degradation of chlorophenols with Fenton's Reagent, *Chemosphere,* 16:2225-2237, 1987.

Barckholtz, C., T.A. Barckholtz, C.M. Hadad, C-H and N-H bond dissociation energies of small aromatic hydrocarbons, *J. Am. Chem. Soc.*, 121(3):491-500, 1999.

Bear, J., *Dynamics of Fluids in Porous Media*, American Elsevier Pub. Co., New York, 1972.

Beltran, F.J., M. Gonzalex, F.J. Rivas and P. Alvarez, Fenton Reagent advanced oxidation of polynuclear aromatic hydrocarbons in water, *Water Air and Soil Pollution*, 105(3):685-700, 1998.

Bielski, B.H.J., D.E. Cabelli, R.L., Arudi, Reactivity of H_2O_2/O_2-radicals in aqueous solution. *J. Phys. Chem. Ref. Data*, 14(4):1041-1100, 1985

Buxton, G.V., C.L. Greenstock, W.P. Helman, and A.B. Ross, Critical review of rate constants for reactions of hydrated electrons, hydrogen atoms and hydroxyl radicals ($\cdot OH/\cdot O^-$) in aqueous solution, *J. Phys. Chem. Ref. Data*, 17(2):513-886, 1988.

Chao, T.T., Selective dissolution of manganese oxides from soils and sediments with acidified hydroxylamine hydrochloride, *Soil Sci. Soc. Amer. Proc*., 36:764-768, 1972.

Chatzis, I., N.R. Morrow, and H.T. Lim, Magnitude and detailed structure of residual oil saturation, *Soc. Pet. Eng. J*., April:311-326. 1983.

Cherry, J.A., S. Feenstra, and D.M. Mackay, Developing a conceptual framework and rational goals for groundwater at DNAPL sites. Subsurface restoration conference. *Third International Conference on Groundwater Quality Research*, Dallas, Texas. 1992.

Clar, E., *The Aromatic Sextet*, Wiley, London, 1972.

Clar, E., *Polycyclic Hydrocarbons, Volume 1*. Academic Press Inc. London, 1964a.

Clar, E., *Polycyclic Hydrocarbons, Volume 2*. Academic Press Inc. London, 1964b.

Corey, A.T., *Mechanics of Immiscible Fluids in Porous Media*, Water Resour. Publ., Fort Collins Colo., 1986.

CRC Handbook of Chemistry and Physics, **2003,** 83, http://www.hbcpnetbase.com/

Daus, A.D., E. Frind, and E.A. Sudicky, Comparative error analysis in finite element formulations of advection-dispersion equation, *Adv. Water Resour.*, 8:86-95, 1985.

Devlin, J.F., *Enhanced in situ Biodegradation of Carbon Tetrachloride and Trichloroethene using a Permeable Wall Injection System*. Ph. D. Thesis, Department of Earth Sciences, University of Waterloo, Waterloo ON, 1994.

Dewar, M. J. S., A molecular orbital theory of organic chemistry. VI. Aromatic substitution and addition, *J. Am. Chem. Soc.,* 74:3357-3363, 1952.

Dipple, A, R.C. Moschel, and C. A. H. Bigger, Chemical Carcinogens, 2nd ed.; Searle, C.E., Ed.; *Am. Chem. Soc., ACS Monograph 182*, 1:41-164, 1984.

Durant, J. L., W. F., R. Busby, A. L. Lafleur, B.W. Penman, and C.L. Crespi, Human cell mutagenicity of oxygenated, nitrated and unsubstituted aromatic hydrocarbons associated with urban aerosols, *Mutation Res.* 371:123-127, 1996.

Dyreborg, S., and E. Arvin, Creosote leaching from a contaminated saturated sand column. *Environ. Technol*. 15:871-878, 1994.

Eisenhauer, H.R., Oxidation of phenolic wastes. Part I, oxidation with hydrogen peroxide and ferrous salt reagent, *J. Water Pollut. Control Fed*., 36(9):1116-1128, 1964.

Feenstra, S., Evaluation of multi-component DNAPL sources by monitoring of dissolved-phase concentrations, Presented at the conference on *Subsurface Contamination by Immiscible Fluids*, (IAH), Calgary AB, April, 18-20, 1990.

Fessenden, J. F. and J.S. Fessenden, *Organic Chemistry* 6th Ed. Brooks/Cole Pub. Co., Pacific Grove, CA. 1998.

Ficek, K.J., *Potassium Permanganate for Iron and Manganese Removal and Taste and Odour Control*, Ann Arbor Science Pub., Inc., Ann Arbor, MI., 1978.

Flotron, V., C. Deltei, A. Bermond, V. Camel, Remediation of matrices contaminated by polycyclic aromatic hydrocarbons: use of Fenton's Reagent. *Polycyclic Aromatic Compounds. 2003.*, 23(4):353-401, 2003.

Freeze, R.A. and J.A. Cherry, *Groundwater*, Prentice-Hall Ltd., Englewood Cliffs, NJ, 1979.

Frind, E.O., J.W. Molson, M. Schirmer, and N. Guiguer, Dissolution and mass transfer of multiple organics under field conditions: The Borden emplaced source, *Water Resour. Res.*, 35(3):683-694, 1999.

Gates-Anderson, B.D., R.L. Siegrist, and S.R Cline, Comparison of potassium permanganate and hydrogen peroxide as chemical oxidants for organically contaminated soils, *J. Environ. Eng,* 127:337-347, 2001.

Geller, J.T. and J.R. Hunt, Mass transfer from nonaqueous phase organic liquids in water-saturated porous media, *Water. Resour. Res*., 29(4):833-845, 1993.

Gilman, H., W.G. Bywater, and P.T. Parker, Dibenzofuran. IV. Orientation and relative aromaticities of the 2,-3- and 4-dibensofuryl radicals, *J. Am. Chem. Soc.,* 57:885-887, 1935.

Gutman, I., and S.J. Cyvin, *Introduction to the Theory of Benzenoid Hydrocarbons*, Springer-Verlag, Berlin Heidlberg, 1989.

Hall, R. J., P.V.R. Shannon, A.M.F. Oliveira-Campos, and M.J.R.P. Queiroz, The synthesis of 7,9-dimethoxy-5,11-dimethyl-6H-pyrido-[4,3-b]carbazole (7,9-dimethoxyellipticine) via a regioselective bromiation and some bromination and ipso substitution reactions of the 2,4-dimthoxycarbazole, *J. Chem. Res. Synop*. 1:2-3, 1992

Hand, S.E., S.C. Johnson, and D.C., Baker, Magnesium methyl carbonate-activated alkylation of methyl ketones with an α-halo nitrile, esters, and amides, *J. Org. Chem*., 62(5):1348-1355, 1997.

Hood, E.D. *Permanganate Flushing of DNAPL Source Zones: Experimental and Numerical Investigation.* Ph. D. Thesis, Department of Civil Engineering, University of Waterloo, Waterloo, ON, 2000.

Imhoff, P.T., P.R. Jaffe, and G.F. Pinder, Experimental investigation of the dissolution dynamics of chlorinated hydrocarbons in porous media. Proceedings of the *International Symposium on Processes Governing the Movement and Fate of Contaminants in the Subsurface Environment,* Stanford University, 1989.

Imhoff, P.T., P.R. Jaffe, and G.F. Pinder, An experimental study of complete dissolution of a nonaqueous phase liquid in saturated porous media. , *Water Resour. Res*., 30(2):307-320, 1994.

Kachurin, O. I., and Y.B Vysotskii, Cation-radicals. Electronic structure and function in electrophilic aromatic substitution, *Rus. J. Org. Chem*., 35(4):548-554, 1999.

Keating, E.J., R.A. Brown, and E.S. Greenberg, Phenolic problems solved with hydrogen peroxide oxidation, *Ind. Water Eng.,* December:22-27, 1987.

King, M.W.G and J.F. Barker, Migration and natural fate of a coal tar creosote plume 1. Overview and plume development, *J. Contam. Hydrol*., 39:249-279, 1999.

Kolthoff, I.M., and A.I Medalia, The reaction between ferrous iron and peroxides. I. Reaction with hydrogen peroxide in the absence of oxygen, *J. Chem. Soc.,* 71:3777-3783, 1949.

Kromkin, E.A., V.E. Tumanov, E.T. Denisov, Evaluation of C-H bond dissociation energies in alkylaromatic hydrocarbons and the enthalpies of corresponding radicals from kinetic data*, Pet. Chem*., 42(1):1-11, 2002.

Kueper, H.B., S. Feesntra, M.O. Rivett, and J.A. Cherry, A series of controlled field experiments to study DNAPL behaviour: Implications for site remediations. *HAZMAT International*, Atlanta City. June 10-12, 1992.

Lamarche, C., *In situ chemical oxidation of an emplaced creosote source*, M.A. Sc. Thesis, Department of Civil Engineering, University of Waterloo, Waterloo, ON, 2002.

Lipczynska-Kochany, E., Degradation of aqueous nitrobenzene by means of the Fenton Reagent, *Chemosphere,* 22(5):592-593, 1991.

Lipczynska-Kochany, E., Degradation of nitrobenzene and nitrophenols in homogeneous solution. Direct photolysis versus photolysis in the presence of hydrogen peroxide and the Fenton reagent, *Water Poll. Res. J. Can.*, 27(1):97-122, 1992.

Lee, D.G., and T. Chen, Oxidation of hydrocarbons. 18. Mechanism of the reaction between permanganate and carbon-carbon double bonds, *J. Am. Chem. Soc.,* 111(19):7534-7538, 1989.

Lee L.S., M. Hagwall, J.J. Delfino, and S.C. Rao, Partitioning of polycyclic aromatic hydrocarbons from diesel fuel and water, *Envron. Sci. Technol*., 26(11):2104-2110, 1992a.

Lee L.S., S.C. Rao and I. Okuda, Equilibrium partitioning of polycyclic aromatic hydrocarbons from coal tar into water, *Envron. Sci. Technol*., 26(11):2110-2115, 1992b.

Lin S.H., and C.C. Lo, Fenton process for treatment of desizing wastewater, *Wat. Res.* 31(8):2050-2056, 1997.

Lobachev, V.L., E.S. Radakov, and E.V. Zaichuk, Kinetics, kinetic isotope effects, and substrate selectivity of alkybenzene oxidation in aqueous permanganate solutions: VI. Reaction with MnO_3^+, *Kinet. Catal.* 38(6):745-761, 1997.

Lou, J.C. and S.S. Lee, Chemical oxidation of BTX using Fenton's reagent, *Haz. Waste and Haz. Mat.,* 12(2):185-193, 1995.

MacKay D.M. D.L. Freyberg and P.V. Roberts, A natural gradient experiment on solute transport in a sand aquifer 1. Approach and overview of plume movement, *Water Resour. Res*., 22(13):2017-2029, 1986.

Mackay, D., W.Y. Shiu, A. Maijanen, and S. Feenstra, Dissolution of non-aqueous phase liquids in groundwater, *J. Contam. Hydrol.*, 8 (1):23-42, 1991.

Malcolmson, H*., Dissolution of an Emplaced Creosote Source, CFB Borden, Ontario.* M.A. Sc. Thesis, Department of Earth Sciences, University of Waterloo, Waterloo, ON, 1992.

Mattraw Jr., H.C., Frabjs, B.J. (Eds), Movement and gate of creosote waste in ground water, Pensacola, Florida: US Geological Survey Toxic Waste-Ground-Water Contamination Program, Water Supply Paper 2285, 1986.

Mercer, J.W. and R.M. Cohen, A review of immiscible fluid in the subsurface: Properties, models, characterization and remediation, *J. Cont. Hydrology*., 6:107-163, 1990.

Merz, J.H., and W.A. Waters, The oxidation of aromatic compounds by means of the free hydroxyl radical, *J. Chem. Soc.,* S15:2427-2433, 1949.

Miller M.M., S.P. Wasik, G.L. Huang, W.Y. Shiu and D, Mackay, Relationship between octanol-water partition coefficient and aqueous solubility, *Environ. Sci. Technol.*, 19(6):522-529, 1985.

Miller C.T., M.M. Poirier-McNeill, and A.S. Mayer, Dissolution of trapped nonaqueous phase liquids: Mass transfer characteristics, *Water Resour. Res*., 26(11):2783-2796, 1990.

Moffett, J.W. and Zika R.G., Reaction kinetics of hydrogen peroxide with copper and iron in seawater, *Environ. Sci. Technol.,* 21(8):804-810, 1987.

Montgomery, J.M., Consulting Engineers, *Water Treatment Principles and Designs*, J. Wiley and Sons, Toronto, 1985.

Morrow, N.R., I. Chatzis, and J.J. Taber, Entrapment and mobilization of residual oil in bead packs, *SPE Reservoir Eng.*, 3(3):927-934, 1988.

Mueller, J.G., P.J. Chapman, and P.H. Pritchard, Creosote-contaminated sites. *Environ. Sci. Technol.*, 23(10):1197-1201, 1989.

Neta, P., V. Madhavan, H. Zemei, and R.W. Fessenden, Rate constants and mechanism of reaction of $SO_4^{\bullet -}$ with aromatic compounds, *J. Am. Chem. Soc*., 99(1):163-164, 1977.

Norman, R.O.C., Application of E.S.R. spectroscopy to kinetics and mechanism in organic chemistry, *Chem. Soc. Rev.,* 1:1-27, 1979.

Pearlman, R.S., S.H. Yalkowsky, S. Banerjee, Water solubilities of polynuclear aromatic and heteroaromatic compounds, *J. Phys. Chem Ref. Data*, 13(2):555-562, 1984.

Perry, R.H., D.G. Green, and J.O Moloney, eds., *Perry's Chemical Engineer's Hand Book*, 6th Ed. McGraw-Hill Inc., New York, 1984.

Peters, C.A. and R.G. Luthy, Coal Tar dissolution in water-miscible solvents, *Environ. Sci. Technol.*, 27(13):2831-2843, 1993.

Powers, S.E., L.M. Abriola, and W.J. Weber Jr., An experimental investigation of nonaqueous phase liquid dissolution in saturated subsurface systems: Steady state mass transfer rate, W*ater Resour. Res.,* 28(10):2691-2705, 1992.

Priddle, M.W., and T.B. MacQuarrie, Dissolution of creosote in groundwater: an experimental and modelling investigation, *J. Contam. Hydrology.*, 15:27-56, 1994.

Reitsma, S., Equilibrium and non-equilibrium composition alcohol flooding models for recovery of immiscible liquids from porous media, Ph.D. Thesis, Dep. of Civ. Eng., Queens University, Kingston ON, 1996.

Rudakov, E. S., and V.L. Loachev, Kinetics, kinetic isotope effects, and substrate selectivity of alkylbenzene oxidation in aqueous permanganate solutions: I Reactions with MnO_4^- anion, *Kinet. Catal.,* 35(2):175-179, 1994.

Rudakov, E. S., V.L. Loachev, and E.V. Zaichuk, Kinetics, kinetic isotope effects, and substrate selectivity of alkylbenzene oxidation in aqueous permanganate solutions: V. Activation parameters for reactions with $HMnO_4$, *Kinet. Catal.,* 37(4):500-507, 1996.

Sahloul, N.A., M.A. Ioannidis and I. Chatzis, Dissolution of residual non-aqueous phase liquids in porous media: pore-scale mechanisms and mass transfer rates, *Adv. Water Resources*., 25:33-49, 2001.

Sedlak, D.L., and A.W. Andren, Oxidation of chlorobenzene with Fenton's reagent. *Environ. Sci. Technol.,* 25(4):777-782, 1991.

Schnarr, J.M., *An In Situ Oxidative Technique to Remove Residual DNAPL from Soils*. M. A. Sc. Thesis, Department of Civil Engineering, University of Waterloo, Waterloo ON, 1992.

Schwarzenbach, R.P., P.M. Gschwend, and D.M. Imboden, *Environmental organic chemistry*, J. Wiley and Sons, New York, 1993.

Schwille, F., *Dense Chlorinated Solvents in Porous and Fractured Media - Model Experiments*. J.F. Pankow (trans.), Chelsea, MI, Lewis Pub. Inc., 1988.

Shiu, W.Y., A. Maijanen, A.L.Y. Ng, and D. Mackay, Preparation of aqueous solutions of sparingly soluble organic substances: II. Multicomponent systems-hydrocarbons mixtures and petroleum products. *Environ. Toxicol. Chem.*, 7:125-137, 1988.

Shui, W.Y., and K.C. Ma, Temperature dependence of physical-chemical properties of selected chemicals of environmental interest I. Mononuclear and polynuclear aromatic hydrocarbons, *J. Phys. Chem Ref. Data*, 29(1):41-130, 2000.

Sherwood, T.K., R.L Pigford and C.L. Wilke, *Mass Transfer*, McGraw-Hill, New York, 1975.

Skoog, D.A., and D.M. West, *Fundamentals of Analytical Chemistry*, 3rd Ed. Holt, Reinhar and Winston, New York, 1976.

Streitwieser, A., and C.H. Heathcock, *Introduction to Organic Chemistry*, 2nd Ed. Macmillan Pub. Co., New York. 1981.

Stone A.T., Reductive dissolution of manganese(III/IV) oxides by substituted phenols, *Environ. Sci. Technol,* 21(10):979-987, 1987.

Taylor, R., *Electrophilic Aromatic Substitution*, J. Wiley and Sons Ltd, West Sussex, 1990.

Ulrich H.J., and A.T. Stone, Oxidation of chlorophenols adsorbed to manganese oxide surfaces, *Environ. Sci. Technol.,* 23(4):421-428, 1989.

Zhang, S., Z. Danhong, and Y. Jinzong, Nitration of carbazle and N-alkylcarbazoles, *Dyes and Pigments,* 27(4):287-296, 1995.

Walling C., Fenton's reagent revisited, *Acc. Chem. Res.*, 8:125-131, 1975.

Walling C., and A. Goosen, Mechanism of the ferric ion catalysed decomposition of hydrogen peroxide: effects of organic substrate. *J. Am. Chem. Soc.,* 95(9):2987-2991, 1973.

Walling C., and R.A. Johnson, Fenton's reagent. V. Hydroxylation and side-chain cleavage of aromatics, *J. Am. Chem. Soc.,* 97(2):363-367, 1975.

Walling, C. and T. Weil, The ferric ion catalyzed decomposition of hydrogen peroxide in perchloric acid Solution, *J. Chem. Kinetics*, 6:507-516, 1974.

Walling C., and S. Kato, The oxidation of alcohols by Fenton's reagent: the effect of copper ion, *J. Am. Chem. Soc.,* 93(17):4275-4281, 1971

Watts, R.J., M.D. Udell, P.A. Rauch, and S.W. Leung, Treatment of pentachlorophenol-contaminated soils using Fenton's reagent. *Haz. Waste and Haz. Mat.,* 7(4):335-345, 1990.

Appendix 1

Balanced Oxidation/Reduction Reactions

Compound	Balance Oxidation/Reduction Reactions
PAH's	
Biphenyl	$C_{12}H_{10} + 19\frac{1}{3}MnO_4^- + 19\frac{1}{3}H^+ \rightarrow 19\frac{1}{3}MnO_2 + 12CO_2 + 14\frac{2}{3}H_2O$
Naphthalene	$C_{10}H_8 + 16MnO_4^- + 16H^+ \rightarrow 16MnO_2 + 10CO_2 + 12H_2O$
Anthracene	$C_{14}H_{10} + 18\frac{2}{3}MnO_4^- + 18\frac{2}{3}H^+ \rightarrow 18\frac{2}{3}MnO_2 + 14CO_2 + 14\frac{1}{3}H_2O$
Phenanthrene	$C_{14}H_{10} + 18\frac{2}{3}MnO_4^- + 18\frac{2}{3}H^+ \rightarrow 18\frac{2}{3}MnO_2 + 14CO_2 + 14\frac{1}{3}H_2O$
Fluoranthene	$C_{16}H_{10} + 24\frac{2}{3}MnO_4^- + 24\frac{2}{3}H^+ \rightarrow 24\frac{2}{3}MnO_2 + 16CO_2 + 17\frac{1}{3}H_2O$
Chrysene	$C_{18}H_{12} + 28MnO_4^- + 28H^+ \rightarrow 28MnO_2 + 18CO_2 + 20H_2O$
Pyrene	$C_{16}H_{10} + 24\frac{2}{3}MnO_4^- + 24\frac{2}{3}H^+ \rightarrow 24\frac{2}{3}MnO_2 + 16CO_2 + 17\frac{1}{3}H_2O$
Heterocyclic PAH's	
Carbazole	$C_{12}H_9N + 20\frac{2}{3}MnO_4^- + 19\frac{2}{3}H^+ \rightarrow 20\frac{2}{3}MnO_2 + 14CO_2 + NO_3^- + 14\frac{1}{3}H_2O$
Dibenzofuran	$C_{12}H_8O + 18MnO_4^- + 18H^+ \rightarrow 18MnO_2 + 12CO_2 + 13H_2O$
Substituted PAH's	
1-methylnaphthalene	$C_{11}H_{10} + 18MnO_4^- + 18H^+ \rightarrow 18MnO_2 + 11CO_2 + 14H_2O$
2-methylnaphthalene	$C_{11}H_{10} + 18MnO_4^- + 18H^+ \rightarrow 18MnO_2 + 11CO_2 + 14H_2O$
Fluorene	$C_{13}H_{10} + 20\frac{2}{3}MnO_4^- + 20\frac{2}{3}H^+ \rightarrow 20\frac{2}{3}MnO_2 + 13CO_2 + 15\frac{1}{3}H_2O$
Acenaphthene	$C_{12}H_{10} + 19\frac{1}{3}MnO_4^- + 19\frac{1}{3}H^+ \rightarrow 19\frac{1}{3}MnO_2 + 12CO_2 + 14\frac{2}{3}H_2O$
Benzene and substituted benzenes	
Benzene	$C_6H_6 + 10MnO_4^- + 10H^+ \rightarrow 10MnO_2 + 6CO_2 + 8H_2O$
Toluene	$C_7H_8 + 12MnO_4^- + 12H^+ \rightarrow 12MnO_2 + 7CO_2 + 10H_2O$
Ethylbenzene	$C_8H_{10} + 14MnO_4^- + 14H^+ \rightarrow 14MnO_2 + 8CO_2 + 12H_2O$
Isopropylbenzene	$C_9H_{12} + 16MnO_4^- + 16H^+ \rightarrow 16MnO_2 + 9CO_2 + 14H_2O$
t-Butylbenzene	$C_{10}H_{14} + 18MnO_4^- + 18H^+ \rightarrow 18MnO_2 + 10CO_2 + 16H_2O$

Appendix 2

Experimental Data for Kinetic Experiments

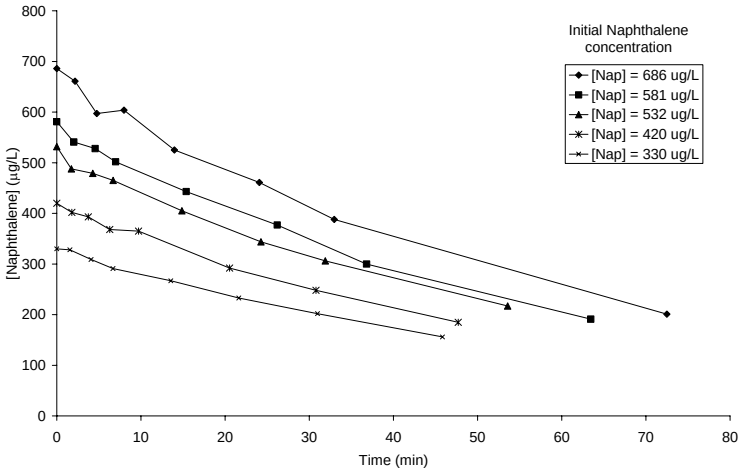

Figure A2. 1. Naphthalene oxidation. [$KMnO_4$] = 3.8 ± 0.1 g/L

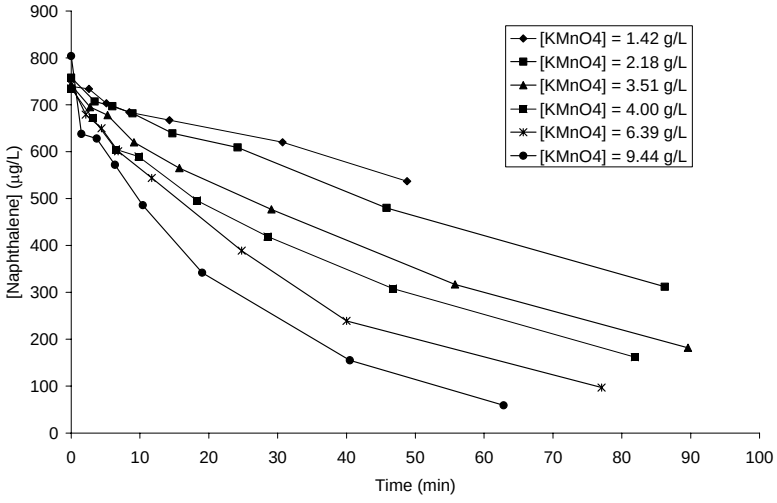

Figure A2. 2. Naphthalene oxidation: [Naphthalene] = 753 ± 26 µg/L

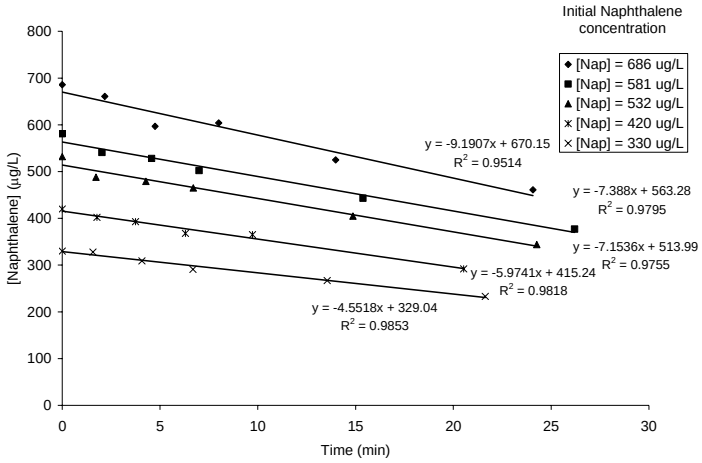

Figure A2. 3. Naphthalene oxidation: Initial rates of reaction. $[KMnO_4] = 3.8 \pm 0.1$ g/L. Slope = r_0

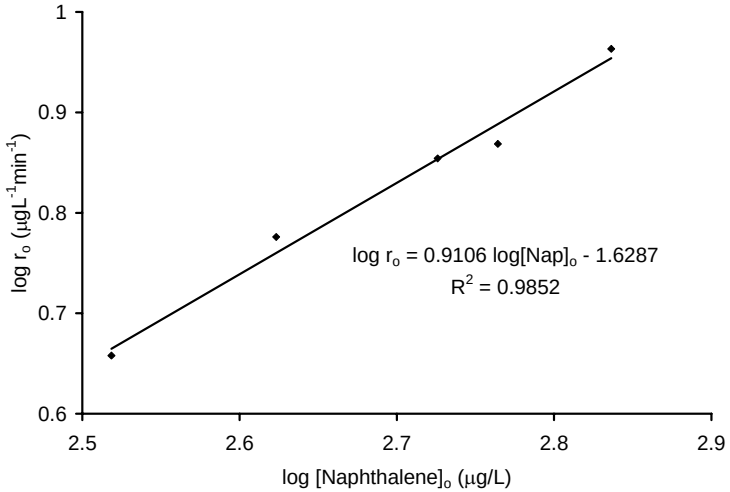

Figure A2. 4. Naphthalene oxidation: Determination of the rate order alpha. Slope = alpha

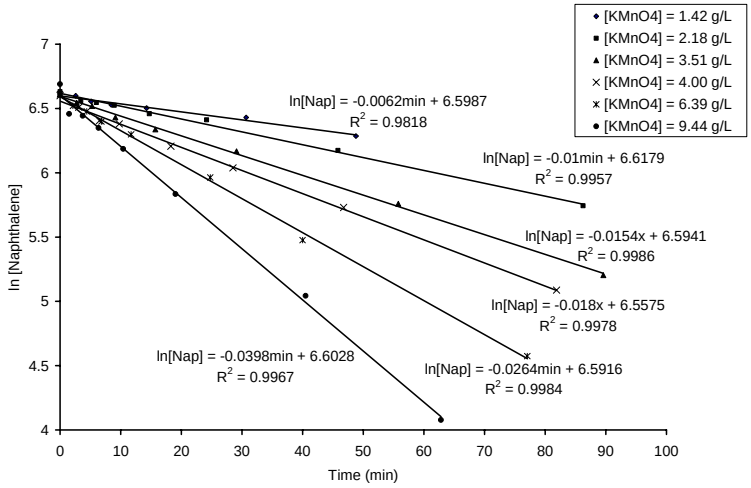

Figure A2. 5. First order decomposition of Naphthalene: [Naphthalene] = 753 ± 26 µg/L. Slope = k_{obs}.

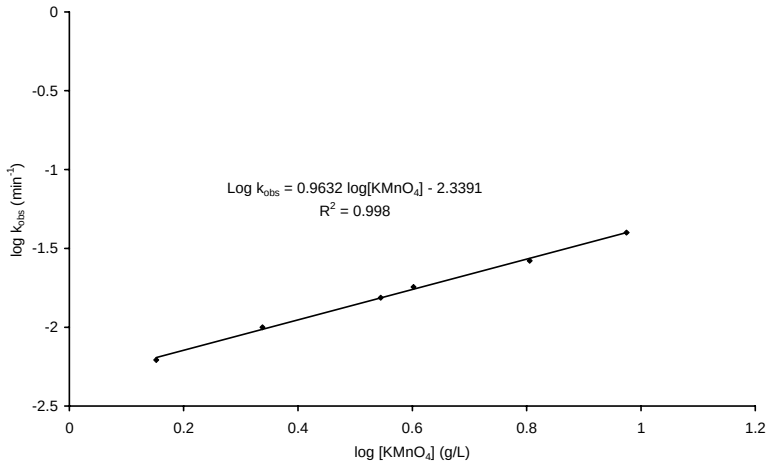

Figure A2. 6. Naphthalene oxidation: Determination of the rate order beta, [Naphthalene] = 753 ± 26 μg/L. Slope = beta

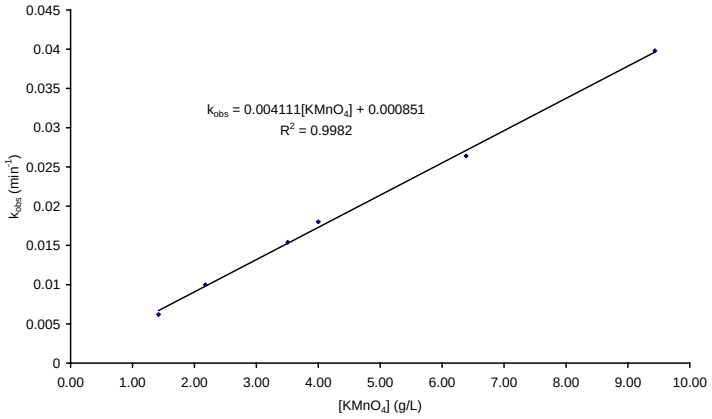

Figure A2. 7. Naphthalene oxidation: Determination of second-order-rate constant, Slope = second-order-rate constant.

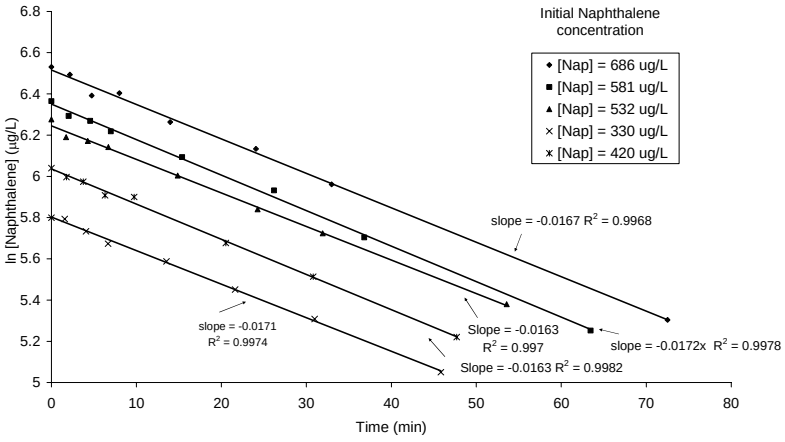

Figure A2. 8. Naphthalene oxidation: Pseudo-first order plots, [$KMnO_4$] = 3.8 ± 0.1 g/L. Dividing the slope of the plots by the $KMnO_4$ concentration provides the second-order-rate constant.

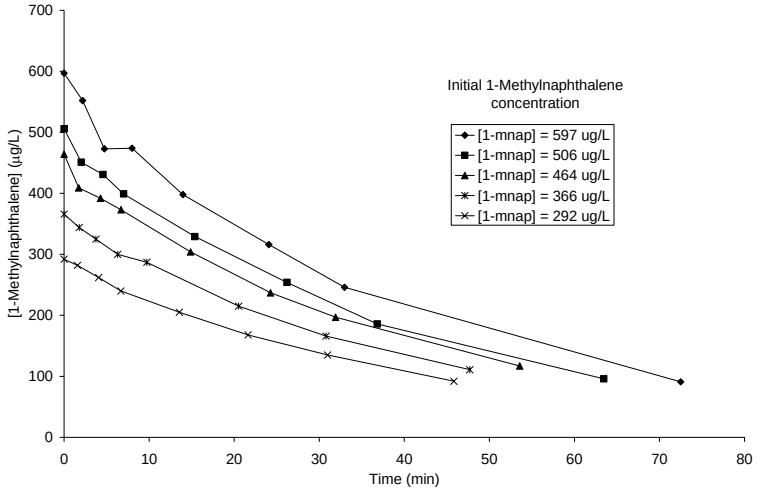

Figure A2. 9. 1-Methylnaphthalene oxidation: [$KMnO_4$] = 3.8 ± 0.1 g/L

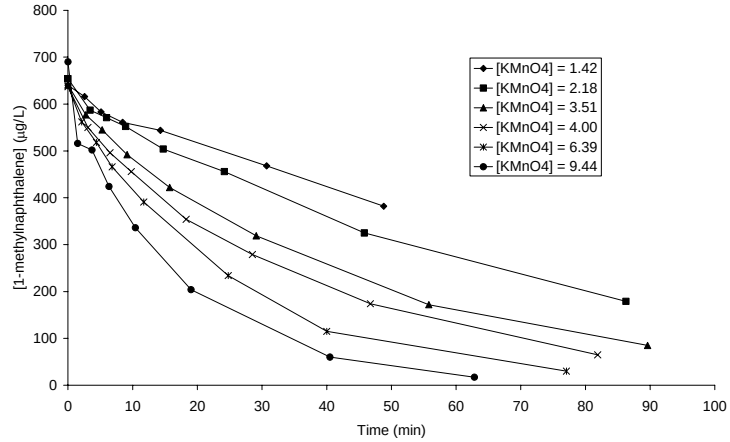

Figure A2. 10. 1-Methylnaphthalene oxidation: [1-Methylnaphthalene] = 650 ± 20 µg/L

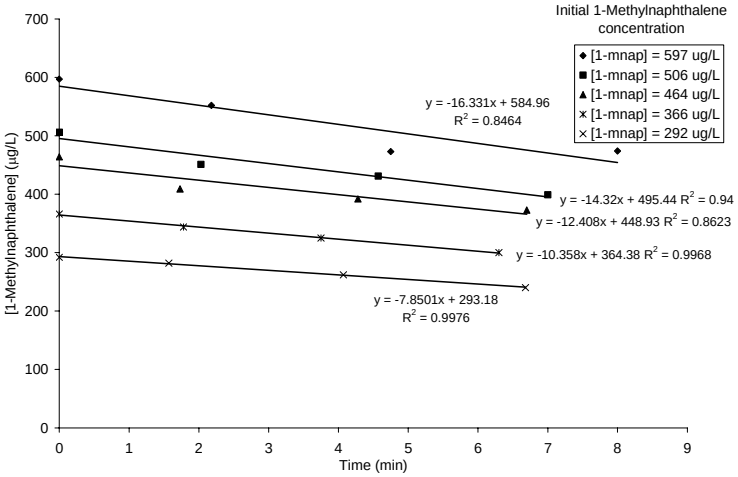

Figure A2. 11. 1-Methylnaphthalene oxidation: Initial rates of reaction. [$KMnO_4$] = 3.8 ± 0.1 g/L. slope = r_0

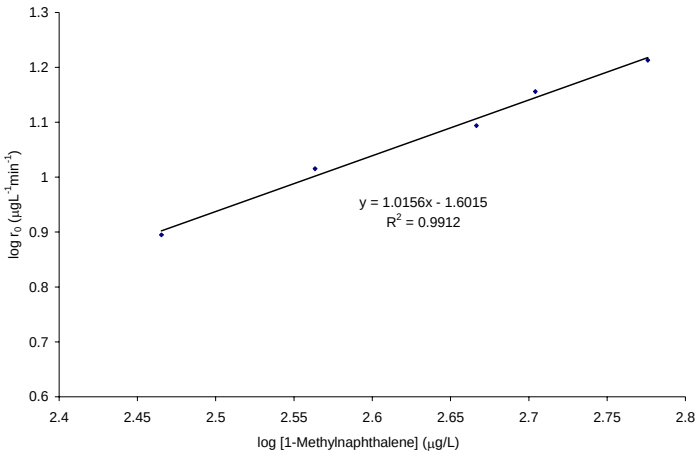

Figure A2. 12. 1-Methylnaphthalene oxidation: Determination of the rate order alpha. Slope = alpha

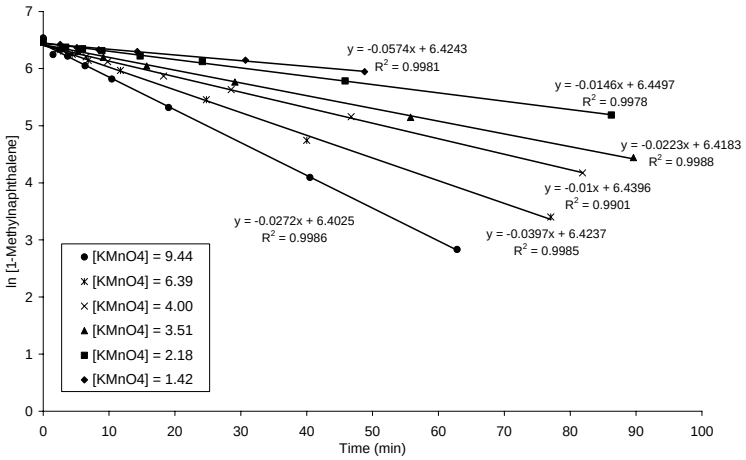

Figure A2. 13. First order decomposition of 1-methylnaphthalene: [1-Methylnaphthalene] = 650 ± 20 μg/L

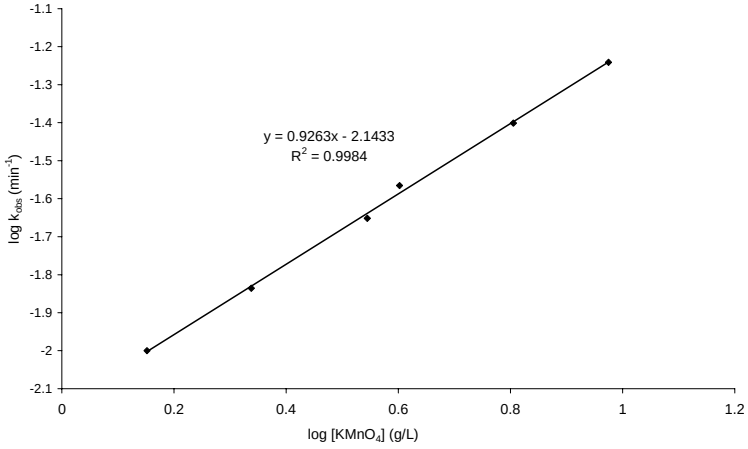

Figure A2. 14. 1-Methylnaphthalene oxidation: Determination of the rate order beta. [1-Methylnaphthalene] = 650 ± 20. Slope = beta

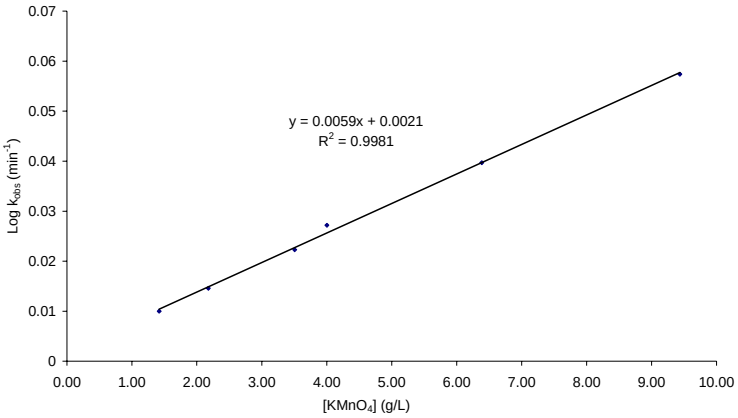

Figure A2. 15. 1-Methylnaphthalene oxidation: Determination of second-order-rate constant. Slope = second-order-rate constant.

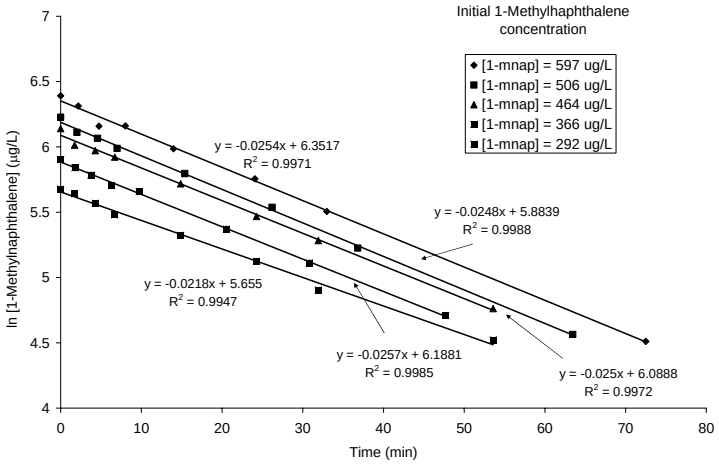

Figure A2. 16. 1-Methylnaphthalene oxidation: Pseudo-first order plots. [$KMnO_4$] = 3.8 ± 0.1 g/L. Dividing the slope of the plots by the $KMnO_4$ concentration provides the second-order-rate constant.

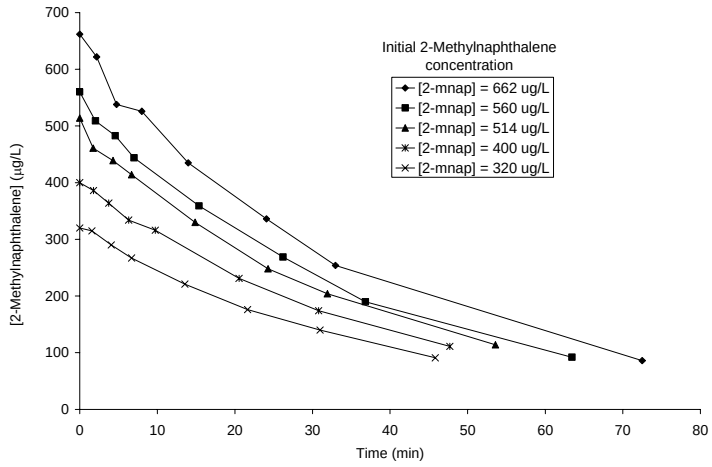

Figure A2. 17. 2-Methylnaphthalene oxidation: [$KMnO_4$] = 3.8 ± 0.1 g/L

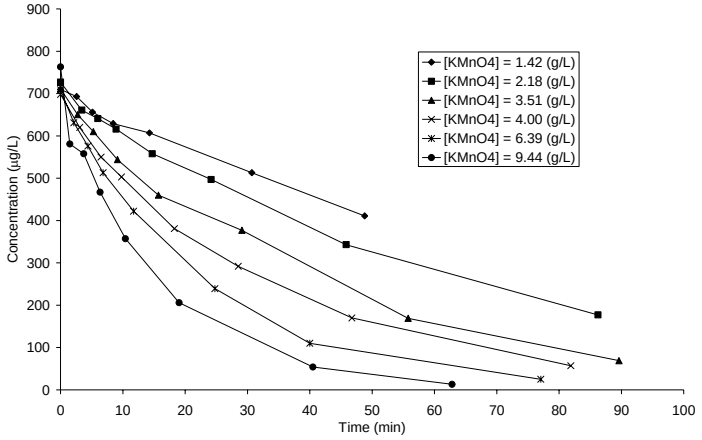

Figure A2. 18. 2-Methylnaphthalene oxidation: [2-Methylnaphthalene] = 719 ± 23 µg/L

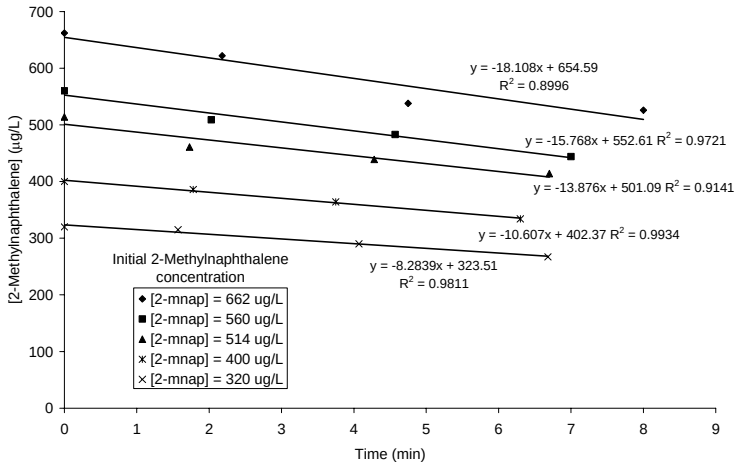

Figure A2. 19. 2-Methylnaphthalene oxidation: Initial rates of reaction. [$KMnO_4$] = 3.8 ± 0.1 g/L. Slope = r_0

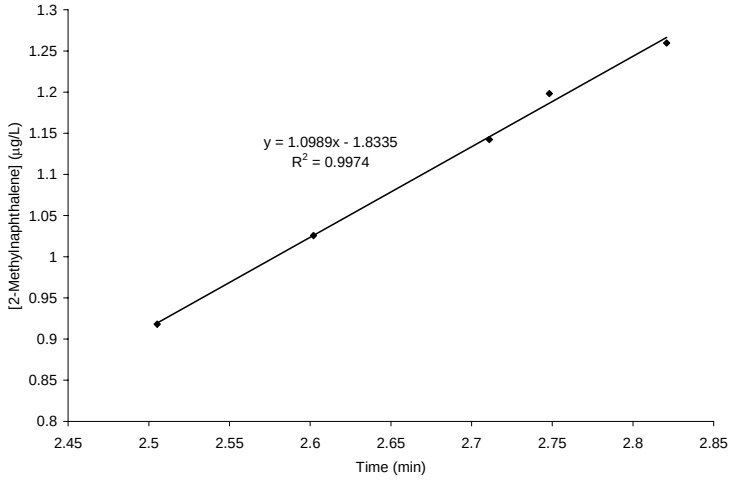

Figure A2. 20. 2-Methylnaphthalene oxidation: Determination of the rate order alpha. Slope = alpha

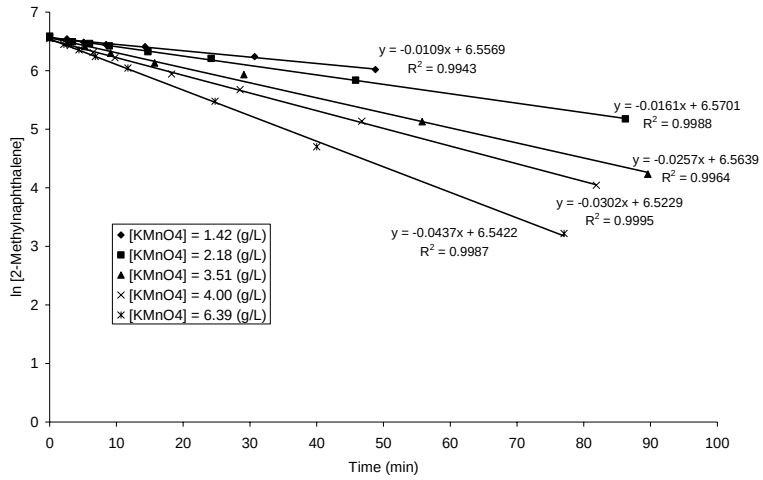

Figure A2. 21. First order decomposition of 2-methylnaphthalene: [2-Methylnaphthalene] = 719 ± 23 μg/L

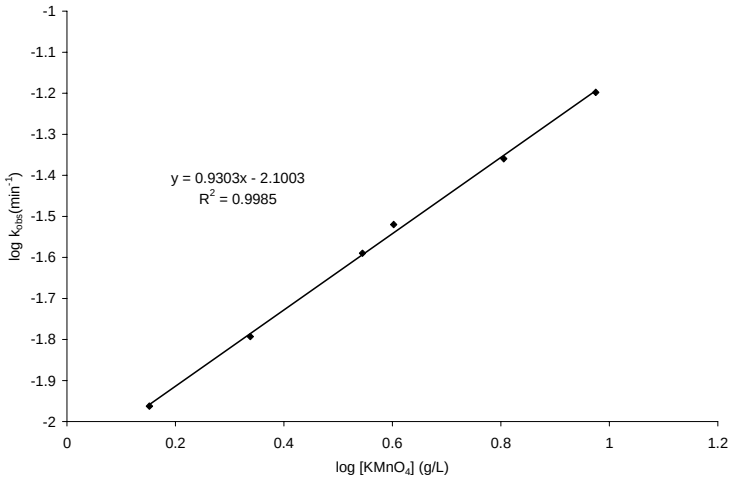

Figure A2. 22. 2-Methylnaphthalene oxidation: Determination of the rate order beta. [2-Methylnaphthalene] = 719 ± 23. Slope = beta

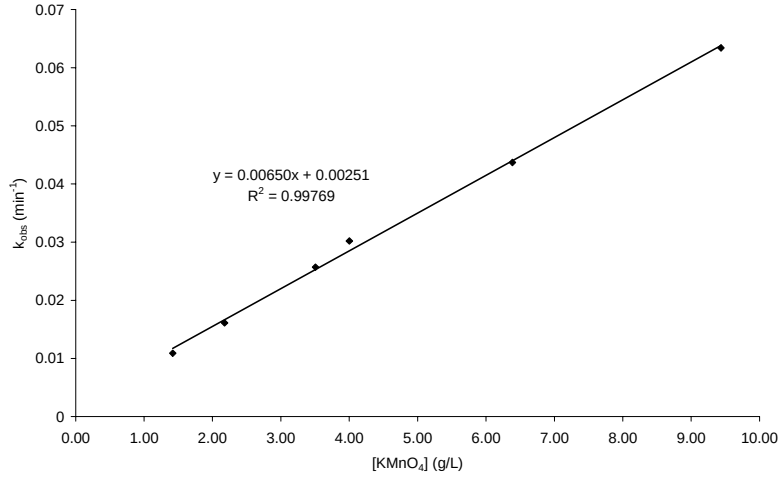

Figure A2. 23. 2-Methylnaphthalene oxidation: Determination of second-order-rate constant. Slope = second-order-rate constant

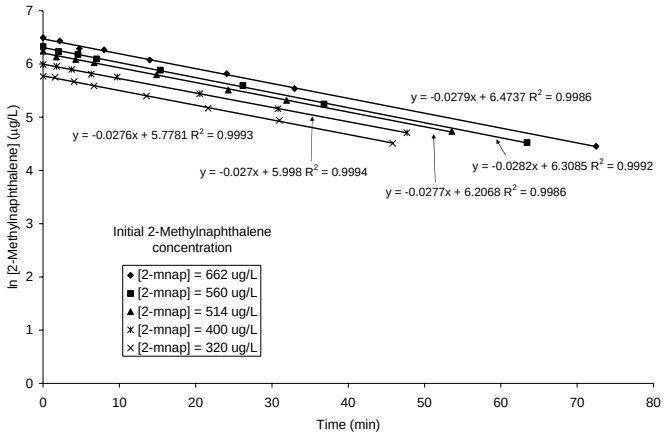

Figure A2. 24. 2-Methylnaphthalene oxidation: Pseudo-first order plots. [$KMnO_4$] = 3.8 ± 0.1 g/L. Dividing the slope of the plots by the $KMnO_4$ concentration provides the second-order-rate constant.

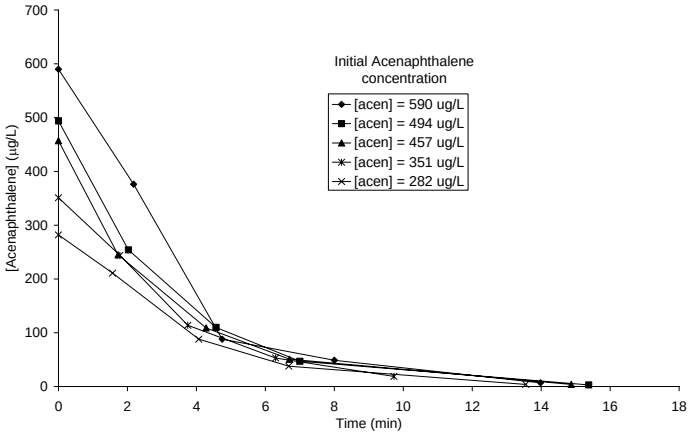

Figure A2. 25. Acenaphthene oxidation: [$KMnO_4$] = 3.8 ± 0.1 g/L

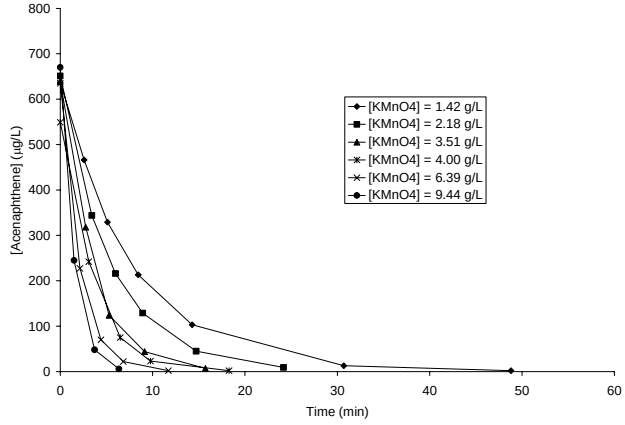

Figure A2. 26. Acenaphthene oxidation: [Acenaphthene] = 630 ± 42 µg/L

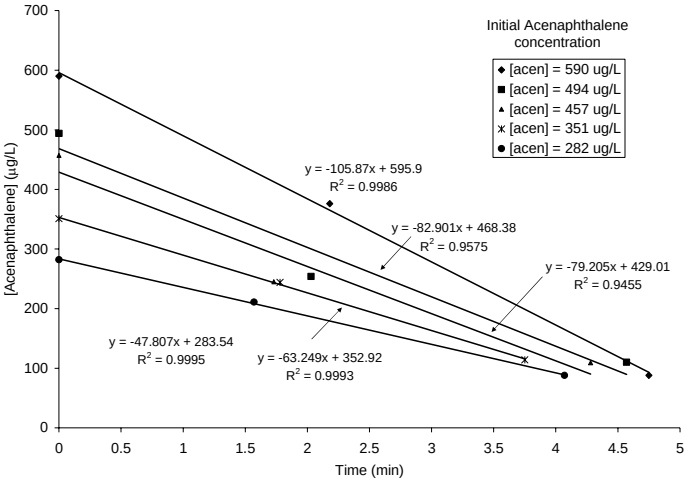

Figure A2. 27. Acenaphthene oxidation: Initial rates of reaction. $[KMnO_4] = 3.8 \pm 0.1$ g/L. Slope = r_0

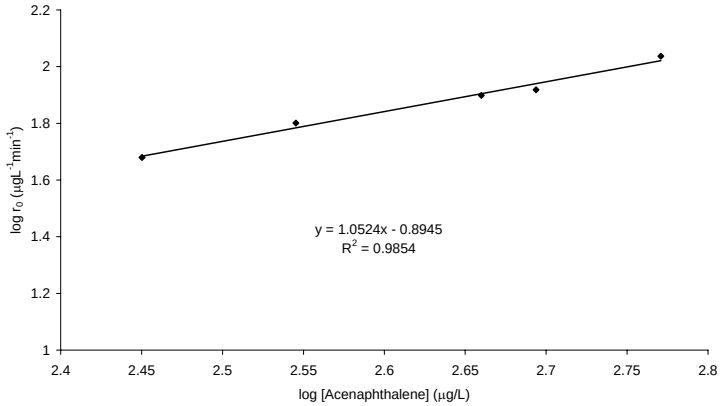

Figure A2. 28. Acenaphthene oxidation: Determination of the rate order alpha. Slope = alpha

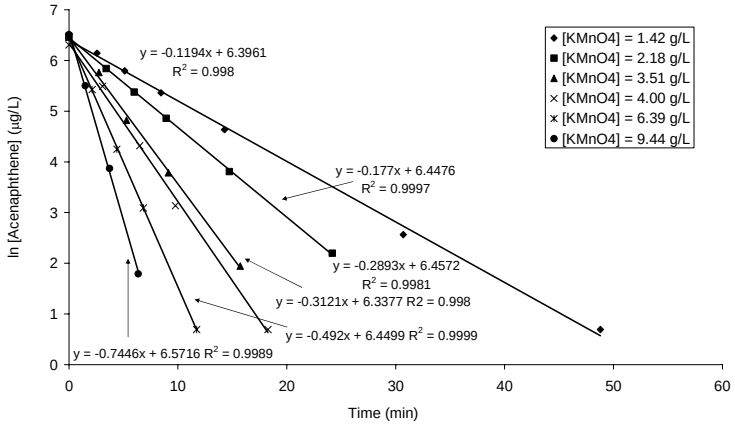

Figure A2. 29. First order decomposition of Acenaphthene: [Acenaphthene] = 630 ± 42 µg/L

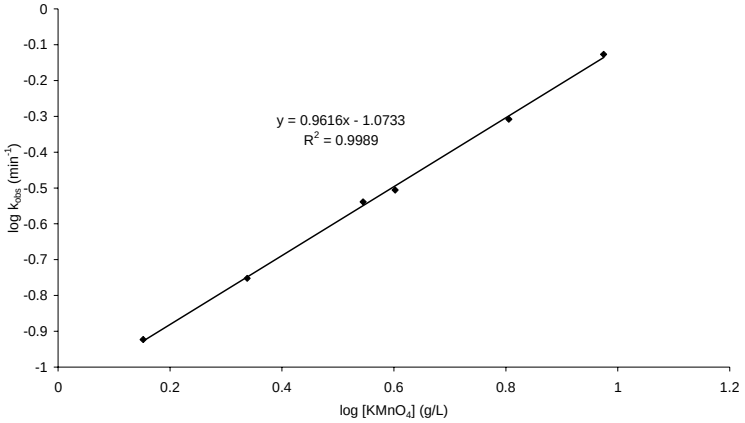

Figure A2. 30. Acenaphthene oxidation: Determination of the rate order beta. [Acenaphthene] = 630 ± 42 μg/L. Slope = beta

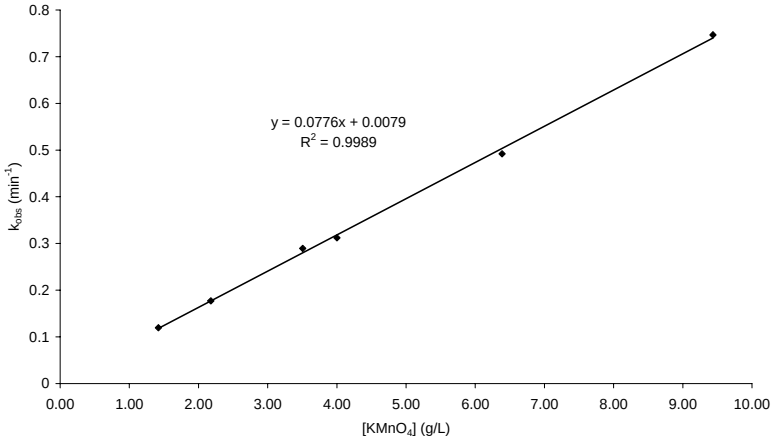

Figure A2. 31. Acenaphthene oxidation: Determination of second-order-rate constant. Slope = second-order-rate constant

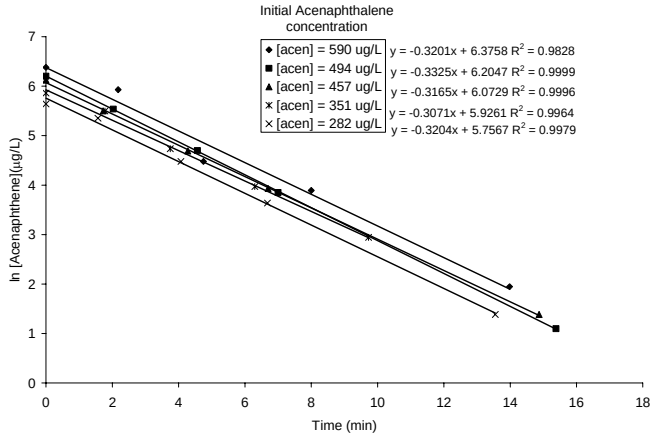

Figure A2. 32. Acenaphthene oxidation: Pseudo-first order plots. [$KMnO_4$] = 3.8 ± 0.1 g/L. Dividing the slope of the plots by the $KMnO_4$ concentration provides the second-order-rate constant.

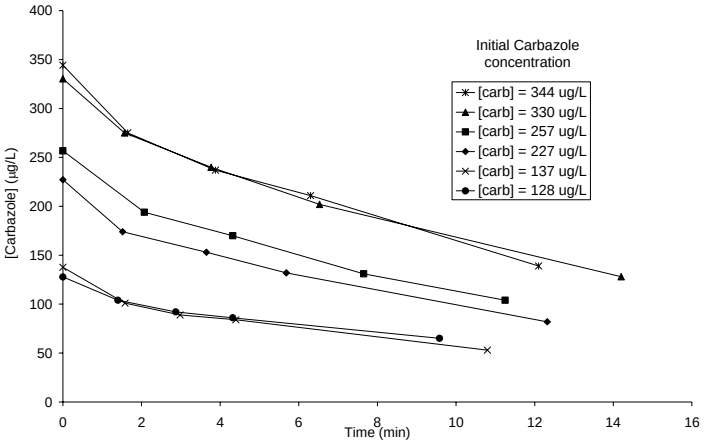

Figure A2. 33. Carbazole oxidation: $[KMnO_4] = 0.46 \pm 0.02$ g/L

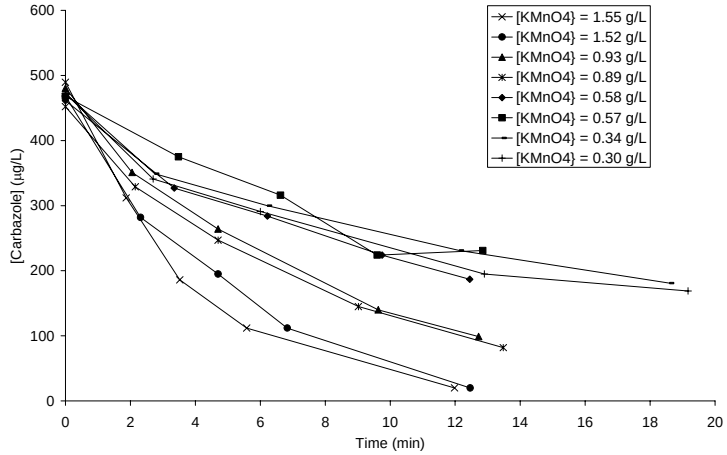

Figure A2. 34. Carbazole oxidation: [Carbazole] = 471 ± 14 µg/L

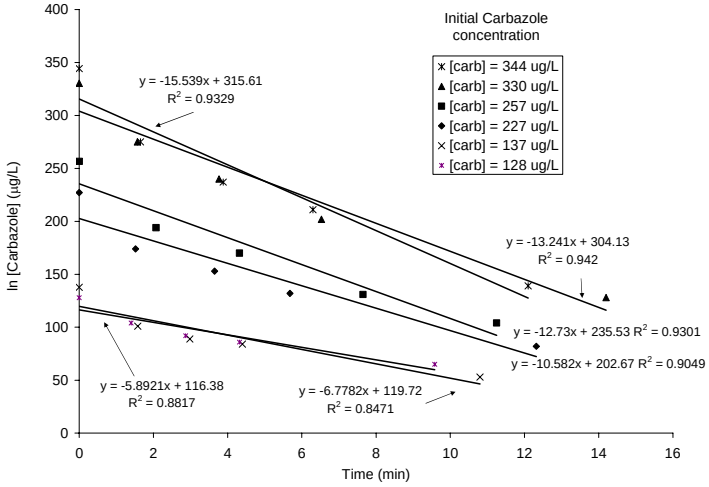

Figure A2. 35. Carbazole oxidation: Initial rates of reaction. $[KMnO_4] = 0.46 \pm 0.02$ g/L. Slope = r_0

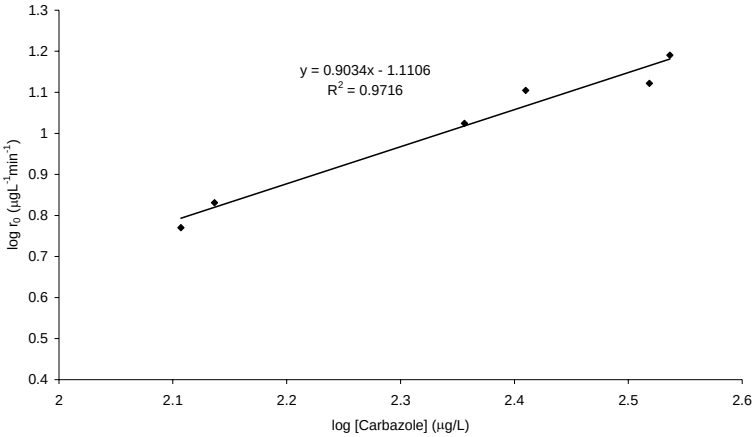

Figure A2. 36. Carbazole oxidation: Determination of the rate order alpha. Slope = alpha

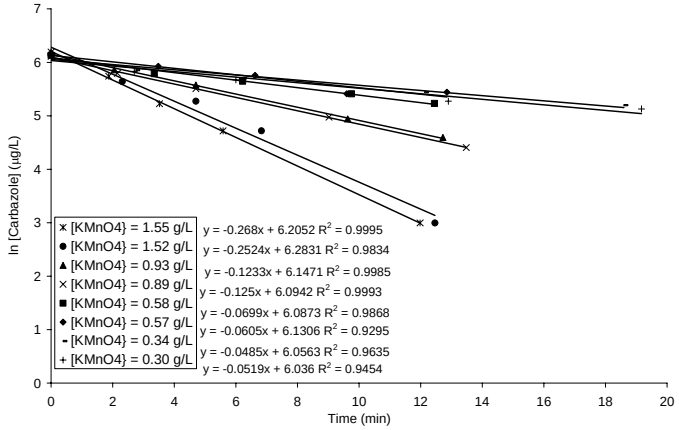

Figure A2. 37. First order decomposition of Carbazole: [Carbazole] = 471 ± 14 μg/L

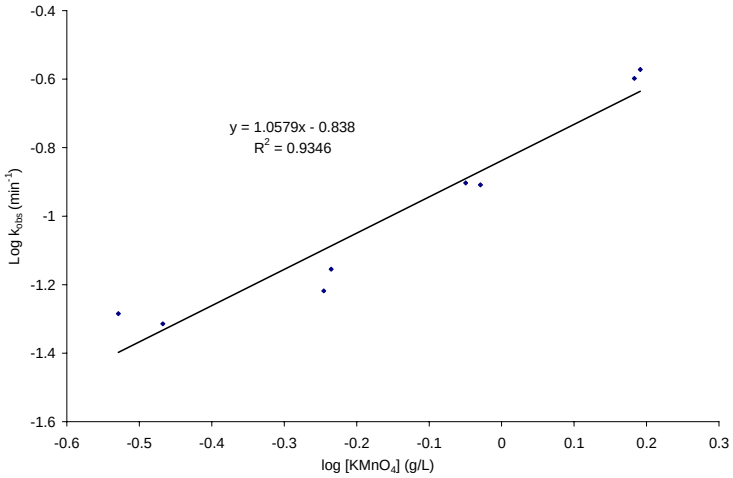

Figure A2. 38. Carbazole oxidation: Determination of the rate order beta. [Carbazole] = 471 ± 14 μg/L. Slope = beta

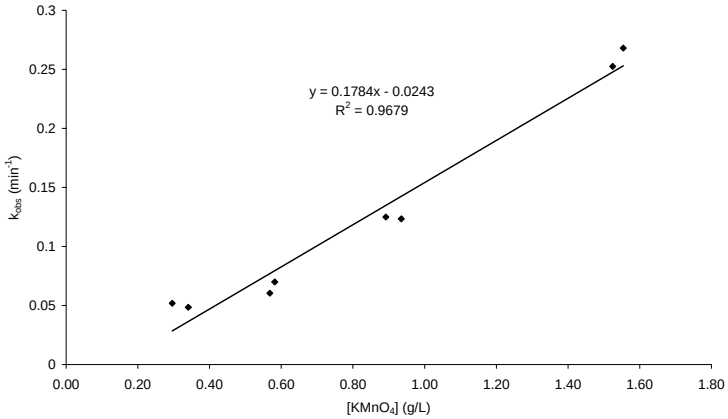

Figure A2. 39. Carbazole oxidation: Determination of second-order-rate constant. Slope = second-order-rate constant

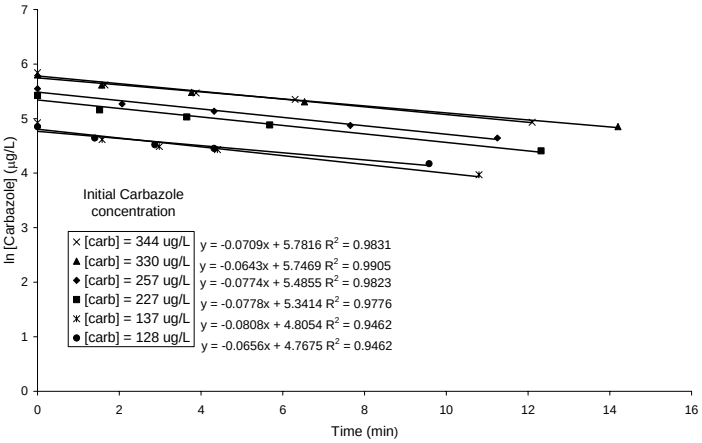

Figure A2. 40. Carbazole oxidation: Pseudo-first order plots. $[KMnO_4] = 0.46 \pm 0.02$ g/L. Dividing the slope of the plots by the $KMnO_4$ concentration provides the second-order-rate constant.

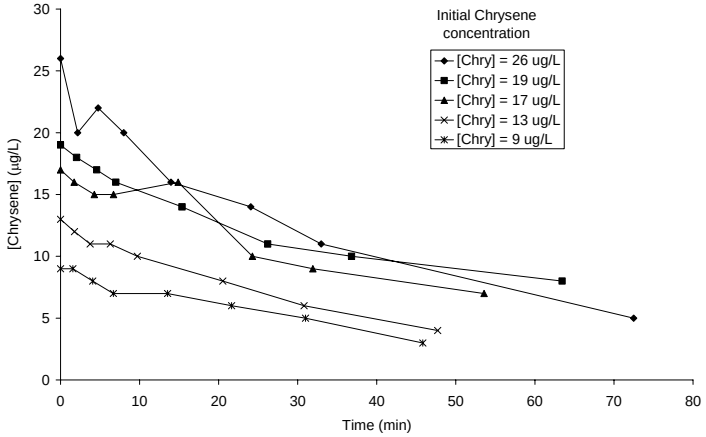

Figure A2. 41. Chrysene oxidation: $[KMnO_4] = 3.8 \pm 0.1$ g/L

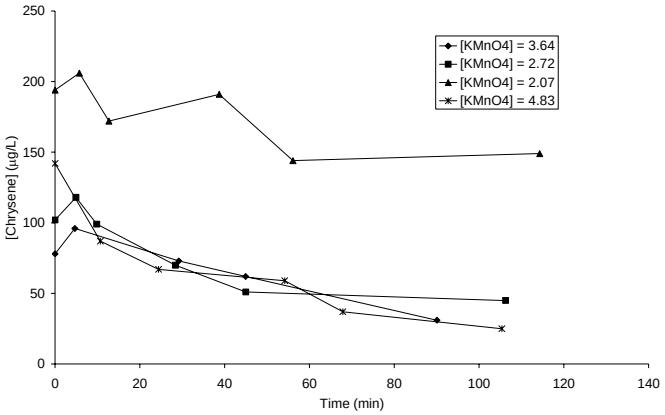

Figure A2. 42. Chrysene oxidation: [Chrysene] = 129 ± 50 µg/L

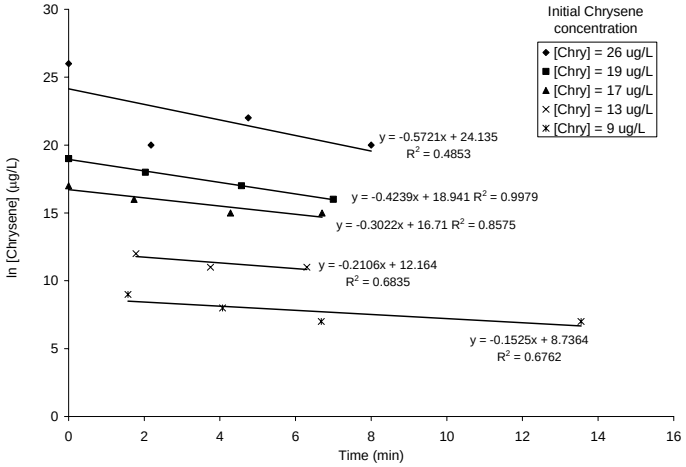

Figure A2. 43. Chrysene oxidation: Initial rates of reaction. $[KMnO_4]$ = 3.8 ± 0.1 g/L. Slope = r_0

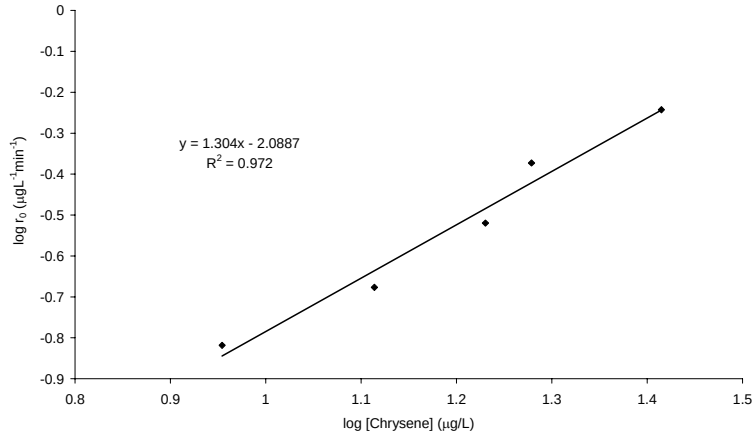

Figure A2. 44. Chrysene oxidation: Determination of the rate order alpha. Slope = alpha

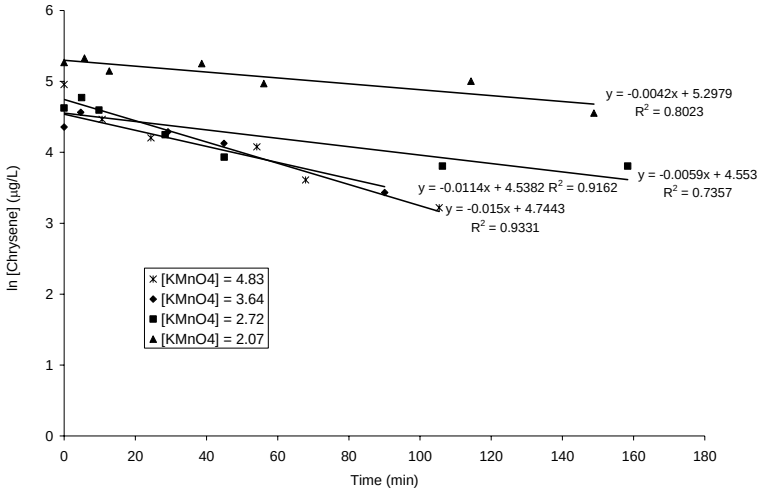

Figure A2. 45. First order decomposition of Chrysene: [Chrysene] = 129 ± 50 µg/L

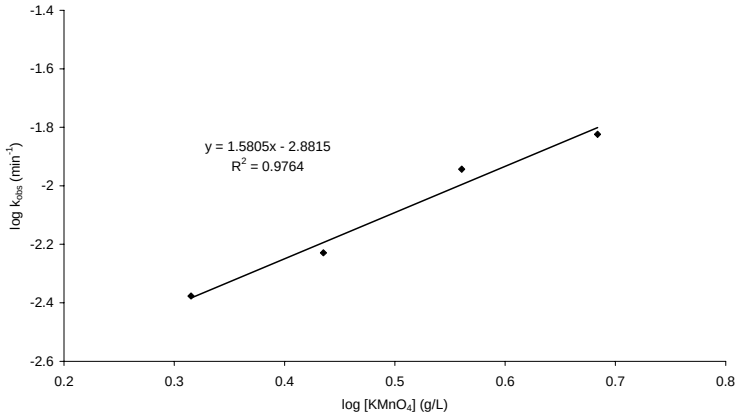

Figure A2. 46. Chrysene oxidation: Determination of the rate order beta. [Chrysene] = 129 ± 50 µg/L. Slope = beta

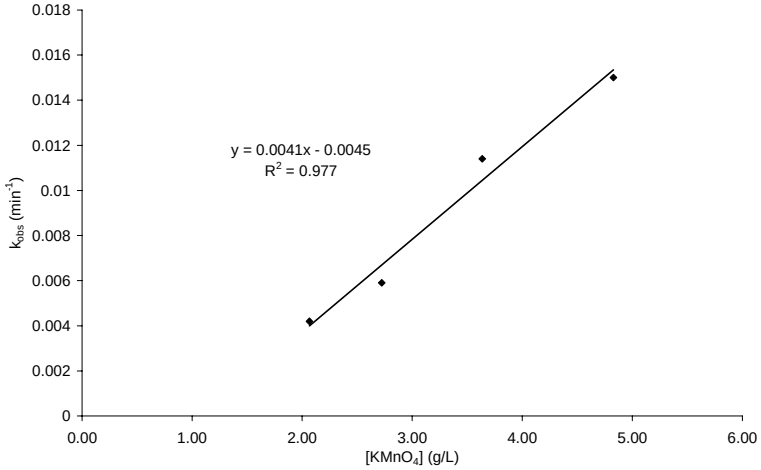

Figure A2. 47. Chrysene oxidation: Determination of second-order-rate constant. Slope = second-order-rate constant

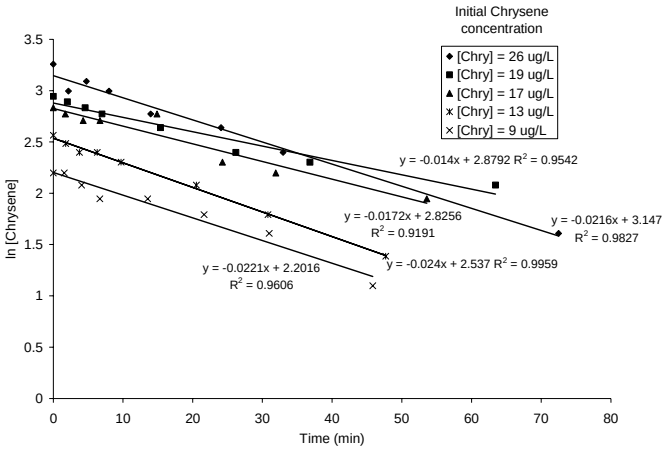

Figure A2. 48. Chrysene oxidation: Pseudo-first order plots. $[KMnO_4] = 3.8 \pm 0.1$ g/L. Dividing the slope of the plots by the $KMnO_4$ concentration provides the second-order-rate constant.

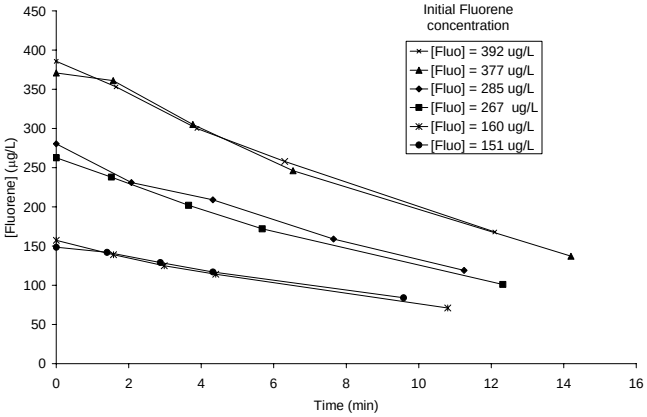

Figure A2. 49. Fluorene oxidation: $[KMnO_4] = 0.46 \pm 0.02$ g/L

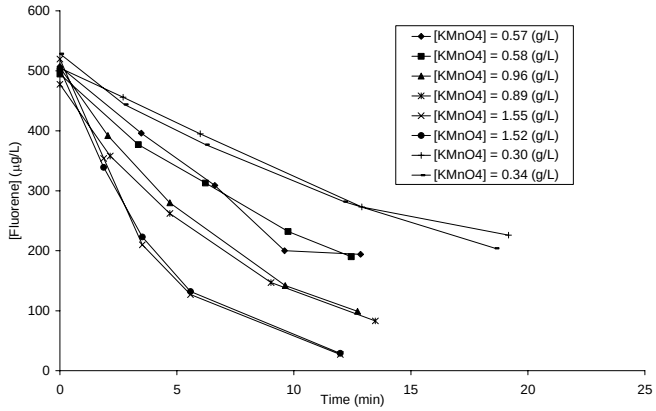

Figure A2. 50. Fluorene oxidation: [Fluorene] = 505 ± 13 µg/L

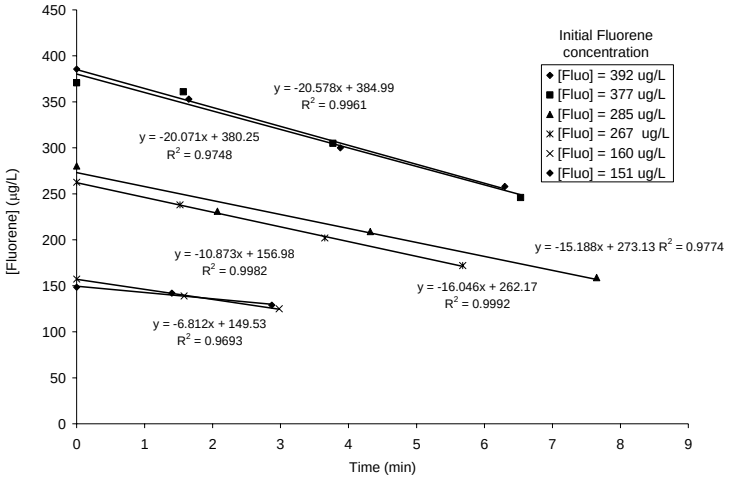

Figure A2. 51. Fluorene oxidation: Initial rates of reaction $[KMnO_4] = 0.46 \pm 0.02$ g/L. Slope = r_0

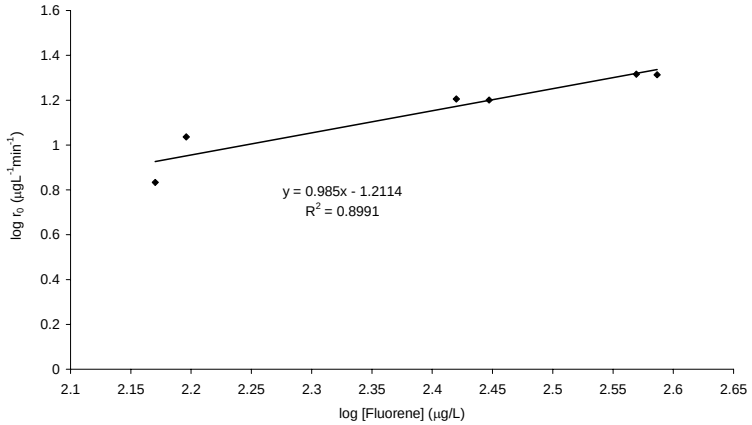

Figure A2. 52. Fluorene oxidation: Determination of the rate order alpha. Slope = alpha

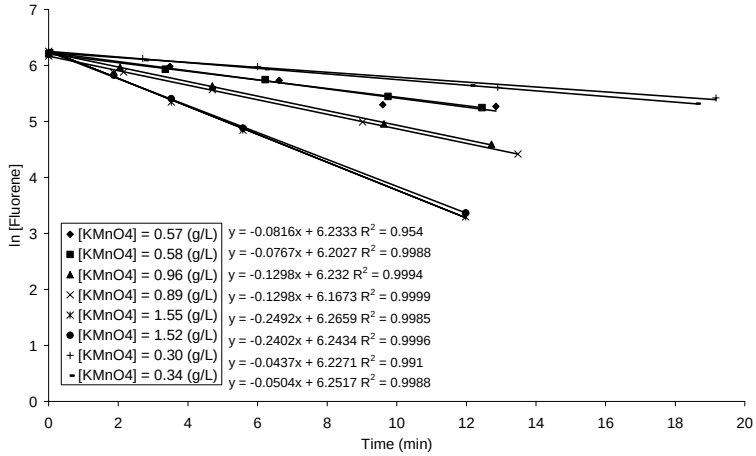

Figure A2. 53. First order decomposition of Fluorene: [Fluorene] = 505 ± 13 µg/L

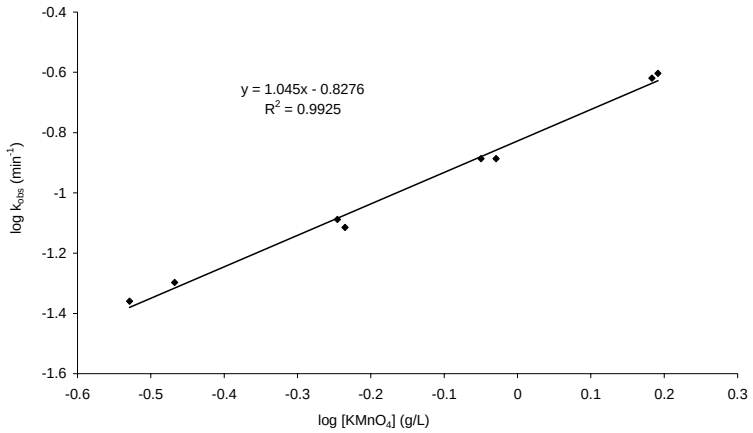

Figure A2. 54. Fluorene oxidation: Determination of the rate order beta. [Fluorene] = 505 ± 13 µg/L. Slope = beta

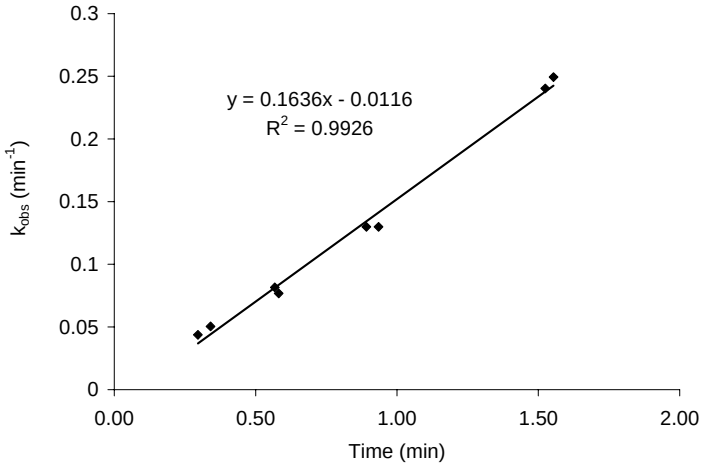

Figure A2. 55. Fluorene oxidation: Determination of second-order-rate constant. Slope = second-order-rate constant

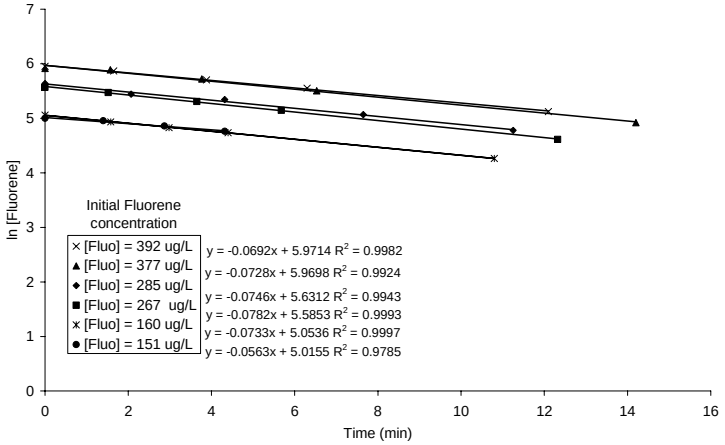

Figure A2. 56. Fluorene oxidation: Pseudo-first order plots. [$KMnO_4$] = 0.46 ± 0.02 g/L. Dividing the slope of the plots by the $KMnO_4$ concentration provides the second-order-rate constant.

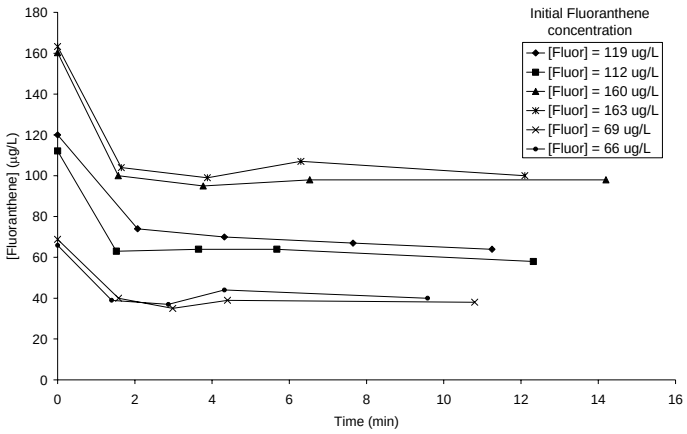

Figure A2. 57. Fluoranthene oxidation: $[KMnO_4] = 0.46 \pm 0.02$ g/L

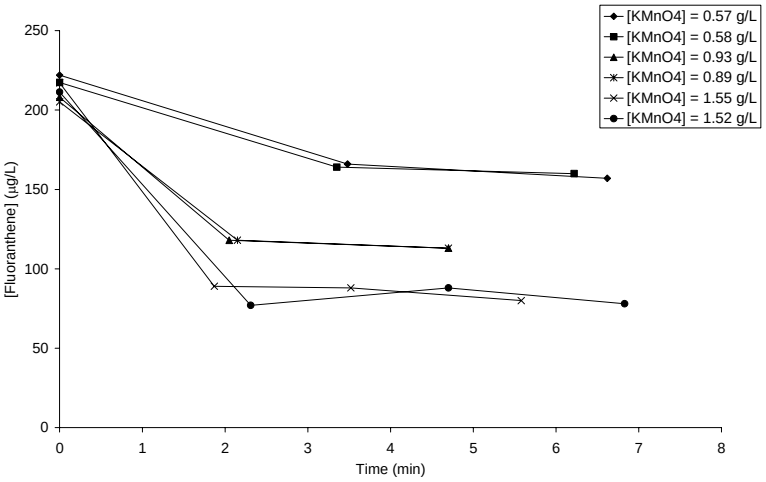

Figure A2. 58. Fluoranthene oxidation: [Fluoranthene] = 217 ± 9 µg/L

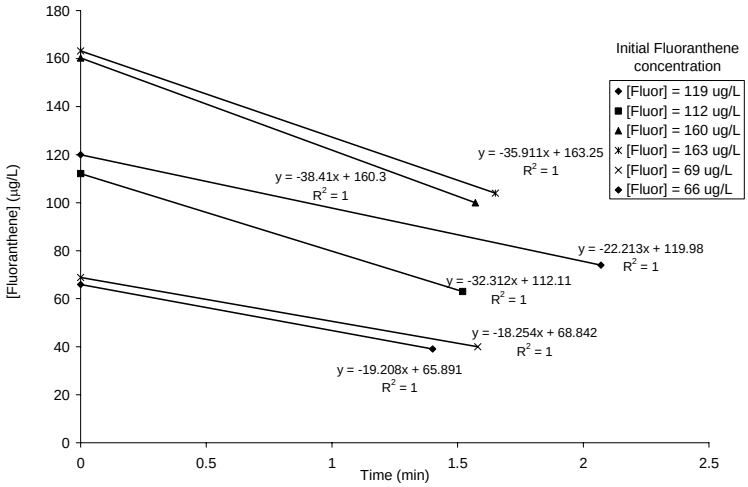

Figure A2. 59. Fluoranthene oxidation: Initial rates of reaction; Note only two data points are used $[KMnO_4] = 0.46 \pm 0.02$ g/L. Slope = r_0

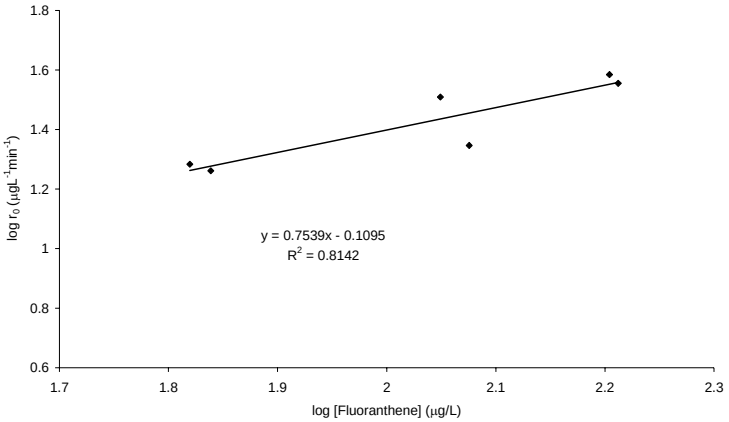

Figure A2. 60. Fluoranthene oxidation: Determination of the rate order alpha. Slope = alpha

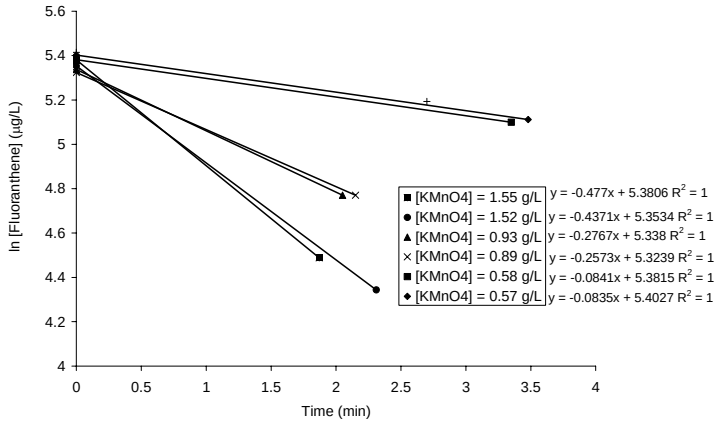

Figure A2. 61. First order decomposition of Fluoranthene: Note only two points are used. [Fluoranthene] = 217 ± 9 µg/L

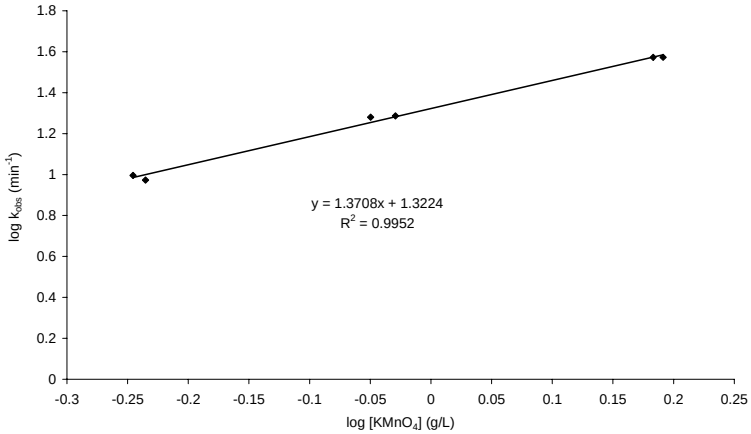

Figure A2. 62. Fluoranthene oxidation: Determination of the rate order beta. [Fluoranthene] = 217 ± 9 µg/L. Slope = beta

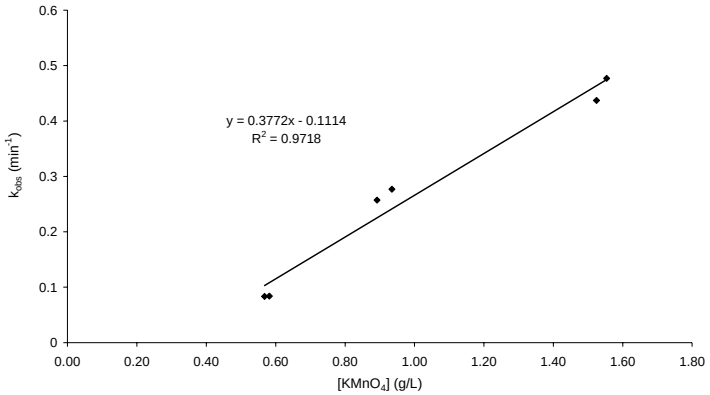

Figure A2. 63. Fluoranthene oxidation: Determination of second-order-rate constant, Slope = second-order-rate constant

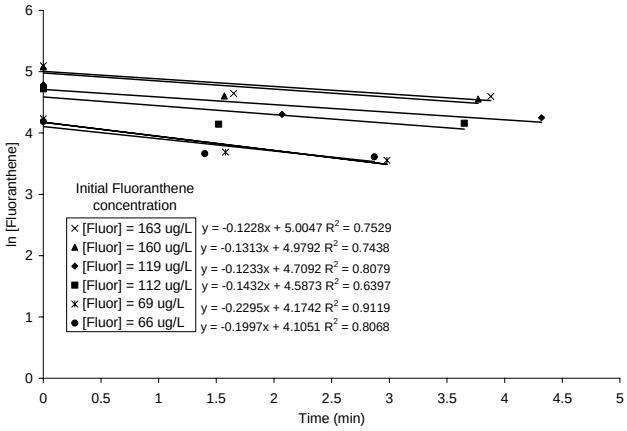

Figure A2. 64. Fluoranthene oxidation; Pseudo-first order plots: $[KMnO_4] = 0.46 \pm 0.02$ g/L. Dividing the slope of the plots by the $KMnO_4$ concentration provides the second-order-rate constant.

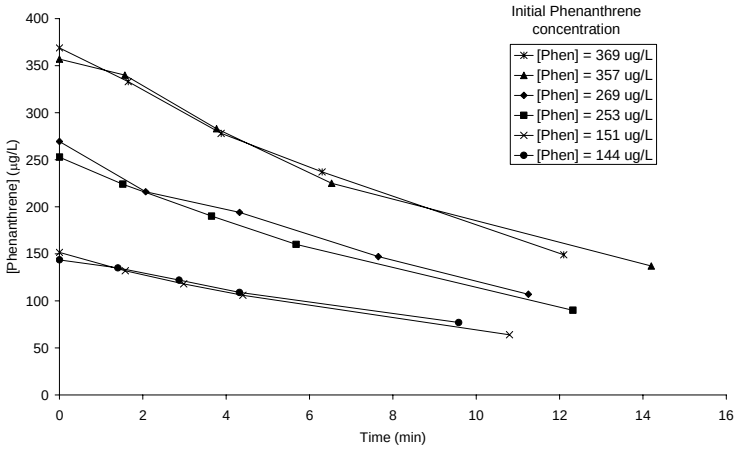

Figure A2. 65. Phenanthrene oxidation: $[KMnO_4] = 0.46 \pm 0.02$ g/L

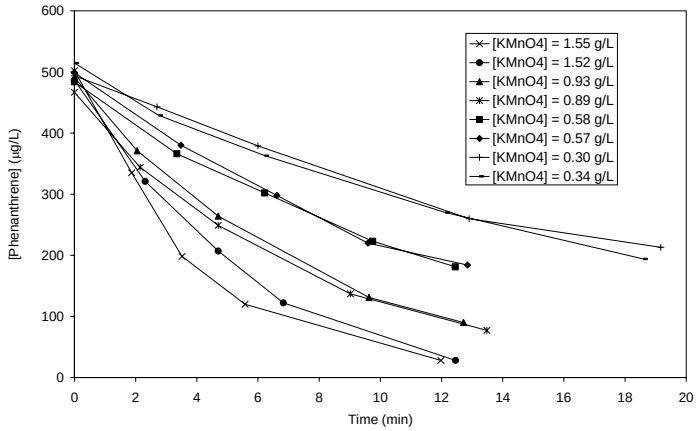

Figure A2. 66. Phenanthrene oxidation: [Phenanthrene] = 491 ± 14 µg/L

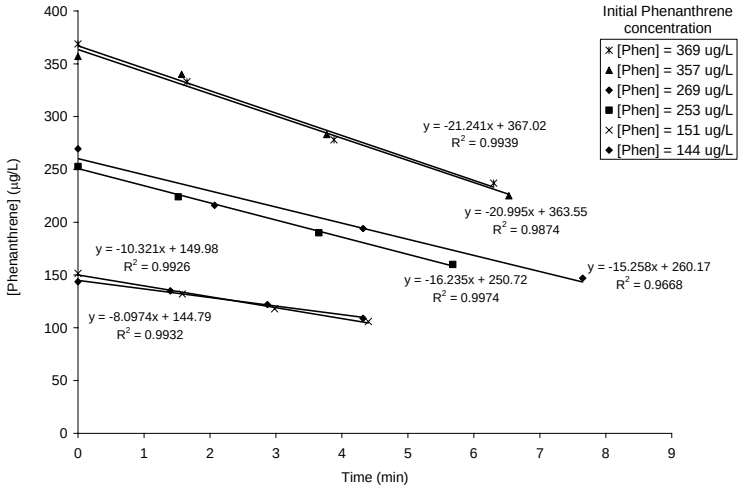

Figure A2. 67. Phenanthrene oxidation: Initial rates of reaction. $[KMnO_4]$ = 0.46 ± 0.02 g/L. Slope = r_0

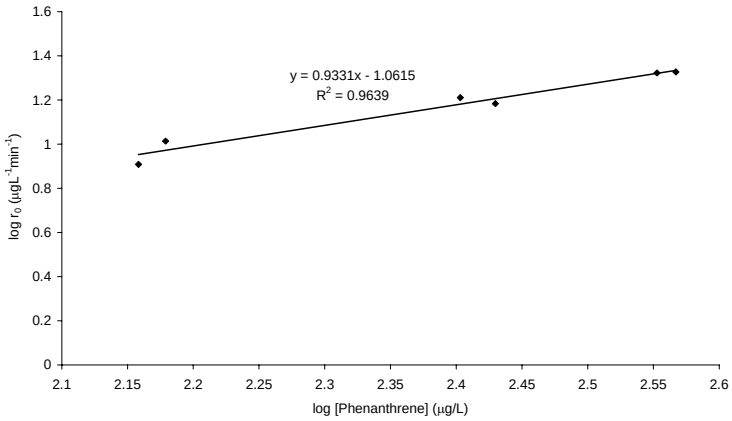

Figure A2. 68. Phenanthrene oxidation: Determination of the rate order alpha. Slope = alpha

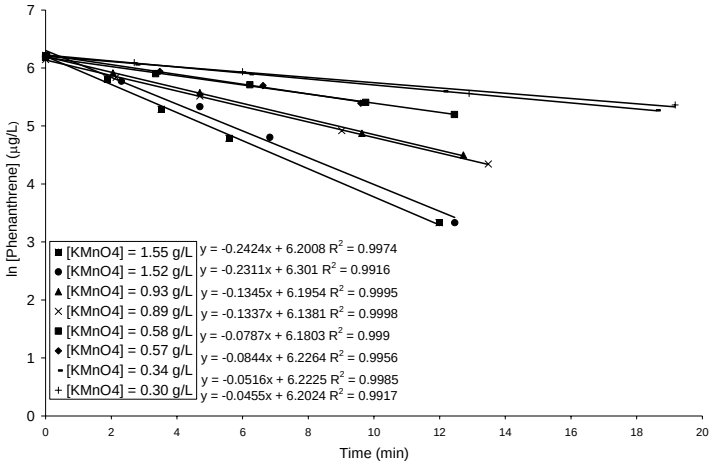

Figure A2. 69. First order decomposition of Phenanthrene: [Phenanthrene] = 491 ± 14 µg/L

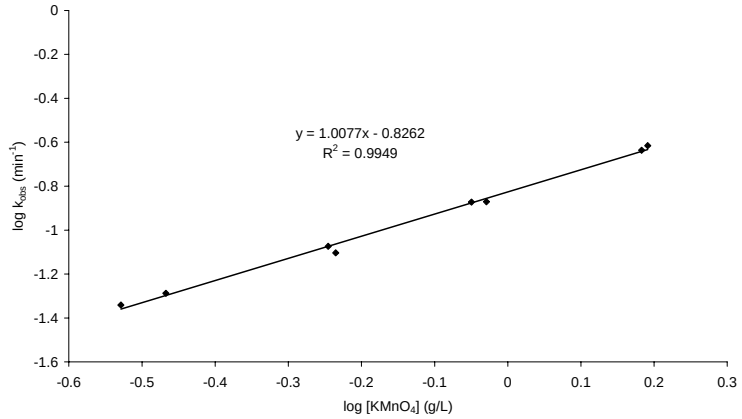

Figure A2. 70. Phenanthrene oxidation: Determination of the rate order beta. [Phenanthrene] = 491 ± 14 µg/L. Slope = beta

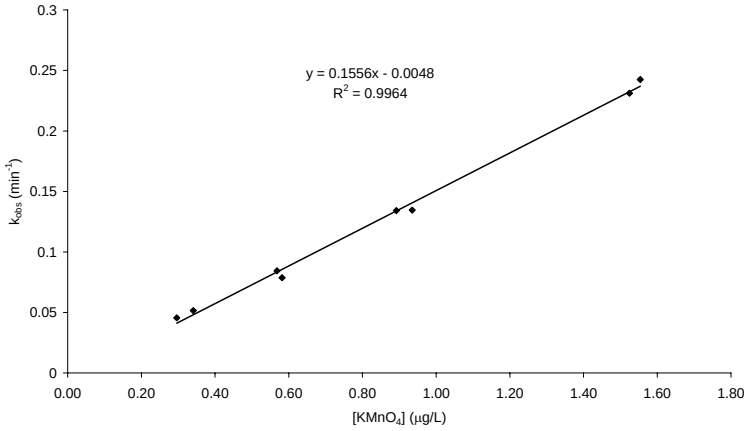

Figure A2. 71. Phenanthrene oxidation: Determination of second-order-rate constant. Slope = second-order-rate constant

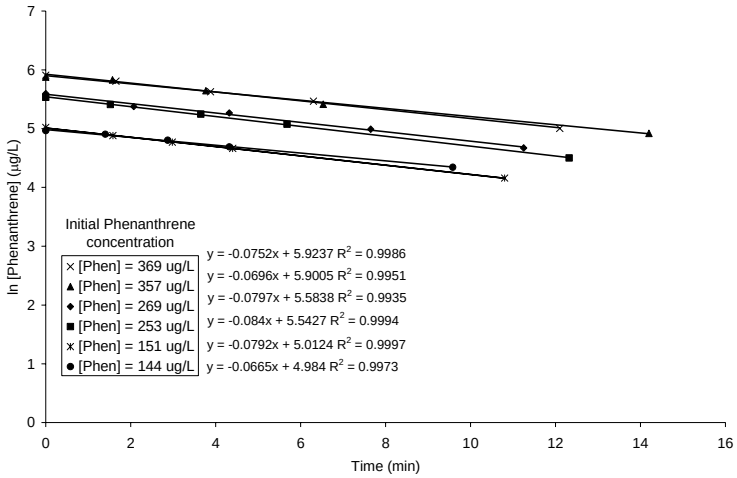

Figure A2. 72. Phenanthrene oxidation: Pseudo-first order plots. [$KMnO_4$] = 0.46 ± 0.02 g/L. Dividing the slope of the plots by the $KMnO_4$ concentration provides the second-order-rate constant.

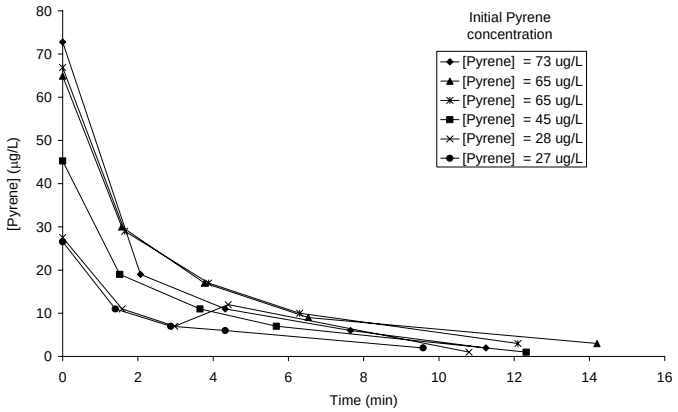

Figure A2. 73. Pyrene oxidation: [$KMnO_4$] = 0.46 ± 0.02 g/L

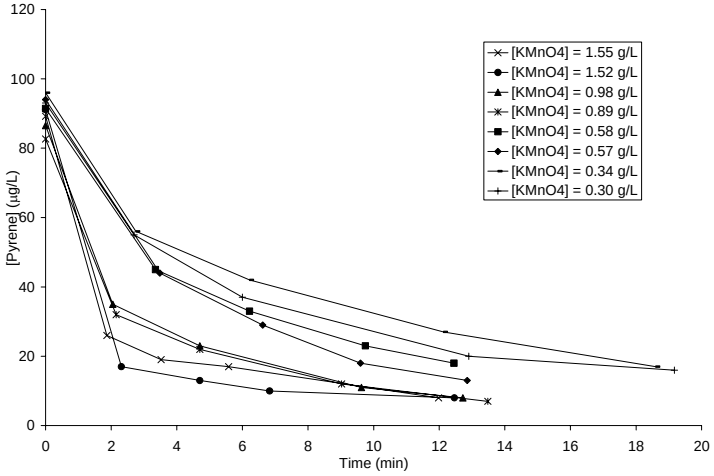

Figure A2. 74. Pyrene oxidation: [Pyrene] = 90 ± 3 µg/L

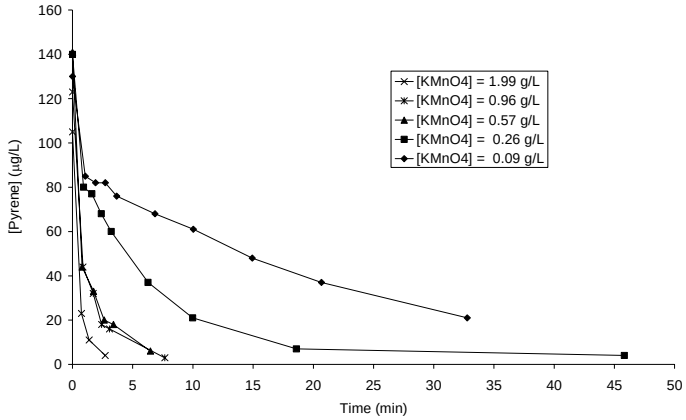

Figure A2. 75. Pyrene oxidation: [Pyrene] = 127 ± 15 µg/L

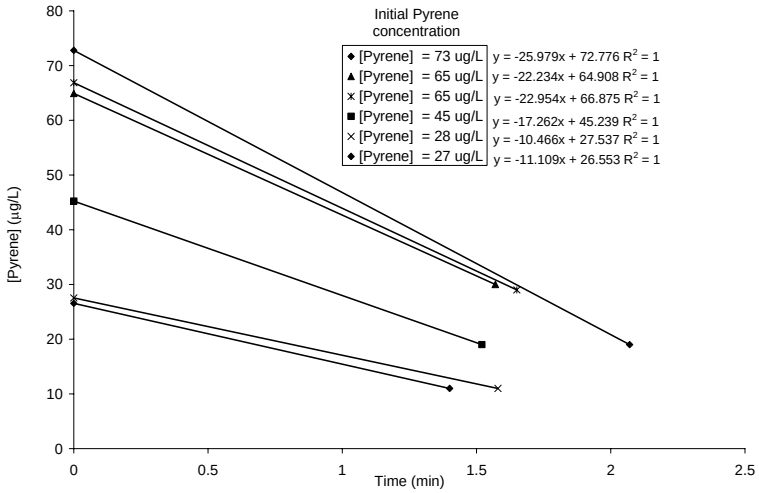

Figure A2. 76. Pyrene oxidation: Initial rates of reaction. $[KMnO_4]$ = 0.46 ± 0.02 g/L. Slope = r_0
Only two data points were used to determine r_0.

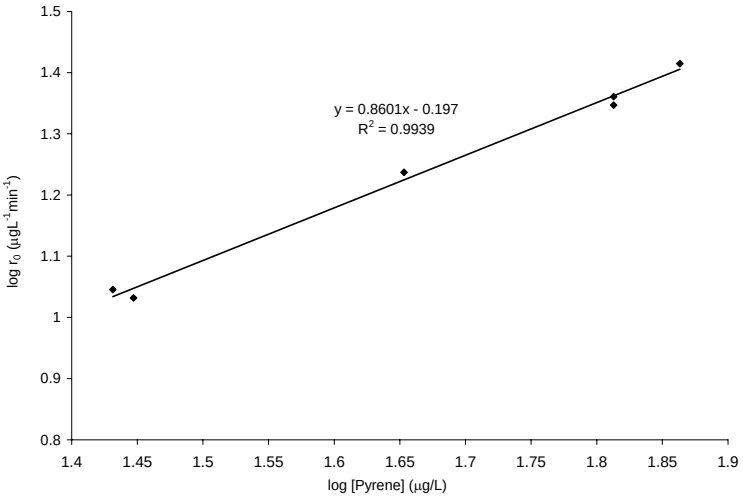

Figure A2. 77. Pyrene oxidation: Determination of the rate order alpha. Slope = alpha

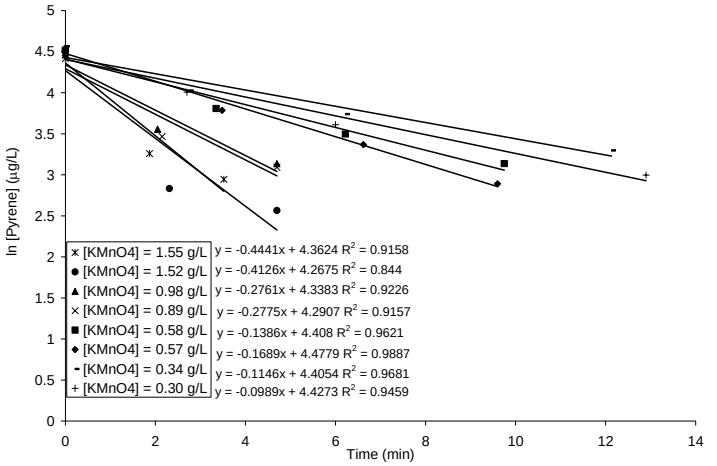

Figure A2. 78. First order decomposition of Pyrene: [Pyrene] = 90 ± 3 µg/L.

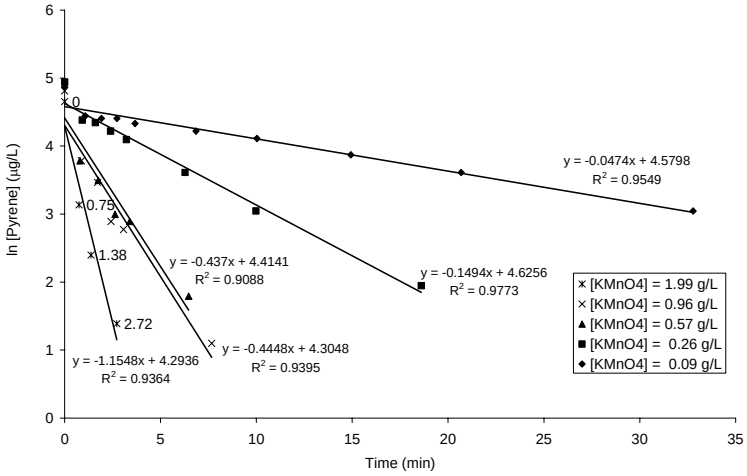

Figure A2. 79. First order decomposition of Pyrene: [Pyrene] = 127 ± 15 µg/L.

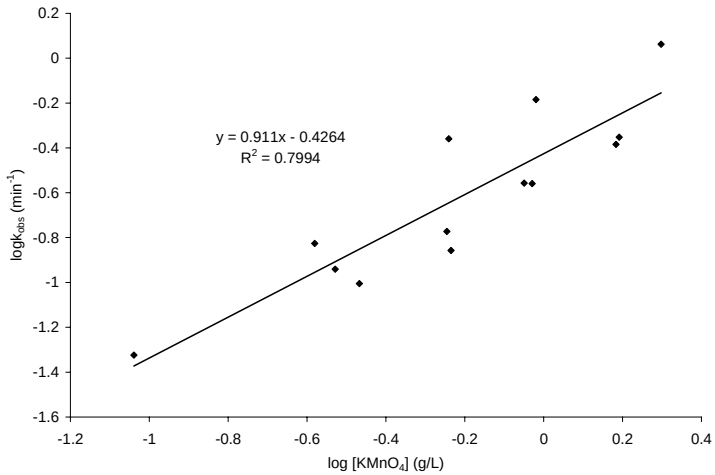

Figure A2. 80. Pyrene oxidation: Determination of the rate order beta. Slope = beta

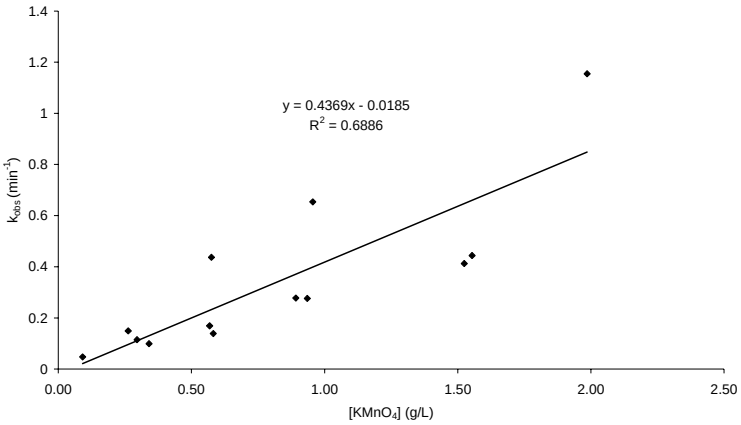

Figure A2. 81. Pyrene oxidation: Determination of second-order-rate constant. Slope = second-order-rate constant

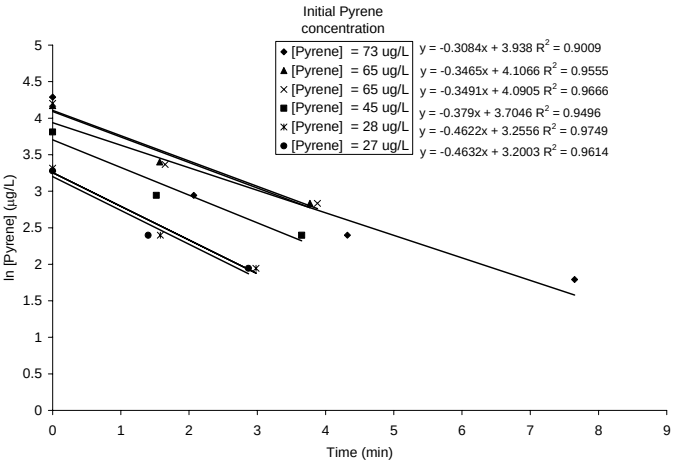

Figure A2. 82. Pyrene oxidation: Pseudo-first order plots. $[KMnO_4] = 0.46 \pm 0.02$ g/L. Dividing the slope of the plots by the $KMnO_4$ concentration provides the second-order-rate constant.

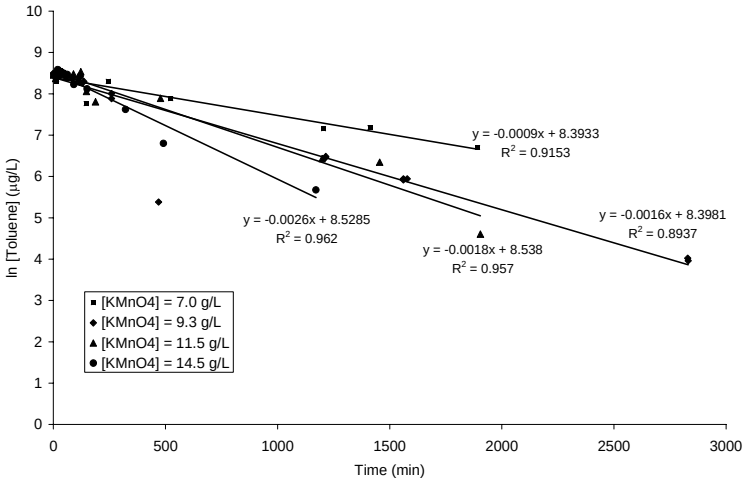

Figure A2. 83. First order decomposition of Methylbenzene: [Methylbenzene] = 4397 ± 307 µg/L

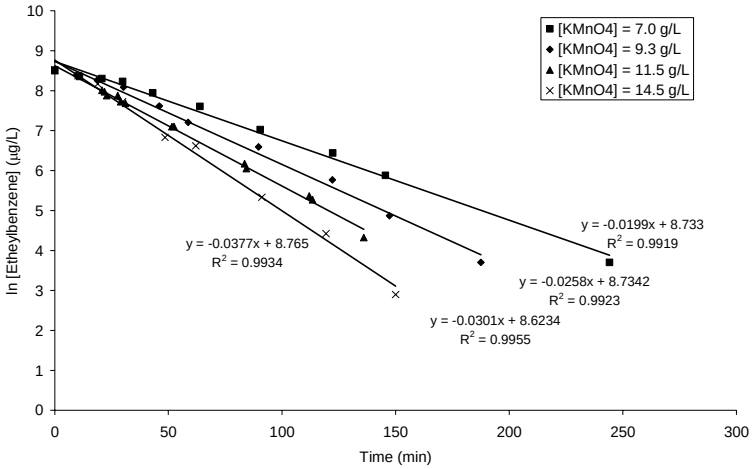

Figure A2. 84. First order decomposition of Ethylbenzene: [Ethylbenzene] = 4995 ± 406 µg/L

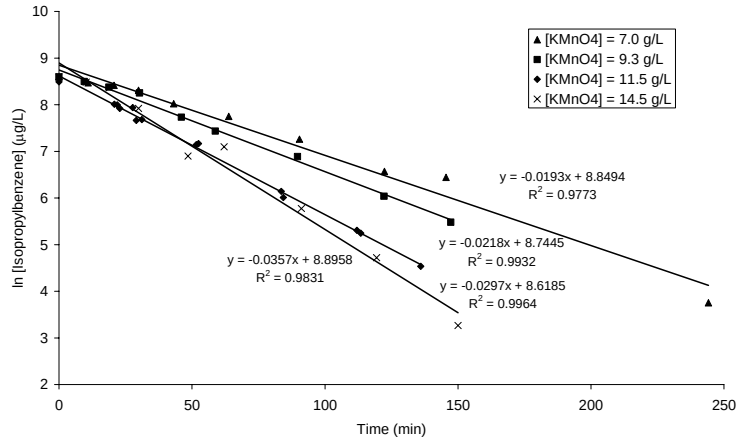

Figure A2. 85. First order decomposition of Isopropylbenzene: [Isopropylbenzene] = 5418 ± 268 µg/L

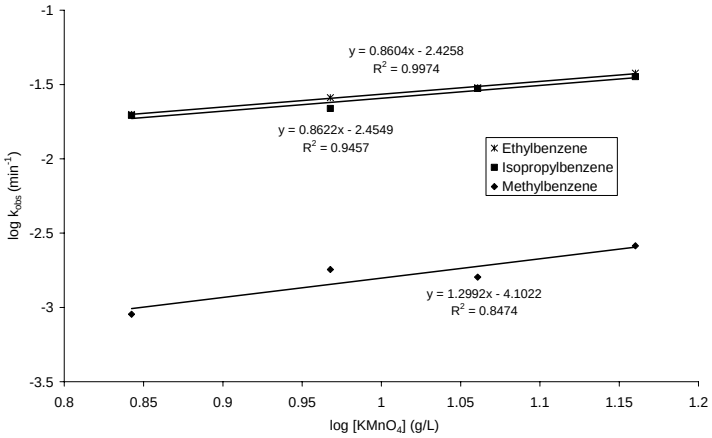

Figure A2. 86. Methylbenzene, Ethylbenzene and Isopropyl oxidation: Determination of the rate order beta. [Methylbenzene] = 4397 ± 307 µg/L, [Ethylbenzene] = 4995 ± 406 µg/L, Isopropylbenzene] = 5418 ± 268 µg/L. Slope = beta

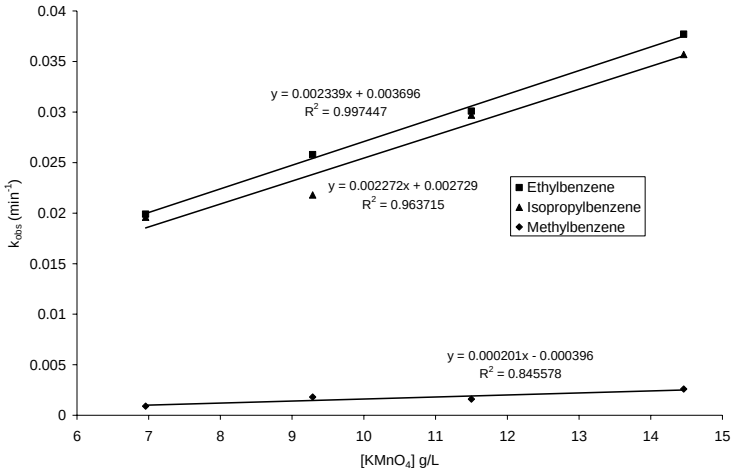

Figure A2. 87. Methylbenzene, Ethylbenzene and Isopropyl oxidation: Determination of second-order-rate constant. Slope = second-order-rate constant

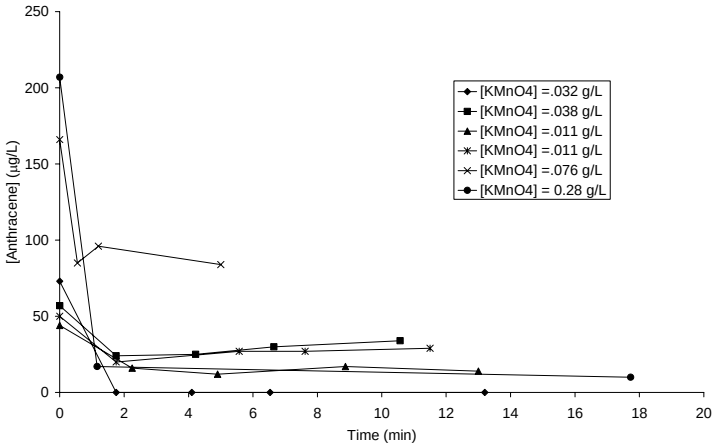

Figure A2. 88. Anthracene oxidation.

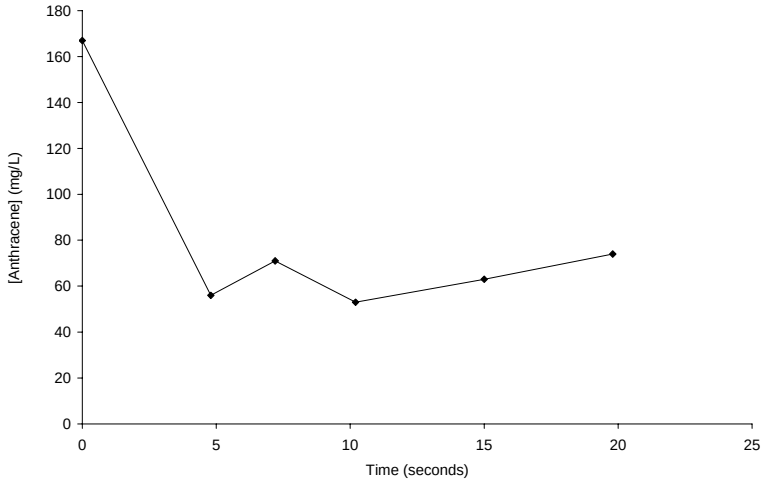

Figure A2. 89. Anthracene oxidation: Early times, the reaction has stopped after 5 seconds.

Appendix 3

Volatile and semi volatile aromatic hydrocarbon analysis

The following procedure was modified for the analysis of creosote and creosote compounds for the experiments conducted in this thesis. Modifications are presented in the individual chapters.

Organic Geochemistry Laboratory
Department of Earth Sciences
Telephone: 519 888 4567 ext 5180/6370

(benzene, toluene, ethylbenzene, p+m-xylene, o-xylene, trimethylbenzenes (1,3,4; 1,2,3 and 1,2,5), naphthalene, indole + 2-methylnaphthalene, 1-methylnaphthalene, biphenyl, acenaphthylene, acenaphthene, dibenzofuran, fluorene, phenanthrene, anthracene, carbazole, fluoranthene, pyrene, benzo (a) anthracene, chrysene, benzo(b+k)fluoranthene, benzo (a) pyrene, indeno(1,2,3,cd)pyrene + dibenzo(ah)anthracene, and benzo(g,h,i)perylene)

Introduction: A gas chromatographic technique is described to determine volatile aromatic components of gasoline and some polycyclic aromatic components of creosote, in groundwater samples (the components are listed above). Typically, these compounds are determined by purge and trap or exhaustive extraction techniques. However, because the may require many anlyses to define the shape, movement and attenuation of a trace contaminant plume, purge and trap methods are too time consuming to use on a routine basis. Separatory funnel or continuous solvent extraction techniques are not only slow and labor intensive but can also suffer from volatilization losses. The methodology presented here was derived from an extraction previously described by Henderson et al., 1976. The technique required that the partitioning of the analyte be at equilibrium between the phases, as opposed to being exhaustively extracted from the water.

Apparatus: Aqueous groundwater samples and methanolic standards are extracted in 18 mL crimp-tip hypovials with Telfon®-faced silicone septa. The determinations are performed on a gas chromatograph equipped with a splitless injection port, a 0.25 mm x 30 m glass DB5 capillary column with a film thickness of 0.25 μm and a flame ionization detector. The chromatographic conditions are as follows: injection port temperature, 275 ^{o}C; initial column temperature, 35 ^{o}C; initial time, 0.5 min; heating rate, 15 ^{o}C/min; final temperature 300 ^{o}C; final time, 10.0 min; detector temperature, 325 ^{o}C; column flow rate, 3 ml/min helium.

Procedure: *Sample bottle preparation*: Bottles and other glassware are soaked in a commercial alkaline cleaning solution for several hours, then rinsed with deionized

water, dilute nitric acid, and more deionized water. The bottles are then baked overnight at 110 ^{o}C.

Sample collection and handling: Each 18 mL hypovial sample bottle is filled without headspace, quickly crimped sealed with a Teflon® setpa and then stored at 4 ^{o}C until extracted (7-14 day time limit). Prior to capping, sodium azide (200 µl of a 10% solution) may be added to the sample bottle as a preservative, if the analysis will not occur within 7 days.

To solvent extract a sample (or standard), the septum cap of the vial is quickly removed and 2.0 mL if water is removed with a syringe. This is followed by the addition of 1.0 mL of dichloromethane, containing the internal standards m-fluorotoluene and 2-fluorobiphenyl. The vial is quickly resealed and agitated on its side at a maximum speed of 350 rpm on a platform shaker for 15 min. After shaking, the vial is inverted and the phases are allowed to separate for 10 to 30 min. Approximately 0.7 mL of the dichloromethane phase is removed from the inverted vial with syringe (through the septum) and placed in a sealed auto sampler vial for injection into the gas chromatograph.

Quality control: Samples and standards are equilibrated to room temperature (approx. 22 ^{o}C) before extraction. A calibration is made in internal standard mode and standards are run in triplicate at four different levels (or more) convering the expected sample range. A multiple point linear regression is performed to determine linearity and slope of the calibration curve. Standards are prepared by spiking water with a concentrated methanolic stock standard, and are extracted in the same manner as the other samples. Three methanolic stock standards are used, each an order of magnitude above the other. The methanolic stock standard is prepared gravimetrically, injecting the various pure compounds through a septum into on 60 mL aliquot of methanol, or are purchased commercially.

Matrix spikes are performed by spiking a known amount of mid-range standards into a duplicate field sample and then calculating the amount recovered after extraction. Reagent water blanks are run on a daily basis. The methanolic stock standards are stored in a freezer when not in use and are replaced when accuracy becomes unacceptable.

Method Detection Limit

Aug 4, 1999
Units are ug/L (ppb)

	N	X_0	X	S	MDL
benzene	9	23.91	28.82	1.29	3.75
toluene	9	22.55	27.91	3.53	10.22
ethylbenzene	9	22.82	25.34	1.26	3.64
p+m-xylene	9	45.64	49.56	1.99	5.76
o-xylene	9	23.64	25.66	1.03	3.00
1,3,4-trimethylbenzene	9	23.64	26.05	0.84	2.43
1,2,3-trimethylbenzene	9	23.36	25.28	0.85	2.45
1,2,5-trimethylbenzene	9	24.72	26.18	0.86	2.49
naphthalene	9	15.69	16.93	1.50	4.34
indole + 2-methylnaphthalene	9	31.25	24.67	1.61	4.66
1-methylnaphthalene	9	15.69	16.89	0.93	2.68
biphenyl	9	30.44	33.07	1.66	4.80
acenaphthylene	9	15.69	17.00	0.92	2.67
acenaphthene	8	15.63	19.21	0.78	2.27
dibenzofuran	9	15.46	14.89	0.89	2.68
fluorene	9	15.69	18.14	0.92	2.67
phenanthrene	9	15.69	17.69	2.23	6.75
anthracene	9	15.69	16.12	1.25	3.63
carbazole	8	16.87	13.44	1.58	4.75
fluoranthene	9	15.69	18.82	1.79	5.17
pyrene	9	15.63	19.26	1.49	4.30
benzo(a)anthracene	8	15.63	10.91	1.09	3.26
chrysene	8	15.69	22.42	2.10	6.30
benzo(b+k)fluoranthene	8	31.25	16.88	6.71	20.11
benzo (a)pyrene	8	15.69	15.69	10.29	24.40
indeno(1,2,3,cd)pyrene+dibenzo(ah)anthracene	9	62.63	62.63		>62.63
benzo(g,h,i)perylene)	9	31.38	31.38		>31.38

N = Sample size
X_0 = True value of standard
X = Average calculated value of standards
S = Standard deviation
MDL = Methode detection limit

Literature cited: Henderson, K.E. G.R. Peyton and W.H. Glaze . *A convenient liquid-liquid extraction method for the determination of halomethanes in water at parts-per-billion level*. IN: Identification and analysis of organic pollutants in water. Keith, L.H. ed. Ann Arbor Science Publishers Inc., Ann Arbor, MI. 1976.